

# Studies of Quantum Phase Transitions in Dirac Electron Systems

by

Hennadii Yerzhakov

A thesis submitted in partial fulfillment of the  
requirements for the degree of  
Doctor of Philosophy

Department of Physics  
University of Alberta

© Hennadii Yerzhakov, 2021

# Abstract

This thesis is dedicated to the study of quantum phase transitions in 2D Dirac semimetals. In Chapter 1, we first briefly review how Dirac fermions emerge in condensed matter systems and then briefly review the physics of quantum phase transitions. Chapter 2 is devoted to the field-theoretic study of the isotropic-nematic phase transition on the surface of a 3D topological insulator with a single Dirac cone in its band structure. Unlike spin-degenerate Fermi liquids, due to the spin-orbit-coupled nature of topological insulators, the nematic order parameter necessarily mixes spin and spatial degrees of freedom. First, using mean-field theory, we find that the system undergoes a first-order phase transition at zero temperature in the undoped limit, which then becomes continuous at a finite-temperature tricritical point. In the doped limit, the phase transition is continuous at zero temperature. We discuss several signatures of the nematic order, among which is the partial breakdown of spin-momentum locking. In many regards, the effects of fluctuations about the mean-field solution are qualitatively the same as for spin-degenerate Fermi liquids. However, we show that nematic fluctuations may induce spin fluctuations. In Chapter 3, we use the double epsilon expansion method of renormalization group theory to study the interplay of interactions and weak uncorrelated disorder on the superconducting phase transition in a 2D Dirac semimetal described by the chiral XY Gross-Neveu-Yukawa model. When the num-

ber of fermion flavors in the system is greater than one, we find new disordered quantum critical points, some of which are of stable-focus type. In Chapter 4, we extend this study to the Ising and Heisenberg Gross-Neveu-Yukawa models, appropriate to charge-density-wave and spin-density-wave transitions, and include long-range correlated disorder. A controlled treatment of the latter requires the introduction of another small parameter; the double epsilon expansion method is thus generalized into the triple epsilon expansion method. We find new short- and long-range disordered fixed points and show that for some regions of physical parameters, the critical behavior is controlled by a stable limit cycle.

# Preface

The thesis is based on three papers:

- [1] R. Lundgren, H. Yerzhakov, and J. Maciejko. Nematic order on the surface of a three-dimensional topological insulator. *Phys. Rev. B*, 96(23):235140, 2017;
- [2] H. Yerzhakov and J. Maciejko. Disordered fermionic quantum critical points. *Phys. Rev. B*, 98(19):195142, 2018;
- [3] H. Yerzhakov and J. Maciejko. Random-mass disorder in the critical Gross-Neveu-Yukawa models, *Nucl. Phys. B*, 962:115241, 2021,

which are presented with a few changes in Chapters 2, 3, and 4. The motivation and models for the projects are proposed, and all three projects are supervised by Joseph Maciejko. The first paper is coauthored with Rex Lundgren, who is the first author. Some of the calculations were performed by Rex and Joseph first. A portion of these calculations was later recalculated by me after a refinement of the model. Such is the “Fluctuation effects” section in the paper except for the self-energy subsection. The self-energy calculations for a generic angle and mean-field calculations for the undoped case were performed in parallel by me and Rex. The self-energy for special angles was calculated by me after the refinement of the model.

# Acknowledgments

First of all, I want to thank my supervisor, Joseph Maciejko. The entanglement of intellect and humanity makes him a singular point in this universe. And even if I am wrong with the previous statement, at least, the singularity is rounded into a giant with a huge heart and shoulders<sup>1</sup>.

I thank the CMT group at the University of Alberta in faces of Joel Hutchinson — my thoughtful superorganized officemate<sup>2</sup>, Rufus Boyack — a superconducting dragon<sup>3</sup>, Mason Protter — who seems to be an expert in everything, Shankar Ganesh — an example of curiosity and dedication, Pramodh UniversityofAlbertaSenarath Yapa — a man of multiple talents, who can be everything he wants to be<sup>4</sup>, Youssef Kora — a raw power of computational<sup>5</sup> muscles, Chun Chen — thank you for the reference, Sepideh Mirabi — thank you for your smiles, and Majid Kheirkhah — thank you for seriousness, for creating a deep intellectual background. Outside the CMT group, this extends to Jens Boos and Kento Osuga — thank you for organizing and contributing to the weekly Student Meetings — a spacetime domain for learning and discussion of extracurricular topics, and to Andrei Tretiakov — also, thank you for the book, which I still might return. I appreciate all the efforts of the CMT professors to teach us beyond the standard curriculum.

I thank my committee members, Dr. Alexander Penin, Dr. Frank Marsiglio, and Dr. Igor Herbut, for valuable critical comments and questions. I also thank my other committee

---

<sup>1</sup>a reference is implied.

<sup>2</sup>a personal opinion.

<sup>3</sup>probably, a public opinion.

<sup>4</sup>fluid like helium.

<sup>5</sup>as well as theoretical.

member, Dr. Marc de Montigny, for playing a “good cop” role.

Over the years, I attended many great lectures. In this regard, I want to emphasize Dr. Massimo Boninsegni, who delivered the most engaging and passionate lectures I have ever experienced.

I appreciate the financial support from the University of Alberta, Alberta Innovates, and Alberta Advanced Education, which facilitated the faster progress in my research.

Outside the academy, the nights were mostly dark with a few stars — thanks to Anna Tendera and Sofia Karabatsos.

Also, without any additional explanations, I thank my mother.

# Contents

<b>Abstract</b>	<b>ii</b>
<b>Preface</b>	<b>iv</b>
<b>Acknowledgments</b>	<b>v</b>
<b>List of Tables</b>	<b>xi</b>
<b>List of Figures</b>	<b>xii</b>
<b>Abbreviations</b>	<b>xviii</b>
<b>1 Introduction</b>	<b>1</b>
1.1 Dirac fermions in condensed matter physics . . . . .	2
1.2 Quantum phase transitions . . . . .	11
1.3 Structure of the thesis . . . . .	15
<b>2 Nematic phase transition on the surface of a 3D topological insulator</b>	<b>16</b>
2.1 Model and Nematic Order Parameter . . . . .	19
2.2 Mean-Field Theory . . . . .	22
2.2.1 Undoped limit . . . . .	23
2.2.2 Doped limit . . . . .	30
2.3 Fluctuation effects . . . . .	34
2.3.1 Collective modes . . . . .	36

2.3.2	Helical non-Fermi liquid behavior . . . . .	41
2.4	Conclusion . . . . .	44
<b>3</b>	<b>Short-range correlated disorder and Dirac semimetal-superconductor transition</b>	<b>45</b>
3.1	Introduction . . . . .	45
3.2	Model . . . . .	48
3.3	RG in the double epsilon expansion . . . . .	52
3.3.1	Bare vs renormalized actions . . . . .	54
3.3.2	Renormalization constants . . . . .	57
3.3.3	Beta functions and anomalous dimensions . . . . .	59
3.4	RG flow analysis . . . . .	62
3.4.1	Fixed points . . . . .	62
3.4.2	Linear stability analysis . . . . .	64
3.4.3	RG flows . . . . .	65
3.5	Critical exponents and phase diagram . . . . .	69
3.6	Conclusion . . . . .	74
<b>4</b>	<b>Long range-correlated random-mass disorder in GNY models</b>	<b>78</b>
4.1	Introduction . . . . .	78
4.2	The random-mass GNY models . . . . .	80
4.3	RG in the triple epsilon expansion . . . . .	84
4.3.1	Bare vs renormalized actions . . . . .	85
4.3.2	Renormalization constants . . . . .	87
4.3.3	Beta functions and anomalous dimensions . . . . .	91
4.4	Fixed points and critical exponents . . . . .	92
4.4.1	Fixed points . . . . .	92
4.4.1.1	Fixed points with short-range correlated disorder . . . . .	93
4.4.1.2	Fixed points with long-range correlated disorder . . . . .	95

4.4.2	Linear stability analysis . . . . .	99
4.4.2.1	Stability of the clean fixed point . . . . .	100
4.4.2.2	Stability of short-range disordered fixed points . . . . .	101
4.4.2.3	Stability of long-range disordered fixed points . . . . .	101
4.4.3	Critical exponents . . . . .	105
4.5	RG flows and bifurcations . . . . .	111
4.5.1	Transcritical and saddle-node bifurcations . . . . .	111
4.5.2	Supercritical Hopf bifurcation and limit-cycle fermionic quantum criticality . . . . .	115
4.5.3	Schematic phase diagrams . . . . .	116
4.6	Conclusion . . . . .	118
<b>5</b>	<b>Conclusion</b>	<b>121</b>
	<b>Bibliography</b>	<b>124</b>
<b>A</b>	<b>Calculations for Chapter 2</b>	<b>148</b>
A.1	Mean-field phase diagram . . . . .	148
A.1.1	Undoped limit, zero temperature . . . . .	151
A.1.2	Undoped limit, finite temperature . . . . .	152
A.1.3	Doped limit, zero temperature . . . . .	155
A.2	Spin susceptibility in the nematic phase . . . . .	157
A.2.1	Undoped Limit . . . . .	158
A.2.2	Doped Limit . . . . .	159
A.3	Inverse propagator for the nematic field . . . . .	160
A.3.1	Static limit . . . . .	163
A.3.2	Dynamical Limit . . . . .	164
A.3.3	Inverse propagator in the nematic phase . . . . .	167
A.4	Electron self-energy . . . . .	168

A.4.1	Quantum Critical Point . . . . .	171
A.4.2	Nematic phase . . . . .	175
A.5	Spin-nematic susceptibility . . . . .	178
<b>B</b>	<b>Calculations for Chapters 3 and 4</b>	<b>182</b>
B.1	Replica trick: general idea . . . . .	182
B.1.1	Replica trick: application . . . . .	183
B.2	Field-theoretic RG . . . . .	184
B.2.1	Calculating traces . . . . .	190
B.3	Calculating Feynman diagrams . . . . .	193
B.3.1	Boson two-point function . . . . .	193
B.3.2	Fermion two-point function . . . . .	195
B.3.3	Boson self-interaction . . . . .	196
B.3.4	Disorder strength . . . . .	199
B.4	Yukawa coupling . . . . .	200
B.5	Long-range correlated disorder contributions . . . . .	201
B.5.1	Boson two-point function . . . . .	202
B.5.2	Boson self-interaction . . . . .	203
B.5.3	Short-range correlated disorder strength . . . . .	203
B.5.4	Long-range correlated disorder strength . . . . .	205
B.6	Absence of fermionic short-range disordered fixed point at $\mathcal{O}(\sqrt{\epsilon_\tau})$ in the chiral Ising GNY model . . . . .	207
B.7	Oscillatory corrections to scaling . . . . .	211
B.8	Log-periodic scaling laws from limit-cycle criticality . . . . .	213
B.9	Relation between two-component and four-component formulations of the chiral XY GNY model . . . . .	215

# List of Tables

3.1	Critical exponents for the boson superfluid-Mott glass transition. . . . .	54
3.2	Critical exponents at the CFP, DFP 1, and DFP 2. . . . .	69

# List of Figures

1.1	a) Honeycomb lattice of graphene. b) Energy-momentum dispersion in graphene. The gap closes at the six corners of the hexagonal first Brillouin zone. . . .	3
1.2	a) Evolution of band edges in $\text{Bi}_{1-x}\text{Sb}_x$ alloy as a function of Sb concentration $x$ , as measured by magnetoreflexion and cyclotron resonance techniques [4]. As $x$ increases, the gap between $L_s$ and $L_a$ bands closes and reopens, which is accompanied by band inversion. For intermediate values of $x$ the insulating state is topologically nontrivial. The figure is taken with permission from Ref. [5]. b) Schematic evolution of the atomic $p$ orbitals of Be and Se atoms into the conduction and valence bands of $\text{Bi}_2\text{Se}_3$ . Stages (I), (II), and (III) denote turning on the chemical bonding, crystal field splitting, and spin-orbit coupling, respectively. The dashed blue line is the Fermi level. The figure is taken with permission from Ref. [6]. . . . .	8
1.3	a) Spin-momentum locking in a 3D TI with a single surface Dirac cone. Red circle – the FS, blue vectors – the expectation value of spin on the FS. b) High-resolution ARPES measurements of the surface band dispersion in $\text{Bi}_2\text{Se}_3$ . The figure is taken with permission from Ref. [7]. . . . .	10

2.1	Examples of classical liquid crystal phases: a) Nematic; b) Smectic A - molecules are normal to the layers; c) Smectic C - molecules are tilted inside the layers. For parts b) and c), the original image is taken from <a href="#">Wikipedia</a> and split into two. For part a), the image is also taken from <a href="#">Wikipedia</a> . Both images used for parts a), b), and c) are created by Kebes and are licensed under <a href="#">CC BY-SA 3.0</a> . . . . .	17
2.2	First-order isotropic-nematic quantum phase transition in the undoped limit ( $\mu = 0$ ). Plots of the mean-field ground state energy density $\mathcal{E}(\Delta)$ in units of $v_F\Lambda^3/3\pi^2$ are given as a function of the dimensionless nematic order parameter $\Delta$ , for $\lambda < \lambda_c$ (blue curve), $\lambda = \lambda_c$ (black curve), and $\lambda > \lambda_c$ (red curve), where $\lambda$ is the dimensionless interaction strength with critical value $\lambda_c \approx 1.31$ at the transition. The leading correction to linear dispersion is given by $\alpha = -0.61$ . . . . .	24
2.3	Finite-temperature isotropic-nematic transition in the undoped limit ( $\mu = 0$ ): (a) Jump in the dimensionless nematic order parameter at the first-order phase transition as a function of temperature; (b) Mean-field phase diagram in the plane of temperature $T$ and dimensionless interaction strength $\lambda$ . A first-order transition (red line) at low temperature turns into a continuous transition (blue line) above a tricritical point (black dot). Dotted lines correspond to limits of metastability of the isotropic ( $T^*$ ) and nematic ( $T^{**}$ ) phases. . . . .	27
2.4	Plot of the dimensionless function $F(x)$ defined in Eq. (2.28). . . . .	30
2.5	Partial breakdown of spin-momentum locking in the nematic phase. Blue dashed line: FS in the isotropic phase ( $\Delta_F = 0$ ); orange dashed line: FS in the nematic phase (here shown for $\Delta_F = 0.18$ ). The red (black) vectors represent the expectation value of spin on the FS in the isotropic (nematic) phase. Except at four special momenta (green dots), spin in the nematic phase is no longer perpendicular to momentum, nor is it tangential to the (distorted) FS. . . . .	33
2.6	One-loop diagrams for (a) the spin-nematic susceptibility [Eq. (2.66)]; (b) the electron self-energy [Eq. (2.71)]. . . . .	39

3.1	Random- $T_c$ disorder is generated from random potential disorder at two-loop order (dotted lines: order parameter fluctuations, solid lines: fermions, box: disorder-induced four-fermion coupling). . . . .	52
3.2	Schematic Feynman rules associated with the replicated action; $a, b$ are replica indices, $i$ is a fermion flavor index, and $q_0, \mathbf{q}$ denotes the frequency-momentum transfer from top to bottom. The extra $\delta(q_0)$ factor prevents frequency/energy transfer between replicas which is a direct consequence of the elastic scattering off the random perturbation. . . . .	58
3.3	One-loop diagrams for the renormalization of (a,b,c) the boson two-point function; (d) the fermion two-point function; (e,f,g) the boson self-interaction $\lambda^2$ ; (h,i) the disorder strength $\Delta$ . At this order there is no renormalization of the Yukawa coupling $h$ . . . . .	60
3.4	Plot of $f(c^2)$ in Eq. (3.44), with $c^2 = (c_f/c_b)^2$ the velocity ratio squared; $f(0) = 0$ , $f(1) = \frac{1}{2}$ , and $f(\infty) = 1$ . . . . .	63
3.5	Critical velocity parameters $c_*^2$ at the first disordered fixed point (DFP 1), the second disordered fixed point (DFP 2), and the clean fixed point (CFP, $c_*^2 = 1$ ), as a function of $N \geq 2$ . . . . .	64
3.6	RG flows for $N = 1$ , with marginal flow (brown line) away from the CFP. . . . .	66
3.7	RG flows for different $N$ . . . . .	68
3.8	Inverse correlation length exponent $\nu^{-1}$ for $\epsilon_\tau = 1$ , as a function of $N \geq 2$ . . . . .	71
3.9	Correction $z - 1$ to the dynamic critical exponent for $\epsilon_\tau = 1$ at the two disordered fixed points, as a function of $N$ . . . . .	71
3.10	Exponents $\omega'$ and $\omega''$ appearing in oscillatory corrections to scaling at DFP 2 for $N \geq 7$ , for $\epsilon_\tau = 1$ . . . . .	72
3.11	Cuts of the separatrix surface at constant $\lambda^2$ for $N = 8$ . . . . .	73

3.12	Schematic phase diagrams in the plane of tuning parameter $r$ and disorder strength $\Delta$ for $N \geq 2$ . SM: Dirac semimetal; DSM: disordered semimetal; SC: superconductor. For sufficiently small initial values of $\lambda^2$ and $h^2$ , the universality class of the transition changes beyond a critical disorder strength from that of the CFP to that of one of the two disordered fixed points: (a) $N = 2$ and $N = 3$ ; (b) $N = 4$ ; (c) $N \geq 5$ . For sufficiently large $\lambda^2$ and/or $h^2$ , beyond a second critical disorder strength there is a reentrant critical regime controlled by the CFP [plotted in (d) for $N \geq 5$ , but an analogous effect occurs for $2 \leq N \leq 4$ ]. . . . .	75
4.1	Schematic momentum-space Feynman rules for the random-mass GNY models, omitting fermion flavor, $O(n)$ , and replica indices. Solid line: fermion propagator, dashed line: boson propagator. Here $p = (p_0, \mathbf{p})$ is the momentum of a propagator line, with $\not{p} = \gamma_\mu p_\mu$ , and $q = (q_0, \mathbf{q})$ is the momentum transfer in a boson four-point vertex. . . . .	88
4.2	Schematic one-loop Feynman diagrams for the random-mass GNY models. Renormalization of (a,b,c,d) the boson two-point function; (e) the fermion two-point function; (f) the Yukawa vertex $h$ ; (g,h,i,j) the boson self-interaction vertex $\lambda^2$ ; (i,k,l,m) the short-range correlated disorder vertex $\Delta$ ; and (j,l,m) the long-range correlated disorder vertex $v$ . . . . .	89
4.3	Stability in the subspace $(\lambda^2, \Delta, v)$ of couplings of (a,b) LDFP1 and (c,d) LDFP2 in the chiral Ising GNY model ( $n = 1$ ), as a function of $N$ and $\delta$ . I: one relevant eigenvalue; II: one relevant eigenvalue, two complex-conjugate irrelevant eigenvalues; III: two relevant eigenvalues. . . . .	102

4.4	Stability in the subspace $(\lambda^2, \Delta, v)$ of couplings of (a,b) LDFP1 and (c,d) LDFP2 in the chiral XY GNY model ( $n = 2$ ), as a function of $N$ and $\delta$ . Regions I-III are defined as in Fig. 4.3. IV: two complex-conjugate relevant eigenvalues; V: no relevant eigenvalues; VI: no relevant eigenvalues, two complex-conjugate irrelevant eigenvalues. . . . .	103
4.5	Stability in the subspace $(\lambda^2, \Delta, v)$ of couplings of (a,b) LDFP1 and (c) LDFP2 in the chiral Heisenberg GNY model ( $n = 3$ ), as a function of $N$ and $\delta$ . Regions are labeled as in Fig. 4.4. . . . .	104
4.6	Dynamical critical exponent $z$ at SDFPs for all three chiral GNY symmetry classes, as a function of $N$ . . . . .	106
4.7	Dynamical critical exponent $z$ in the chiral Ising GNY model ( $n = 1$ ) at (a,b) LDFP1 and (c,d) LDFP2, as a function of $N$ and $\delta$ . . . . .	107
4.8	Dynamical critical exponent $z$ in the chiral XY GNY model ( $n = 2$ ) at (a,b) LDFP1 and (c,d) LDFP2, as a function of $N$ and $\delta$ . . . . .	108
4.9	Dynamical critical exponent $z$ in the chiral Heisenberg GNY model ( $n = 3$ ) at (a,b) LDFP1 and (c) LDFP2, as a function of $N$ and $\delta$ . . . . .	109
4.10	Inverse correlation length exponent $\nu^{-1}$ for the CFP and SDFPs in all three chiral GNY symmetry classes, as a function of $N$ . . . . .	110
4.11	Schematic bifurcation diagrams for (a) the transcritical bifurcation, (b) the saddle-node bifurcation, and (c) the supercritical Hopf bifurcation. The horizontal axis represents a direction in the $N$ - $\delta$ plane, and the vertical axis, the space of running couplings (critical hypersurface). Solid red symbolizes an RG attractor, dashed blue a repeller, and schematic RG trajectories are shown in black. . . . .	112
4.12	Phenomenology of the saddle-node bifurcation at $\delta = \delta_D$ . (a) Curvilinear coordinate $g$ along RG trajectories for $\delta > \delta_D$ ; (b) Wilsonian beta function near the bifurcation; (c) crossover from disordered quasi-critical behavior to clean critical behavior for $\delta$ slightly below $\delta_D$ . . . . .	114

4.13 Schematic RG flow and critical ( $r = 0$ ) phase diagrams for generic $N$ and $\delta_{c,1} < \delta < \delta_{c,2}$ in region IV (see Figs. 4.4-4.5), for (a,b) the chiral Heisenberg GNY model and (c,d) the chiral XY model. In the Heisenberg case, the transition is controlled by a stable limit cycle (LC) for generic bare values of the short-range correlated ( $\Delta$ ) and long-range correlated ( $v$ ) disorder strengths. In the XY case, the transition is controlled by the limit cycle for weak short-range disorder and by a disordered fixed point (SDFP1) for strong short-range disorder. . . . .	117
A.1 Temperature dependence of $a_4$ (a) and $a_6$ (b) in Eq. (A.25). . . . .	154

# Abbreviations

<b>QPT</b>	Quantum phase transition
<b>IQHE</b>	Integer quantum Hall effect
<b>QSH</b>	Quantum spin Hall
<b>3D TI</b>	3D topological insulator
<b>QCP</b>	Quantum critical point
<b>QFT</b>	Quantum field theory
<b>RG</b>	Renormalization group
<b>FP</b>	Fixed point
<b>FL</b>	Fermi liquid
<b>QP</b>	Quasiparticle
<b>FS</b>	Fermi surface
<b>ARPES</b>	Angle-resolved photoemission spectroscopy
<b>GNY</b>	Gross-Neveu-Yukawa
<b>VBS</b>	valence-bond-solid
$\overline{\text{MS}}$	Modified minimal subtraction
<b>MC</b>	Monte Carlo
<b>DFP</b>	Disordered fixed point
<b>CFP</b>	Clean fixed point
<b>SDFP</b>	Short-range disordered fixed point
<b>LDFP</b>	Long-range disordered fixed point
<b>QED<sub>3</sub></b>	(2+1)D quantum electrodynamics

# Chapter 1

## Introduction

Condensed matter physics deals with assemblies of a macroscopically large number (typically on the order of  $10^{23}$ ) of particles distributed on macroscopic length scales (typically on the order of 1 cm). Interactions between these particles may produce phenomena not observable on microscopic scales, such as superfluidity and superconductivity. Such a situation is captured by the notion of emergence, which more broadly encompasses concepts, phenomena, and laws that make sense or manifest only on macroscopic scales. Another facet of the concept of emergence in condensed matter physics is the notion of emergent massless Dirac fermions, which have a relativistic-like linear spectrum as opposed to the ordinary quadratic energy-momentum dispersion of electrons in conventional metals. Unlike superfluidity and superconductivity given as examples above, Dirac fermions do not necessarily rely on the presence of interactions. They already emerge in the electronic band structure of certain materials in the low-energy, long-distance limit. Such is the case for graphene and the boundaries of 3D topological insulators. However, Dirac fermions may also emerge as a result of interactions, e.g., in unconventional superconductors and spin liquids. An important direction in current condensed matter research is to understand the effect of interactions in materials which exhibit such emergent Dirac fermions. In particular, we will be interested in situations where interactions lead to a qualitative change in the 2D Dirac fermion system — quantum phase transitions (QPTs). In general, these are

strongly-correlated problems that are not well described by conventional perturbation expansions about mean-field theories. Another difficult but important research question is to understand the effect on such QPTs of disorder, ubiquitously present in real condensed matter systems and which may drastically affect the physics of the clean systems.

In the rest of this chapter, we first review in more detail how the relativistic Dirac dispersion emerges in nonrelativistic condensed matter systems. We then summarize the basic physics of QPTs. Throughout this thesis, we use natural units ( $\hbar = c = k_B = 1$ ).

## 1.1 Dirac fermions in condensed matter physics

Perhaps the best known example of Dirac fermion system in condensed matter physics is graphene [8] — a single layer of carbon atoms forming a 2D honeycomb lattice, see Fig. 1.1(a). Its triangular Bravais lattice unit cell includes two atoms,  $A$  and  $B$ , and the primitive Bravais lattice vectors may be chosen to be  $\mathbf{a}_1 = a(\frac{3}{2}, \frac{\sqrt{3}}{2})$  and  $\mathbf{a}_2 = a(\frac{3}{2}, -\frac{\sqrt{3}}{2})$ , where  $a$  is the nearest-neighbor distance (see Fig. 1.1(a)), which we may set to 1. The simplest tight-binding model describing fermions hopping on this lattice has the following form in second quantization,

$$\hat{H} = \sum_{\mathbf{k}} \begin{pmatrix} c_{A,\mathbf{k}}^\dagger & c_{B,\mathbf{k}}^\dagger \end{pmatrix} \begin{pmatrix} 0 & -tf(\mathbf{k}) \\ -tf^*(\mathbf{k}) & 0 \end{pmatrix} \begin{pmatrix} c_{A,\mathbf{k}} \\ c_{B,\mathbf{k}} \end{pmatrix}, \quad (1.1)$$

where  $-t$  is a nearest-neighbor hopping matrix element,  $f(\mathbf{k})$  may be written as  $f(\mathbf{k}) = 1 + e^{i\mathbf{k}\cdot\mathbf{a}_1} + e^{i\mathbf{k}\cdot\mathbf{a}_2}$  (there are other physically equivalent expressions related by gauge transformations), and  $c_{A/B,\mathbf{k}}^{(\dagger)}$  is the annihilation (creation) operator for a fermion on sublattice  $A/B$  with crystal momentum  $\mathbf{k}$ . After diagonalizing this Hamiltonian, one finds the energy dispersion  $\epsilon_{\mathbf{k}\pm}$ , plotted in Fig. 1.1(b) in units of  $t$ ,

$$\epsilon_{\mathbf{k}\pm} = \pm t |f(\mathbf{k})| = \pm t \sqrt{3 + 4 \cos\left(\frac{3k_x}{2}\right) \cos\left(\frac{\sqrt{3}k_y}{2}\right) + 2 \cos(\sqrt{3}k_y)}. \quad (1.2)$$

The energy gap  $\epsilon_{\mathbf{k}+} - \epsilon_{\mathbf{k}-}$  vanishes at the six corners of the first Brillouin zone, but

only two of these corners are inequivalent, and we may choose them to be at  $\mathbf{K} = \frac{2\pi}{3}(1, \frac{1}{\sqrt{3}})$  and  $\mathbf{K}' = \frac{2\pi}{3}(1, -\frac{1}{\sqrt{3}})$ .

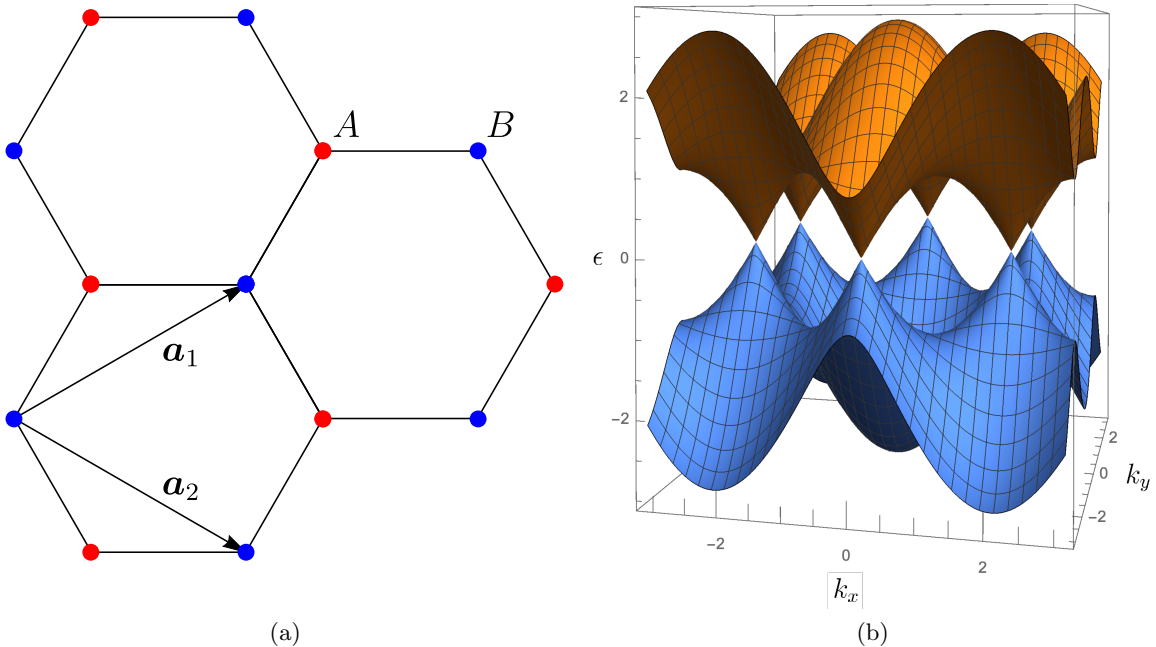


Figure 1.1: a) Honeycomb lattice of graphene. b) Energy-momentum dispersion in graphene. The gap closes at the six corners of the hexagonal first Brillouin zone.

If one is interested in physics at energies much less than the bandwidth, which is about 8.4 eV ( $t \approx 2.8$  eV) in graphene [9], then it is acceptable to Taylor expand the Hamiltonian in momentum in the vicinity of these points and retain only the leading order terms. In this way one obtains a massless Dirac-like expression for the Hamiltonian matrix  $H_{\mathbf{k}}$ :  $H_{\mathbf{k}} = v_F \boldsymbol{\sigma} \cdot \mathbf{k}$ , where  $\mathbf{k}$  is now a deviation in momentum space from the Dirac points  $\mathbf{K}, \mathbf{K}'$ ,  $\boldsymbol{\sigma}$  is a vector of Pauli matrices acting in “pseudospin” (sublattice) space, and  $v_F$  is the Fermi velocity, which is on the order of  $10^6$  m/s in graphene [9].

In fact, this degeneracy of energy levels at  $\mathbf{K}$  and  $\mathbf{K}'$ , which leads to a massless Dirac dispersion in the vicinity of these points, is due to inversion and time-reversal  $\mathcal{T}$  symmetries present in graphene. Focusing on the region of a possible touching of two bands, we may

write down a generic two-band Hamiltonian:

$$H_{\mathbf{k}} = d_0(\mathbf{k})\sigma_0 + \mathbf{d}(\mathbf{k}) \cdot \boldsymbol{\sigma}, \quad (1.3)$$

where  $\sigma_0$  is a  $2 \times 2$  identity matrix. The eigenenergies of this Hamiltonian are given by  $E_{\mathbf{k}\pm} = d_0(\mathbf{k}) \pm \sqrt{\mathbf{d}(\mathbf{k})^2}$ . Thus, the eigenenergy corresponding to momentum  $\mathbf{k}$  is degenerate if  $\mathbf{d}(\mathbf{k}) = 0$ , which, according to the von Neumann-Wigner theorem [10], generically happens only in 3D. Indeed, this condition requires us to satisfy three equations  $d_i(\mathbf{k}) = 0$ ,  $i = x, y, z$ , which in 3D corresponds to a point of intersection of three surfaces given by  $d_i(k_x, k_y, k_z) = 0$ . In the absence of specific constraints, this generically happens at some point in 3D momentum space. In 2D, to satisfy such a condition, one has to find a point of intersection of three curves. In graphene, a combination of inversion and  $\mathcal{T}$  symmetries provides a specific condition for this to happen. In graphene, inversion symmetry requires  $H(\mathbf{k}) = \sigma_x H(-\mathbf{k}) \sigma_x$ , and  $\mathcal{T}$  symmetry (for simplicity, we consider spinless electrons) requires  $H(\mathbf{k}) = H(-\mathbf{k})^*$ , where  $H(\mathbf{k})$  is the two-band tight-binding Hamiltonian appearing in Eq. (1.1). The combination of this gives  $H(\mathbf{k}) = \sigma_x H(\mathbf{k})^* \sigma_x$ . Thus, a generic two-band Hamiltonian must satisfy

$$d_0(\mathbf{k})\sigma_0 + \mathbf{d}(\mathbf{k}) \cdot \boldsymbol{\sigma} = \sigma_x (d_0(\mathbf{k})\sigma_0 + \mathbf{d}(\mathbf{k}) \cdot \boldsymbol{\sigma})^* \sigma_x = d_0(\mathbf{k})\sigma_0 + d_x(\mathbf{k})\sigma_x + d_y(\mathbf{k})\sigma_y - d_z(\mathbf{k})\sigma_z, \quad (1.4)$$

which means that  $d_z(\mathbf{k}) = 0$ . Only two equations must now be satisfied to have a degeneracy,  $d_i(k_x, k_y) = 0$ ,  $i = x, y$ , which will generically happen at specific points. However, in fact, a weak spin-orbit coupling present in graphene creates a tiny gap (on the order of  $10^{-3}$  meV) at the Dirac points [11]. In 3D, where energy degeneracies generically occur at specific momentum points called Weyl nodes, the material is called a Weyl semimetal if the Fermi surface additionally consists exclusively of such nodes (unless terms linear in  $(\mathbf{k} - \mathbf{K})$  vanish in the low-energy Hamiltonian) [12, 13]. At 3D Weyl nodes, the dispersion is also linear, however, the corresponding particles have a definite chirality and are known in high-energy

physics as Weyl fermions (in 3D, a Dirac fermion is a pair of right- and left-handed Weyl fermions).

Another class of condensed matter systems, where massless Dirac fermions dwell, are edges and surfaces of topological materials. With the discovery of the integer quantum Hall effect (IQHE) in 1980 [14], it was realized that the Landau paradigm of classifying states of matter according to the symmetries they break [15, 16] is insufficient. The symmetries of two quantum Hall states might be the same, but the two states are still separated by a sharp phase transition. In the IQHE, the transition is accompanied by a jump in the quantized Hall conductivity  $\sigma_{xy}$ , which is a topological property. Topology deals with properties of systems that remain unchanged under smooth deformations. In mathematics, the number of holes in surfaces remains unchanged under smooth deformations of their shapes. This number is called the genus,  $g$ . The insensitivity of the genus to smooth changes in the geometry of a surface is captured by the Gauss-Bonnet theorem, which states that the integral of the Gaussian curvature,  $K$ , over a closed surface  $S$  is a topological invariant:

$$\frac{1}{2\pi} \int_S K dS = \chi, \quad (1.5)$$

where  $\chi = 2 - 2g$  is called the Euler characteristic. In physics, topology concerns itself with quantized macroscopic properties that are unchanged under smooth deformations of the Hamiltonian.

Many topological properties are captured in noninteracting Hamiltonians. In 1D, an example of topologically nontrivial phase is the Su-Schrieffer-Heeger model of polyacetylene [17]; in 2D, one may name the IQHE, the Chern insulator [18], and the quantum spin Hall (QSH) effect [11]. An important quantity to understand how topology can arise in condensed matter systems is the Berry phase [19] — a quantum mechanical phase accumulated as a system's Hamiltonian undergoes slow changes via variation of an external parameter. Let us denote by  $H(\mathbf{R})$  a Hamiltonian with nondegenerate levels, where  $\mathbf{R} = \mathbf{R}(t)$  is a vector of external parameters slowly changing with time  $t$  such that it traces a closed path

$C$  after time  $T$ , and let us also denote by  $|\psi(\mathbf{R})\rangle$  an energy eigenstate. Then, after time  $T$ , one finds that the state evolves into  $|\psi(\mathbf{R}(T))\rangle = e^{i\gamma_C} |\psi(\mathbf{R}(0))\rangle$ , where the Berry phase  $\gamma_C = \oint_C \mathbf{a}(\mathbf{R}) \cdot d\mathbf{R}$ . Here  $\mathbf{a}(\mathbf{R}) = i \langle \psi(\mathbf{R}) | \nabla_{\mathbf{R}} | \psi(\mathbf{R}) \rangle$  is called the Berry connection. One may also use Stokes' theorem and express the Berry phase through the Berry curvature,  $\gamma_C = \int_S \mathbf{B}(\mathbf{R}) \cdot d\mathbf{S}$ , where  $\mathbf{B}(\mathbf{R}) = \nabla_{\mathbf{R}} \times \mathbf{a}(\mathbf{R})$ , and  $S$  is an arbitrary surface bounded by  $C$ . In crystalline matter with a finite energy gap, the role of the parameter  $\mathbf{R}$  is played by the momentum  $\mathbf{k}$  in the first Brillouin zone. For the IQHE, the integral of the Berry curvature over the first Brillouin zone,  $C_1 = \frac{1}{2\pi} \int_{1BZ} \mathbf{B}(\mathbf{R}) \cdot d\mathbf{S}$ , called the first Chern number, is an integer topological invariant conceptually similar to the Euler characteristic of Eq. (1.5), but in momentum space rather than real space. It determines the off-diagonal component of the conductivity tensor  $\sigma_{xy} = \frac{e^2}{h} \nu$ , where  $\nu$  is the sum of Chern numbers of the occupied bands. It is essential for the quantum Hall effect that the  $\mathcal{T}$  symmetry is broken in the presence of magnetic field: the first Chern number for a  $\mathcal{T}$ -invariant system is zero. Haldane [18] showed that a topologically nontrivial state analogous to the IQHE, the Chern insulator, may exist in the absence of net magnetic flux. As implied by its name, the Chern insulator is characterized by a nonzero Chern number. It was later realized by Kane and Mele [11] that nontrivial topological states may also exist in  $\mathcal{T}$ -invariant systems in the presence of spin-orbit coupling, which leads to the phenomenon of band inversion, whereby conduction and valence bands cross and exchange roles. In 2D, this is the QSH state (2D topological insulator), which may be considered as two copies of Chern insulators with opposite spins and Chern numbers. As was mentioned above, due to  $\mathcal{T}$ -invariance the net Chern number of the QSH state is zero, and its topological state is characterized by a  $\mathbb{Z}_2$  invariant, which may only take two values corresponding to trivial and nontrivial topological states [20, 21]. What is common among these topological states is that there are edge modes on the boundary, and the topological invariant determines the number (or the number modulo 2, for a  $\mathbb{Z}_2$  invariant) of such edge modes. A heuristic argument for their existence is as follows. Topological properties remain unchanged unless a non-smooth change in the band structure happens, namely gap closure and reopening. Let us consider

a topological insulator in contact with a trivial insulator. Then, somewhere across the interface, the gap should close, leading to a gapless edge mode. In the vicinity of the Fermi level, which lies in the bulk gap for an insulator, these edge states are also characterized by a 1D massless Dirac (for QSH insulators) or Weyl (for the IQHE and Chern insulators) dispersion.

So far, we have briefly discussed 2D topological states, which can have 1D massless Dirac modes on their boundary. However, in this thesis we focus on 2D Dirac fermions. In fact, there are also 3D versions of  $\mathcal{T}$ -invariant topological insulators hosting 2D massless Dirac fermions on their surfaces [22]. As in the 2D QSH topological insulator, a topologically nontrivial state in 3D  $\mathcal{T}$ -invariant band insulators occurs due to the presence of strong spin-orbit coupling leading to band inversion. 3D topological insulators (3D TIs) are also characterized by a  $\mathbb{Z}_2$  invariant, which in the noninteracting case may be represented using an integral over the Brillouin zone. In 3D, the integrand is not the Berry curvature, but the Chern-Simons form of the Berry connection [23]. There are two classes of 3D TIs: weak and strong. Weak 3D TIs may be considered as a stack of 2D QSH states; they exhibit surface states only on surfaces made by the edges of 2D QSH systems. In contrast, strong 3D TIs can not be reduced to 2D QSH states. As suggested by their name, strong 3D TIs are more robust than their weak counterparts, in which surface states might be gapped without breaking  $\mathcal{T}$  symmetry. Henceforth, we will concentrate on strong 3D TIs and omit the word “strong” while referring to them. The first 3D TI was theoretically predicted in the bismuth antimony alloy  $\text{Bi}_{1-x}\text{Sb}_x$  [24], and shortly thereafter experimentally confirmed [25]. This material is not easily described by a simple model Hamiltonian due to its alloy structure, but the observed behavior of its electronic structure conveniently illustrates the effect of spin-orbit coupling, see Fig. 1.2(a). As the Sb concentration increases, the effective spin-orbit coupling strength increases as well, and, as a consequence, the gap between  $L_s$  and  $L_a$  bands closes and reopens, which is accompanied by band inversion. A class of materials with a simpler theoretical description and exhibiting a nontrivial topological state are the stoichiometric crystals  $\text{Bi}_2\text{Se}_3$ ,  $\text{Bi}_2\text{Te}_3$ ,  $\text{Sb}_2\text{Te}_3$  [6, 7] with a single Dirac cone in their surface

electronic structure. From the definition of the  $\mathbb{Z}_2$  invariant it may be deduced that a 3D TI can support only an odd number of surface Dirac fermions [22]. For example, the aforementioned alloy  $\text{Bi}_{1-x}\text{Sb}_x$  supports  $N = 5$  Dirac cones.

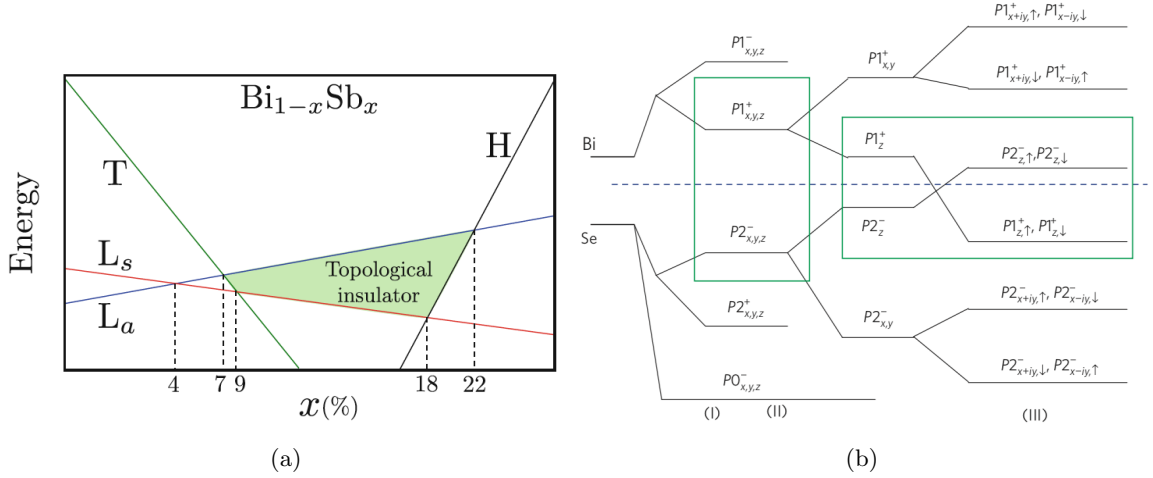


Figure 1.2: a) Evolution of band edges in  $\text{Bi}_{1-x}\text{Sb}_x$  alloy as a function of Sb concentration  $x$ , as measured by magnetoreflexion and cyclotron resonance techniques [4]. As  $x$  increases, the gap between  $L_s$  and  $L_a$  bands closes and reopens, which is accompanied by band inversion. For intermediate values of  $x$  the insulating state is topologically nontrivial. The figure is taken with permission from Ref. [5]. b) Schematic evolution of the atomic  $p$  orbitals of Bi and Se atoms into the conduction and valence bands of  $\text{Bi}_2\text{Se}_3$ . Stages (I), (II), and (III) denote turning on the chemical bonding, crystal field splitting, and spin-orbit coupling, respectively. The dashed blue line is the Fermi level. The figure is taken with permission from Ref. [6].

The minimal model describing a 3D TI should contain four bands, since due to  $\mathcal{T}$  invariance, Kramers' theorem guarantees that both the conduction and valence bands must be doubly degenerate at  $\mathcal{T}$ -invariant points. For a  $\mathcal{T}$  and inversion invariant insulator such as  $\text{Bi}_2\text{Se}_3$ , at the  $\Gamma$  point the minimal four-band Hamiltonian up to  $O(k^2)$  has the form [6, 26]

$$H(\mathbf{k}) = \epsilon_0(\mathbf{k})\mathbf{I}_{4 \times 4} + \begin{pmatrix} \mathcal{M}(\mathbf{k}) & A_1 k_z & 0 & A_2 k_- \\ A_1 k_z & -\mathcal{M}(\mathbf{k}) & A_2 k_- & 0 \\ 0 & A_2 k_+ & \mathcal{M}(\mathbf{k}) & -A_1 k_z \\ A_2 k_+ & 0 & -A_1 k_z & -\mathcal{M}(\mathbf{k}) \end{pmatrix} + o(k^2), \quad (1.6)$$

where  $k_{\pm} = k_x \pm ik_y$ ,  $\epsilon_0(\mathbf{k}) = C + D_1k_z^2 + D_2k_{\perp}^2$ ,  $\mathcal{M}(\mathbf{k}) = M - B_1k_z^2 - B_2k_{\perp}^2$ , and  $k_{\perp}^2 = k_x^2 + k_y^2$ . This is essentially a 3D Dirac equation with unidirectionally anisotropic velocity  $\mathbf{v} = (A_2, A_2, A_1)$  and anisotropic  $\mathbf{k}$ -dependent mass  $\mathcal{M}(\mathbf{k})$ .

The band inversion for Bi<sub>2</sub>Se<sub>3</sub> is schematically illustrated in Fig. 1.2(b). If one would imagine gradually increasing the strength of spin-orbit coupling, one would observe closure and reopening of the bulk gap accompanied by the band inversion process. In the effective Hamiltonian (1.6), this corresponds to the parameter  $M$  crossing through zero and changing sign.

From the bulk Hamiltonian (1.6) one may find an effective surface Hamiltonian by projection to the surface and truncation of the spectrum to exclude gapped bulk states. In the presence of a surface perpendicular to the  $z$  axis, only  $k_x$  and  $k_y$  are good quantum numbers. One may then find analytically surface states  $|\Psi_1\rangle, |\Psi_2\rangle$  for open boundary conditions at  $k_x = k_y = 0$ ; such states are degenerate by Kramers' theorem. Then one may project  $H(k_x, k_y, -i\frac{\partial}{\partial z})$  onto the subspace spanned by  $|\Psi_1\rangle, |\Psi_2\rangle$ . This approximation is adequate as long as the bulk gap is large. In this way, one finds the effective surface Hamiltonian [26]:

$$H_{\text{surface}} = C + \frac{D_1M}{B_1} + \left(D_2 - B_2\frac{D_1}{B_1}\right)k^2 + A_2\sqrt{1 - \left(\frac{D_1}{B_1}\right)^2}(\sigma_x k_y - \sigma_y k_x), \quad (1.7)$$

which to first order in momentum (or in the isotropic case  $D_1 = D_2$ ,  $B_1 = B_2$ ) and neglecting the constant offset is

$$H_{\text{eff}} = v_{\text{F}}(\mathbf{p} \times \boldsymbol{\sigma})_z, \quad (1.8)$$

the massless 2D Dirac Hamiltonian, which can be used for studying the properties of surface states. This is unitarily equivalent to the massless Dirac Hamiltonian in graphene, but here the Pauli matrices correspond to the physical electron spin (as opposed to the pseudospin/sublattice degree of freedom in graphene).

A peculiar feature of this Hamiltonian is spin-momentum locking: spin is always

perpendicular to the momentum, see Fig. 1.3 (a); thus, the surface states are helical with dispersion linear in momentum near the Dirac point,  $E_{p\pm} = \pm v_F p$ , which is confirmed via ARPES measurements, e.g. in  $\text{Bi}_2\text{Se}_3$  [7] (see Fig. 1.3(b)). The corresponding eigenstates are  $|\Psi_{\pm}\rangle = \frac{1}{\sqrt{2}} \begin{pmatrix} \pm e^{-i\phi_{\mathbf{p}}} \\ i \end{pmatrix}$ , where “ $\pm$ ” denotes upper/lower helicity branches, and  $\phi_{\mathbf{p}} = \arctan(p_y/p_x)$  is the direction of in-plane (surface) momentum.

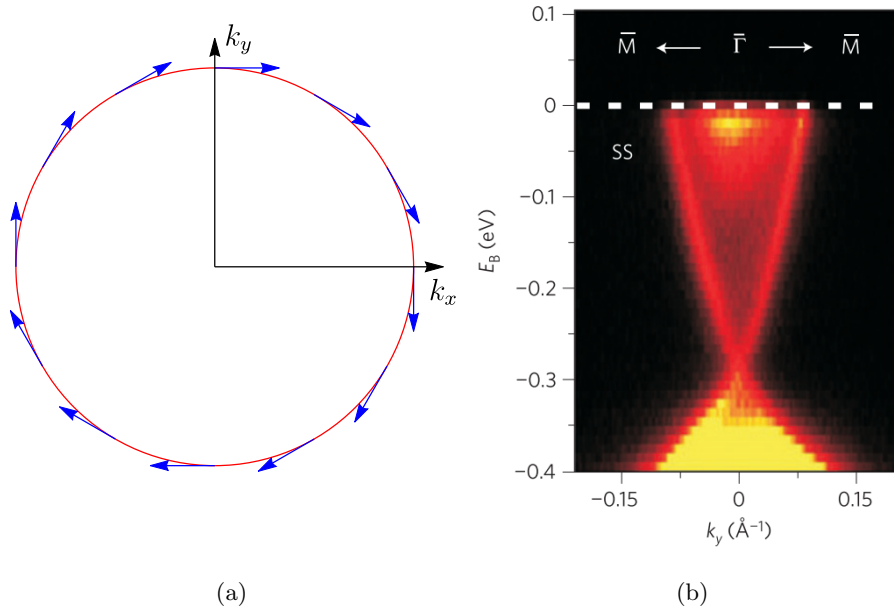


Figure 1.3: a) Spin-momentum locking in a 3D TI with a single surface Dirac cone. Red circle – the FS, blue vectors – the expectation value of spin on the FS. b) High-resolution ARPES measurements of the surface band dispersion in  $\text{Bi}_2\text{Se}_3$ . The figure is taken with permission from Ref. [7].

In this thesis, we will be working primarily with the systems described above, known collectively as 2D Dirac semimetals, where Dirac fermions emerge already in the absence of electron-electron interactions. However, we note that Dirac fermions also arise as low-energy excitations as a consequence of interactions in other condensed matter systems. These include algebraic spin liquids, which may be described as a system of electrically neutral Dirac spin- $\frac{1}{2}$  fermions coupled to a fluctuating  $U(1)$  gauge field [27], and unconventional  $d$ -

wave superconductors, in which Bogoliubov quasiparticles exhibit a Dirac spectrum [28,29].

## 1.2 Quantum phase transitions

Inevitably, interactions are present in all systems, including the 2D Dirac semimetals discussed thus far at the single-particle level. Here we will be focusing on the spontaneous symmetry-breaking QPTs, which may be induced by these interactions. Unlike ordinary thermal phase transitions, QPTs happen at zero temperature and the associated critical phenomena, in the case of continuous QPTs, are driven by quantum fluctuations [30]. In a QPT, the role of temperature is played by an interaction strength  $g$  in the interacting Hamiltonian  $H = H_0 + gV$ , where  $H_0$  is the Hamiltonian of the noninteracting system (here the unperturbed Dirac semimetal) and  $V$  is an interaction term. Essentially, quantum phases are equivalence classes of many-body ground states. In the thermodynamic limit, as  $g$  varies, an excited state and the ground state may cross in the coupling-energy plane. If the transition is continuous, the point  $g_c$  at which this happens is called a quantum critical point (QCP) and is also a point of nonanalyticity in the partition function  $Z$ . For the symmetry-breaking QPTs we will be studying, the disordered phase at  $g < g_c$  is adiabatically connected to a noninteracting Dirac semimetal and respects all its symmetries, while the ordered phase at  $g > g_c$  develops a nonzero order parameter, bilinear in fermion operators, that breaks one or more of those symmetries. If the ordered phase is gapped, the energy gap  $\Delta$  behaves near the QCP as  $\Delta \sim (g - g_c)^{\nu z}$ . Here  $\nu$  and  $z$  are the correlation length and dynamic critical exponents, respectively. The correlation length is a characteristic length beyond which the two-point correlation function for the fluctuations of the order parameter effectively decays to zero. It usually diverges at the QCP as a power law,  $\xi \sim |g - g_c|^{-\nu}$ . In many cases, a QPT in  $d$  spatial dimensions might be considered as a classical phase transition in  $d + 1$  dimensions, via the so-called quantum-to-classical mapping [30]. Indeed, at a QCP, fluctuations are long-ranged in both spatial and temporal (imaginary time) directions, and the latter acts as an additional “spatial” dimension. In

turn, temporal and spatial coordinates may enter into the action in a different way, thus the spatial  $\xi$  and temporal  $\xi_\tau \sim 1/\Delta$  correlation lengths may also have different scaling exponents. This anisotropy is reflected by the dynamic critical exponent  $\xi_\tau \sim \xi^z$ . Other thermodynamic quantities of interest, such as the order parameter and its susceptibility, also exhibit power-law behavior with corresponding exponents. Other quantities, in principle measurable, are the order parameter spectral function  $\chi(\mathbf{p}, \omega)$  and the Dirac fermion spectral function  $A(\mathbf{k}, \omega)$ :

$$\chi(\mathbf{p}, \omega) \sim \frac{\Theta(\omega^2 - \mathbf{p}^2) \operatorname{sgn} \omega}{|\omega^2 - \mathbf{p}^2|^{1-\eta_\phi/2}}, \quad (1.9)$$

$$A(\mathbf{p}, \omega) \sim \frac{(\omega - \alpha \cdot \mathbf{p}) \Theta(\omega^2 - \mathbf{p}^2) \operatorname{sgn} \omega}{(\omega^2 - \mathbf{p}^2)^{1-\eta_\psi/2}}, \quad (1.10)$$

where  $\eta_\phi$  and  $\eta_\psi$  are the boson (order parameter) and fermion anomalous dimensions,  $\alpha_i = i\gamma_0\gamma_i$ ,  $i = 1, 2$ , and  $\Theta(x)$  is the Heaviside step function. Equations (1.9) and (1.10) are written for  $z = 1$ , which applies when the emergent Lorentz invariance of the free Dirac semimetal persists at the QCP. For  $z \neq 1$ , one should replace  $\omega \rightarrow |\omega|^{1/z} \operatorname{sgn} \omega$ . At a fermionic QCP,  $\eta_\psi$  is typically greater than zero. As such, instead of quasiparticle poles, the fermion Green's function has branch points, and at the QCP the fermionic liquid is a non-Fermi liquid. Even though there might be many critical exponents, only a few of them are independent. For example, for a classical ferromagnetic transition there are six critical exponents, but only two should be measured to find the others. As a matter of fact, (very) different physical systems may display the same set of critical exponents forming a universality class. In general, the set of critical exponents depends on the dimensionality, symmetries, and the range of interactions of physical systems. Additionally, as discussed below, the presence of itinerant fermions can give rise to new universality classes even with the same dimensionality and symmetries.

The critical behavior of condensed matter systems is dominated by long-range fluctuations. Thus, to study this critical behavior, we may coarse-grain the system and study the continuous quantum field theory (QFT) models that result from such coarse-graining.

For the interaction-driven QPTs we are interested in, these are interacting QFTs. However, regular perturbation theory in the interaction strength is not suitable for studying critical phenomena. To see this, let us consider the action of a classical  $\phi^4$  theory in  $d$  dimensions, where  $\phi$  is the coarse-grained order parameter:  $S = \int d^d x [(\partial\phi)^2 + r\phi^2 + \lambda^2\phi^4]$ . Since the action is dimensionless (we use  $\hbar = 1$ ), the dimension of the interaction strength  $\lambda^2$  is  $[\lambda^2] = [L]^{d-4}$ , where  $[L]$  is a unit of length. The only scale in the continuous model we have is the correlation length  $\xi$ . This allows us to switch to dimensionless quantities via scaling. In particular, setting  $x' = x/\xi$ , we obtain  $\int d^d x' [(\partial'\phi')^2 + r'\phi'^2 + \lambda'^2\phi'^4]$ , where  $\phi' = \xi^{(d-2)/2}\phi$  and  $\lambda'^2 = \xi^{4-d}\lambda^2$ . We see that in physical  $d = 3$  dimensions, applicable to QPTs in two spatial dimensions via the quantum-to-classical mapping, the dimensionless interaction strength is  $\lambda'^2 = \xi\lambda^2$ . Recalling that  $\xi$  diverges as the system approaches the critical point, we see that the dimensionless coupling  $\lambda'^2$  diverges as well, which makes ordinary perturbation theory inapplicable.

The proper method to study critical phenomena was introduced by K. Wilson [31], based on the renormalization group (RG). The Wilsonian renormalization group method is based on the idea of scale invariance at the critical point. Consider an action  $S[\phi] = S_0[\phi] + \int d^d x \sum g_i O_i[\phi]$ , where the second term is a general interaction term with couplings  $g_i$ . In condensed matter, there is a natural cutoff lengthscale  $\Lambda^{-1}$  on the order of the lattice constant  $a$ . Then, assuming translational invariance, the integration in momentum space is restricted to values of  $|\mathbf{k}| < \Lambda$ . In Wilson's momentum-shell scheme, one represents the order parameter field  $\phi$  as a sum of slow and fast modes (i.e. Fourier modes with small and large momentum) and integrates out fast modes for  $\frac{\Lambda}{b} < |\mathbf{k}| < \Lambda$ , where  $b$  is slightly larger than one. Then, after rescaling the new cutoff  $\frac{\Lambda}{b}$  to the previous one  $\Lambda$ , the action acquires the same form (up to irrelevant new operators) with new, renormalized couplings  $g'_i$ . Iterating the same steps and defining  $b = e^\ell$ , where  $\ell$  is called the RG parameter or RG time, one obtains the Gell-Mann-Low equations  $\frac{dg}{d\ell} = \beta(\mathbf{g})$ , which define the flow of running couplings  $g_i(\ell)$  in coupling space. Due to scale invariance, QCPs correspond to fixed points of the Gell-Mann-Low equations, i.e. they are determined by  $\beta(\mathbf{g}) = 0$ . Couplings

which flow to zero in the limit of infinite RG time are irrelevant to the physics of critical phenomena. This circumstance explains universality phenomena, as in typical condensed matter systems only finitely many couplings are relevant. At this point, it is still not clear how to practically perform the averaging over fast modes in an interacting QFT as there is still no small parameter one can use for an expansion. One way to introduce it is to consider a system close to its upper critical dimension  $D_c$ , which is 4 in the  $\phi^4$  theory discussed above. For  $D > D_c$  all the couplings are irrelevant and the long-range physics is described by the noninteracting action, which has a single Gaussian fixed point (FP)  $\mathbf{g} = 0$ . Analytically continuing to real  $D$ , one expects that for  $D = D_c - \epsilon$  just below  $D_c$  new fixed points will appear close to the Gaussian FP at couplings  $g_i$   $\epsilon$ -small in amplitude. Thus, one may implement a perturbative expansion using  $\epsilon$  as a small parameter [32].

In the preceding brief discussion of the RG, we did not explicitly talk about itinerant fermion systems, our prime concern. The important difference from bosonic systems is that fermionic systems have Fermi surfaces. For the Fermi surfaces, as in conventional metals, an early approach to quantum criticality by Hertz [33] and Millis [34] was to integrate out fermionic modes completely to obtain a pure bosonic theory. However, by doing this we lose the information about the Fermi surface. This is just a handwaving argument to stress the importance of keeping low-lying fermionic excitations. More precisely, it can be shown that Hertz-Millis theory is applicable in  $d \geq 3$  dimensions, but fails otherwise [30]. Several approaches to address the  $d = 2$  problem were developed, such as the patch RG approach by Metlitski and Sachdev [35]. For the point-like Fermi surfaces we will deal with in this thesis, the situation is technically simpler. However, it is still important to keep gapless fermionic modes at all steps in the RG procedure. In particular, even for point-like Fermi surfaces a complete integration of fermionic modes à la Hertz-Millis gives rise to problematic infrared divergences in the remaining bosonic action [36]. In Chaps. 3 and 4 we will apply RG techniques to coupled boson-fermion field theories of the chiral Gross-Neveu-Yukawa type.

Initially, the RG originated in high-energy physics as a calculational tool with no

obvious relation to the Wilsonian approach, which provided the former with a transparent physical interpretation (in high-energy physics one has to assume the existence of a fundamental cutoff  $\Lambda$ ). Though physically obscure from a condensed matter standpoint, methods developed in high-energy physics are of great practical use, and in this thesis we are going to exploit the modified minimal subtraction ( $\overline{\text{MS}}$ ) RG scheme [37] instead of the Wilsonian momentum-shell approach. At the order at which we perform our calculations, the Gell-Mann-Low equations, and the physical conclusions drawn thereof, are independent of the chosen RG scheme.

Another aspect this thesis investigates is the effect of quenched disorder, unavoidable in real condensed matter systems, on QPTs. We postpone a discussion of disorder until Chap. 3, where we will discuss some results of the short-range correlated disorder on the superconducting quantum phase transition in 2D Dirac electron semimetals.

### 1.3 Structure of the thesis

The thesis is organized as follows. In Chap. 2, we build a field-theoretic description of the nematic phase transition on the surface of a 3D TI, details of calculations for which are placed in Appendix A. Chaps. 3 and 4 are devoted to studies of the effects of quenched disorder on different QPTs in 2D Dirac semimetals described in the clean limit by the family of chiral Gross-Neveu-Yukawa models. In particular, Chap. 3 considers how weak short-range correlated disorder affects the superconducting phase transition. This study is extended to other QPTs in Chap. 4, which also considers long-range correlated disorder.

## Chapter 2

# Nematic phase transition on the surface of a 3D topological insulator

Nature allows for the electronic liquid to exist in many phases, including electronic liquid crystals [38]. These are phases whose set of symmetries lies somewhere between the symmetries of liquids and crystals. Since at this point we talk about symmetries only, we may introduce the subject using classical counterparts – classical liquid crystals [39]. Liquids are characterized by the absence of any kind of long-range order whatsoever, thus having (on average) the highest degree of symmetry. In contrast, crystals have long-range positional and rotational orders, having only a set of discrete translational and point group symmetries forming a space group. The nematic phase is an example of phase with an intermediate degree of symmetry: it breaks rotational symmetry to  $C_2$ , the group of two-fold rotations, but has full translational symmetry. The hexatic phase [40] breaks rotational symmetry to  $C_6$ , the group of six-fold rotations. In smectic (or stripe) phases, in addition to the breaking of rotational symmetry the translational symmetry is also broken, leading to a positional order in one direction. For classical liquids, these phases originate from the elongated rod-

like shape of the constituting molecules (see Fig. 2.1). While we cannot think of electrons as elongated objects, electronic liquid crystalline phases indeed are observed in experiments. Observations of spontaneous anisotropy in transport in the GaAs/GaAlAs heterostructures in high magnetic fields [41, 42] and the strongly correlated material  $\text{Sr}_3\text{Ru}_2\text{O}_7$  [43] strongly suggest the existence of the nematic phase in these materials. There is also evidence for nematic phases in cuprate- [44, 45] and iron-based [46–48] superconductors.

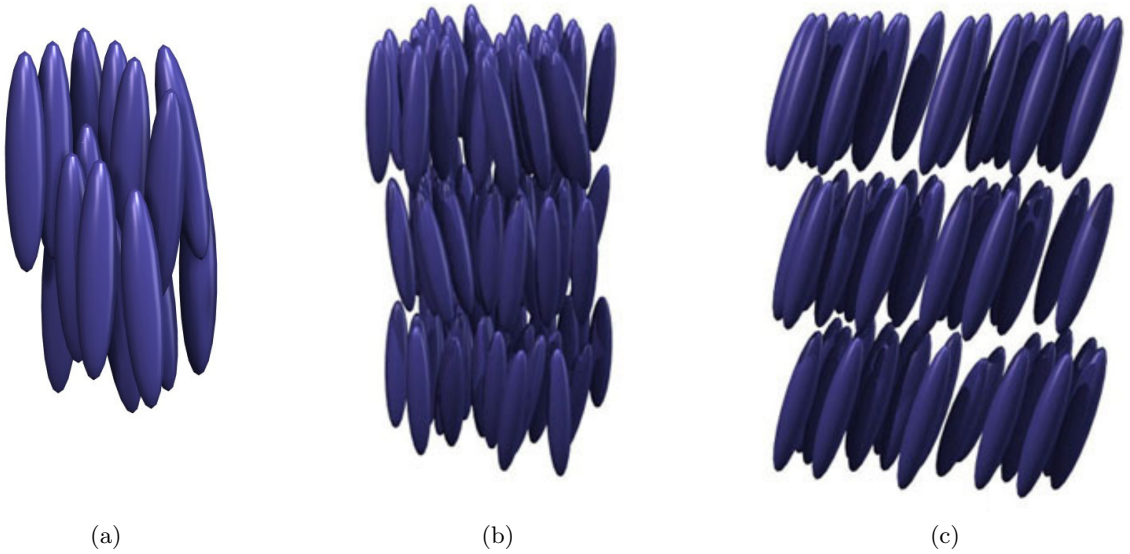


Figure 2.1: Examples of classical liquid crystal phases: a) Nematic; b) Smectic A - molecules are normal to the layers; c) Smectic C - molecules are tilted inside the layers. For parts b) and c), the original image is taken from [Wikipedia](#) and split into two. For part a), the image is also taken from [Wikipedia](#). Both images used for parts a), b), and c) are created by Kebes and are licensed under [CC BY-SA 3.0](#).

One way for the formation of the nematic state is the quantum melting of stripe electronic phases [49]. In this strong-coupling perspective, the nematic phase is formed via the proliferation of dislocations in the stripe phase. An alternative weak-coupling perspective considers the emergence of the nematic phase out of the isotropic Fermi liquid (FL) via the Pomeranchuk instability [50]. In the Landau theory of the Fermi liquid [51], interacting fermionic systems are described as a collection of quasiparticles (QPs) over the sharply defined Fermi surface (FS) with the momentum distribution function  $n_{\mathbf{p}}$ . For a conven-

tional spin-degenerate FL in three dimensions, interactions between these quasiparticles are parametrized by two Landau parameters, and the energy functional may be written in the following form:

$$\delta E[\delta n(\mathbf{p})] = \sum_{\sigma} \int \varepsilon(p) \delta n_{\sigma}(\mathbf{p}) \frac{d^3 p}{(2\pi)^3} + \frac{1}{2} \sum_{\sigma} \sum_{\sigma'} \int f_{\sigma\sigma'}(\mathbf{p}, \mathbf{p}') \delta n_{\sigma}(\mathbf{p}) \delta n_{\sigma'}(\mathbf{p}') \frac{d^3 p d^3 p'}{(2\pi)^6}, \quad (2.1)$$

where  $f_{\sigma\sigma'}(\mathbf{p}, \mathbf{p}') = f^S(\mathbf{p}, \mathbf{p}') + \sigma\sigma' f^A(\mathbf{p}, \mathbf{p}')$  characterizes an effective interaction between QPs,  $\sigma, \sigma' = \pm 1$  are spin indices, and  $\delta n_{\sigma}(\mathbf{p}) = n_{\sigma}(\mathbf{p}) - n_{\sigma}^{(0)}(\mathbf{p})$  is the deviation of the momentum distribution function from its form in the ground state. At low energies, the most important contribution to the integral in Eq. (2.1) comes from momenta close to  $\mathbf{p}_F$ , and we may approximate  $f(\mathbf{p}, \mathbf{p}')$  with its values on the FS  $p = p_F$ , where it becomes a function of an angle  $\theta$  between the vectors  $\mathbf{p}, \mathbf{p}'$ . Pomeranchuk argued that the isotropic FS will be stable against distortions  $\delta n(\mathbf{p})$  if the change in energy  $\delta E[\delta n(\mathbf{p})] > 0$ . He showed that this is satisfied if  $1 + \frac{F_l^{S,A}}{2l+1} \geq 0$ , where  $F_l^{S,A}$  are proportional to the coefficients of the expansion in angular harmonics of  $f^{S,A}(\theta)$  — the Landau parameters for each angular momentum channel. Violation of this condition in the  $l = 2$  channel leads to a spontaneous quadrupolar distortion of the FS. In 2D, the FS acquires an elliptical shape.

In contrast, the FL theory for the helical surface states in a 3D TI with a single Dirac cone needs ten Landau parameters: one in the charge-charge interaction channel, four in the spin-charge channel, and five in the spin-spin channel [52]. This is because of the strong spin-orbit coupling present in the system, which reduces the amount of symmetries compared to the conventional FL. Unless the FS is exactly at the Dirac point, and at sufficiently low temperatures, one may project this theory onto the FS, leaving only a branch of one helicity (see Fig. 1.3). Due to spin-momentum locking, this resulting projected theory looks effectively spinless:

$$\delta \bar{E}[\delta \bar{n}_{\mathbf{p}}] = \int \frac{d^2 p}{(2\pi)^2} \epsilon_{\mathbf{p}}^0 \delta \bar{n}_{\mathbf{p}} + \frac{1}{2} \sum_{l=0}^{\infty} \int \frac{d^2 p}{(2\pi)^2} \frac{d^2 p'}{(2\pi)^2} \bar{f}_l \cos l\theta_{\mathbf{p}\mathbf{p}'} \delta \bar{n}_{\mathbf{p}} \delta \bar{n}_{\mathbf{p}'}, \quad (2.2)$$

where  $\bar{n}_{\mathbf{p}} = \langle \psi_{\mathbf{p}+}^\dagger \psi_{\mathbf{p}+} \rangle$  is the momentum distribution for a single helicity branch and  $\bar{f}_l = f_l^{\text{cc}} - f_l^{\text{sc},3} - \frac{1}{4}f_l^{\text{ss},5} + \frac{1}{8} \left( f_{l-1}^{\text{ss},1} - f_{l-1}^{\text{ss},3} + f_{l+1}^{\text{ss},1} + f_{l+1}^{\text{ss},3} \right)$  — the Landau parameter per angular momentum channel of the projected theory. The terms  $f_l$  with superscripts stand for the Landau parameters per momentum channel of the unprojected theory, where cc, sc, and ss refer to the charge-charge, spin-charge, and spin-spin channels, respectively. The last formula means that the interaction in the  $l$ -th angular momentum channel of the unprojected theory may produce interactions in the  $(l \pm 1)$ -th channel, a direct consequence of spin-momentum locking on the FS. It is not hard to notice that Pomeranchuk’s ideas apply for this case as well.

In the following sections, to provide a more microscopic basis for these phenomenological ideas, we build the field-theoretic description of the nematic phase transition on the surface of a 3D TI with a single, rotationally invariant Dirac cone. We give details of calculations in Appendix A.

## 2.1 Model and Nematic Order Parameter

In this section, we introduce our field-theoretic model for the isotropic-nematic transition on the surface of a 3D topological insulator. We follow largely the approach of Ref. [53], with important caveats due to the presence of strong spin-orbit coupling, as will be seen below. While nematic order in 2D electron gases with Rashba spin-orbit coupling has been studied before [54, 55], such systems have two degenerate concentric FSs and are thus qualitatively distinct from the single, nondegenerate helical FS considered here.

The Hamiltonian that describes the noninteracting gapless surface state of a topological insulator with a single Dirac cone is given by [56, 57] (in units where  $\hbar = k_B = 1$ )

$$H_0 = \int \frac{d^2k}{(2\pi)^2} \psi_{\mathbf{k}}^\dagger (h(\mathbf{k}) - \mu) \psi_{\mathbf{k}}, \quad (2.3)$$

where  $\psi_{\mathbf{k}} = (\psi_{\mathbf{k}\uparrow}, \psi_{\mathbf{k}\downarrow})$  is a two-component Dirac spinor,  $v_F$  is the Fermi velocity,  $\mu$  is the

chemical potential, and

$$h(\mathbf{k}) = v_F \hat{\mathbf{z}} \cdot (\boldsymbol{\sigma} \times \mathbf{k}) = v_F \begin{pmatrix} 0 & ike^{-i\theta_{\mathbf{k}}} \\ -ike^{i\theta_{\mathbf{k}}} & 0 \end{pmatrix}, \quad (2.4)$$

where  $\boldsymbol{\sigma}$  is a vector of Pauli matrices,  $\theta_{\mathbf{k}} = \tan^{-1}(k_y/k_x)$  and  $k = \sqrt{k_x^2 + k_y^2}$ . The Hamiltonian (2.3) has a continuous spatial  $SO(2)$  rotation symmetry,  $[J_z, h(\mathbf{k}) - \mu] = 0$ , where

$$J_z = -i \frac{\partial}{\partial \theta_{\mathbf{k}}} + \frac{1}{2} \sigma_z, \quad (2.5)$$

is the  $z$  component of total angular momentum.

In order to study the isotropic-nematic transition we need a suitable microscopic definition of the nematic order parameter in terms of the fermionic fields  $\psi, \psi^\dagger$ . In general, nematic order is described by a quadrupolar order parameter  $Q_{ab}$  which transforms as a real, traceless symmetric rank-two tensor under rotations [58]. Because of spin-orbit coupling, here the relevant rotations are simultaneous rotations in real space and spin space, generated by the total angular momentum (2.5). Therefore, unlike for spin rotationally invariant Fermi liquids [53] the nematic order parameter can involve both the spatial (charge) and spin degrees of freedom of the electron. To lowest order in the electron momentum, the appropriate generalization of the nematic order parameter considered in Ref. [53] for spin rotationally invariant Fermi liquids to the surface state of 3D topological insulators is

$$\hat{Q}_{ab}(\mathbf{r}) = -\frac{i}{k_A} \psi^\dagger(\mathbf{r}) (\sigma_a \overset{\leftrightarrow}{\partial}_b + \sigma_b \overset{\leftrightarrow}{\partial}_a - \delta_{ab} \boldsymbol{\sigma} \cdot \overset{\leftrightarrow}{\boldsymbol{\partial}}) \psi(\mathbf{r}), \quad (2.6)$$

where  $a, b = 1, 2$ , and  $\overset{\leftrightarrow}{\boldsymbol{\partial}} = (\overset{\leftrightarrow}{\partial}_x, \overset{\leftrightarrow}{\partial}_y)$  is a vector of symmetrized derivatives whose action is defined as  $\psi^\dagger \overset{\leftrightarrow}{\partial}_a \psi \equiv \frac{1}{2} (\psi^\dagger \partial_a \psi + (\partial_a \psi^\dagger) \psi)$ . This ensures  $\hat{Q}_{ab}(\mathbf{r})$  is a Hermitian operator. Finally, for technical purposes it is convenient to define the parameter  $k_A$  differently depending on whether one is in the doped or undoped limit. We consider that four-fermion interactions, to be written out explicitly below, only act within a high-energy cutoff that

can be converted to a momentum cutoff  $\Lambda$  by dividing by  $v_F$ . In the undoped limit  $\mu = 0$ , we define  $k_A \equiv \Lambda$  and the order parameter is local in space. This order parameter was first introduced in the context of nematic instabilities of the Majorana surface state of superfluid  ${}^3\text{He-B}$  [59], and its 3D analog was proposed as an order parameter for parity-breaking phases of spin-orbit coupled bulk metals [60, 61]. In the doped limit, defined as  $\mu \gg v_F \Lambda$ , only (angular) degrees of freedom on the FS are relevant and we define  $k_A \equiv |\boldsymbol{\partial}|$  [62]. As discussed below, this should be understood from a momentum space perspective, and is equivalent to projecting the order parameter onto the Fermi surface.

In the spirit of Ref. [53], we consider an attractive four-fermion interaction in the quadrupolar ( $l = 2$ ) channel,

$$H_{\text{int}} = -\frac{f_2}{4} \int d^2r \text{tr} \left( \hat{Q}(\mathbf{r})^2 \right), \quad (2.7)$$

where  $\text{tr}$  denotes a trace over the spatial (nematic) indices  $a, b$ . The action in imaginary time is then

$$S[\psi^\dagger, \psi] = \int_0^{1/T} d\tau \int d^2r \left[ \psi^\dagger (\partial_\tau - iv_F \hat{\mathbf{z}} \cdot (\boldsymbol{\sigma} \times \boldsymbol{\partial}) - \mu) \psi - \frac{f_2}{4} \text{tr} \left( \hat{Q}(\mathbf{r})^2 \right) \right], \quad (2.8)$$

where  $T$  is temperature. As our focus is the vicinity of the isotropic-nematic transition, interactions in other angular momentum channels have been ignored. Indeed, in the doped limit, as long as such interactions are less than the critical value for a  $l \neq 2$  Pomeranchuk instability, they will simply lead to a finite renormalization of physical quantities such as the Fermi velocity [52]. While the phenomenological Landau Fermi liquid description does not strictly apply to the undoped case, we will assume in this case that interactions in  $l \neq 2$  channels are sufficiently weak so there are no competing instabilities.

## 2.2 Mean-Field Theory

To investigate a possible isotropic-nematic phase transition in the action (2.8), we first analyze it in the mean-field approximation. Introducing a real auxiliary scalar field  $Q_{ab}(\tau, \mathbf{r})$  to decouple the four-fermion term via the Hubbard-Stratonovich transformation, we have

$$S[\psi^\dagger, \psi, Q_{ab}] = \int_0^{1/T} d\tau \int d^2r \left[ \psi^\dagger (\partial_\tau - iv_F \hat{\mathbf{z}} \cdot (\boldsymbol{\sigma} \times \boldsymbol{\partial}) - \mu) \psi - \frac{iQ_{ab}}{k_A} \psi^\dagger (\sigma_a \overleftrightarrow{\partial}_b + \sigma_b \overleftrightarrow{\partial}_a - \delta_{ab} \boldsymbol{\sigma} \cdot \overleftrightarrow{\boldsymbol{\partial}}) \psi + \frac{1}{f_2} \text{tr}(\hat{Q}^2) \right]. \quad (2.9)$$

Assuming a uniform and static order parameter  $Q_{ab}(\tau, \mathbf{r}) = \bar{Q}_{ab}$ , and integrating out the fermions, we obtain the following saddle-point free energy density,

$$\mathcal{F}(\bar{Q}) = \frac{2}{f_2} \bar{Q}^2 - \frac{T}{V} \sum_{ik_n} \sum_{\mathbf{k}} \ln [(k_n - i\mu)^2 + \epsilon_{\mathbf{k}}(\bar{Q})^2], \quad (2.10)$$

where  $k_n = (2n + 1)\pi T$ ,  $n \in \mathbb{Z}$  is a fermionic Matsubara frequency. We have rotated the order parameter such that  $\bar{Q}_{11} = -\bar{Q}_{22} = 0$ ,  $\bar{Q}_{12} = \bar{Q}_{21} = \bar{Q}$  without loss of generality (corresponding to the principal axes of the distorted FS being parallel to the  $x$  and  $y$  axes<sup>1</sup>), and

$$\epsilon_{\mathbf{k}}(\bar{Q}) = \sqrt{(\epsilon_{\mathbf{k}}^0)^2 - 4\bar{Q}\epsilon_{\mathbf{k}}^0 \frac{k}{k_A} \cos 2\theta_{\mathbf{k}} + 4\bar{Q}^2 \left(\frac{k}{k_A}\right)^2}, \quad (2.11)$$

is the mean-field dispersion relation of fermionic quasiparticles in the nematic phase (for  $\bar{Q} \neq 0$ ), where  $\epsilon_{\mathbf{k}}^0 = v_F k$  is the dispersion relation in the isotropic phase. This corresponds to an anisotropic Dirac cone (in the doped limit,  $\epsilon_{\mathbf{k}}(\bar{Q})$  is only meant to model the dispersion of quasiparticles on the FS, with  $k \approx k_F \equiv \mu/v_F$ ). Here  $k_A$  is to be understood in momentum space, i.e.,  $k_A = \Lambda$  in the undoped limit and  $k_A = k$  in the doped limit. Performing the

---

<sup>1</sup>There is a  $\pi/4$  angle difference between the naive orientation of  $\hat{Q}_{ab}$  in Eq. (2.6) and the principal axes of the distorted FS, or equivalently, the orientation of the effective spinless nematic order parameter that results from projection to the FS [52].

sum over Matsubara frequencies, and ignoring constant terms, we obtain

$$\mathcal{F}(\bar{Q}) = \frac{2}{f_2} \bar{Q}^2 - T \sum_s \int \frac{d^2k}{(2\pi)^2} \ln \left( 1 + e^{-(s\epsilon_{\mathbf{k}}(\bar{Q}) - \mu)/T} \right), \quad (2.12)$$

where  $s = \pm 1$  corresponds to the upper and lower branches of the Dirac cone, respectively, and we have taken the infinite volume limit  $V \rightarrow \infty$ . At zero temperature, Eq. (2.12) becomes the ground state energy density,

$$\mathcal{E}(\bar{Q}) = \frac{2}{f_2} \bar{Q}^2 - \frac{1}{2} \sum_s \int \frac{d^2k}{(2\pi)^2} |s\epsilon_{\mathbf{k}}(\bar{Q}) - \mu|. \quad (2.13)$$

In the following our analysis is performed at constant  $\mu$ .

### 2.2.1 Undoped limit

We first evaluate the free energy density in the undoped limit ( $\mu = 0$ ). At zero temperature, we have

$$\mathcal{E}(\bar{Q}) = \frac{2}{f_2} \bar{Q}^2 - \int_{|\mathbf{k}| < \Lambda} \frac{d^2k}{(2\pi)^2} \epsilon_{\mathbf{k}}(\bar{Q}), \quad (2.14)$$

where we have imposed the momentum cutoff  $\Lambda$ . The integral over momentum can be performed exactly, and we obtain

$$\mathcal{E}(\Delta) = \frac{v_F \Lambda^3}{3\pi^2} \left[ \frac{\Delta^2}{\lambda} - |\Delta - 1| E \left( -\frac{4\Delta}{(\Delta - 1)^2} \right) \right], \quad (2.15)$$

where  $E(m)$  is the complete elliptic integral of the second kind, and we define a dimensionless nematic order parameter  $\Delta = 2\bar{Q}/v_F\Lambda$  and a dimensionless interaction strength  $\lambda = 2f_2\Lambda/3\pi^2v_F$ . A strongly first-order isotropic-nematic transition is found at a critical value  $\lambda_c \approx 2.13$ , with a jump of order one in the order parameter  $\Delta$  at the transition, corresponding to a value of  $\bar{Q}$  on the order of the high-energy cutoff  $v_F\Lambda$ . This is to be expected since  $\bar{Q}$  has units of energy, and in the undoped limit the only energy scale in the

problem is the cutoff (the critical value of the interaction strength  $f_2$  is also determined by the cutoff, since the interaction (2.7) is perturbatively irrelevant at the Dirac point). Expanding (2.15) in powers of  $\Delta$  in the limit  $|\Delta| \ll 1$ , we find

$$\mathcal{E}(\Delta) - \mathcal{E}(0) = \frac{v_F \Lambda^2}{3\pi^2} \left[ \left( \frac{1}{\lambda} - \frac{\pi}{8} \right) \Delta^2 + \dots \right], \quad (2.16)$$

hence the limit of metastability of the isotropic phase (corresponding to the divergence of the nematic susceptibility) is  $\lambda^* = 8/\pi \approx 2.55$ , but this is preempted by the first-order transition at  $\lambda_c \approx 2.13$ . The limit of metastability of the nematic phase can be found numerically, and is  $\lambda^{**} \approx 1.90$ .

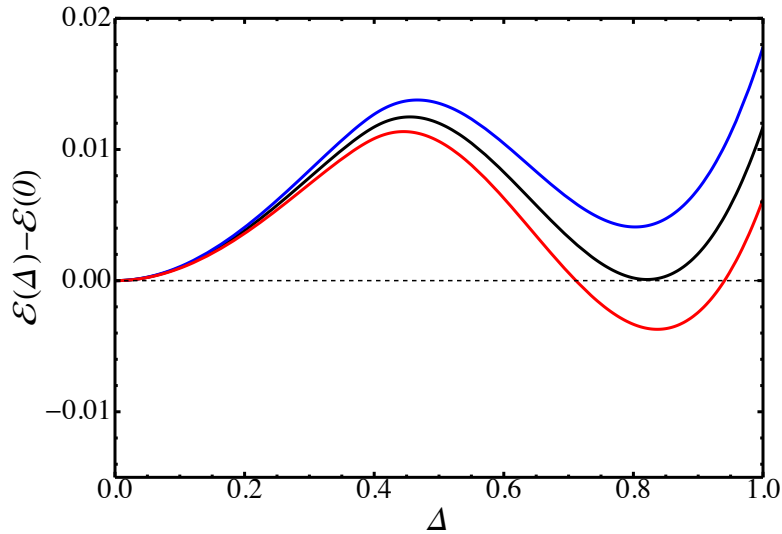


Figure 2.2: First-order isotropic-nematic quantum phase transition in the undoped limit ( $\mu = 0$ ). Plots of the mean-field ground state energy density  $\mathcal{E}(\Delta)$  in units of  $v_F \Lambda^3 / 3\pi^2$  are given as a function of the dimensionless nematic order parameter  $\Delta$ , for  $\lambda < \lambda_c$  (blue curve),  $\lambda = \lambda_c$  (black curve), and  $\lambda > \lambda_c$  (red curve), where  $\lambda$  is the dimensionless interaction strength with critical value  $\lambda_c \approx 1.31$  at the transition. The leading correction to linear dispersion is given by  $\alpha = -0.61$ .

The magnitude of the order parameter jump at the transition can be reduced some-

what by considering the effects of nonzero band curvature at the Dirac point, i.e., deviations from a perfectly linear dispersion (which are present anyway in real topological insulator materials). In other words, we replace  $v_F$  in the noninteracting dispersion  $\epsilon_{\mathbf{k}}^0$  by a  $k$ -dependent Fermi velocity

$$v_F(k) = v_F \left[ 1 + \alpha \left( \frac{k}{\Lambda} \right)^2 + \dots \right], \quad (2.17)$$

with the dimensionless parameter  $\alpha$  representing the leading correction. Such corrections are formally irrelevant in the low-energy limit  $k \ll \Lambda$  but affect the free energy [53, 63], which depends on the noninteracting dispersion at all wavevectors up to the cutoff. In the presence of such terms the energy density cannot be evaluated analytically and one must resort to numerical integration. A typical plot of the ground state energy density in the vicinity of the transition for nonzero  $\alpha$  is given in Fig. 2.2. We have found that negative values of  $\alpha$  reduce both the critical interaction strength and order parameter jump at the transition below their values for a strictly linear dispersion.

The appearance of a first-order transition is somewhat surprising, since Landau theory predicts a continuous isotropic-nematic transition in 2D (unlike in 3D, there are no cubic invariants). Expanding the quasiparticle dispersion relation  $\epsilon_{\mathbf{k}}(\bar{Q})$  in powers of  $\bar{Q}$  in Eq. (2.14), and performing the integral over  $\mathbf{k}$ , we obtain the Landau theory

$$\mathcal{E}(\Delta) - \mathcal{E}(0) \stackrel{?}{=} \frac{v_F \Lambda^2}{3\pi^2} \left[ \left( \frac{1}{\lambda} - \frac{\pi}{8} \right) \Delta^2 + \sum_{n=2}^{\infty} c_{2n} \Delta^{2n} \right], \quad (2.18)$$

where  $c_{2n} < 0$  for all  $n \geq 2$ . We have checked that the only way to get a quartic term  $\propto \Delta^4$  with positive coefficient is to consider a  $k$ -dependent Fermi velocity  $v_F(k)$  that becomes negative at a certain value of  $k$  below the cutoff  $\Lambda$ , in clear contradiction with the assumption of a single Dirac point in the low-energy spectrum. Therefore, the Landau theory (2.18) is unbounded from below for sufficiently large  $\Delta$ , in disagreement with the exact energy density (2.15) which behaves qualitatively like in Fig. 2.2. As a result, there must be nonanalytic terms in Eq. (2.15), but missed by the Landau expansion around  $\Delta = 0$ , that stabilize

the energy density. Such nonanalytic terms are ultimately responsible for the first-order character of the phase transition. In fact, for  $|\Delta| \gg 1$  the energy density (2.15) becomes

$$\mathcal{E}(\Delta) - \mathcal{E}(0) \approx \frac{v_F \Lambda^2}{3\pi^2} \left( \frac{\Delta^2}{\lambda} - \frac{\pi}{2} |\Delta| \right), \quad |\Delta| \gg 1. \quad (2.19)$$

Thus the energy density is stabilized at large  $\Delta$  by the “bare” (tree-level) mass term  $\Delta^2/\lambda$ , which grows faster than the negative  $|\Delta|$  term coming from the one-loop fermion determinant, i.e., the integral over quasiparticle energies in Eq. (2.14). The latter is in fact negative for all  $\Delta$ . We note that a first-order Ising nematic transition at zero temperature was also found for a model of interacting electrons on the square lattice [64]. In this case van Hove singularities in the quasiparticle density of states, corresponding to Lifshitz transitions tuned by the value of  $\bar{Q}$ , are responsible for nonanalyticities in the energy density and the first-order character of the transition.

At finite temperature the free energy density in the undoped limit is given by

$$\mathcal{F}(\bar{Q}) = \frac{2}{f_2} \bar{Q}^2 - T \sum_s \int_{|\mathbf{k}| < \Lambda} \frac{d^2 k}{(2\pi)^2} \ln \left( 1 + e^{-s\epsilon_{\mathbf{k}}(\bar{Q})/T} \right). \quad (2.20)$$

In the remainder of this section we focus on the limit of strict linear dispersion  $v_F(k) = v_F$ . The integral over the magnitude of  $k$  can be evaluated analytically in terms of dilogarithms  $\text{Li}_2(x)$  and trilogarithms  $\text{Li}_3(x)$  (see Appendix A); the remaining angular integral must be performed numerically. In Fig. 2.3a we plot the jump  $\Delta_c$  in the order parameter at the transition as a function of temperature  $T$ . The jump decreases smoothly from its value at zero temperature, eventually vanishing above a certain temperature  $T_{\text{TCP}}$  corresponding to a tricritical point; for  $T > T_{\text{TCP}}$  the transition is continuous (a similar behavior was found in Ref. [64]). Since  $\Delta$  vanishes at the tricritical point, to find  $T_{\text{TCP}}$  we expand the free energy density (2.12) in powers of  $\Delta$ . To describe the tricritical point we must expand to sixth order,

$$\mathcal{F}(\Delta, T) - \mathcal{F}(0, T) = \frac{v_F \Lambda^3}{3\pi^2} (a_2 \Delta^2 + a_4 \Delta^4 + a_6 \Delta^6), \quad (2.21)$$

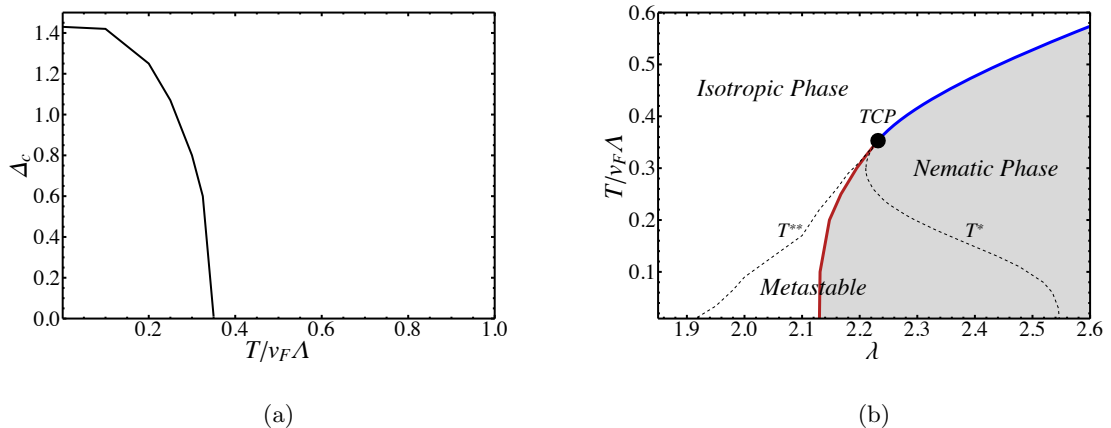


Figure 2.3: Finite-temperature isotropic-nematic transition in the undoped limit ( $\mu = 0$ ): (a) Jump in the dimensionless nematic order parameter at the first-order phase transition as a function of temperature; (b) Mean-field phase diagram in the plane of temperature  $T$  and dimensionless interaction strength  $\lambda$ . A first-order transition (red line) at low temperature turns into a continuous transition (blue line) above a tricritical point (black dot). Dotted lines correspond to limits of metastability of the isotropic ( $T^*$ ) and nematic ( $T^{**}$ ) phases.

where  $a_2, a_4, a_6$  are functions of  $T$ . We find that  $a_6 > 0$  for  $0.2 \lesssim T/v_F\Lambda \lesssim 0.6$ , which comprises the tricritical point (Fig. 2.3a). The tricritical point  $(T_{\text{TCP}}, \lambda_{\text{TCP}})$  is found from the condition  $a_2 = a_4 = 0$ , from which we find  $T_{\text{TCP}} \approx 0.35$  and  $\lambda_{\text{TCP}} \approx 2.23$ . The finite-temperature phase diagram is shown in Fig. 2.3b, in which we also plot the limits of metastability of the isotropic ( $T^*$ ) and nematic ( $T^{**}$ ) phases. Note that the first-order phase boundary and limits of metastability are obtained from the numerically evaluated, exact free energy density (2.12) rather than from the Landau expansion (2.21), which is accurate only in the vicinity of the continuous transition. Strictly speaking, the finite-temperature phase transition for  $T > T_{\text{TCP}}$  is a Kosterlitz-Thouless transition and the nematic phase only exhibits quasi-long-range order at finite  $T$  (but is truly long-range ordered at  $T = 0$ ).

At the mean-field level, the nematic phase is a theory of noninteracting Dirac quasi-particles with anisotropic dispersion, with Hamiltonian  $H_{\text{MF}} = \sum_{\mathbf{k}} \psi_{\mathbf{k}}^\dagger \mathcal{H}_{\mathbf{k}} \psi_{\mathbf{k}}$  where

$$\mathcal{H}_{\mathbf{k}} = v_F \hat{\mathbf{z}} \cdot (\boldsymbol{\sigma} \times \mathbf{k}) + \frac{\bar{Q}_{ab}}{\Lambda} (\sigma_a k_b + \sigma_b k_a - \delta_{ab} \boldsymbol{\sigma} \cdot \mathbf{k}). \quad (2.22)$$

Without loss of generality we choose  $\bar{Q}_{12} = \bar{Q}_{21} = \bar{Q}$ ,  $\bar{Q}_{11} = -\bar{Q}_{22} = 0$ , and thus

$$\mathcal{H}_{\mathbf{k}} = v_F \hat{\mathbf{z}} \cdot (\boldsymbol{\sigma} \times \mathbf{k}) + \frac{2\bar{Q}}{\Lambda} (\sigma_x k_y + \sigma_y k_x). \quad (2.23)$$

The velocities in the  $x$  and  $y$  directions (i.e., parallel to the principal axes of the nematic order parameter) at the Dirac point are

$$v_x = v_F |1 - \Delta|, \quad v_y = v_F |1 + \Delta|. \quad (2.24)$$

Away from  $\Delta = \pm 1$ , the density of states remains linear near the Dirac point,  $\mathcal{N}(\epsilon) \propto |\epsilon|$ . In the limit of strict linear dispersion  $v_F(k) = v_F$ , the value  $\Delta = 1$  ( $\Delta = -1$ ) thus corresponds to a Lifshitz transition where the quasiparticle dispersion vanishes along  $x$  ( $y$ ) and degenerates into the intersection of two planes, i.e., a quasi-1D Dirac dispersion with formally infinite density of states. In the presence of nonzero band curvature however [Eq. (2.17)], this degeneracy is lifted, and the flat direction acquires a cubic dispersion at small momenta,

$$\epsilon_{\mathbf{k}}(\Delta = 1) \approx v_F \sqrt{4k_y^2 + \frac{\alpha^2}{\Lambda^4} k_x^6}, \quad \mathbf{k} \rightarrow 0, \quad (2.25)$$

with  $k_x$  and  $k_y$  interchanged for  $\Delta = -1$ . This corresponds to a density of states of the form  $\mathcal{N}(\epsilon) \propto |\epsilon|^{1/3}$  near the Dirac point  $\epsilon = 0$ .

An interesting signature of the unusual type of nematic order described here is anisotropy in the in-plane spin susceptibility in the absence of any time-reversal symmetry breaking. To compute the spin susceptibility we augment the mean-field Hamiltonian matrix (2.35) with a Zeeman term,

$$\delta\mathcal{H}_{\mathbf{k}}^Z = -\frac{1}{2} g \mu_B \mathbf{B} \cdot \boldsymbol{\sigma}, \quad (2.26)$$

where  $g$  is the  $g$ -factor,  $\mu_B$  is the Bohr magneton, and  $\mathbf{B}$  is an in-plane magnetic field. To

linear order in  $\Delta$ , we find

$$\chi_{xx}(T) - \chi_{yy}(T) = -\frac{g^2 \mu_B^2 \Lambda}{32\pi v_F} F\left(\frac{T}{v_F \Lambda}\right) \Delta(T), \quad (2.27)$$

where  $\chi_{ij}(T)$  is the spin susceptibility tensor at temperature  $T$ ,  $\Delta(T)$  is the dimensionless nematic order parameter at temperature  $T$ , and  $F$  is a smooth function of temperature (Fig. 2.4) defined as

$$F(x) = x \int_0^{1/x} dy \left[ \sinh y + y \left( y \tanh \frac{y}{2} - 1 \right) \right] \operatorname{sech}^2 \frac{y}{2}. \quad (2.28)$$

Thus anisotropy in the in-plane susceptibility is a direct measure of nematic order. For  $T > T_{\text{TCP}}$ , the transition is continuous (blue curve in Fig. 2.3b) thus  $\Delta(T)$  is small near  $T_c$  and the expression (2.27) can be used in the vicinity of the transition. We thus expect

$$\chi_{xx}(T) - \chi_{yy}(T) \propto F\left(\frac{T_c}{v_F \Lambda}\right) \Delta(T) \propto (T_c - T)^\beta, \quad (2.29)$$

on the nematic side of the transition, for  $(T_c - T)/T_c \ll 1$ . Thus the susceptibility anisotropy can give a direct measure of the order parameter critical exponent  $\beta$ , which is 1/2 in mean-field theory. In the first-order region, since  $\Delta$  may not be small Eq. (2.27) cannot be directly used, but we nonetheless expect the anisotropy to be nonzero everywhere in the nematic phase and to vanish in the isotropic phase.

From a qualitative standpoint, the observation of in-plane spin susceptibility anisotropy in the absence of time-reversal symmetry breaking distinguishes the unusual type of nematic order discussed here from other types of order. For conventional nematic order in spin rotationally invariant systems [53], the breaking of rotation symmetry is in the charge sector and does not cause anisotropy in the spin sector. In-plane ferromagnetic order would lead to anisotropy in the spin response, but requires time-reversal symmetry breaking.

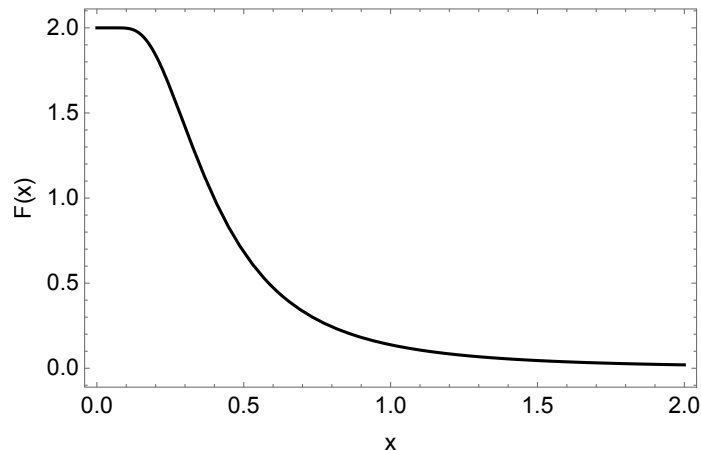


Figure 2.4: Plot of the dimensionless function  $F(x)$  defined in Eq. (2.28).

### 2.2.2 Doped limit

In the doped limit  $\mu \gg v_F \Lambda$ , the cutoff is imposed around the FS,

$$\int_{|k-k_F|<\Lambda} \frac{d^2 k}{(2\pi)^2} \equiv \int_{k_F-\Lambda}^{k_F+\Lambda} \frac{dk k}{2\pi} \int_0^{2\pi} \frac{d\theta_{\mathbf{k}}}{2\pi}, \quad (2.30)$$

where  $k_F \equiv \mu/v_F$  is the (isotropic) Fermi momentum of noninteracting electrons. We obtain the ground state energy density (2.13) to leading order in  $\Lambda/k_F$  as

$$\mathcal{E}(\bar{Q}) - \mathcal{E}(0) = \left( \frac{2}{f_2} - \mathcal{N}(\mu) \right) \bar{Q}^2 + \frac{\mathcal{N}(\mu)}{4\mu^2} \bar{Q}^4 + \mathcal{O}(\bar{Q}^6), \quad (2.31)$$

where  $\mathcal{N}(\mu) = \mu/(2\pi v_F^2)$  is the noninteracting density of states at the FS. Since the coefficient of the  $\bar{Q}^4$  term is positive, we therefore find a continuous quantum phase transition at a critical value of the interaction strength  $f_2$  given by

$$\mathcal{N}(\mu) f_2 = 2. \quad (2.32)$$

From general considerations we expect a line of finite- $T$  Kosterlitz-Thouless phase transitions that terminates at this quantum critical point. We note also that Eq. (2.32) corre-

sponds precisely to the  $l = 2$  Pomeranchuk criterion

$$\bar{F}_2 = -1, \quad (2.33)$$

derived from the phenomenological Landau helical Fermi liquid theory discussed in the introduction to this chapter [52]. In this context the dimensionless “projected” Landau parameters  $\bar{F}_l$  are defined as  $\bar{F}_l = \frac{1}{2}\mathcal{N}(\mu)f_l$  for  $l \geq 1$ , where  $f_l$  is the quasiparticle interaction strength in angular momentum channel  $l$ . The difference in sign arises simply from the fact that in Eq. (2.7) an attractive interaction corresponds to  $f_2 > 0$ , while in Ref. [52] it corresponds to  $f_2 < 0$ .

A first observable signature of nematic order of the type we have described in the doped limit is the partial breakdown of spin-momentum locking. In the doped limit, the mean-field Hamiltonian for fermionic quasiparticles is  $H_{\text{MF}} = \sum_{\mathbf{k}} \psi_{\mathbf{k}}^\dagger \mathcal{H}_{\mathbf{k}} \psi_{\mathbf{k}}$  where

$$\mathcal{H}_{\mathbf{k}} = v_F \hat{\mathbf{z}} \cdot (\boldsymbol{\sigma} \times \mathbf{k}) - \mu + \bar{Q}_{ab}(\sigma_a \hat{k}_b + \sigma_b \hat{k}_a - \delta_{ab} \boldsymbol{\sigma} \cdot \hat{\mathbf{k}}), \quad (2.34)$$

and  $\hat{k}_a = k_a/k$ . Without loss of generality we choose  $\bar{Q}_{12} = \bar{Q}_{21} = \bar{Q}$ ,  $\bar{Q}_{11} = -\bar{Q}_{22} = 0$ , and thus

$$\mathcal{H}_{\mathbf{k}} = v_F \hat{\mathbf{z}} \cdot (\boldsymbol{\sigma} \times \mathbf{k}) - \mu + 2\bar{Q}(\sigma_x \hat{k}_y + \sigma_y \hat{k}_x). \quad (2.35)$$

Eq. (2.35) describes an anisotropic FS. Near the FS, the eigenstates have positive helicity (assuming  $\mu > 0$ , thus above the Dirac point) and are given by

$$|\psi_+(\mathbf{k})\rangle = \frac{1}{\sqrt{2}} \begin{pmatrix} i e^{i\theta_{\mathbf{k}}} \frac{f(\theta_{\mathbf{k}}, \Delta_F)}{e^{2i\theta_{\mathbf{k}}} - \Delta_F} \\ 1 \end{pmatrix}, \quad (2.36)$$

where we define

$$f(\theta_{\mathbf{k}}, \Delta_F) \equiv \sqrt{1 + \Delta_F^2 - 2\Delta_F \cos 2\theta_{\mathbf{k}}}. \quad (2.37)$$

We introduce a new dimensionless order parameter  $\Delta_F \equiv 2\bar{Q}/\mu$  for the doped limit. The expectation value  $\mathbf{s}_{\mathbf{k}} \equiv \langle \psi_+(\mathbf{k}) | \boldsymbol{\sigma} | \psi_+(\mathbf{k}) \rangle$  of the spin operator on the FS is in plane, with components

$$s_{\mathbf{k}}^x = \frac{(1 + \Delta_F) \sin \theta_{\mathbf{k}}}{f(\theta_{\mathbf{k}}, \Delta_F)}, \quad s_{\mathbf{k}}^y = -\frac{(1 - \Delta_F) \cos \theta_{\mathbf{k}}}{f(\theta_{\mathbf{k}}, \Delta_F)}, \quad (2.38)$$

thus nematic order affects the spin polarization on the FS. To leading order in  $\Delta_F$ , the angle  $\delta(\theta_{\mathbf{k}})$  between the spin vectors in the presence and absence of nematic order is

$$\delta(\theta_{\mathbf{k}}) \approx \Delta_F |\sin 2\theta_{\mathbf{k}}|. \quad (2.39)$$

Thus except for four points on the FS  $\theta_{\mathbf{k}} = 0, \pi/2, \pi, 3\pi/2$ , spin and momentum are no longer orthogonal (Fig. 2.5). However, one might naively think that spin-momentum locking is preserved in the sense that the spin vector remains tangent to the FS even if the latter is distorted. This is not true: defining a unit vector  $\hat{\mathbf{t}}_{\mathbf{k}}$  tangent to the distorted FS (that winds around the FS clockwise), we have

$$\hat{\mathbf{z}} \cdot (\mathbf{s}_{\mathbf{k}} \times \hat{\mathbf{t}}_{\mathbf{k}}) \approx \Delta_F \sin 2\theta_{\mathbf{k}}, \quad (2.40)$$

to leading order in  $\Delta_F$ , thus the spin vector is tangent to the FS only at four points,  $\theta_{\mathbf{k}} = 0, \pi/2, \pi, 3\pi/2$  (Fig. 2.5). This partial breakdown of spin-momentum locking except at high-symmetry points could be detected experimentally using spin-resolved angle-resolved photoemission spectroscopy (ARPES), using for instance the setups described in Ref. [7].

As in the undoped case, nematic order of the type considered here would lead to anisotropy in the in-plane spin susceptibility. Here the transition is continuous already at zero temperature, and in the vicinity of the zero temperature quantum critical point we find

$$\chi_{xx} - \chi_{yy} = \frac{1}{4} g^2 \mu_B^2 \mathcal{N}(\mu) \frac{\Lambda}{k_F} \Delta_F, \quad (2.41)$$

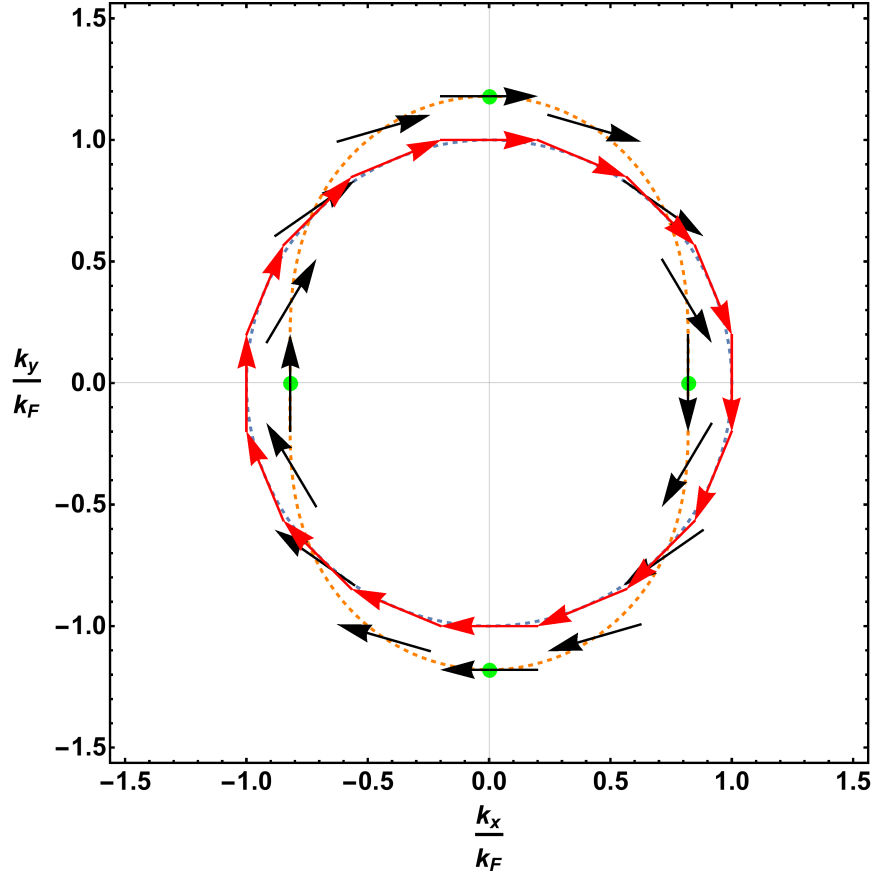


Figure 2.5: Partial breakdown of spin-momentum locking in the nematic phase. Blue dashed line: FS in the isotropic phase ( $\Delta_F = 0$ ); orange dashed line: FS in the nematic phase (here shown for  $\Delta_F = 0.18$ ). The red (black) vectors represent the expectation value of spin on the FS in the isotropic (nematic) phase. Except at four special momenta (green dots), spin in the nematic phase is no longer perpendicular to momentum, nor is it tangential to the (distorted) FS.

to leading order in  $\Delta_F$ . More conventional measures of nematicity, such as anisotropy in the in-plane resistivity [53, 65], apply here as well. Considering scattering on nonmagnetic impurities modelled by a collision time  $\tau$ , a calculation of the conductivity using the Kubo formula and impurity-averaged Green's functions in the first Born approximation gives<sup>2</sup>

$$\frac{\rho_{xx} - \rho_{yy}}{\rho_{xx} + \rho_{yy}} \approx \Delta_F, \quad (2.42)$$

to leading order in  $\Delta_F$  and assuming weak disorder  $1/(\mu\tau) \ll 1$ . By symmetry we anticipate an analogous result in the undoped case.

### 2.3 Fluctuation effects

We now go beyond the mean-field level and investigate the effect of fluctuations in the vicinity of the quantum critical point in the doped limit  $k_F \gg \Lambda$ . Following Ref. [53], we rewrite the order parameter in terms of the Pauli matrices  $\tau_z$  and  $\tau_x$ ,

$$\hat{Q} = \psi^\dagger \Delta_1 \psi \tau_z + \psi^\dagger \Delta_2 \psi \tau_x, \quad (2.43)$$

where

$$\Delta_1 = -i(\sigma_x \hat{\partial}_x - \sigma_y \hat{\partial}_y), \quad \Delta_2 = -i(\sigma_x \hat{\partial}_y + \sigma_y \hat{\partial}_x), \quad (2.44)$$

and we define  $\hat{\boldsymbol{\partial}} \equiv \overleftrightarrow{\boldsymbol{\partial}}/|\boldsymbol{\partial}|$  in the sense of Fourier transforms (see Eq. (2.6)). We can now rewrite the imaginary-time action in a vectorial form,

$$S[\psi^\dagger, \psi] = \int_0^{1/T} d\tau \int d^2r \left[ \psi^\dagger \hat{\mathcal{G}}_0^{-1} \psi - \frac{f_2}{2} (\psi^\dagger \boldsymbol{\Delta} \psi)^2 \right], \quad (2.45)$$

where  $\boldsymbol{\Delta} = (\Delta_1, \Delta_2)$  and

$$\hat{\mathcal{G}}_0^{-1} = \partial_\tau - iv_F \hat{\mathbf{z}} \cdot (\boldsymbol{\sigma} \times \boldsymbol{\partial}) - \mu, \quad (2.46)$$

---

<sup>2</sup>This calculation was performed by R. Lundgren.

is the noninteracting Green's operator. Introducing a bosonic auxiliary field  $\mathbf{n} = (n_1, n_2)$  to decouple the four-fermion term, we have

$$S[\psi^\dagger, \psi, \mathbf{n}] = \int_0^{1/T} d\tau \int d^2r \left[ \psi^\dagger (\hat{\mathcal{G}}_0^{-1} - \mathbf{n} \cdot \boldsymbol{\Delta}) \psi + \frac{1}{2f_2} \mathbf{n}^2 \right]. \quad (2.47)$$

After integrating out the fermions to second order in  $\mathbf{n}$ , we find the effective action

$$S_{\text{eff}}[\mathbf{n}] = \frac{1}{2} \sum_{iq_n, \mathbf{q}} \mathbf{n}(\mathbf{q}, iq_n)^T \chi^{-1}(\mathbf{q}, iq_n) \mathbf{n}(-\mathbf{q}, -iq_n), \quad (2.48)$$

where the inverse propagator for the auxiliary field is given to lowest order in momentum  $\mathbf{q}$  and Matsubara frequency  $q_n$  by

$$\chi_{ij}^{-1}(\mathbf{q}, iq_n) = \delta_{ij}(r + \kappa q^2) + M_{ij}(\mathbf{q}, iq_n). \quad (2.49)$$

Here  $r = f_2^{-1} - \mathcal{N}(\mu)/2$  is the distance from criticality which gives a mass to the auxiliary field,  $\kappa = \mathcal{N}(\mu)/(8k_F^2)$  gives it a finite stiffness, and

$$M(\mathbf{q}, iq_n) = is\mathcal{N}(\mu) \int_0^{2\pi} \frac{d\phi}{2\pi} \frac{1}{is - \cos(\phi - \theta_{\mathbf{q}})} \begin{pmatrix} \sin^2 2\phi & -\sin 2\phi \cos 2\phi \\ -\sin 2\phi \cos 2\phi & \cos^2 2\phi \end{pmatrix}, \quad (2.50)$$

is a dynamical term, where  $s \equiv q_n/(v_F q)$  and  $\theta_{\mathbf{q}}$  is the angle between  $\mathbf{q}$  and the  $x$  axis. Performing the integral over  $\phi$ , we have

$$M(\mathbf{q}, iq_n) = \frac{\mathcal{N}(\mu)}{2} \frac{|s|}{\sqrt{s^2 + 1}} \left[ 1 - \left( \sqrt{s^2 + 1} - |s| \right)^4 (\sigma_z \cos 4\theta_{\mathbf{q}} + \sigma_x \sin 4\theta_{\mathbf{q}}) \right], \quad (2.51)$$

which, after a rotation of  $\theta_{\mathbf{q}}$  by  $\pi/4$ , gives the same inverse propagator as for the spinless nematic Fermi fluid [53]. The effective action (2.48) can be diagonalized by a rotation

$\mathbf{n} \rightarrow \mathbf{n}'$ ,  $\chi^{-1} \rightarrow \chi'^{-1}$ , where

$$\mathbf{n}'(\mathbf{q}, iq_n) = R(4\theta_{\mathbf{q}})^T \mathbf{n}(\mathbf{q}, iq_n) = \begin{pmatrix} \hat{\mathbf{d}}_{\mathbf{q}} \cdot \mathbf{n}(\mathbf{q}, iq_n) \\ \hat{\mathbf{z}} \cdot (\hat{\mathbf{d}}_{\mathbf{q}} \times \mathbf{n}(\mathbf{q}, iq_n)) \end{pmatrix}. \quad (2.52)$$

Here  $R(\phi) = e^{-i\sigma_y \phi/2}$  is an orthogonal rotation matrix and  $\hat{\mathbf{d}}_{\mathbf{q}} \equiv (\cos 2\theta_{\mathbf{q}}, \sin 2\theta_{\mathbf{q}})$ . Thus  $n'_1$  and  $n'_2$  correspond to the longitudinal and transverse components of  $\mathbf{n}$ , respectively. The transformed inverse propagator is

$$\chi'^{-1}(\mathbf{q}, iq_n) = R(4\theta_{\mathbf{q}})^T \chi^{-1}(\mathbf{q}, iq_n) R(4\theta_{\mathbf{q}}) = \begin{pmatrix} \chi_1'^{-1}(\mathbf{q}, iq_n) & 0 \\ 0 & \chi_2'^{-1}(\mathbf{q}, iq_n) \end{pmatrix}. \quad (2.53)$$

For small  $s$ , we have

$$\chi_1'^{-1}(\mathbf{q}, iq_n) = r + \kappa q^2 + 2\mathcal{N}(\mu)s^2 + \dots, \quad (2.54)$$

$$\chi_2'^{-1}(\mathbf{q}, iq_n) = r + \kappa q^2 + \mathcal{N}(\mu)|s| + \dots \quad (2.55)$$

### 2.3.1 Collective modes

Since the inverse propagator of nematic fluctuations is the same as in the spinless case, the number and dispersion of collective modes, given by the condition

$$\det \chi^{-1}(\mathbf{q}, iq_n) = 0, \quad (2.56)$$

is also the same. Analytically continuing Eq. (2.54)-(2.55) to real frequencies  $iq_n \rightarrow \omega + i\delta$ , we find

$$\chi_1'^{-1}(\mathbf{q}, \omega) = r + \kappa q^2 - 2\mathcal{N}(\mu) \left( \frac{\omega}{v_F q} \right)^2, \quad (2.57)$$

$$\chi_2'^{-1}(\mathbf{q}, \omega) = r + \kappa q^2 - \mathcal{N}(\mu) \frac{i\omega}{v_F q}, \quad (2.58)$$

to leading order in  $\omega/(v_F q)$ . At criticality  $r \rightarrow 0^+$ , the collective mode dispersions are

$$\omega_1(q) \approx \sqrt{\frac{\kappa}{2\mathcal{N}(\mu)}} v_F q^2, \quad \omega_2(q) \approx -\frac{i v_F \kappa}{\mathcal{N}(\mu)} q^3, \quad (2.59)$$

thus  $\omega_1$  is an undamped  $z = 2$  mode and  $\omega_2$  is an overdamped  $z = 3$  mode. Since  $\omega_2 \ll \omega_1$  in the long-wavelength limit  $q \rightarrow 0$ , the overdamped mode dominates the long-wavelength response and the dynamic critical exponent at the transition is  $z = 3$  [53].

We note that although  $\omega_1$  corresponds to longitudinal fluctuations of  $\mathbf{n}$ , when projecting to the FS the longitudinal (11 and 22) components of the order parameter (2.6) map to the transverse (12 and 21) components of the usual spinless nematic order parameter

$$\psi^\dagger (\partial_a \partial_b - \frac{1}{2} \delta_{ab} \partial^2) \psi, \quad (2.60)$$

where the effectively spinless field  $\psi^\dagger$  creates electrons of the appropriate helicity on the FS, i.e., in the single-particle state Eq. (2.36) or its negative-helicity counterpart. Likewise, under projection the transverse components of (2.6) are mapped to the longitudinal components of (2.60). Thus in this sense  $\omega_1$  ( $\omega_2$ ) is the transverse (longitudinal) mode, in accordance with the terminology of Ref. [53].

In the nematic phase ( $r < 0$ ), we consider Gaussian fluctuations about the classical saddle point, which we take to be  $\bar{\mathbf{n}} = (\bar{n}, 0)$  without loss of generality. Near the critical point where  $\bar{n}$  is small, the leading change in the effective action for fluctuations compared to the isotropic phase is to the uniform and static part ( $\mathbf{q} = iq_n = 0$ ) of the inverse propagator [53],

$$\chi^{-1}(\mathbf{q}, iq_n) = \begin{pmatrix} 2|r| + \kappa q^2 + M_{11}(\mathbf{q}, iq_n) & M_{12}(\mathbf{q}, iq_n) \\ M_{21}(\mathbf{q}, iq_n) & \kappa q^2 + M_{22}(\mathbf{q}, iq_n) \end{pmatrix}, \quad (2.61)$$

i.e., the longitudinal (amplitude) mode  $\delta n_1$  acquires a mass  $2|r|$  and the transverse (Goldstone) mode  $\delta n_2$  is massless. Deep in the nematic phase (i.e.,  $\bar{n}$  not small), the  $q^2$  part

and the dynamical part  $M_{ij}$  will be modified from their form at  $\bar{n} = 0$ , but our conclusions drawn from the small  $\bar{n}$  limit will not be affected in a major way (for instance, a finite  $\bar{n}$  would lead to a difference  $\kappa_{\perp} \neq \kappa_{\parallel}$  in stiffness for the amplitude and Goldstone modes). The two eigenvalues  $\chi_{\perp}^{-1}$  and  $\chi_{\parallel}^{-1}$  of the inverse propagator (2.61) give the spectrum of collective modes in the nematic phase. The inverse transverse propagator, given by

$$\chi_{\perp}^{-1}(\mathbf{q}, iq_n) = \kappa q^2 + \mathcal{N}(\mu)|s| \cos^2 2\theta_{\mathbf{q}} - \mathcal{N}(\mu) \left( \cos 4\theta_{\mathbf{q}} + \frac{\mathcal{N}(\mu)}{16|r|} \sin^2 4\theta_{\mathbf{q}} \right) 2s^2 + \mathcal{O}(s^3), \quad (2.62)$$

corresponds to the gapless nematic Goldstone mode, which is overdamped due to Landau damping except along the principal axes of the distorted FS ( $\theta_{\mathbf{q}} = \pm\pi/4, \pm 3\pi/4$  for the saddle point considered, corresponding to  $\bar{Q}_{11} = -\bar{Q}_{22} \neq 0$ ). Along those directions the inverse transverse propagator reduces to Eq. (2.54) and the Goldstone mode disperses quadratically according to  $\omega_1(q)$  in Eq. (2.59). Those undamped directions also correspond to the FS momenta where spin-momentum locking is preserved (green dots in Fig. 2.5). The inverse longitudinal propagator is given by

$$\chi_{\parallel}^{-1}(\mathbf{q}, iq_n) = 2|r| + \kappa q^2 + \mathcal{N}(\mu)|s| \sin^2 2\theta_{\mathbf{q}} + \mathcal{N}(\mu) \left( \cos 4\theta_{\mathbf{q}} + \frac{\mathcal{N}(\mu)}{16|r|} \sin^2 4\theta_{\mathbf{q}} \right) 2s^2 + \mathcal{O}(s^3), \quad (2.63)$$

and describes gapped amplitude fluctuations, as expected.

Despite the number and dispersion of collective modes being formally the same as in the spinless nematic Fermi fluid, their physical nature is very different: in the latter case only charge degrees of freedom fluctuate, while fluctuations of the spin-orbit-coupled nematic order parameter (2.6) strongly mix charge and spin. An important observable consequence of this difference is that nematic fluctuations in the helical liquid considered here should strongly couple to the spin sector. While static nematic order does not break time-reversal symmetry and thus cannot induce a static spin polarization, nematic fluctuations can in principle induce spin fluctuations. To quantify this effect, one can use linear response:

a nematic fluctuation  $\delta\mathbf{n}(\mathbf{q}, \omega)$  with momentum  $\mathbf{q}$  and frequency  $\omega$  should induce a spin fluctuation  $\delta\langle\mathbf{s}(\mathbf{q}, \omega)\rangle$  with the same momentum and frequency,

$$\delta\langle s_i(\mathbf{q}, \omega)\rangle \propto \Pi_{ij}^R(\mathbf{q}, \omega)\delta n_j(\mathbf{q}, \omega), \quad (2.64)$$

if a suitably defined retarded spin-nematic susceptibility  $\Pi_{ij}^R(\mathbf{q}, \omega)$  is nonzero. An appropriate definition is

$$\Pi_{ij}^R(\mathbf{r}, t) = -i\theta(t) \left\langle \left[ (\psi^\dagger \sigma_i \psi)_{(\mathbf{r}, t)}, (\psi^\dagger \Delta_j \psi)_{(\mathbf{0}, 0)} \right] \right\rangle, \quad (2.65)$$

in real space and time, where  $\psi^\dagger \sigma \psi$  is the spin operator and  $\psi^\dagger \Delta \psi$  is the operator that couples to nematic fluctuations in Eq. (2.47). Eq. (2.65) will differ in the isotropic and nematic phases; here we compute  $\Pi_{ij}^R$  in the isotropic phase and find a nonzero result, but we expect a nonzero result in the nematic phase as well.

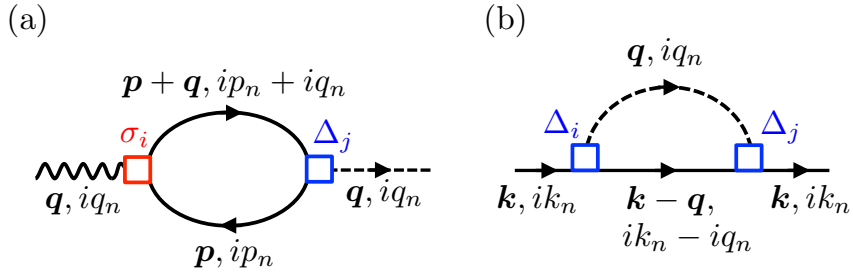


Figure 2.6: One-loop diagrams for (a) the spin-nematic susceptibility [Eq. (2.66)]; (b) the electron self-energy [Eq. (2.71)].

In the Matsubara frequency domain, the spin-nematic susceptibility is given by the bubble diagram in Fig. 2.6(a),

$$\Pi_{ij}(\mathbf{q}, iq_n) = \frac{T}{V} \sum_{\mathbf{p}, ip_n} \text{tr} \sigma_i \mathcal{G}_0(\mathbf{p} + \mathbf{q}, ip_n + iq_n) \Delta_j(\mathbf{p}, \mathbf{p} + \mathbf{q}) \mathcal{G}_0(\mathbf{p}, ip_n), \quad (2.66)$$

where

$$\Delta_1(\mathbf{k}, \mathbf{k}') \equiv \sigma_x \left( \frac{\hat{k}_x + \hat{k}'_x}{2} \right) - \sigma_y \left( \frac{\hat{k}_y + \hat{k}'_y}{2} \right), \quad (2.67)$$

$$\Delta_2(\mathbf{k}, \mathbf{k}') \equiv \sigma_x \left( \frac{\hat{k}_y + \hat{k}'_y}{2} \right) + \sigma_y \left( \frac{\hat{k}_x + \hat{k}'_x}{2} \right), \quad (2.68)$$

are the Fourier transform of the nematic vertices (2.44) and  $\mathcal{G}_0$  is the unperturbed electron Green's function, given by

$$\mathcal{G}_0(\mathbf{p}, ip_n) = \frac{ip_n + \mu + v_F \hat{\mathbf{z}} \cdot (\boldsymbol{\sigma} \times \mathbf{p})}{(ip_n + \mu)^2 - v_F^2 \mathbf{p}^2}. \quad (2.69)$$

The retarded spin-nematic susceptibility  $\Pi_{ij}^R(\mathbf{q}, \omega)$  is obtained from (2.66) by analytic continuation  $iq_n \rightarrow \omega + i\delta$ . We evaluate its imaginary part  $\Pi_{ij}''(\mathbf{q}, \omega)$  at zero temperature and in the long-wavelength  $q \ll k_F$ , low-energy  $|\omega| \ll \mu$  limits. To leading order in  $\omega/v_F q$ , we find

$$\Pi_{ij}''(\mathbf{q}, \omega) \sim \frac{\omega}{\mu} \begin{pmatrix} \cos \theta_{\mathbf{q}} & \sin \theta_{\mathbf{q}} \\ -\sin \theta_{\mathbf{q}} & \cos \theta_{\mathbf{q}} \end{pmatrix} - 3 \frac{\omega}{\mu} \begin{pmatrix} \cos 3\theta_{\mathbf{q}} & \sin 3\theta_{\mathbf{q}} \\ \sin 3\theta_{\mathbf{q}} & -\cos 3\theta_{\mathbf{q}} \end{pmatrix}. \quad (2.70)$$

ignoring an overall constant prefactor (we are only interested in showing that the response does not vanish). From time-reversal symmetry one can show that  $\Pi_{ij}''(\mathbf{q}, \omega) = \Pi_{ij}''(-\mathbf{q}, -\omega)$ , which is obeyed since all components in the matrices of Eq. (2.70) are odd in both  $\mathbf{q}$  and  $\omega$ . Kramers-Kronig relations imply that the real part  $\Pi_{ij}'(\mathbf{q}, \omega)$  approaches a constant at low frequencies and has the same structure in momentum space. By virtue of Eq. (2.64), nematic fluctuations can thus induce spin fluctuations, by contrast with the spinless (or spin degenerate) nematic Fermi fluid.

### 2.3.2 Helical non-Fermi liquid behavior

We now turn to the fermion self-energy on the FS. In the random phase approximation (RPA), i.e., at the one-loop level, the self-energy is given by the diagram in Fig. 2.6(b),

$$\Sigma(\mathbf{k}, ik_n) = \frac{T}{V} \sum_{\mathbf{q}, iq_n} \sum_{ij} \Delta_i(\mathbf{k}, \mathbf{k} - \mathbf{q}) \mathcal{G}_0(\mathbf{k} - \mathbf{q}, ik_n - iq_n) \Delta_j(\mathbf{k} - \mathbf{q}, \mathbf{k}) \chi_{ij}(\mathbf{q}, iq_n), \quad (2.71)$$

where  $\chi_{ij}$  is the propagator of nematic fluctuations given in Eq. (2.49). Here we only consider the effect of longitudinal fluctuations (i.e., the  $z = 3$  overdamped mode) which are expected to dominate at low energies. At the critical point  $r = 0$ , we find

$$\Sigma(\mathbf{k}, ik_n) = \left(1 + \hat{\mathbf{z}} \cdot (\boldsymbol{\sigma} \times \hat{\mathbf{k}})\right) \Sigma_0(\mathbf{k}, ik_n), \quad (2.72)$$

for  $|k - k_F| \ll k_F$  and  $|k_n| \ll \mu$ , where

$$\Sigma_0(\mathbf{k}, ik_n) = -i\omega_0^{1/3} |k_n|^{2/3} \text{sgn } k_n, \quad (2.73)$$

and  $\omega_0 \sim \mathcal{N}(\mu)^{-1} (v_F \kappa)^{-2}$ , ignoring factors of order one. Near the FS, we can ignore the lower helicity branch (assuming  $\mu > 0$ ) and the electron Green's function  $\mathcal{G}(\mathbf{k}, ik_n) = [\mathcal{G}_0(\mathbf{k}, ik_n) - \Sigma(\mathbf{k}, ik_n)]^{-1}$  is given approximately by

$$\mathcal{G}(\mathbf{k}, ik_n) \approx \frac{1}{2} \frac{1 + \hat{\mathbf{z}} \cdot (\boldsymbol{\sigma} \times \hat{\mathbf{k}})}{2i\omega_0^{1/3} |k_n|^{2/3} \text{sgn } k_n - \xi_{\mathbf{k}}}, \quad (2.74)$$

where  $\xi_{\mathbf{k}} = v_F |\mathbf{k}| - \mu$ . Thus to a first approximation the critical Green's function retains the same helicity structure as in the noninteracting limit,

$$\mathcal{G}_0(\mathbf{k}, ik_n) \approx \frac{1}{2} \frac{1 + \hat{\mathbf{z}} \cdot (\boldsymbol{\sigma} \times \hat{\mathbf{k}})}{ik_n - \xi_{\mathbf{k}}}, \quad (2.75)$$

but exhibits non-Fermi liquid behavior with vanishing quasiparticle residue as  $\omega \rightarrow 0$ . The spectral function is of the form

$$A(\mathbf{k}, \omega) \sim \frac{1}{2} \left( 1 + \hat{\mathbf{z}} \cdot (\boldsymbol{\sigma} \times \hat{\mathbf{k}}) \right) \frac{\omega_0^{1/3} |\omega|^{2/3}}{\xi_{\mathbf{k}}^2}, \quad (2.76)$$

in the limit  $\omega_0^{1/2} |\omega|^{2/3} \ll |\xi_{\mathbf{k}}| \ll \mu$ . Apart from the helicity structure, this is fully analogous to the spinless case [53]. In analogy with Ref. [66], we conjecture that the transverse ( $z = 2$ ) fluctuations will give a finite anomalous dimension  $\eta_\psi$  to the electron propagator, replacing the denominator  $\xi_{\mathbf{k}}^2$  in Eq. (2.76) by  $|\xi_{\mathbf{k}}|^{2-\eta_\psi}$ .

In the nematic phase, the longitudinal modes are gapped [see Eq. (2.63)] and one must look at the effect of the transverse Goldstone modes described by the inverse propagator (2.62). Because the symmetry generator  $J_z$  that is broken in the nematic phase does not commute with translations, on general grounds one expects non-Fermi liquid behavior in the nematic phase as well [67]. By contrast with the electron self-energy at the critical point (2.72)-(2.73) however, we expect the self-energy in the nematic phase to reflect the broken rotational symmetry.

To estimate the self-energy in the nematic phase, we observe that on the FS  $|\mathbf{k}| = k_F$ , the electron Green's function appearing in Eq. (2.71) can be approximated by

$$\mathcal{G}_0(\mathbf{k} - \mathbf{q}, ik_n - iq_n) \approx \frac{1}{2} \frac{1 + \hat{\mathbf{z}} \cdot (\boldsymbol{\sigma} \times \hat{\mathbf{k}})}{ik_n - iq_n + v_F \hat{\mathbf{k}} \cdot \mathbf{q}}, \quad (2.77)$$

since the momentum  $\mathbf{q}$  of the collective mode is much smaller than the Fermi momentum. Here we assume we are close to the quantum critical point such that the distortion of the FS is small and can be neglected in the calculation of the self-energy; this is an  $\mathcal{O}(\bar{n})$  effect, and can be understood in mean-field theory (Sec. 2.2.2), whereas the breakdown of Fermi liquid theory in the nematic phase appears at “zeroth” order in  $\bar{n}$  as will be seen. In the low-energy limit (i.e., on the FS  $k_n \rightarrow 0$ ) Eq. (2.77) is peaked at  $\theta_{\mathbf{q}} = \theta_{\mathbf{k}} \pm \pi/2$ , thus in

Eq. (2.71) one can replace  $\theta_{\mathbf{q}}$  in the Goldstone mode propagator (2.62) by  $\theta_{\mathbf{k}} \pm \pi/2$  [68, 69],

$$\chi_{\perp}^{-1}(\mathbf{q}, iq_n) \approx \kappa q^2 + \mathcal{N}(\mu)|s| \cos^2 2\theta_{\mathbf{k}}. \quad (2.78)$$

We obtain

$$\begin{aligned} \Sigma(\mathbf{k}, ik_n) &= (1 - \sigma_y \cos 3\theta_{\mathbf{k}} - \sigma_x \sin 3\theta_{\mathbf{k}}) |\cos 2\theta_{\mathbf{k}}|^{-2/3} \\ &\times \Sigma_0(\mathbf{k}, ik_n), \end{aligned} \quad (2.79)$$

where  $\Sigma_0$  is defined in Eq. (2.73). Ignoring the lower helicity branch, we obtain the Green's function

$$\mathcal{G}(\mathbf{k}, ik_n) \approx \frac{1}{2} \frac{1 + \hat{\mathbf{z}} \cdot (\boldsymbol{\sigma} \times \hat{\mathbf{k}})}{2i\omega_0^{1/3} |\cos 2\theta_{\mathbf{k}}|^{4/3} |k_n|^{2/3} \text{sgn } k_n - \xi_{\mathbf{k}}}, \quad (2.80)$$

and the spectral function

$$A(\mathbf{k}, \omega) \sim \frac{1}{2} \left(1 + \hat{\mathbf{z}} \cdot (\boldsymbol{\sigma} \times \hat{\mathbf{k}})\right) \frac{\omega_0^{1/3} |\cos 2\theta_{\mathbf{k}}|^{4/3} |\omega|^{2/3}}{\xi_{\mathbf{k}}^2}, \quad (2.81)$$

which are analogous to the spinless results [53] apart from the helicity structure. Equations (2.79)-(2.81) hold for generic angles  $\theta_{\mathbf{k}} \neq \pm\pi/4, \pm 3\pi/4$  on the FS away from the principal axes of the nematic. Along the principal axes  $\theta_{\mathbf{k}} = \pm\pi/4, \pm 3\pi/4$ , we find that after projection to the upper helicity branch the self-energy scales as  $\sim |\omega|^{3/2}$ , as in Ref. [53], corresponding to long-lived quasiparticles along those directions. Equations (2.76) and (2.81) correspond to a ‘‘helical non-Fermi liquid’’ in which the destruction of long-lived quasiparticles over most (in the nematic phase) or all (at the quantum critical point) of the FS coexists with a Berry phase of  $\pi$  in spin space.

## 2.4 Conclusion

In this chapter, we have developed a field-theoretic description of nematic order for a single Dirac cone on the surface of a 3D topological insulator. Due to spin-orbit coupling present in topological insulators, the nematic order parameter for helical Fermi liquids involves both spin and momentum, in contrast to the case of regular Fermi liquids which just involves momentum. In the undoped limit at zero temperature, we found a first-order isotropic-nematic transition at the mean-field level, in contrast with the expectation of a continuous transition based on Landau theory. The transition becomes continuous at a finite-temperature tricritical point. In the doped limit the transition was found to be continuous even at zero temperature. The spin-orbit coupled nature of nematic order was shown to lead to the partial breakdown of spin-momentum locking on the distorted FS and anisotropy in the in-plane spin susceptibility in both the doped and undoped limits. The number and dispersion of collective modes in the doped limit, as well as the prediction of non-Fermi liquid behavior at the quantum critical point and in the nematic phase, were seen to be the same as for spin rotationally invariant nematic Fermi fluids. However, in the helical case it was shown that nematic fluctuations can induce spin fluctuations, owing once again to the spin-orbit coupled nature of nematic order in these systems.

## Chapter 3

# Short-range correlated disorder and Dirac semimetal- superconductor transition

### 3.1 Introduction

In this and the following chapter, we study the effects of disorder on quantum phase transitions in Dirac fermion systems.

Disorder is ubiquitous in real physical systems, and almost inevitable in engineered ones. It may come as point-like defects (vacancies and interstitials), line defects (edge and screw dislocations), or volume defects (e.g., grain boundaries and voids). In many cases, disorder can be considered stationary. In this case, it is called quenched disorder, on which we focus in this thesis. The study of the effects of disorder is a broad topic. In particular, it may lead to spatial localization of the single-particle wavefunctions in noninteracting systems [70]. Localization also may happen in interacting systems and is dubbed many-body localization [71]. Disorder may lead to unique random phases of matter [72–76], destabilize phases and transitions of pure systems, or round sharp features of phase transitions. While other cases are possible (e.g., disorder in the phase of a complex order parameter

or directions of easy axes in magnets), disorder often enters into a system's effective Lagrangian in the form of random-field or random-mass terms. The former has the form  $-\mathbf{h}(\mathbf{r}) \cdot \boldsymbol{\phi}(\mathbf{r})$ , where  $\boldsymbol{\phi}(\mathbf{r})$  is an order parameter field, and  $\mathbf{h}(\mathbf{r})$  is a spatially random field. This term usually emerges when disorder locally breaks the internal symmetry of the order parameter field [77]. The second type of disorder, random-mass disorder, also called random- $T_c$  disorder, does not break the symmetry of the order parameter, and introduces a spatially random correction to the mass term  $\delta r(\mathbf{r})\boldsymbol{\phi}(\mathbf{r})^2$  into the Lagrangian. It has been shown that random-field disorder prevents spontaneous symmetry breaking in  $d \leq 2$  and  $d \leq 4$  spatial dimensions for discrete and continuous symmetries of the order parameter, respectively [78–81].

Random-mass disorder does not destabilize phases but may destabilize phase transitions. The Harris criterion [82] characterizes the stability of clean critical points, both classical and quantum: if  $d\nu > 2$ , where  $\nu$  is the correlation length exponent, the clean critical point is stable. If it is stable, the disorder strength flows (in the RG sense) to zero in the long-wavelength limit, and the system is self-averaging, i.e., the width of the distribution of physical observables across different realizations of disorder is zero in the thermodynamic limit. If the clean critical point is unstable, there are two alternatives. In the first, the disorder strength flows to infinity, and in the second, the disorder strength is finite in the long-wavelength limit corresponding to a finite-disorder random critical point. The Chayes inequality [83] states that the correlation length exponent at such a random critical point should itself obey the Harris criterion.

With the discovery of materials with a pseudo-relativistic spectrum, much research has been done on the effects of disorder in such materials, both for Weyl [84–99] and Dirac [100–105] semimetals. However, most studies focused on noninteracting systems. The interplay of disorder and interactions has been considered, in particular, in Refs. [106–108] and Refs. [109–111] for the surface of 3D topological insulators and superconductors, respectively; in Ref. [112] for the integer quantum Hall plateau transition; in Refs. [113–118] for graphene. Recent work has also demonstrated the possibility of novel critical

phases in massless (2+1)D relativistic quantum electrodynamics in the presence of quenched disorder [119–121], with possible applications to disordered spin liquids. However, with a few exceptions discussed below, none of the above studies considered the effect of disorder on symmetry-breaking quantum phase transitions, such as those focused on in this thesis.

In this Chapter, we consider the interplay of disorder and interactions on the semimetal-superconductor quantum phase transition in a system of 2D Dirac fermions at charge neutrality. In the BCS theory of superconductivity, the transition temperature  $T_c \sim \exp\left(-\frac{1}{\mathcal{N}(\mu)g}\right)$ , where  $\mathcal{N}(\mu)$  is the density of states at the Fermi level and  $g$  is the BCS coupling. Thus, at zero temperature, one expects that the system is always in the superconducting state, eliminating the possibility of a quantum phase transition. However, naively, from the given formula, for a vanishing density of states at the Fermi level, one concludes that  $T_c$  approaches zero, and a quantum phase transition is possible.

The effect of quenched disorder on the semimetal-superconductor quantum phase transition of 2D Dirac fermions at charge neutrality has already been partially addressed using mean-field [106, 118] and standard epsilon expansion [106] methods. Here we revisit this problem using the double epsilon expansion [122–124] which is better suited to the study of quantum critical phenomena in disordered systems. While the double epsilon expansion has traditionally been applied to purely bosonic systems, e.g., the  $O(n)$  vector model with random- $T_c$  disorder [122–124], here we show that it can be applied to fermionic quantum critical points (QCPs) described by quantum field theories of the Gross-Neveu-Yukawa (GNY) type [125, 126], exploiting the fact that, like the  $O(n)$  vector model, such theories have an upper critical dimension of four absent quenched disorder. We consider a model of 2D Dirac semimetal with  $N$  flavors of two-component Dirac fermions, and show that at leading (one-loop) order in the double epsilon expansion, a Harris-stable clean QCP gives way beyond a certain critical disorder strength to a finite-disorder QCP [127] with non-Gaussian critical exponents and noninteger dynamic critical exponent  $z > 1$ . Furthermore, Dirac fermions and bosonic order parameter fluctuations are strongly coupled at this QCP. The latter is therefore a first example of *disordered fermionic QCP*, which combines the phenomenology

of finite-disorder bosonic QCPs [128] with that of (clean) fermionic QCPs, where coupling between bosonic order parameter fluctuations and gapless fermionic modes leads to new universality classes beyond those of the purely bosonic Landau-Ginzburg-Wilson paradigm. We do not discuss the possibility of Griffiths phases due to rare regions effects [77]. However, according to the classification developed in Refs. [129–131], the problem we consider belongs to class A, in which the effective rare region dimensionality  $d_{RR}$  is less than the lower critical dimension  $d_c^-$ . In our case, we have  $d_{RR} = 1$  (disorder is completely correlated in time dimension) and  $d_c^- = 2$ . In this class, Griffiths singularities [132–134] are essential singularities, and rare region effects are exponentially weak.

The rest of this chapter is structured as follows. In Sec. 3.2 we present our model for the semimetal-superconductor transition in the presence of quenched disorder. In Sec. 3.3 we outline the basic steps of the renormalization group (RG) approach in the double epsilon expansion and present the beta functions describing the flow under renormalization of various coupling constants in the theory. In Sec. 3.4 we find RG fixed points, analyze their stability, and determine how they are connected under the RG flow. In Sec. 3.5 we determine the critical exponents at the various fixed points and derive implications of the RG flow analysis for the phase diagram of the system. A brief conclusion follows in Sec. 3.6, and the details of derivations are contained in Appendix B.

## 3.2 Model

We consider a model of  $N$  flavors of two-component Dirac fermions  $\psi^1, \psi^2, \dots, \psi^N$  in 2+1 dimensions, which in the absence of interactions are described by the low-energy imaginary-time Lagrangian

$$\mathcal{L}_\psi = \sum_{i=1}^N i\bar{\psi}^i(\gamma_0\partial_\tau + c_f\boldsymbol{\gamma}\cdot\nabla)\psi^i, \quad (3.1)$$

where  $\gamma_0$  and  $\boldsymbol{\gamma} = (\gamma_1, \gamma_2)$  denote Euclidean  $2 \times 2$  Dirac matrices in 2+1 dimensions, obeying the  $SO(3)$  Clifford algebra  $\{\gamma_\mu, \gamma_\nu\} = 2\delta_{\mu\nu}\mathbb{I}_{2 \times 2}$ ,  $\mu, \nu = 0, 1, 2$ , with  $\mathbb{I}_{2 \times 2}$  the  $2 \times 2$  identity

matrix, and  $\bar{\psi}^i = -i\psi^{i\dagger}\gamma_0$  is the Dirac conjugate. In a condensed matter system on a lattice the  $N$  flavors would correspond to  $N$  symmetry-related linear band crossings in the Brillouin zone, with a common Dirac velocity  $c_f$ . We also assume the underlying microscopic model is particle-hole symmetric, which excludes any possible tilt of the Dirac cones. For a 3D topological insulator the two components of the spinor  $\psi^i$  correspond to physical spin; for a 2D Dirac semimetal like graphene an equivalent four-component formulation is more natural (see Appendix B.9).

We will be interested in superconducting instabilities, and consider subjecting the Dirac fermions to sufficiently short-range attractive interactions. At low energies, the various possible superconducting order parameters will transform according to irreducible representations of the symmetry group of (3.1). We will assume the microscopic interactions are such that in a certain range of couplings they favor pairing in the flavor-symmetric,  $s$ -wave, spin-singlet channel, with an order parameter

$$\sum_{i=1}^N \langle \psi^{iT} i\sigma_2 \psi^i \rangle, \quad (3.2)$$

where  $T$  denotes the transpose and  $\sigma_1, \sigma_2, \sigma_3$  are the Pauli spin matrices, which act on the physical spin degrees of freedom. We consider first the clean limit, and assume that the chemical potential is exactly at the Dirac point. The transition from Dirac semimetal to superconductor at zero temperature proceeds via a QCP at finite attraction strength, since the density of states of the Dirac semimetal vanishes at the Fermi energy [106, 135–139]. The critical behavior at the QCP is governed by the so-called chiral XY GNY model [126],

$$\mathcal{L}_{\text{clean}} = \mathcal{L}_\psi + \mathcal{L}_\phi + \mathcal{L}_{\phi\psi\psi}, \quad (3.3)$$

where

$$\mathcal{L}_\phi = |\partial_\tau \phi|^2 + c_b^2 |\nabla \phi|^2 + r |\phi|^2 + \lambda^2 |\phi|^4, \quad (3.4)$$

$$\mathcal{L}_{\phi\psi\psi} = h\phi^* \sum_{i=1}^N \psi^{iT} i\sigma_2 \psi^i + \text{H.c.} \quad (3.5)$$

The Lagrangian (3.3) describes gapless Dirac fermions interacting with bosonic order parameter fluctuations  $\phi$  with velocity  $c_b$ ;  $r$  is a tuning parameter for the transition ( $r > 0$  in the semimetal phase,  $r < 0$  in the superconducting phase, and  $r = 0$  at criticality), and the coupling constants  $\lambda^2$  and  $h$  obey  $\lambda^2 > 0$  and  $h^2 > 0$ . The absence of a term  $\phi^* \partial_\tau \phi$  linear in time derivatives is a consequence of the assumed particle-hole symmetry of the underlying microscopic model. The effective low-energy Lagrangian (3.3) exhibits an emergent  $O(N)$  flavor symmetry under  $\psi^i \rightarrow W_{ij} \psi^j$ , with  $W$  an arbitrary orthogonal  $N \times N$  matrix, and its critical properties for any  $N$  can be accessed via an RG analysis in  $D = 4 - \epsilon$  space-time dimensions [126, 139–141]. For  $N = 1$ , the model is applicable to the superconducting transition on the surface of a 3D topological insulator with a single Dirac cone, and features a QCP with emergent  $\mathcal{N} = 2$  supersymmetry [140, 142–149]. For  $N = 4$ , the model describes the superconducting transition in graphene [139]. Also, for  $N = 4$  and  $N = 2$ , the model describes a quantum phase transition from a Dirac semimetal (spinful or spinless, respectively) to an insulator with Kekulé valence-bond-solid (VBS) order on the honeycomb lattice [139, 150], or to an insulator with columnar VBS order on the  $\pi$ -flux square lattice [151]. The spontaneously broken symmetries in those examples are discrete  $\mathbb{Z}_3$  and  $\mathbb{Z}_4$  point group symmetries, respectively, but those anisotropies are irrelevant perturbations at the  $O(2)$ -symmetric GNY fixed point, at least in the large- $N$  limit [152, 153]. However, in those VBS realizations of chiral XY GNY criticality, spatial randomness necessarily couples linearly to the VBS order parameter: it thus acts as random-field disorder, which destroys the  $d = 2$  critical point. In Appendix B.9 we establish an equivalence between the two-component formulation with Yukawa coupling to the Majorana mass used here and in Ref. [147], and a four-component formulation with normal and axial Dirac masses typically

used in discussions of graphene [139, 140], where the  $U(1)$  symmetry is realized as an axial symmetry.

Focusing on the superconducting transition, we now consider the effect of quenched disorder on this transition. We assume a random spin-independent perturbation that is smooth on the scale of the microscopic lattice constant, i.e., that is sufficiently long-range so as to not scatter Dirac fermions between different valleys (see, e.g., Ref. [154]). Furthermore, we assume exact particle-hole symmetry at the microscopic level. An example type of microscopic disorder in graphene that preserves that symmetry is random-bond disorder, i.e., randomness in the nearest-neighbor fermion hopping [155]. The perturbation then couples identically to all fermion flavors,

$$\mathcal{L}_{\text{dis}} = V(\mathbf{x}) \sum_{i=1}^N \bar{\psi}^i M \psi^i, \quad (3.6)$$

where the matrix  $M$  depends on the precise type of disorder, and  $V(x)$  is a random variable. Proceeding as in Ref. [106], we assume a Gaussian disorder distribution with zero mean and variance  $\Delta_V$ ,

$$P[V(\mathbf{x})] \propto e^{-\int d^2\mathbf{x} V(\mathbf{x})^2/2\Delta_V}, \quad (3.7)$$

and perform the quenched disorder average using the replica trick (see Appendix B.1 and Refs. [30, 156, 157]). This generates a four-fermion interaction nonlocal in time,

$$S_{\text{dis,f}} = -\frac{\Delta_V}{2} \sum_{a,b=1}^m \sum_{i,j=1}^N \int d^2\mathbf{x} d\tau d\tau' (\bar{\psi}_a^i M \psi_a^i)(\mathbf{x}, \tau) (\bar{\psi}_b^j M \psi_b^j)(\mathbf{x}, \tau'), \quad (3.8)$$

where the replica limit  $m \rightarrow 0$  is to be taken at the end of the calculation. This effective interaction preserves all the symmetries of the clean limit, including translation symmetry and  $O(N)$  flavor symmetry. As will be explained in greater detail in Sec. 3.3, in the context of an RG analysis near four dimensions the four-fermion interaction term (3.8) is strongly irrelevant in perturbation theory, and thus would not appear to affect critical behavior in the

scaling limit. However, at two-loop order this interaction generates an effective four-boson interaction,

$$S_{\text{dis,b}} = -\frac{\Delta}{2} \sum_{a,b=1}^m \int d^2\mathbf{x} d\tau d\tau' |\phi_a|^2(\mathbf{x}, \tau) |\phi_b|^2(\mathbf{x}, \tau'), \quad (3.9)$$

where  $\Delta \propto h^4 \Delta_V$  at leading order in perturbation theory (Fig. 3.1). The four-boson interaction (3.9) is identical to one generated by Gaussian disorder in the coefficient of the  $|\phi|^2$  term in Eq. (4.2), i.e., random- $T_c$  disorder. By contrast with Eq. (3.8), this interaction is relevant below four dimensions [158] and must be included in an RG analysis of the critical behavior, to which we now turn.

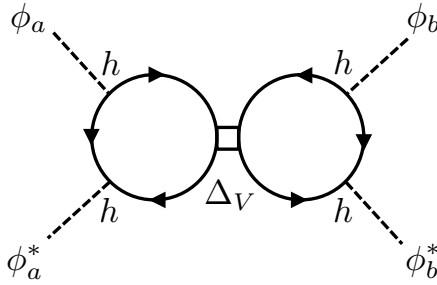


Figure 3.1: Random- $T_c$  disorder is generated from random potential disorder at two-loop order (dotted lines: order parameter fluctuations, solid lines: fermions, box: disorder-induced four-fermion coupling).

### 3.3 RG in the double epsilon expansion

In the limit of a unique fermion flavor  $N = 1$ , the problem so far described has been studied in Ref. [106] using the  $\epsilon$  expansion in  $D = 4 - \epsilon$  spacetime dimensions. In this expansion the four-fermion coupling  $\Delta_V$  in Eq. (3.8) has an engineering dimension  $-1 + \epsilon$ , and is thus strongly irrelevant at the Gaussian fixed point for small  $\epsilon$ , while the induced four-boson coupling  $\Delta$  in Eq. (3.9) has an engineering dimension  $1 + \epsilon$ , which is strongly relevant at the Gaussian fixed point. In the  $\epsilon$  expansion one thus finds that disorder is relevant at the clean

QCP also [106], since dimensions of operators at this QCP only receive  $\mathcal{O}(\epsilon)$  corrections relative to their engineering dimensions. In fact, the conventional  $\epsilon$  expansion below four dimensions generally predicts runaway flows near QCPs with random- $T_c$  disorder [30]. While such runaway flows are often interpreted as an indication that critical behavior is destroyed, they really only signal the breakdown of the conventional  $\epsilon$  expansion as well as the need for another small parameter with which to tame RG flows generated by disorder. Here we will follow one particular approach to fulfill this need, which consists in working in  $d = 4 - \epsilon$  spatial and  $\epsilon_\tau$  time dimensions [122–124]. In  $d = 4 - \epsilon$  spatial and  $\epsilon_\tau$  imaginary time dimensions, the order parameter field  $\phi$  and the fermion field  $\psi$  have engineering dimensions  $\Delta_\phi = (2 - \epsilon + \epsilon_\tau)/2$  and  $\Delta_\psi = (3 - \epsilon + \epsilon_\tau)/2$ , respectively. Thus, the couplings  $\lambda^2$  and  $\Delta$  have mass dimensions  $\epsilon - \epsilon_\tau$  and  $\epsilon$ ; and the Yukawa coupling  $h$  has mass dimension  $(\epsilon - \epsilon_\tau)/2$ . Treating  $\epsilon$  and  $\epsilon_\tau$  as small parameters, a controlled perturbative RG analysis can be performed. In the present case, to access the physical problem in 2+1 dimensions one extrapolates  $\epsilon \rightarrow 2$  and  $\epsilon_\tau \rightarrow 1$ . The four-fermion disorder-induced coupling  $\Delta_V$  in Eq. (3.8) has dimension  $d + 2\epsilon_\tau - [\psi^\dagger \psi \psi^\dagger \psi] = -2 + \epsilon$ , which is strongly irrelevant for small  $\epsilon, \epsilon_\tau$ , and thus we may exclude  $\Delta_V$  from the consideration. (For a study of quantum critical phenomena in disordered 3D Dirac semimetals using a different type of double epsilon expansion, see Ref. [159].)

For an  $O(n)$  generalization of scalar  $\phi^4$  theory with  $n > 1$ , a stable DFP with  $\lambda_*^2 \sim \mathcal{O}(\epsilon, \epsilon_\tau)$ ,  $\Delta_* \sim \mathcal{O}(\epsilon, \epsilon_\tau)$  on the critical hypersurface  $r = 0$  is found at one-loop order, with critical exponents <sup>1</sup>:

$$\nu = \frac{1}{2} + \frac{3n\epsilon + (2n + 4)\epsilon_\tau}{32(n - 1)}, \quad (3.10)$$

$$z = 1 + \frac{(4 - n)\epsilon + (2n + 4)\epsilon_\tau}{16(n - 1)}. \quad (3.11)$$

For  $n = 2$ , and extrapolating  $\epsilon_\tau$  to 1 and  $\epsilon$  to 2 or 1, relevant to the boson superfluid-Mott

---

<sup>1</sup>The one-loop exponents (3.10-3.11) correspond to those given in Refs. [160] and [124], and we have also independently reproduced those results. Note that the result for  $\nu$  quoted in Eq. (21.22) of Ref. [30] is the incorrect result for  $\nu_\perp = (2 - \gamma_{\phi^2}^*)^{-1}$  given in the original paper by Boyanovsky and Cardy [123], which was later corrected in Refs. [124, 160].

glass transition in (2+1)D and (3+1)D, respectively, one obtains exponents in reasonable agreement with those found in numerical Monte Carlo (MC) simulations (Table 3.1).

	MC [161, 162]	$\mathcal{O}(\epsilon, \epsilon_\tau)$
$\nu$ , (2+1)D	1.16(5)	1.125
$z$ , (2+1)D	1.52(3)	1.75
$\nu$ , (3+1)D	0.90(5)	0.9375
$z$ , (3+1)D	1.67(6)	1.625

Table 3.1: Critical exponents for the boson superfluid-Mott glass transition.

### 3.3.1 Bare vs renormalized actions

Focusing first on the critical theory  $r = 0$ , we thus study the replicated action

$$\begin{aligned}
S = \sum_a \int d^d \mathbf{x} d^{\epsilon_\tau} \tau & \left( i\bar{\psi}_a(\not{\partial}_\tau + c_f \not{\nabla})\psi_a + |\partial_\tau \phi_a|^2 + c_b^2 |\nabla \phi_a|^2 + \lambda^2 |\phi_a|^4 + h(\phi_a^* \psi_a^T i\sigma_2 \psi_a + \text{H.c.}) \right) \\
& - \frac{\Delta}{2} \sum_{ab} \int d^d \mathbf{x} d^{\epsilon_\tau} \tau d^{\epsilon_\tau} \tau' |\phi_a|^2(\mathbf{x}, \tau) |\phi_b|^2(\mathbf{x}, \tau'), \tag{3.12}
\end{aligned}$$

where  $a, b = 1, \dots, m$  are replica indices, we denote  $\not{\partial}_\tau \equiv \gamma_0 \partial_\tau$  and  $\not{\nabla} \equiv \boldsymbol{\gamma} \cdot \nabla$  for simplicity, and we group the  $N$  fermion flavors for each replica  $a$  into an  $O(N)$  vector,  $\psi_a \equiv (\psi_a^1, \psi_a^2, \dots, \psi_a^N)$ . By rescaling the fermion and boson fields as well as the time coordinate, and redefining the couplings in the Lagrangian, one can eliminate the velocities  $c_f$  and  $c_b$  from the Lagrangian at the expense of multiplying  $|\partial_\tau \phi_a|^2$  by the ratio  $(c_f/c_b)^2$ , which we will denote  $c^2$ .

To carry out an RG analysis of the above theory, we compare the bare action

$$\begin{aligned}
S_B = \sum_a \int d^d \mathbf{x}_B d^{\epsilon_\tau} \tau_B & \left( i\bar{\psi}_{a,B}(\not{\partial}_{\tau_B} + \not{\nabla}_B)\psi_{a,B} + c_B^2 |\partial_{\tau_B} \phi_{a,B}|^2 + |\nabla_B \phi_{a,B}|^2 + \lambda_B^2 |\phi_{a,B}|^4 \right. \\
& \left. + h_B(\phi_{a,B}^* \psi_{a,B}^T i\sigma_2 \psi_{a,B} + \text{H.c.}) \right) - \frac{\Delta_B}{2} \sum_{ab} \int d^d \mathbf{x}_B d^{\epsilon_\tau} \tau_B d^{\epsilon_\tau} \tau'_B |\phi_{a,B}|^2(\mathbf{x}_B, \tau_B) |\phi_{b,B}|^2(\mathbf{x}_B, \tau'_B), \tag{3.13}
\end{aligned}$$

to the renormalized action

$$\begin{aligned}
S = \sum_a \int d^d \mathbf{x} d^{\epsilon_\tau} \tau & \left( Z_1 i \bar{\psi}_a \not{\partial}_\tau \psi_a + Z_2 i \bar{\psi}_a \nabla \psi_a + Z_3 c^2 |\partial_\tau \phi_a|^2 + Z_4 |\nabla \phi_a|^2 + Z_5 \lambda^2 \mu^{\epsilon - \epsilon_\tau} |\phi_a|^4 \right. \\
& \left. + Z_6 h \mu^{(\epsilon - \epsilon_\tau)/2} (\phi_a^* \psi_a^T i \sigma_2 \psi_a + \text{H.c.}) \right) - Z_7 \frac{\Delta}{2} \mu^\epsilon \sum_{ab} \int d^d \mathbf{x} d^{\epsilon_\tau} \tau d^{\epsilon_\tau} \tau' |\phi_a|^2(\mathbf{x}, \tau) |\phi_b|^2(\mathbf{x}, \tau'),
\end{aligned} \tag{3.14}$$

where the renormalized couplings  $c^2$ ,  $\lambda^2$ ,  $h$ ,  $\Delta$  are dimensionless, and we have introduced a renormalization scale  $\mu$ . The renormalization constants  $Z_1, \dots, Z_7$  are to be calculated in perturbation theory. The bare and renormalized kinetic terms for the fermion match if one takes  $\mathbf{x}_B = \mathbf{x}$ ,  $\tau_B = \eta\tau$ , and

$$\sqrt{Z_1} \psi_a(\mathbf{x}, \tau) = \eta^{(\epsilon_\tau - 1)/2} \psi_{a,B}(\mathbf{x}_B, \tau_B), \tag{3.15}$$

$$\sqrt{Z_2} \psi_a(\mathbf{x}, \tau) = \eta^{\epsilon_\tau/2} \psi_{a,B}(\mathbf{x}_B, \tau_B), \tag{3.16}$$

which implies  $\eta = Z_2/Z_1$ . The dynamic critical exponent  $z$  describes the relative scaling of space and time, which in dimensionless units reads  $\mu\tau \sim (\mu|\mathbf{x}|)^z$ . Defining the anomalous dimensions

$$\gamma_i = \frac{d \ln Z_i}{d \ln \mu}, \quad i = 1, \dots, 7, \tag{3.17}$$

this implies [120]

$$z = 1 + \gamma_1 - \gamma_2, \tag{3.18}$$

since the bare coordinate  $\mathbf{x}_B$  and time  $\tau_B$  do not depend on  $\mu$ . Likewise, the  $|\nabla\phi|^2$  terms match if one requires

$$\sqrt{Z_4} \phi_a(\mathbf{x}, \tau) = \eta^{\epsilon_\tau/2} \phi_{a,B}(\mathbf{x}_B, \tau_B). \tag{3.19}$$

From Eq. (3.15)-(3.16) and (3.19) we find that the bare and renormalized coupling constants are related by

$$c^2 = Z_3^{-1} Z_4 \left( \frac{Z_1}{Z_2} \right)^2 c_B^2, \quad (3.20)$$

$$\lambda^2 = \mu^{-(\epsilon - \epsilon_\tau)} \left( \frac{Z_1}{Z_2} \right)^{\epsilon_\tau} Z_4^2 Z_5^{-1} \lambda_B^2, \quad (3.21)$$

$$h^2 = \mu^{-(\epsilon - \epsilon_\tau)} \left( \frac{Z_1}{Z_2} \right)^{\epsilon_\tau} Z_2^2 Z_4 Z_6^{-2} h_B^2, \quad (3.22)$$

$$\Delta = \mu^{-\epsilon} Z_4^2 Z_7^{-1} \Delta_B, \quad (3.23)$$

from which we obtain the RG beta functions  $\beta_g \equiv dg/d \ln \mu$ ,  $g \in \{c^2, \lambda^2, h^2, \Delta\}$ ,

$$\beta_{c^2} = (2\gamma_1 - 2\gamma_2 - \gamma_3 + \gamma_4)c^2, \quad (3.24)$$

$$\beta_{\lambda^2} = (-\epsilon + \epsilon_\tau) + \epsilon_\tau(\gamma_1 - \gamma_2) + 2\gamma_4 - \gamma_5 \lambda^2, \quad (3.25)$$

$$\beta_{h^2} = (-\epsilon + \epsilon_\tau) + \epsilon_\tau(\gamma_1 - \gamma_2) + 2\gamma_2 + \gamma_4 - 2\gamma_6 h^2, \quad (3.26)$$

$$\beta_\Delta = (-\epsilon + 2\gamma_4 - \gamma_7)\Delta, \quad (3.27)$$

using the fact that the bare couplings  $c_B^2$ ,  $\lambda_B^2$ ,  $h_B^2$ , and  $\Delta_B$  are independent of  $\mu$ . For  $\epsilon > \epsilon_\tau > 0$ , the couplings  $\lambda^2$ ,  $h^2$ , and  $\Delta$  are relevant at the Gaussian fixed point, and one may hope to find a controlled fixed point in perturbation theory for small  $\epsilon, \epsilon_\tau$ .

To determine the correlation length exponent  $\nu$  one needs to compute the RG eigenvalue of the scalar field mass term  $|\phi|^2$  at the QCP, which is done by adding the term  $\sum_a r_B |\phi_{a,B}|^2$  to the bare Lagrangian and  $\sum_a Z_r r \mu^2 |\phi_a|^2$  to its renormalized counterpart. Equating the two gives the relation

$$r = \mu^{-2} Z_4 Z_r^{-1} r_B, \quad (3.28)$$

which yields the usual expression for the inverse correlation length exponent [163],

$$\nu^{-1} = 2 - \gamma_4 + \gamma_r, \quad (3.29)$$

defining  $\gamma_r = d \ln Z_r / d \ln \mu$  as for the other renormalization constants. Finally, the fermion  $\gamma_\psi$  and boson  $\gamma_\phi$  anomalous dimensions are obtained from  $\gamma_{\psi,\phi} = d \ln Z_{\psi,\phi} / d \ln \mu$  where we define  $Z_\psi$  and  $Z_\phi$  via

$$\psi_{a,B}(\mathbf{x}_B, \tau_B) = \sqrt{Z_\psi} \psi_a(\mathbf{x}, \tau), \quad (3.30)$$

$$\phi_{a,B}(\mathbf{x}_B, \tau_B) = \sqrt{Z_\phi} \phi_a(\mathbf{x}, \tau). \quad (3.31)$$

Using Eq. (3.15)-(3.16) and (3.19) we find

$$\gamma_\psi = \gamma_2 + \epsilon_\tau(z - 1), \quad (3.32)$$

$$\gamma_\phi = \gamma_4 + \epsilon_\tau(z - 1). \quad (3.33)$$

### 3.3.2 Renormalization constants

To derive the beta functions (3.24)-(3.27) one must first compute the renormalization constants  $Z_1, \dots, Z_7$ , and to determine the correlation length exponent one must calculate  $Z_r$ . Here we adopt the field-theoretic approach, with renormalization constants calculated at one-loop order in the modified minimal subtraction ( $\overline{\text{MS}}$ ) scheme with dimensional regularization. As is customary for these types of problems (see, e.g., Ref. [140]), we adopt a naive dimensional-regularization prescription according to which all Dirac matrices anti-commute [164] and spinor traces over products of an odd number of Dirac matrices vanish<sup>2</sup>. With the dimensional-regularization prescription just mentioned, perturbative results only depend on the total number of (complex) fermionic degrees of freedom, i.e., the dimension of

---

<sup>2</sup>In Ref. [140], a modified prescription that includes  $\text{tr} \gamma_\mu \gamma_\nu \gamma_\lambda \propto \epsilon_{\mu\nu\lambda}$ , which holds in three dimensions with a 2D representation of the Clifford algebra, was shown to give results at variance with those obtained with the naive prescription used here, but only starting at four-loop order. Since we perform calculations at one-loop order only, the naive prescription is sufficient for our purposes.

the chosen representation of the Dirac algebra, times the number of flavors. The Feynman rules associated with the massive replicated action are illustrated schematically in Fig. 3.2; the fermion and boson propagators are given by

$$G_{ab}^{ij}(p) = \langle \psi_a^i(p) \bar{\psi}_b^j(p) \rangle = \delta_{ab} \delta^{ij} \frac{\not{p}}{p^2}, \quad (3.34)$$

$$D_{ab}(p) = \langle \phi_a(p) \phi_b^*(p) \rangle = \frac{\delta_{ab}}{c^2 p_0^2 + \mathbf{p}^2 + \mu^2 r}, \quad (3.35)$$

denoting the spacetime momentum by  $p = (p_0, \mathbf{p})$  and  $\not{p} = \gamma_\mu p_\mu$ .

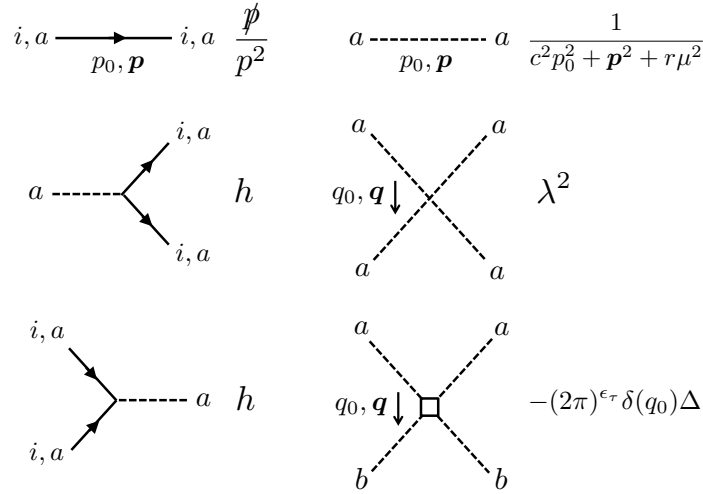


Figure 3.2: Schematic Feynman rules associated with the replicated action;  $a, b$  are replica indices,  $i$  is a fermion flavor index, and  $q_0, \mathbf{q}$  denotes the frequency-momentum transfer from top to bottom. The extra  $\delta(q_0)$  factor prevents frequency/energy transfer between replicas which is a direct consequence of the elastic scattering off the random perturbation.

In the  $\overline{\text{MS}}$  scheme, the renormalization constants are computed order by order in the loop expansion by writing  $Z_i = 1 + \delta Z_i$ ,  $i = 1, \dots, 7, r$  and demanding that the  $\delta Z_i$  cancel the ultraviolet divergences of the one-particle irreducible (1PI) effective action. In dimensional regularization, this means that at one-loop order the  $\delta Z_i$ , which are computed from the Feynman diagrams in Fig. 3.3, contain simple poles in  $\epsilon$  and  $\epsilon - \epsilon_\tau$ . We present

the details of the calculation in Appendix B; here we simply quote the results (after taking the replica limit  $m \rightarrow 0$ ):

$$Z_1 = 1 - \frac{8h^2}{\epsilon - \epsilon_\tau} f(c^2), \quad (3.36)$$

$$Z_2 = 1 - \frac{4h^2}{\epsilon - \epsilon_\tau}, \quad (3.37)$$

$$Z_3 = 1 - \frac{2\Delta}{\epsilon} - \frac{4Nh^2c^{-2}}{\epsilon - \epsilon_\tau}, \quad (3.38)$$

$$Z_4 = 1 - \frac{4Nh^2}{\epsilon - \epsilon_\tau}, \quad (3.39)$$

$$Z_5 = 1 + \frac{20\lambda^2}{\epsilon - \epsilon_\tau} - \frac{16Nh^4\lambda^{-2}}{\epsilon - \epsilon_\tau} - \frac{12\Delta}{\epsilon}, \quad (3.40)$$

$$Z_6 = 1, \quad (3.41)$$

$$Z_7 = 1 + \frac{16\lambda^2}{\epsilon - \epsilon_\tau} - \frac{8\Delta}{\epsilon}, \quad (3.42)$$

$$Z_r = 1 + \frac{8\lambda^2}{\epsilon - \epsilon_\tau} - \frac{2\Delta}{\epsilon}, \quad (3.43)$$

where we have rescaled the coupling constants according to  $g/(4\pi)^2 \rightarrow g$ ,  $g \in \{\lambda^2, h^2, \Delta\}$ , and we define the dimensionless function (see Fig. 3.4),

$$f(c^2) = \frac{c^2(c^2 - 1 - \ln c^2)}{(c^2 - 1)^2}. \quad (3.44)$$

### 3.3.3 Beta functions and anomalous dimensions

To calculate the beta functions, we first use the chain rule to write

$$\gamma_i = \frac{1}{Z_i} \frac{dZ_i}{d \ln \mu} = \frac{1}{Z_i} \sum_g \frac{\partial Z_i}{\partial g} \beta_g, \quad (3.45)$$

for  $i = 1, \dots, 7$  and  $g \in \{c^2, \lambda^2, h^2, \Delta\}$ , which when substituted into the expressions (3.24)-(3.27) gives a linear system of equations for the beta functions. Expanding the beta functions

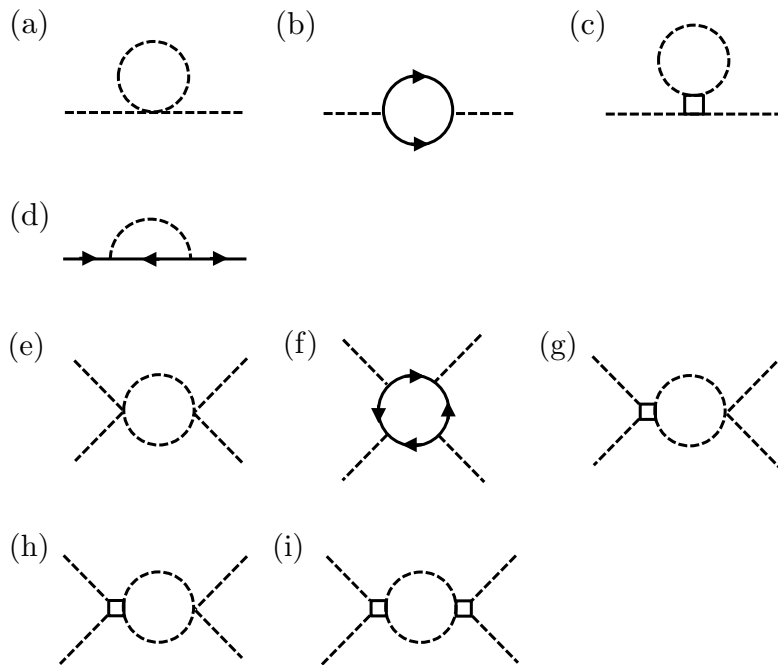


Figure 3.3: One-loop diagrams for the renormalization of (a,b,c) the boson two-point function; (d) the fermion two-point function; (e,f,g) the boson self-interaction  $\lambda^2$ ; (h,i) the disorder strength  $\Delta$ . At this order there is no renormalization of the Yukawa coupling  $h$ .

to quadratic order in the couplings, we find that all poles in  $\epsilon$  and  $\epsilon - \epsilon_\tau$  cancel, and obtain

$$\beta_{c^2} = -2c^2\Delta + 4h^2 [c^2 (4f(c^2) + N - 2) - N], \quad (3.46)$$

$$\beta_{\lambda^2} = -(\epsilon - \epsilon_\tau)\lambda^2 - 12\Delta\lambda^2 + 20\lambda^4 + 8Nh^2\lambda^2 - 16Nh^4, \quad (3.47)$$

$$\beta_{h^2} = -(\epsilon - \epsilon_\tau)h^2 + 4(N + 2)h^4, \quad (3.48)$$

$$\beta_\Delta = -\epsilon\Delta - 8\Delta^2 + 16\Delta\lambda^2 + 8N\Delta h^2. \quad (3.49)$$

Setting  $\epsilon_\tau = 0$  and  $\Delta = 0$ , Eq. (3.48) and (3.47) reduce to the one-loop beta functions of the chiral XY GNY model in the ordinary  $4 - \epsilon$  expansion (e.g., Eq. (19)-(20) in Ref. [141] in the  $e^2 = 0$  limit). Note that the above beta functions are perturbative in  $\lambda^2$ ,  $h^2$ , and  $\Delta$ , but exact in the relative velocity parameter  $c^2$ .

Using Eq. (3.45), from the renormalization constants (3.36)-(3.42) and the beta functions (3.46)-(3.49) we can calculate the anomalous dimensions  $\gamma_i$ , and from those the critical exponents  $\nu^{-1}$ ,  $z$ ,  $\gamma_\psi$ , and  $\gamma_\phi$ . We obtain

$$\nu^{-1} = 2 - 4Nh^2 - 8\lambda^2 + 2\Delta, \quad (3.50)$$

$$z = 1 + 4h^2(2f(c^2) - 1), \quad (3.51)$$

$$\gamma_\psi = 4h^2 [1 + (2f(c^2) - 1)\epsilon_\tau], \quad (3.52)$$

$$\gamma_\phi = 4Nh^2 \left[ 1 + (2f(c^2) - 1) \frac{\epsilon_\tau}{N} \right], \quad (3.53)$$

which are meant to be evaluated at the RG fixed points  $(c_*^2, \lambda_*^2, h_*^2, \Delta_*)$  discussed in the following section. At one-loop order  $h_*^2 \sim \mathcal{O}(\epsilon, \epsilon_\tau)$ , thus the subleading correction proportional to  $\epsilon_\tau$  in the fermion (3.52) and boson (3.53) anomalous dimensions should be discarded. In other words, at one-loop order the correction  $z - 1$  to the dynamic critical exponent is  $\mathcal{O}(\epsilon, \epsilon_\tau)$ , which gives a term quadratic in  $\epsilon, \epsilon_\tau$  in Eq. (3.32)-(3.33) that should be treated on par with two-loop corrections to  $\gamma_2, \gamma_4$ , and thus eliminated when working at one-loop order.

## 3.4 RG flow analysis

We now search for fixed points of the flow equations (3.46)-(3.49), i.e., common zeros  $(c_*^2, \lambda_*^2, h_*^2, \Delta_*)$  of the beta functions, which correspond to possible (multi)critical points for the semimetal-superconductor transition. In the double epsilon expansion, the nature of the fixed points and their stability depend sensitively on the ratio  $\epsilon/\epsilon_\tau$  (especially for disordered fixed points with  $\Delta_* \neq 0$ ) [122–124]. Since we are interested in the limit  $\epsilon \rightarrow 2$  and  $\epsilon_\tau \rightarrow 1$ , corresponding to 2+1 dimensions, we set  $\epsilon = 2\epsilon_\tau$  and expand to leading order in  $\epsilon_\tau$ .

### 3.4.1 Fixed points

First considering possible clean fixed points with  $\Delta_* = 0$ , we find the Gaussian fixed point  $(c_*^2, 0, 0, 0)$  and  $O(2)$  Wilson-Fisher fixed point  $(c_*^2, \frac{\epsilon_\tau}{20}, 0, 0)$ , where  $c_*^2$  is arbitrary since the velocity parameter flows under RG only in the presence of disorder or a nonzero Yukawa coupling [Eq. (3.46)]. We also find a GNY fixed point for all  $N$ ,

$$\left(1, \frac{2 - N + \sqrt{N^2 + 76N + 4}}{40(N + 2)}\epsilon_\tau, \frac{\epsilon_\tau}{4(N + 2)}, 0\right), \quad (3.54)$$

corresponding to the semimetal-superconductor QCP in the clean limit, and in agreement with earlier studies [126, 139–141]. Note that  $\lambda_*^2 > 0$  for all  $N \geq 1$ . Since  $f(1) = \frac{1}{2}$  (see Fig. 3.4), from Eq. (3.51) one finds  $z = 1$ , and the clean QCP has emergent Lorentz invariance.

We now look for possible disordered fixed points with  $\Delta_* \neq 0$ . Since at one-loop order  $\beta_{h^2}$  depends on  $h^2$  alone [Eq. (3.48)], we can separately consider the cases with  $h_*^2$  zero and nonzero. For  $h_*^2 = 0$ , we find the fixed point  $(0, \frac{\epsilon_\tau}{2}, 0, \frac{3\epsilon_\tau}{4})$  for all  $N$ <sup>3</sup>, which corresponds

---

<sup>3</sup>Note that naively substituting  $h_*^2 = 0$  into Eq. (3.51) would imply that this fixed point has  $z = 1$ , which is incorrect. The issue is that this fixed point has  $c_*^2 = 0$ , but the renormalization constants (3.36)-(3.43) are calculated assuming  $c^2 \neq 0$ . To calculate  $z$  at the bosonic disordered fixed point one should rescale fields and redefine couplings in Eq. (3.12) in such a way as to eliminate the parameter  $c^2$  in front of  $|\partial_\tau \phi_a|^2$  at the expense of multiplying  $i\bar{\psi}_a \not{\partial}_\tau \psi_a$  by  $1/c$ . The dynamic critical exponent is then given by  $z = 1 + \frac{1}{2}(\gamma_3 - \gamma_4) = 1 + \frac{3\epsilon_\tau}{4}$ , in agreement with known results (see Eq. (3.11) with  $n = 2$ ).

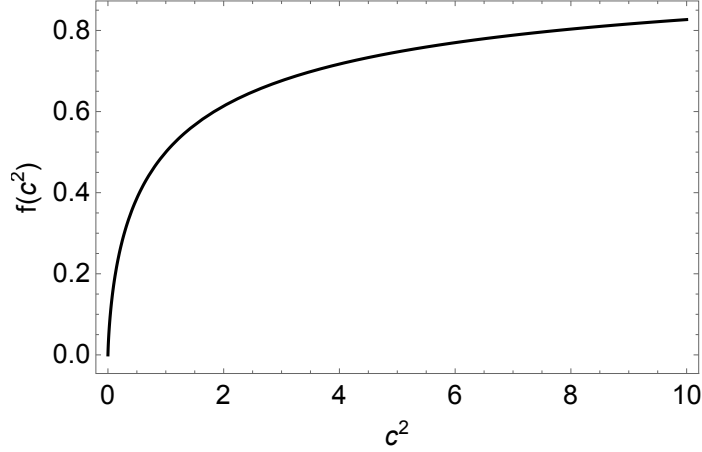


Figure 3.4: Plot of  $f(c^2)$  in Eq. (3.44), with  $c^2 = (c_f/c_b)^2$  the velocity ratio squared;  $f(0) = 0$ ,  $f(1) = \frac{1}{2}$ , and  $f(\infty) = 1$ .

to the disordered fixed point of the purely bosonic  $O(2)$  model [122–124] and describes the superfluid-Mott glass transition in the presence of exact particle-hole symmetry [165]. For  $h_*^2 \neq 0$ , as already mentioned one necessarily has  $h_*^2 = \epsilon_\tau/[4(N+2)]$  like at the clean fixed point (CFP) in Eq. (3.54), regardless of the values of  $\lambda_*^2$  and  $\Delta_*$ . Solving for a common zero of  $\beta_{\lambda^2}$  and  $\beta_\Delta$ , we find two nontrivial disordered fixed points (DFP),

$$\text{DFP 1: } \left( c_{*,\text{DFP1}}^2, \frac{\epsilon_\tau}{N+2}, \frac{\epsilon_\tau}{4(N+2)}, \frac{3\epsilon_\tau}{2(N+2)} \right), \quad (3.55)$$

$$\text{DFP 2: } \left( c_{*,\text{DFP2}}^2, \frac{N\epsilon_\tau}{4(N+2)}, \frac{\epsilon_\tau}{4(N+2)}, \frac{(N-1)\epsilon_\tau}{2(N+2)} \right). \quad (3.56)$$

As they occur at finite Yukawa coupling, and thus involve strongly coupled bosonic *and* fermionic critical fluctuations, we will term these fixed points *fermionic* disordered fixed points. The critical couplings  $\lambda_*^2$ ,  $h_*^2$ , and  $\Delta_*$  are strictly positive, and thus physical, for all  $N \geq 2$ . Inserting (3.55) and (3.56) into  $\beta_{c^2}$ , one numerically finds that in both cases  $\beta_{c^2}$  has a unique zero at a positive value of  $c^2$  for all  $N \geq 2$  (Fig. 3.5). For DFP 1, one can derive the lower bound  $c_{*,\text{DFP1}}^2 \geq N/(N-1)$ , and  $c_{*,\text{DFP1}}^2$  tends to one as  $N$  increases. For DFP 2,  $c_{*,\text{DFP2}}^2$  increases without bound as  $N$  increases, and we have  $c_{*,\text{DFP2}}^2 \geq N/3$ .

The cases  $N = 1$  and  $N = 4$  are special. As  $N$  approaches one from above, DFP

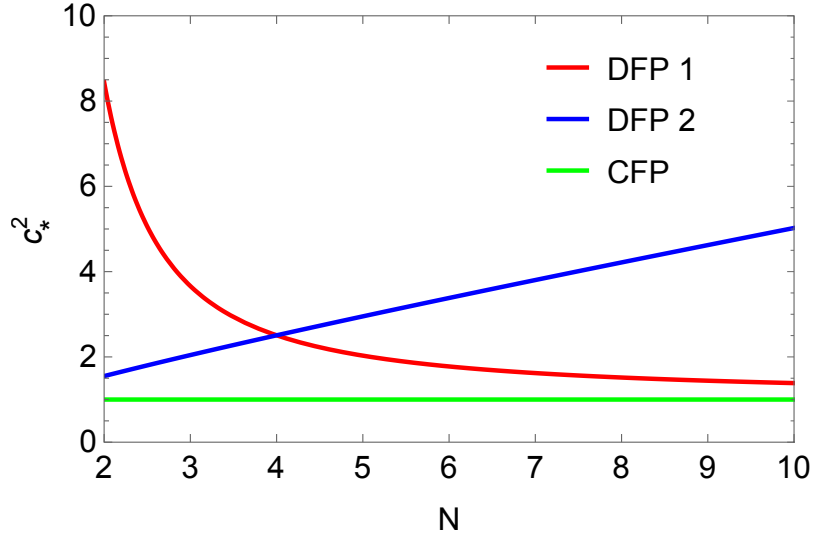


Figure 3.5: Critical velocity parameters  $c_*^2$  at the first disordered fixed point (DFP 1), the second disordered fixed point (DFP 2), and the clean fixed point (CFP,  $c_*^2 = 1$ ), as a function of  $N \geq 2$ .

2 merges with the clean fixed point, with  $c_{*,\text{DFP2}}^2 \rightarrow c_{*,\text{CFP}}^2 = 1$ , while DFP 1 moves off to infinite coupling ( $c_{*,\text{DFP1}}^2 \rightarrow \infty$ ). As can be gleaned by looking at Eq. (3.55)-(3.56) and Fig. 3.5, as  $N \rightarrow 4$  DFP 1 and DFP 2 also merge. In accordance with the general scenario governing the pairwise merging of fixed points [166, 167], and as will be elaborated upon below, in the presence of disorder we expect to find marginal scaling at the clean fixed point for  $N = 1$  and at the (unique) fermionic disordered fixed point for  $N = 4$ .

### 3.4.2 Linear stability analysis

We now perform a linear stability analysis for the fixed points found in the previous section, within the critical hypersurface  $r = 0$ . In the absence of disorder, as found previously [126, 139–141] the Gaussian and  $O(2)$  Wilson-Fisher fixed points have at least one unstable direction, while the CFP is stable and describes the critical behavior at the transition. In the presence of disorder, both the Gaussian and  $O(2)$  Wilson-Fisher fixed points acquire an additional unstable direction. At the CFP, the RG eigenvalue (defined as the negative of

the slope of the ultraviolet beta functions) corresponding to disorder is

$$-\frac{2}{5} \left( \frac{\sqrt{N^2 + 76N + 4} - N - 8}{N + 2} \right) \epsilon_\tau, \quad (3.57)$$

which is strictly negative for all  $N \geq 2$ . Thus disorder is perturbatively irrelevant at the CFP for all  $N \geq 2$ . For  $N = 1$ , the eigenvalue (3.57) vanishes and one has marginal scaling, as expected from the discussion at the end of the last section. Expanding the beta functions to quadratic order in the couplings near the CFP, we find that disorder is marginally relevant.

Turning now to the disordered fixed points, we find that the disordered  $O(2)$  Wilson-Fisher fixed point is destabilized by a nonzero Yukawa coupling for all  $N$ . By contrast, the stability of DFP 1 and DFP 2 depends on  $N$ . For  $N = 2, 3$ , DFP 1 is stable while DFP 2 has one unstable direction; for  $N = 4$ , DFP 1 and DFP 2 merge into a single fermionic disordered fixed point with marginal flow; for  $N \geq 5$ , DFP 1 and DFP 2 exchange their stability properties, i.e., DFP 2 is stable and DFP 1 has one unstable direction. As previously mentioned, for  $N = 1$  no finite-disorder fixed points remain.

### 3.4.3 RG flows

Having investigated the linearized RG flow near the fixed points, we now analyze the full flow in the four-dimensional space of couplings, as given by the solution of the coupled differential equations (3.46)-(3.49). Since the beta function for the Yukawa coupling (3.48) is independent of  $c^2$ ,  $\lambda^2$ , and  $\Delta$ , the CFP, DFP 1, and DFP 2 share a common fixed-point value of  $h_*^2 = \epsilon_\tau/[4(N+2)]$ . Furthermore, we find that the scaling field corresponding to the relative velocity parameter  $c^2$  is irrelevant at each of those fixed points (except for  $N = 1$ , which is discussed separately below). Therefore we will plot the projection of the RG flow in the  $\lambda^2$ - $\Delta$  plane at fixed  $h^2 = h_*^2$ .

In Fig. 3.6 we plot the projected RG flows for  $N = 1$ . There is marginal flow away from the CFP, with nonzero projections along the  $\lambda^2$ ,  $\Delta$ , and  $c^2$  directions. The point

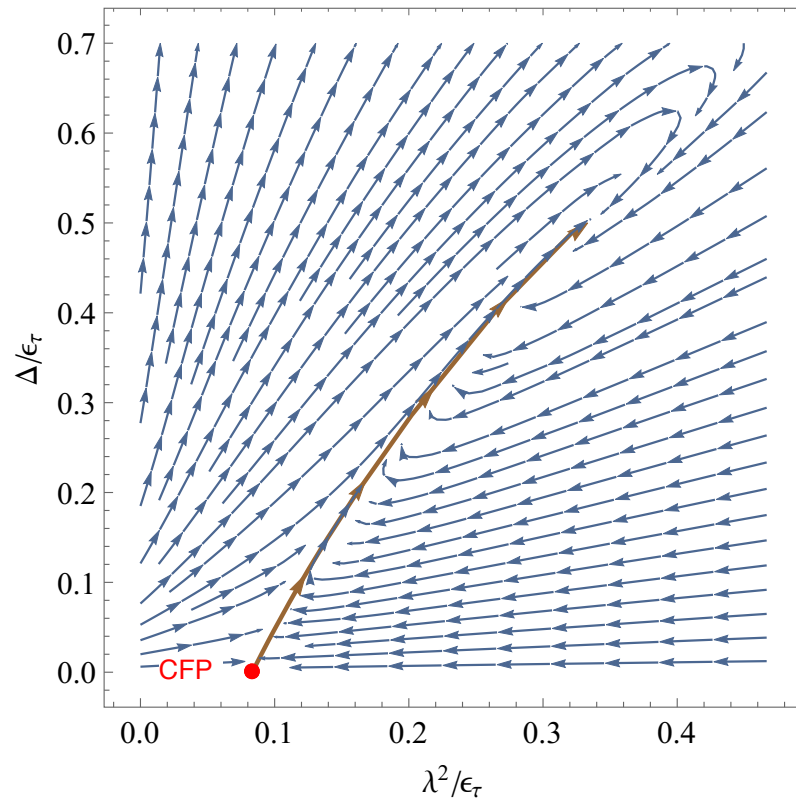


Figure 3.6: RG flows for  $N = 1$ , with marginal flow (brown line) away from the CFP.

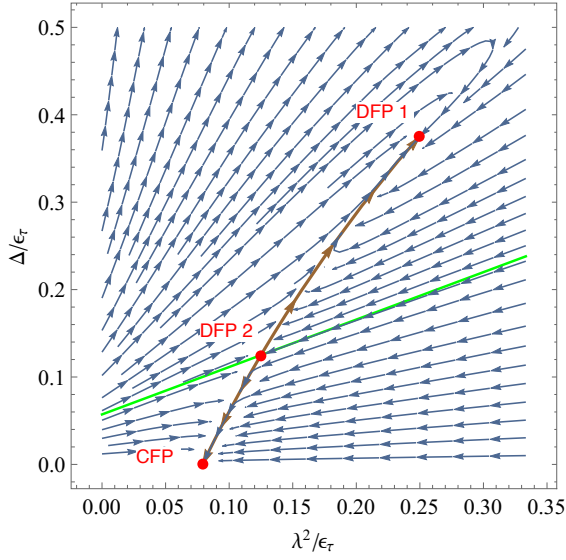
$(\lambda^2, \Delta) = (\epsilon_\tau/3, \epsilon_\tau/2)$  towards which the marginal flow leads in Fig. 3.6 is a remnant of DFP 1 [see Eq. (3.55)], but is not a fixed point as it is impossible to make  $\beta_{c^2}$  vanish there for  $N = 1$ . The marginal flow at the CFP implies the existence of a Landau pole that can be interpreted as a crossover temperature scale  $T^* \sim \Lambda e^{-1/\alpha\Delta_0}$  above which scaling in the quantum critical fan is controlled by the CFP, where  $\Lambda$  is a high-energy cutoff,  $\Delta_0$  is a dimensionless measure of the bare disorder strength, and  $\alpha$  is a numerical factor of order unity. Below  $T^*$  the runaway flow suggests the existence of a new fixed point, not accessible at one-loop order, or a first-order transition.

In Fig. 3.7a we plot the flow diagram for  $N = 2$ . As found in the linear stability analysis, the CFP and DFP 1 are stable fixed points while DFP 2 has one unstable direction, and controls a separatrix surface (appearing as a line in the  $\lambda^2$ - $\Delta$  plane) that separates the basins of attraction of the CFP and DFP 1. For  $N = 3$ , the flow diagram is qualitatively similar but DFP 1 and DFP 2 approach each other; at  $N = 4$  they merge into a single DFP with marginal flow towards the CFP (Fig. 3.7b).

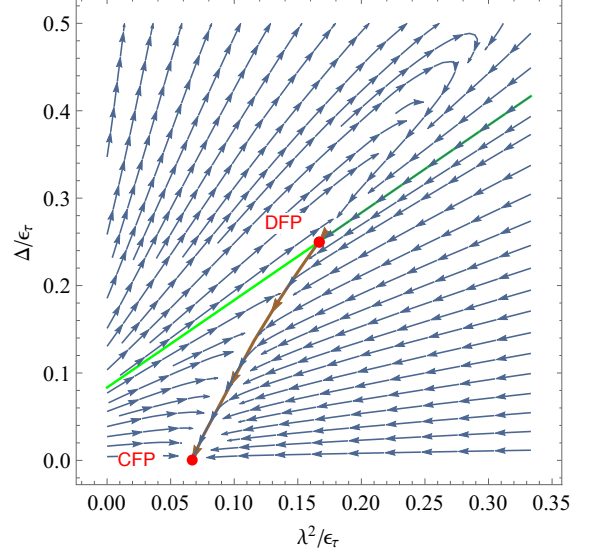
For  $N = 5$  (Fig. 3.7c) and  $N = 6$ , the flow diagram is qualitatively similar as that for  $N = 2$  and  $N = 3$ , but the stability properties of DFP 1 and DFP 2 are interchanged. DFP 1 now controls the separatrix, and DFP 2 is the stable fixed point. For  $N \geq 7$ , this state of affairs remains, but two irrelevant eigenvalues of the stability matrix acquire a nonzero imaginary part. Since the stability matrix is real, they are complex conjugates  $\omega_\pm = \omega' \pm i\omega''$ , but their real part  $\omega'$  (defining  $\omega_\pm$  to be the eigenvalues of the Jacobian matrix of the ultraviolet beta functions) remains positive, since they correspond to irrelevant directions. We obtain

$$\omega_\pm = \frac{N + 8 \pm i\sqrt{3N(5N - 32)}}{2(N + 2)}\epsilon_\tau. \quad (3.58)$$

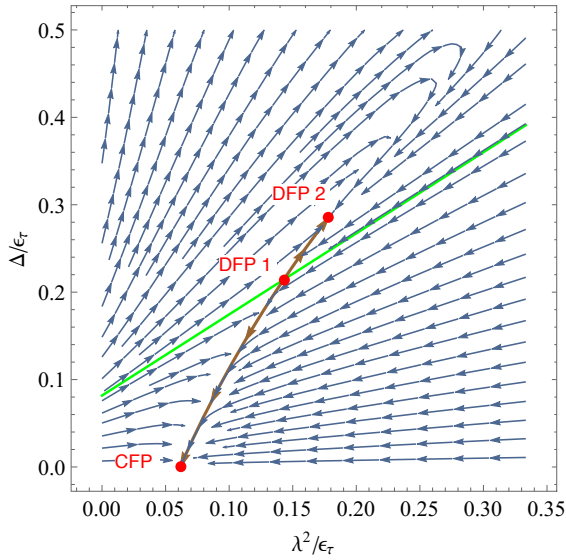
As a consequence of the nonzero imaginary part, RG trajectories spiral around DFP 2, and the latter becomes a fixed point of stable-focus type. Such fixed points have been found before in disordered  $O(n)$  magnets [122, 168], and an unstable-focus point was found



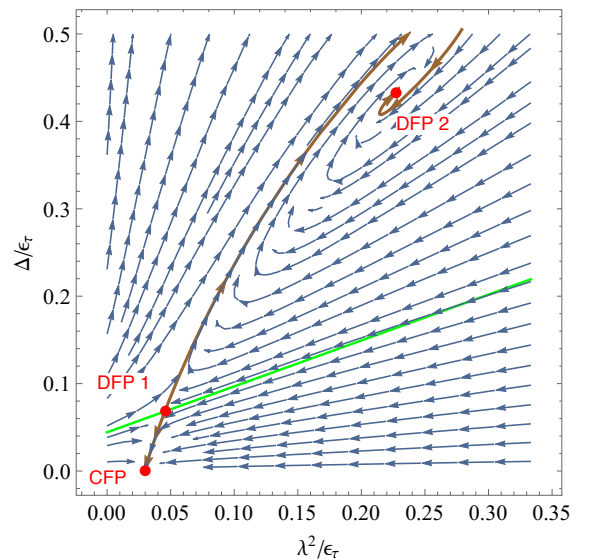
(a) RG flows for  $N = 2$ , with separatrix (green line) controlled by DFP 2 between the CFP and DFP 1.



(b) RG flows for  $N = 4$ : DFP 1 and DFP 2 merge into a single DFP with marginal flow towards the CFP.



(c) RG flows for  $N = 5$ .



(d) RG flows for  $N = 20$ ; DFP 2 is a fixed point of stable-focus type for all  $N \geq 7$ .

Figure 3.7: RG flows for different  $N$ .

in Ref. [169]. As an illustrative example, we plot the RG flows for  $N = 20$  in Fig. 3.7d (stable-focus behavior is obtained for all  $N \geq 7$ , but  $\omega''$  is larger — and thus the spiraling trajectories more easily seen — for larger  $N$ .)

### 3.5 Critical exponents and phase diagram

From Eq. (3.50)-(3.53) and the fixed point couplings (3.54), (3.55), (3.56) we can now determine the critical exponents at the various fixed points (Table 3.2), where  $\eta_\psi, \eta_\phi$  denote the anomalous dimensions  $\gamma_\psi, \gamma_\phi$  evaluated at the fixed point.

Fixed point	$\nu^{-1}$	$z - 1$	$\eta_\psi$	$\eta_\phi$
CFP	$2 - \left( \frac{4N + 2 + \sqrt{N^2 + 76N + 4}}{5(N + 2)} \right) \epsilon_\tau$	0	$\frac{\epsilon_\tau}{N + 2}$	$\frac{N\epsilon_\tau}{N + 2}$
DFP 1	$2 - \left( \frac{N + 5}{N + 2} \right) \epsilon_\tau$	$\frac{3 + \left( \frac{1 - c_*^2}{c_*^2} \right) N}{2(N + 2)} \epsilon_\tau$	$\frac{\epsilon_\tau}{N + 2}$	$\frac{N\epsilon_\tau}{N + 2}$
DFP 2	$2 - \left( \frac{2N + 1}{N + 2} \right) \epsilon_\tau$	$\frac{\frac{N}{c_*^2} - 1}{2(N + 2)} \epsilon_\tau$	$\frac{\epsilon_\tau}{N + 2}$	$\frac{N\epsilon_\tau}{N + 2}$

Table 3.2: Critical exponents at the CFP, DFP 1, and DFP 2.

For  $N = 1$ , the CFP becomes the supersymmetric fixed point with  $\eta_\psi = \eta_\phi = \epsilon_\tau/3$  [140, 142–148]. At the present one-loop order, the fermion/boson anomalous dimensions  $\eta_\phi$  and  $\eta_\psi$  only depend on the Yukawa coupling  $h^2$ , which is the same at each fixed point as observed earlier. This state of affairs will change at higher loop orders, and we expect the anomalous dimensions to differ at different fixed points in general.

We plot the inverse correlation length exponent  $\nu^{-1}$  extrapolated to  $\epsilon_\tau = 1$  as a function of  $N \geq 2$  in Fig. 3.8. In accordance with the linear stability analysis in Sec. 3.4.2, the CFP obeys the Harris criterion [82], according to which clean critical behavior is stable

against random- $T_c$  disorder if

$$\nu^{-1} < d/2, \tag{3.59}$$

where  $d = 2$  is the (physical) spatial dimension and  $\nu^{-1}$  is the inverse correlation length exponent in the clean limit. At the CFP,  $\nu^{-1}$  is strictly less than one for all  $1 < N < \infty$  and reaches one at both  $N = 1$  and  $N = \infty$ ; thus for  $N = 1$  the CFP is Harris marginal, as found in Sec. 3.4. Note that in the context of a perturbative RG analysis, it is more appropriate to use the Harris criterion in the form (3.59), rather than in the usual form  $\nu > 2/d$ , as (3.59) simply expresses the condition of perturbative irrelevance of the disorder-induced interaction (3.9), namely that its scaling dimension  $2(d + \epsilon_\tau - \nu^{-1})$  be larger than the effective spacetime dimensionality  $d + 2\epsilon_\tau$  appropriate for this interaction. However, this makes clear the fact that the Harris criterion is one of perturbative stability, and does not preclude the existence of disordered critical points occurring past a certain finite critical disorder strength, as found here. At the DFP 1 (DFP 2),  $\nu^{-1}$  increases (decreases) monotonically as  $N$  increases, asymptotically reaching 1 (0) at  $N = \infty$ . Thus at all fixed points  $\nu^{-1} \leq 1$ , in agreement with the Chayes inequality  $\nu^{-1} \leq d/2$  for critical points in disordered systems [83].

We also plot the deviation of the dynamic critical exponent  $z$  from unity at DFP 1 and DFP 2 in Fig. 3.9, as a function of  $N \geq 2$ , and extrapolated to  $\epsilon_\tau = 1$  (or equivalently, in units of  $\epsilon_\tau$ ). The dynamic critical exponent depends on the fixed-point value of the relative velocity parameter  $c_*^2$ , itself plotted in Fig. 3.5.

Finally, by contrast with standard RG fixed points of source/sink type where RG trajectories approach the fixed point monotonically, fixed points of stable-focus type, such as the DFP 2 for  $N \geq 7$ , are known to lead to oscillatory corrections to scaling laws [168]. In particular, the uniform, static order parameter susceptibility  $\chi$ , which obeys the usual

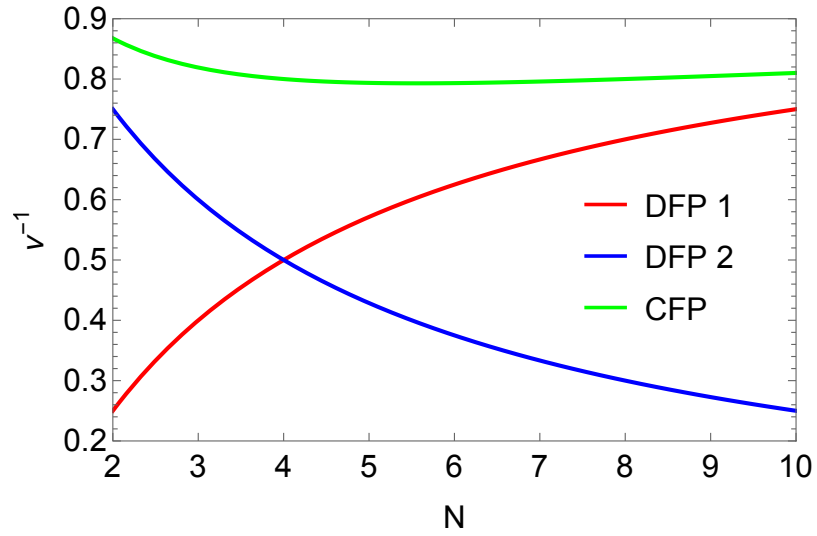


Figure 3.8: Inverse correlation length exponent  $\nu^{-1}$  for  $\epsilon_\tau = 1$ , as a function of  $N \geq 2$ .

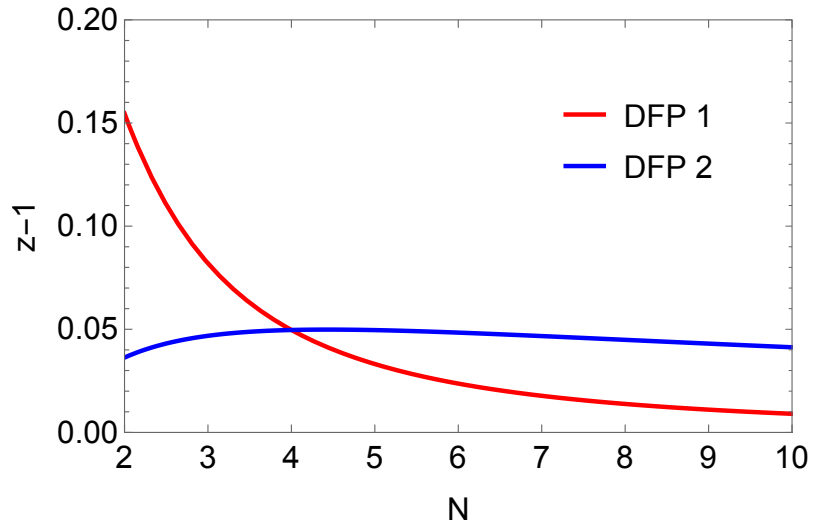


Figure 3.9: Correction  $z-1$  to the dynamic critical exponent for  $\epsilon_\tau = 1$  at the two disordered fixed points, as a function of  $N$ .

scaling law  $\chi \sim |r|^{-\gamma}$  with  $\gamma$  the susceptibility exponent, develops corrections of the form

$$\chi \sim |r|^{-\gamma} \left[ 1 + C \left| \frac{r}{r_0} \right|^{\nu\omega'} \cos \left( \nu\omega'' \ln \left| \frac{r}{r_0} \right| + \phi \right) + \dots \right], \quad (3.60)$$

where  $r_0$ ,  $C$ , and  $\phi$  are nonuniversal constants that depend on the initial distance to the fixed point within the critical hypersurface  $r = 0$ , but the exponents  $\omega'$  and  $\omega''$ , given in Eq. (3.58) and plotted in Fig. 3.10, are universal properties of the fixed point. [See Appendix B.7 for a derivation of Eq. (3.60).]

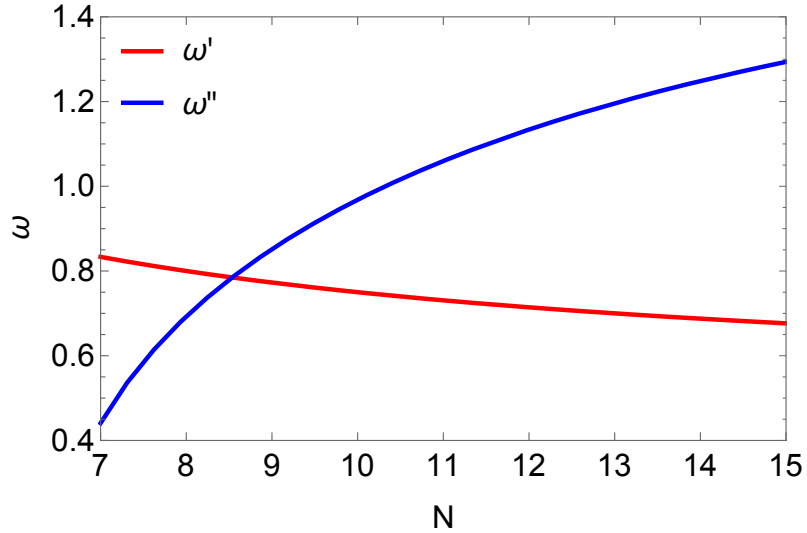


Figure 3.10: Exponents  $\omega'$  and  $\omega''$  appearing in oscillatory corrections to scaling at DFP 2 for  $N \geq 7$ , for  $\epsilon_\tau = 1$ .

The separatrix surface for  $N \geq 2$  mentioned in Sec. 3.4.3 has interesting nonmonotonicity properties. As the direction corresponding to the relative velocity parameter  $c^2$  is always irrelevant at the CFP, DFP 1, and DFP 2 for  $N \geq 2$ , it is sufficient to consider the separatrix as a 2D surface in the 3D reduced parameter space  $(\lambda^2, h^2, \Delta)$ . In Fig. 3.11 we plot three cuts through this surface at constant  $\lambda^2$  that are representative of the qualitative behavior we have observed numerically for all  $N \geq 2$ , and which can be summarized as follows. Let  $\Delta = g_{\lambda^2}(h^2)$  be an equation describing the separatrix curve in the  $h^2$ - $\Delta$

plane for a given  $\lambda^2$ . Then there always exists an interval  $[h_1^2, h_2^2]$ , dependent on  $\lambda^2$ , and a value  $\lambda_1^2$  such that for  $\lambda^2 < \lambda_1^2$ , the function  $g_{\lambda^2}(h^2)$  is double valued. Conversely, consider describing the same separatrix curve by the equation  $h^2 = g_{\lambda^2}^{-1}(\Delta)$  where  $g^{-1}$  is the inverse function. Then likewise there always exists an interval  $[\Delta_1, \Delta_2]$ , dependent on  $\lambda^2$ , and a value  $\lambda_2^2 < \lambda_1^2$  such that for  $\lambda^2 < \lambda_2^2$  the function  $g_{\lambda^2}^{-1}(\Delta)$  is double valued. This double-valued/nonmonotonic behavior of the separatrix surface has potential consequences for the phase diagram of the system as will be discussed below.

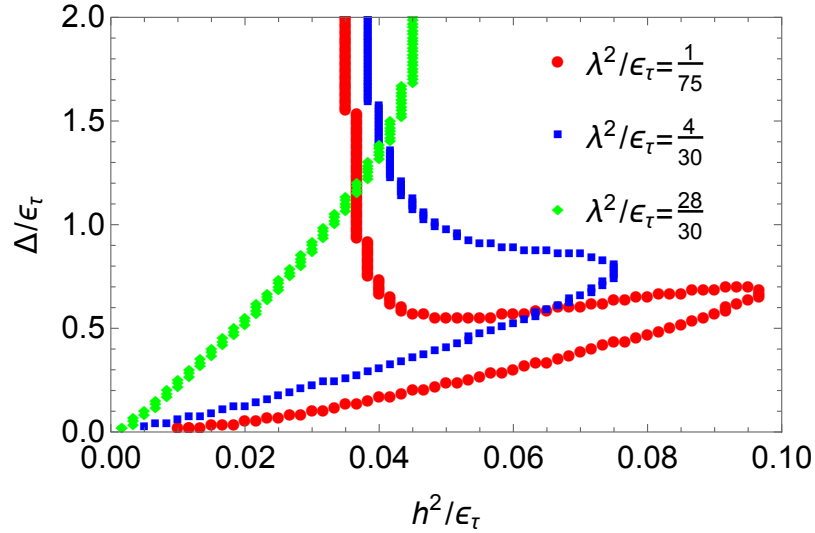


Figure 3.11: Cuts of the separatrix surface at constant  $\lambda^2$  for  $N = 8$ .

By following the RG trajectories from a set of initial conditions for the coupling constants  $(c^2, \lambda^2, h^2, \Delta)$  one can deduce the following implications for the phase diagram of the system. The  $N = 1$  case has already been discussed previously: the one-loop analysis does not allow one to determine the ultimate fate of the quantum critical point, which can either fall in a new universality class or become a first-order transition. For  $N \geq 2$ , consider as tuning variables the critical tuning parameter for the transition,  $r$ , and the disorder strength  $\Delta$ , assuming that  $\lambda^2$  and  $h^2$  are held fixed. For  $\Delta = 0$  the transition is between a clean Dirac semimetal and a superconductor, and is in the universality class of the CFP. For sufficiently small nonzero  $\Delta$ , the initial conditions in parameter space remain in the basin

of attraction of the CFP and the universality class of the transition is still controlled by the latter. For  $\Delta > 0$ , the transition is between a disordered semimetal and a superconductor. Rare-region effects will likely lead to the formation of quantum Griffiths phases on both sides of the transition [128], characterized by essential Griffiths-McCoy singularities, but are expected to produce exponentially small corrections to thermodynamic observables at the critical point [129].

As  $\Delta$  increases, it eventually crosses the separatrix surface at a certain critical value  $\Delta_{c,1}$ , and for  $\Delta > \Delta_{c,1}$  enters the basin of attraction of a disordered fixed point. Thus for  $N = 2$  and  $N = 3$ , the universality class of the transition is controlled by the CFP for  $\Delta < \Delta_{c,1}$ , by DFP 2 for  $\Delta = \Delta_{c,1}$ , which is a multicritical point, and by DFP 1 for  $\Delta > \Delta_{c,1}$  [see Fig. 3.12(a)]. For  $N = 4$ , for  $\Delta > \Delta_{c,1}$  the RG trajectories flow back to the (unique) DFP, such that the universality class of the transition is controlled by the DFP for  $\Delta \geq \Delta_{c,1}$  [Fig. 3.12(b)]. For  $N \geq 5$ , the scenario is the same as for  $N = 2$  and  $N = 3$  but the roles of DFP 1 and DFP 2 are exchanged, with DFP 1 acting as multicritical point at  $\Delta = \Delta_{c,1}$  and DFP 2 controlling the critical behavior for  $\Delta > \Delta_{c,1}$  [Fig. 3.12(c)].

As mentioned earlier and illustrated in Fig. 3.11, for sufficiently small  $\lambda^2$  there is always an interval of values of  $h^2$  for which the separatrix curve is a double-valued function of  $h^2$ . As a result, if the initial value of  $h^2$  is contained in this interval, as the disorder strength  $\Delta$  increases from zero the universality class of the transition will be first controlled by the CFP, then by one of the disordered fixed points (depending on the value of  $N$ ), and then again by the CFP [Fig. 3.12(d)]. However, this counterintuitive behavior may be an artefact of the one-loop approximation.

### 3.6 Conclusion

In conclusion, we have studied the critical properties of the semimetal-superconductor quantum phase transition in a model of 2D Dirac semimetal with  $N$  flavors of two-component Dirac fermions, in the presence of quenched disorder assumed to be uncorrelated, but suf-

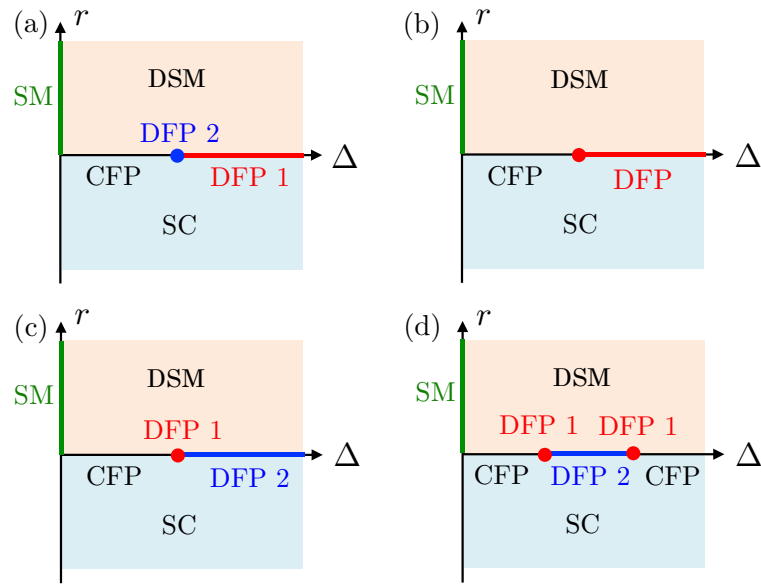


Figure 3.12: Schematic phase diagrams in the plane of tuning parameter  $r$  and disorder strength  $\Delta$  for  $N \geq 2$ . SM: Dirac semimetal; DSM: disordered semimetal; SC: superconductor. For sufficiently small initial values of  $\lambda^2$  and  $h^2$ , the universality class of the transition changes beyond a critical disorder strength from that of the CFP to that of one of the two disordered fixed points: (a)  $N = 2$  and  $N = 3$ ; (b)  $N = 4$ ; (c)  $N \geq 5$ . For sufficiently large  $\lambda^2$  and/or  $h^2$ , beyond a second critical disorder strength there is a reentrant critical regime controlled by the CFP [plotted in (d) for  $N \geq 5$ , but an analogous effect occurs for  $2 \leq N \leq 4$ ].

ficiently smooth so as to make the probability of scattering between different Dirac cones negligible. Our one-loop analysis demonstrated the possibility of a general scenario for critical phenomena in disordered systems, to our knowledge not explicitly discussed in the literature so far: a clean critical point may be stable against disorder according to the Harris criterion, but yet may be replaced by a finite-disorder critical point beyond a certain finite, critical disorder strength. In the model studied here such finite-disorder critical points were characterized by finite fixed-point values of both the boson-boson and fermion-boson couplings, and thus were dubbed disordered fermionic QCPs. Other notable features of the disordered critical points found included a noninteger dynamic critical exponent  $z > 1$ , as well as oscillatory corrections to scaling for sufficiently large  $N$ .

Possible applications of our results include the semimetal-superconductor quantum phase transition in graphene ( $N = 4$ ) and on the surface of a 3D topological insulator ( $N = 1$ ); the experimental results reported in Ref. [170] are encouraging in regards to the latter, although one would need to additionally tune the chemical potential to the Dirac point and reach the quantum critical regime by the application of a nonthermal tuning parameter such as pressure. With those caveats in mind, we also note that the surface of 3D topological crystalline insulators [171, 172] such as SnTe [173],  $\text{Pb}_{1-x}\text{Sn}_x\text{Se}$  [174], and  $\text{Pb}_{1-x}\text{Sn}_x\text{Te}$  [175] supports  $N = 4$  two-component Dirac cones, as in graphene, and that superconductivity has been observed in In-doped SnTe [176, 177], though presumably of bulk origin. Larger values of  $N$  may be accessible in systems of ultracold large-spin alkaline-earth fermions [178] loaded into optical honeycomb lattices, such as those studied theoretically in Ref. [179], but with interactions tuned to be attractive.

To further elucidate the critical behavior at  $N = 1$  in the present model, perturbative calculations at two-loop order would be necessary. The conformal bootstrap [180], perturbative RG studies of the clean chiral XY GNY model at four-loop order [140], as well as quantum Monte Carlo simulations [149] suggest that  $\nu^{-1}$  is slightly above one at the CFP for  $N = 1$ , implying via the Harris criterion that disorder is in fact relevant (as opposed to marginally relevant as found at one-loop order) at the CFP. (Interestingly, for

$N = 4$  quantum Monte Carlo simulations of the Kekulé transition in graphene [152] and naive extrapolation of the four-loop GNY  $\epsilon$ -expansion results [140] predict  $\nu^{-1} > 1$  at the CFP, while Padé extrapolation of the latter results [140] as well as functional RG studies of the Kekulé transition [181] predict  $\nu^{-1} < 1$  in the clean limit, in agreement with our one-loop result.) Beyond perturbative RG, it would be interesting to try to apply strong-disorder RG methods [74, 75, 182] to this problem, as done recently for the 2D bosonic superfluid-Mott insulator transition [183], or to incorporate the effect of quenched disorder in the sign-problem-free quantum Monte Carlo simulations of Ref. [149], as done previously for the disordered attractive Hubbard model [184].

## Chapter 4

# Long range-correlated random-mass disorder in GNY models

### 4.1 Introduction

In the previous chapter, the effect of short-range correlated disorder in the chiral XY GNY model was studied via the double epsilon expansion method. In this chapter we extend this study to the chiral Ising and Heisenberg GNY models [126, 140]. As we briefly review in Sec. 4.2, these chiral GNY models describe a variety of QCPs in condensed matter systems [185]. Unlike in the previous chapter, we also consider random-mass disorder with correlations between two spatial points  $\mathbf{x}, \mathbf{x}'$  that decay asymptotically as a power law,  $\sim |\mathbf{x} - \mathbf{x}'|^{-\alpha}$ , with  $\alpha < d$ . (For  $\alpha > d$ , the correlations are short range, as the disorder correlation function in momentum space remains finite in the long-wavelength limit.) According to the extended Harris criterion, a clean critical point with correlation length exponent  $\nu_{\text{CFP}}$  is perturbatively stable against such long-range correlated disorder if  $\nu_{\text{CFP}} > 2/\min(d, \alpha)$  [186]; this type of disorder thus generally has a stronger effect at phase transitions than uncorrelated disorder.

Our main results are summarized as follows. For the chiral Ising GNY model, we find new disordered multicritical points, and for the chiral XY and Heisenberg GNY models, new disordered critical and multicritical points. As in Chap. 3, some of the disordered QCPs found exhibit usual sink-type RG flows, while others are of stable-focus type. We also explore how the structure of the RG flow on the critical hypersurface evolves upon tuning RG-invariant system parameters, here the number  $N$  of fermion flavors and the exponent  $\alpha$  describing disorder correlations. We are particularly interested in bifurcations of these RG flows [167], where the number or stability properties of fixed points suddenly change as a function of  $N$  and  $\alpha$ , called control parameters in bifurcation theory. We find and analyze instances of the saddle-node bifurcation, also known as the fixed-point annihilation scenario [166], at which a repulsive fixed point and an attractive fixed point coalesce and disappear into the complex plane. This type of bifurcation appears or has been argued to appear in RG flows in a variety of problems of current interest in both high-energy physics [166, 187–193] and condensed matter physics/statistical mechanics [194–202]. The characteristic phenomenology associated with it includes Berezinskii-Kosterlitz-Thouless/Miransky scaling, walking/pseudo-critical behavior, and weakly first-order transitions. In our particular problem, it manifests itself in the existence of an anomalously (i.e., exponentially) large length scale  $L_*$  that governs the crossover between two distinct universality classes of critical behavior. In much previous work, the saddle-node bifurcation is tuned by a parameter such as space(time) dimensionality  $d$  or the integer number  $N$  of components of a fermionic or bosonic field, and thus cannot be approached continuously in practice. Here, for fixed  $d$  and  $N$  the bifurcation can be approached by continuously tuning the exponent  $\alpha$  for disorder correlations.

Besides the saddle-node bifurcation, we also discover instances of more exotic bifurcations [167]: the transcritical bifurcation, at which two fixed points exchange their stability properties without annihilating, and the supercritical Hopf (or Poincaré-Andronov-Hopf) bifurcation [203]. The latter is a bifurcation at which a stable-focus QCP loses its stability by giving birth to a stable limit cycle, which then controls the asymptotic critical behavior.

A possibility first considered by Wilson [204], stable RG limit cycles lead to log-periodic scaling behavior [205], i.e., discrete scale invariance (as opposed to log-periodic behavior of *corrections* to scaling at stable-focus points). Hopf bifurcations in RG flows were found in classical disordered  $O(n)$  models [186, 206], but only the subcritical Hopf bifurcation [203] was found, where an unstable-focus fixed point becomes stable and gives birth to an *unstable* limit cycle. As a result, the models studied in Refs. [186, 206] did not exhibit log-periodic critical scaling behavior in the long-distance limit.

The rest of the chapter is structured as follows. In Sec. 4.2, we briefly describe the chiral GNY models with long-range correlated random-mass quenched disorder. In Sec. 4.3, we describe the perturbative RG scheme used to derive beta functions on the critical hypersurface. By contrast with Chap. 3, where the double epsilon expansion [122–124, 160] was sufficient to tame RG flows in the presence of uncorrelated disorder, here we use a controlled *triple* epsilon expansion [207] at one-loop order that allows us to tame the flow of both interaction and correlated disorder strengths. In Sec. 4.4, we investigate the fixed points of the RG beta functions derived in Sec. 4.3, focusing on DFPs and analyzing their linear stability. We compute critical exponents and anomalous dimensions at all DFPs. In Sec. 4.5, we discuss qualitative features of the RG flow, including various bifurcations that occur under changes of the control parameters  $N$  and  $\alpha$ , and their consequences for critical properties. We conclude in Sec. 4.6 with a summary of our main results and a few directions for further research. The details of calculations are placed in Appendix B.

## 4.2 The random-mass GNY models

Our starting point is the family of chiral  $O(n)$  GNY models in 2+1 dimensions at zero temperature, described by the Euclidean action:

$$S = \int d^2\mathbf{x} d\tau (\mathcal{L}_\phi + \mathcal{L}_\psi + \mathcal{L}_{\psi\phi}), \quad (4.1)$$

where  $\boldsymbol{x}$  denotes spatial coordinates, and  $\tau$  is imaginary time. The model consists of a real  $n$ -component scalar field  $\boldsymbol{\phi} = (\phi^1, \dots, \phi^n)$ , the order parameter, governed by the Lagrangian:

$$\mathcal{L}_\phi = (\partial_\tau \boldsymbol{\phi})^2 + c_b^2 (\nabla \boldsymbol{\phi})^2 + r \boldsymbol{\phi}^2 + \lambda^2 (\boldsymbol{\phi}^2)^2, \quad (4.2)$$

where  $\boldsymbol{\phi}^2 = \boldsymbol{\phi} \cdot \boldsymbol{\phi} = \sum_{i=1}^n (\phi^i)^2$ . It is coupled to a Dirac fermion field  $\psi$ , described by the Lagrangian:

$$\mathcal{L}_\psi = i\bar{\psi}(\gamma_0 \partial_\tau + c_f \boldsymbol{\gamma} \cdot \nabla)\psi. \quad (4.3)$$

The scalar mass squared  $r$  in Eq. (4.2) tunes the model through criticality:  $r < 0$  gives a phase with spontaneously broken  $O(n)$  symmetry,  $r > 0$  is the symmetric phase, and  $r = 0$  is the critical point. (For  $n = 2$ , this is the model studied in the previous chapter.) The parameter  $\lambda^2$  describes self-interactions of the order parameter. We define the Dirac adjoint in Eq. (4.3) as  $\bar{\psi} = -i\psi^\dagger \gamma_0$ . We denote  $\boldsymbol{\gamma} = (\gamma_1, \gamma_2)$ , and  $\gamma_\mu$ ,  $\mu = 0, 1, 2$  are Hermitian Dirac matrices obeying the  $SO(3)$  Clifford algebra  $\{\gamma_\mu, \gamma_\nu\} = 2\delta_{\mu\nu}$ . In the ordinary GNY model, Lorentz invariance (exact or emergent at criticality [208]) demands that the fermion  $c_f$  and boson  $c_b$  velocities be equal, but in the presence of quenched disorder, to be introduced below, the ratio  $c = c_f/c_b$  will flow under RG transformations.

We perform perturbative calculations near four dimensions at one-loop order via the triple epsilon-expansion scheme to be explained below, but we are ultimately interested in (2+1)D physics. We will present our results in terms of the number  $N$  of flavors of two-component Dirac fermions (i.e., the number of linear band crossing points at the Fermi level in a condensed matter system), but they can alternatively be interpreted as pertaining to  $N_f = N/2$  flavors of four-component Dirac fermions when  $N$  is even.

We consider the cases  $n = 1, 2, 3$ , corresponding to the chiral Ising, XY, and Heisenberg GNY models, respectively [126, 140]. The form of the Yukawa coupling  $\mathcal{L}_{\psi\phi}$  in Eq. (4.1) differs in each case. In the chiral Ising GNY model [125], a single real scalar  $\phi$  couples to

the fermion mass  $i\bar{\psi}\psi$ ,

$$\mathcal{L}_{\psi\phi}^{\text{Ising}} = ih\phi\bar{\psi}\psi, \quad (4.4)$$

with coupling strength  $h$ . The Yukawa coupling in the chiral XY GNY model can be formulated in different but equivalent ways, depending on the choice of spinor representation. In the four-component representation, the Yukawa coupling can be written as a coupling to both the ordinary mass  $i\bar{\psi}\psi$  and an axial mass  $\bar{\psi}\gamma_5\psi$ ,

$$\mathcal{L}_{\psi\phi}^{\text{XY}} = ih\bar{\psi}(\phi^1 + i\gamma_5\phi^2)\psi, \quad (4.5)$$

and is equivalent to the Nambu–Jona-Lasinio model [209]. Here, one utilizes a four-dimensional representation  $\gamma_\mu$ ,  $\mu = 0, 1, 2, 3$  of the  $SO(4)$  Clifford algebra, and  $\gamma_5 = \gamma_0\gamma_1\gamma_2\gamma_3$ . In a different spinor representation<sup>1</sup>, the model can be written as a coupling to a Majorana mass,

$$\mathcal{L}_{\psi\phi}^{\text{XY}} = \frac{h}{2}(\phi^*\psi^T i\gamma_2\psi + \text{H.c.}), \quad (4.6)$$

where the  $O(2)$  order parameter  $\phi = (\phi^1, \phi^2)$  is expressed as a complex scalar field  $\phi = \phi^1 + i\phi^2$ . This was the representation used in the previous chapter (upon substitution  $h \rightarrow h/2$ ). Finally, the Yukawa coupling in the chiral Heisenberg GNY model is:

$$\mathcal{L}_{\psi\phi}^{\text{Heis}} = ih\phi \cdot \bar{\psi}\boldsymbol{\sigma}\psi, \quad (4.7)$$

where  $\boldsymbol{\sigma} = (\sigma_1, \sigma_2, \sigma_3)$  forms a spin-1/2 representation of the  $SU(2)$  algebra.

For different values of  $N$ , the  $O(n)$  GNY models introduced above describe a variety of quantum phase transitions in (2+1)D condensed matter systems [185]. For  $N = 4$  (spinful fermions) and  $N = 2$  (spinless fermions), the chiral Ising GNY model ( $n = 1$ ) describes a transition from a Dirac semimetal to an insulator with charge-density-wave order on the

---

<sup>1</sup>See Appendix B.9 for the mapping between the two representations of the chiral XY GNY model.

honeycomb lattice [210]. For  $N = 1$ , the model describes a ferromagnetic transition on the surface of a 3D topological insulator [211]. For  $N = 1/2$ , which can be interpreted as a model containing a single flavor of two-component Majorana fermions, the model describes the time-reversal symmetry-breaking transition on the surface of a 3D topological superconductor [145], which exhibits an emergent  $\mathcal{N} = 1$  supersymmetry [145, 148, 212]. The chiral XY GNY model ( $n = 2$ ) has been considered in Chap. 3, but we recapitulate its applications here for completeness. The cases  $N = 4$  (spinful) and  $N = 2$  (spinless) are applicable to the Kekulé valence-bond-solid (VBS) transition on the honeycomb lattice [139, 150], or to the columnar VBS transition on the  $\pi$ -flux square lattice [151]. In these VBS transitions, spatial randomness acts as random-field disorder destroying the  $d = 2$  critical point<sup>2</sup>. Alternatively, the chiral XY GNY model also describes a semimetal-superconductor transition in a system with  $N$  two-component Dirac fermions ( $N = 4$  for spinful fermions on the honeycomb lattice [139]), in which case the  $U(1) \cong SO(2)$  symmetry is exact and random-field disorder is forbidden by conservation of particle number. For  $N = 1$ , the model describes a superconducting transition on the surface of a 3D topological insulator, and exhibits an emergent  $\mathcal{N} = 2$  supersymmetry [139, 145–148, 214]. Finally, for  $N = 4$  the chiral Heisenberg GNY model ( $n = 3$ ) describes the transition from a Dirac semimetal to an insulator with antiferromagnetic spin-density-wave order on the honeycomb lattice [210].

We model quenched random-mass disorder by randomness in the scalar mass squared,  $r(\mathbf{x}) = r_0 + \delta r(\mathbf{x})$ , where  $\delta r(\mathbf{x})$  is a Gaussian random variable of zero mean and correlation function [186]:

$$\overline{\delta r(\mathbf{x})\delta r(\mathbf{x}')}\propto\Delta\delta(\mathbf{x}-\mathbf{x}')+\frac{v}{|\mathbf{x}-\mathbf{x}'|^\alpha},\tag{4.8}$$

where  $\overline{\dots}$  denotes disorder averaging. The uniform part  $r_0$  is the tuning parameter for the

---

<sup>2</sup>The microscopic Ising/Heisenberg order parameters for charge-density-wave/spin-density-wave transitions on the honeycomb lattice are odd under the  $\mathbb{Z}_2$  symmetry of A-B sublattice exchange, which is explicitly broken by generic disorder configurations. As mentioned in Sec. 3.2, a microscopic example of random-mass disorder for those transitions is randomness in the nearest-neighbor (A-B) fermion hopping (see, e.g., Ref. [155, 213]).

transition, and  $\Delta$  and  $v$  are the short-range and long-range correlated disorder strengths, respectively. Even when considering initial conditions for the RG with only long-range correlated disorder,  $\Delta = 0$ , short-range correlated disorder is generated perturbatively already at one-loop order, see Eq. (4.40), and should be kept in the space of couplings. By contrast, long-range correlated disorder cannot be generated perturbatively from short-range correlated disorder, see Eq. (4.41). We use the replica trick to average over disorder (see Appendix B.1 and Refs. [30,156,157]), which induces an effective two-body interaction,

$$S_{\text{dis}} = -\frac{\Delta}{2} \sum_{ab} \int d^2\mathbf{x} d\tau d\tau' \phi_a^2(\mathbf{x}, \tau) \phi_b^2(\mathbf{x}, \tau') - \frac{v}{2} \sum_{ab} \int d^2\mathbf{x} d^2\mathbf{x}' d\tau d\tau' \frac{\phi_a^2(\mathbf{x}, \tau) \phi_b^2(\mathbf{x}', \tau')}{|\mathbf{x} - \mathbf{x}'|^\alpha}, \quad (4.9)$$

where  $a, b = 1, \dots, m$  are replica indices, and the replica limit  $m \rightarrow 0$  is to be taken at the end of the calculation. The local interaction term was already seen in Chap. 3, but now there is an additional long-range interaction arising from correlated disorder. As in Chap. 3, randomness in the scalar mass squared preserves the exact particle-hole symmetry of the clean GNY action (4.1).

### 4.3 RG in the triple epsilon expansion

The double epsilon expansion method has been explained in Chap. 3. In the presence of long-range correlated disorder, we see from Eq. (4.9) that the coupling constant  $v$  has mass dimension  $4 - \alpha$  at the Gaussian fixed point. While for generic  $\alpha < d < 4$  this coupling is strongly relevant, if we set  $\alpha = 4 - \delta$  and treat  $\delta$  as a small parameter, long-range correlated disorder is only slightly relevant and can be treated perturbatively [186]. This forms the basis of a triple expansion in  $\epsilon, \epsilon_\tau, \delta$  [207], which thus far has only been applied to bosonic systems. Below we employ this triple epsilon expansion to study the GNY models with both short-range and long-range correlated random-mass disorder. As in Chap. 3, fermion disorder is strongly irrelevant in this expansion and does not explicitly appear in the action.

In the presence of three epsilon-like parameters, the nature of the RG fixed points

and their stability depend on two ratios, e.g.,  $\epsilon/\epsilon_\tau$  and  $\delta/\epsilon_\tau$ . As in Chap. 3, we restrict our consideration to  $\epsilon/\epsilon_\tau = 2$ , which in the limit  $\epsilon_\tau \rightarrow 1$  corresponds to (2+1)D systems. Regarding the  $\delta/\epsilon_\tau$  ratio, we consider the range  $0 < \delta/\epsilon_\tau < 4$ . For  $\delta < 0$ , long-range correlated disorder is irrelevant at the Gaussian fixed point, and for  $\delta/\epsilon_\tau > 4$ , the long-range disorder correlations (4.8) with  $\alpha = 4 - \delta$  would have the unphysical feature of increasing rather than decaying with distance in the limit  $\epsilon_\tau \rightarrow 1$ .

### 4.3.1 Bare vs renormalized actions

The basic steps of the RG procedure are the same as in the previous chapter. For the convenience of the reader, we again outline them here using as example the chiral XY GNY model studied in Chap. 3, but now with long-range correlated disorder (4.9). For the chiral Ising and Heisenberg GNY models, the number of components of the order parameter and the form of the Yukawa coupling change [see Eqs. (4.4-4.7)], but the relations (4.16) between bare and renormalized couplings, and the formal expressions (4.17-4.22) for the beta functions in terms of the anomalous dimensions (4.12), remain the same.

As in Refs. [215,216], we rescale the time coordinate as well as the fermion and boson fields, and redefine the couplings in the action (4.1-4.9), to eliminate the velocities  $c_f$  and  $c_b$  in favor of the dimensionless ratio  $c^2 = (c_f/c_b)^2$ , which then appears in front of the time derivative term for the boson field. The replicated bare action for the random-mass chiral XY GNY model is then:

$$\begin{aligned}
S_B = \sum_a \int d^d \mathbf{x}_B d^{\epsilon_\tau} \tau_B & \left( i\bar{\psi}_{a,B} (\gamma_0 \partial_{\tau_B} + \boldsymbol{\gamma} \cdot \nabla_B) \psi_{a,B} + \phi_{a,B}^* (-c_B^2 \partial_{\tau_B}^2 - \nabla_B^2 + r) \phi_{a,B} \right. \\
& \left. + \lambda_B^2 |\phi_{a,B}|^4 + \frac{h_B}{2} (\phi_{a,B}^* \psi_{a,B}^T i\gamma_2 \psi_{a,B} + \text{H.c.}) \right) \\
& - \frac{\Delta_B}{2} \sum_{ab} \int d^d \mathbf{x}_B d^{\epsilon_\tau} \tau_B d^{\epsilon_\tau} \tau'_B |\phi_{a,B}|^2(\mathbf{x}_B, \tau_B) |\phi_{b,B}|^2(\mathbf{x}_B, \tau'_B) \\
& - \frac{v_B}{2} \sum_{ab} \int d^d \mathbf{x}_B d^d \mathbf{x}'_B d^{\epsilon_\tau} \tau_B d^{\epsilon_\tau} \tau'_B \frac{|\phi_{a,B}|^2(\mathbf{x}_B, \tau_B) |\phi_{b,B}|^2(\mathbf{x}'_B, \tau'_B)}{|\mathbf{x}_B - \mathbf{x}'_B|^\alpha}, \tag{4.10}
\end{aligned}$$

where  $a, b = 1, \dots, m$  are replica indices, and the corresponding renormalized action is:

$$\begin{aligned}
S = \sum_a \int d^d \mathbf{x} d^{\epsilon_\tau} \tau & \left( i \bar{\psi}_a (Z_1 \gamma_0 \partial_\tau + Z_2 \boldsymbol{\gamma} \cdot \nabla) \psi_a + \phi_a^* (-Z_3 c^2 \partial_\tau^2 - Z_4 \nabla^2 + Z_r r \mu^2) \phi_a \right. \\
& \left. + Z_5 \lambda^2 \mu^{\epsilon - \epsilon_\tau} |\phi_a|^4 + Z_6 \frac{\hbar}{2} \mu^{(\epsilon - \epsilon_\tau)/2} (\phi_a^* \psi_a^T i \gamma_2 \psi_a + \text{H.c.}) \right) \\
& - Z_7 \frac{\Delta}{2} \mu^\epsilon \sum_{ab} \int d^d \mathbf{x} d^{\epsilon_\tau} \tau d^{\epsilon_\tau} \tau' |\phi_a|^2(\mathbf{x}, \tau) |\phi_b|^2(\mathbf{x}, \tau') \\
& - Z_8 \frac{v}{2} \mu^\delta \sum_{ab} \int d^d \mathbf{x} d^d \mathbf{x}' d^{\epsilon_\tau} \tau d^{\epsilon_\tau} \tau' \frac{|\phi_a|^2(\mathbf{x}, \tau) |\phi_b|^2(\mathbf{x}', \tau')}{|\mathbf{x} - \mathbf{x}'|^\alpha}, \tag{4.11}
\end{aligned}$$

where  $\mu$  is a renormalization scale. Due to the anisotropy between space and time, we set  $\mathbf{x}_B = \mathbf{x}$  and  $\tau_B = \eta \tau$ , and matching the bare and renormalized kinetic terms for the fermion we find that  $\eta = Z_2/Z_1$ . Defining the anomalous dimensions:

$$\gamma_i = \mu \frac{d \ln Z_i}{d \mu}, \quad i = 1, \dots, 8, r, \tag{4.12}$$

we find that the dynamic critical exponent  $z = \mu(d \ln \tau / d \mu)$  [120] is given by:

$$z = 1 + \gamma_1 - \gamma_2. \tag{4.13}$$

The fermion and boson fields are multiplicatively renormalized,

$$\psi_{a,B}(\mathbf{x}_B, \tau_B) = \sqrt{Z_\psi} \psi_a(\mathbf{x}, \tau), \quad \phi_{a,B}(\mathbf{x}_B, \tau_B) = \sqrt{Z_\phi} \phi_a(\mathbf{x}, \tau), \tag{4.14}$$

and the fermion and boson anomalous dimensions,  $\eta_\psi = \mu(d \ln Z_\psi / d \mu)$  and  $\eta_\phi = \mu(d \ln Z_\phi / d \mu)$ , are given by:

$$\eta_\psi = \gamma_2 + \epsilon_\tau (z - 1), \quad \eta_\phi = \gamma_4 + \epsilon_\tau (z - 1). \tag{4.15}$$

Comparing Eqs. (4.10) and (4.11), we obtain relations between the bare and (dimensionless)

renormalized couplings,

$$c^2 = Z_3^{-1} Z_4 \left( \frac{Z_1}{Z_2} \right)^2 c_B^2, \quad \lambda^2 = \mu^{-(\epsilon - \epsilon_\tau)} \left( \frac{Z_1}{Z_2} \right)^{\epsilon_\tau} Z_4^2 Z_5^{-1} \lambda_B^2, \quad h^2 = \mu^{-(\epsilon - \epsilon_\tau)} \left( \frac{Z_1}{Z_2} \right)^{\epsilon_\tau} Z_2^2 Z_4 Z_6^{-2} h_B^2, \\ \Delta = \mu^{-\epsilon} Z_4^2 Z_7^{-1} \Delta_B, \quad v = \mu^{-\delta} Z_4^2 Z_8^{-1} v_B, \quad r = \mu^{-2} Z_4 Z_r^{-1} r_B. \quad (4.16)$$

Using the fact that the bare couplings do not depend on the renormalization scale  $\mu$ , we find the RG beta functions  $\beta_g \equiv \mu(dg/d\mu)$ ,  $g \in \{c^2, \lambda^2, h^2, \Delta, v\}$ , to be:

$$\beta_{c^2} = (2\gamma_1 - 2\gamma_2 - \gamma_3 + \gamma_4)c^2, \quad (4.17)$$

$$\beta_{\lambda^2} = (-\epsilon - \epsilon_\tau + 2\gamma_4 - \gamma_5 + \epsilon_\tau(\gamma_1 - \gamma_2))\lambda^2, \quad (4.18)$$

$$\beta_{h^2} = (-\epsilon - \epsilon_\tau + 2(\gamma_2 - \gamma_6) + \gamma_4 + \epsilon_\tau(\gamma_1 - \gamma_2))h^2, \quad (4.19)$$

$$\beta_\Delta = (-\epsilon + 2\gamma_4 - \gamma_7)\Delta, \quad (4.20)$$

$$\beta_v = (-\delta + 2\gamma_4 - \gamma_8)v, \quad (4.21)$$

$$\beta_r = (-2 + \gamma_4 - \gamma_r)r. \quad (4.22)$$

From Eq. (4.22), we find the inverse correlation length exponent [163],

$$\nu^{-1} = 2 - \gamma_4 + \gamma_r. \quad (4.23)$$

### 4.3.2 Renormalization constants

We calculate the renormalization constants  $Z_i$ ,  $i = 1, \dots, 8, r$  at one-loop order in the modified minimal subtraction ( $\overline{\text{MS}}$ ) scheme with dimensional regularization in  $4 - \epsilon$  space and  $\epsilon_\tau$  time dimensions. The relevant Feynman rules and diagrams are shown schematically in Figs. 4.1 and 4.2, respectively. The fermion and boson propagators are given by:

$$G_{ab}^{IJ}(p) = \langle \psi_a^I(p) \bar{\psi}_b^J(p) \rangle = \delta_{ab} \delta^{IJ} \frac{\not{p}}{p^2}, \quad (4.24)$$

$$D_{ab}^{ij}(p) = \langle \phi_a^i(p) \phi_b^j(-p) \rangle = \delta_{ab} \delta^{ij} \frac{1}{c^2 p_0^2 + \mathbf{p}^2 + r\mu^2}, \quad (4.25)$$

where  $I, J = 1, \dots, N$  and  $i, j = 1, \dots, n$  are fermion flavor and  $O(n)$  indices, respectively, and  $\not{p} = \gamma_\mu p_\mu$ .

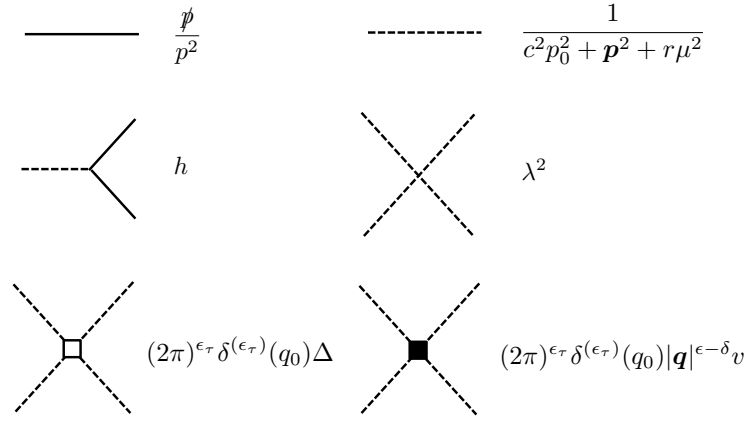


Figure 4.1: Schematic momentum-space Feynman rules for the random-mass GNY models, omitting fermion flavor,  $O(n)$ , and replica indices. Solid line: fermion propagator, dashed line: boson propagator. Here  $p = (p_0, \mathbf{p})$  is the momentum of a propagator line, with  $\not{p} = \gamma_\mu p_\mu$ , and  $q = (q_0, \mathbf{q})$  is the momentum transfer in a boson four-point vertex.

For the chiral XY GNY model ( $n = 2$ ), the diagrams in the clean limit or containing only short-range correlated disorder vertices were already computed in Chap. 3; these results are also easily adapted to  $n = 1$  and  $n = 3$ . The new diagrams containing long-range correlated disorder vertices are evaluated explicitly in Appendix B.5 for  $n = 1, 2, 3$ . Unlike the standard epsilon expansion in  $4 - \epsilon$  dimensions, in the triple epsilon expansion one-loop diagrams contain simple poles not only in  $\epsilon$ , but also in  $\epsilon - \epsilon_\tau$ ,  $\delta$ , and  $2\delta - \epsilon$ . We obtain the

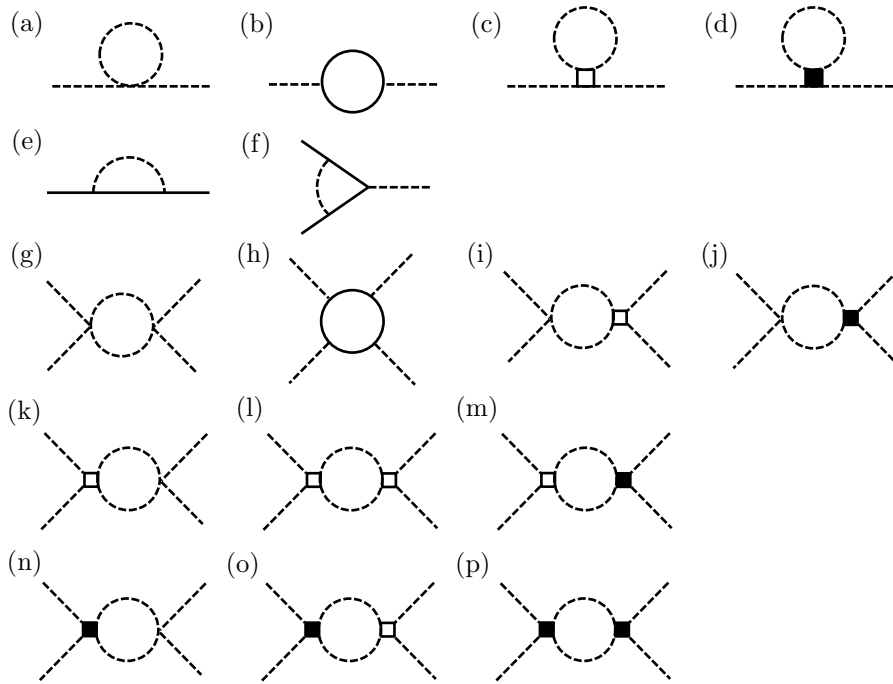


Figure 4.2: Schematic one-loop Feynman diagrams for the random-mass GNY models. Renormalization of (a,b,c,d) the boson two-point function; (e) the fermion two-point function; (f) the Yukawa vertex  $h$ ; (g,h,i,j) the boson self-interaction vertex  $\lambda^2$ ; (i,k,l,m) the short-range correlated disorder vertex  $\Delta$ ; and (j,l,m) the long-range correlated disorder vertex  $v$ .

following renormalization constants:

$$Z_1 = 1 - \frac{nh^2}{\epsilon - \epsilon_\tau} f(c^2), \quad (4.26)$$

$$Z_2 = 1 - \frac{nh^2}{2(\epsilon - \epsilon_\tau)}, \quad (4.27)$$

$$Z_3 = 1 - \frac{2\Delta}{\epsilon} - \frac{2v}{\delta} - \frac{Nh^2c^{-2}}{\epsilon - \epsilon_\tau}, \quad (4.28)$$

$$Z_4 = 1 - \frac{Nh^2}{\epsilon - \epsilon_\tau}, \quad (4.29)$$

$$Z_5 = 1 + \frac{2(n+8)\lambda^2}{\epsilon - \epsilon_\tau} - \frac{Nh^4\lambda^{-2}}{\epsilon - \epsilon_\tau} - \frac{12\Delta}{\epsilon} - \frac{12v}{\delta}, \quad (4.30)$$

$$Z_6 = 1 + (2-n) \frac{h^2}{\epsilon - \epsilon_\tau}, \quad (4.31)$$

$$Z_7 = 1 + \frac{4(n+2)\lambda^2}{\epsilon - \epsilon_\tau} - \frac{8\Delta}{\epsilon} - \frac{12v}{\delta} - \frac{4v^2\Delta^{-1}}{2\delta - \epsilon}, \quad (4.32)$$

$$Z_8 = 1 + \frac{4(n+2)\lambda^2}{\epsilon - \epsilon_\tau} - \frac{4\Delta}{\epsilon} - \frac{4v}{\delta}, \quad (4.33)$$

$$Z_r = 1 + \frac{2(n+2)\lambda^2}{\epsilon - \epsilon_\tau} - \frac{2\Delta}{\epsilon} - \frac{2v}{\delta}. \quad (4.34)$$

We have rescaled the couplings according to  $g/(4\pi)^2 \rightarrow g$ ,  $g \in \{\lambda^2, h^2, \Delta, v, r\}$ , and, as in Chap. 3, we define the dimensionless function,

$$f(c^2) = \frac{c^2(c^2 - 1 - \ln c^2)}{(c^2 - 1)^2}, \quad (4.35)$$

plotted earlier in Fig. 3.4. At one-loop order there is no renormalization of the Yukawa vertex for the chiral XY GNY model, i.e., the diagram in Fig. 4.2(f) vanishes for  $n = 2$  [see Eq. (4.31)], which is easily seen from the form (4.6) of the Yukawa coupling. We also see from the last term in Eq. (4.32) that short-range correlated disorder is generated at one-loop order from long-range correlated disorder, via the diagram in Fig. 4.2(m). By contrast, long-range correlated disorder cannot be generated perturbatively from short-range correlated disorder.

### 4.3.3 Beta functions and anomalous dimensions

Using the chain rule,

$$\gamma_i = \frac{\mu}{Z_i} \frac{dZ_i}{d\mu} = \frac{1}{Z_i} \sum_g \frac{\partial Z_i}{\partial g} \beta_g, \quad (4.36)$$

for  $i = 1, \dots, 8, r$  and  $g \in \{c^2, \lambda^2, h^2, \Delta, v, r\}$  in Eqs. (4.17-4.22), and expanding the beta functions to quadratic order in all couplings except  $c^2$ , we obtain:

$$\beta_{c^2} = -2(\Delta + v)c^2 + h^2[N(c^2 - 1) + nc^2(2f(c^2) - 1)], \quad (4.37)$$

$$\beta_{\lambda^2} = -(\epsilon - \epsilon_\tau)\lambda^2 + 2(n + 8)\lambda^4 + 2Nh^2\lambda^2 - Nh^4 - 12(\Delta + v)\lambda^2, \quad (4.38)$$

$$\beta_{h^2} = -(\epsilon - \epsilon_\tau)h^2 + (N + 4 - n)h^4, \quad (4.39)$$

$$\beta_\Delta = -\epsilon\Delta + 4(n + 2)\lambda^2\Delta + 2Nh^2\Delta - 8\Delta^2 - 12\Delta v - 4v^2, \quad (4.40)$$

$$\beta_v = -\delta v + 4(n + 2)\lambda^2v + 2Nh^2v - 4\Delta v - 4v^2. \quad (4.41)$$

We note that all poles in linear combinations of the small parameters  $\epsilon, \epsilon_\tau, \delta$  properly cancel in the beta functions. Setting  $\epsilon_\tau$  and the disorder couplings to zero, we find that Eqs. (4.38-4.39) agree with the beta functions for the chiral  $O(n)$  GNY models in the clean limit [140]. When setting  $n = 2$  and  $v = 0$ , Eqs. (4.37-4.40) reproduce our previous results for the chiral XY GNY model with short-range correlated disorder in Chap. 3. Finally, when turning off the Yukawa coupling,  $h^2 = 0$ , the beta functions (4.38,4.40,4.41) with both short-range and long-range correlated disorder agree with those given in Refs. [123, 124, 160, 186, 207]. We also note that the above beta functions are perturbative in the couplings  $\lambda^2, h^2, \Delta$ , and  $v$ , but exact in the dimensionless velocity ratio  $c^2$ .

The critical exponents  $\nu^{-1}$ ,  $z$ ,  $\eta_\psi$ , and  $\eta_\phi$  are obtained by evaluating:

$$\nu^{-1} = 2 - Nh^2 - 2(n+2)\lambda^2 + 2(\Delta + v), \quad (4.42)$$

$$z = 1 + \left(f(c^2) - \frac{1}{2}\right)nh^2, \quad (4.43)$$

$$\eta_\psi = \frac{n}{2}h^2 + \epsilon_\tau(z - 1), \quad (4.44)$$

$$\eta_\phi = Nh^2 + \epsilon_\tau(z - 1), \quad (4.45)$$

at RG fixed points  $(c_*^2, \lambda_*^2, h_*^2, \Delta_*, v_*)$ , i.e., common zeros of the set (4.37-4.41) of beta functions. Since  $h_*^2$  will be  $\mathcal{O}(\epsilon, \epsilon_\tau)$  at one-loop order, as can already be seen from Eq. (4.39), for a consistent treatment we have to discard the  $\epsilon_\tau(z - 1)$  terms in the fermion and boson anomalous dimensions, as done in the previous chapter.

## 4.4 Fixed points and critical exponents

In Sec. 4.4.1, we discuss the fixed points of the flow equations (4.37-4.41). Depending on their stability, which is analyzed in Sec. 4.4.2, these are *bona fide* critical points (no relevant direction) or multicritical points (one or more relevant directions). Here, the number of relevant directions refers to the number of such directions on the critical hypersurface, since the tuning parameter  $r$  for the transition (see Sec. 4.2) is a relevant direction at all fixed points. As mentioned in Sec. 4.3, we fix  $\epsilon = 2\epsilon_\tau$ , with the extrapolation  $\epsilon_\tau \rightarrow 1$  corresponding to 2+1 dimensions. Throughout the chapter, we evaluate quantities such as fixed-point couplings, RG eigenvalues, and critical exponents as a function of the control parameters  $N \geq 1$  and  $\delta = 4 - \alpha \in [0, 4]$ , where the latter parameter is to be understood as the ratio  $\delta/\epsilon_\tau$  evaluated at  $\epsilon_\tau = 1$ .

### 4.4.1 Fixed points

We denote the RG fixed points as five-component vectors  $(c_*^2, \lambda_*^2, h_*^2, \Delta_*, v_*)$  in the space of running couplings. Starting with the CFPs ( $\Delta_* = v_* = 0$ ), these include Gaussian fixed

points  $(c_*^2, 0, 0, 0, 0)$  and the  $O(n)$  Wilson-Fisher fixed points  $(c_*^2, \frac{\epsilon_\tau}{2(n+8)}, 0, 0, 0)$ , where  $c_*^2$  is arbitrary and can be set to unity by independent redefinitions of the fermion and boson fields. We also have the GNY fixed points, for all  $n = 1, 2, 3$  and  $N$  given by:

$$\left(1, \frac{4 - n - N + \sqrt{D_C}}{4(n+8)(N+4-n)} \epsilon_\tau, \frac{\epsilon_\tau}{(N+4-n)}, 0, 0\right), \quad (4.46)$$

where  $D_C = N^2 + 2(5n+28)N + (4-n)^2$ , in agreement with earlier studies [140]. The fixed-point couplings are positive for all  $N > 0$ . Since  $c_*^2 = 1$  and  $f(1) = \frac{1}{2}$  (Fig. 3.4), Eq. (4.43) implies that the CFPs are Lorentz invariant ( $z = 1$ ), and are in fact conformally invariant.

We next turn to DFPs, for which  $\Delta_*$  and/or  $v_*$  are nonzero. To be physical, all fixed points must obey the following conditions [186]:

$$c_*^2 > 0, \quad \lambda_*^2 \geq 0, \quad h_*^2 \geq 0, \quad v_* \geq 0, \quad \Delta_* + v_* \geq 0. \quad (4.47)$$

At fermionic DFPs with  $h_*^2 > 0$ , the condition  $\beta_{c^2} = 0$  together with Eq. (4.47) further implies that  $c_*^2 > 1$ . From Eq. (4.37), we find that at a fermionic fixed point,

$$N(c_*^2 - 1) + 2nc_*^2 \left(f(c_*^2) - \frac{1}{2}\right) = \frac{2(\Delta_* + v_*)c_*^2}{h_*^2}. \quad (4.48)$$

Equation (4.47) implies that the right-hand side of this equation is positive. From Fig. 3.4 and Eq. (4.35), we see that  $f(c_*^2) > \frac{1}{2}$  only if  $c_*^2 > 1$ , and  $f(c_*^2) < \frac{1}{2}$  only if  $c_*^2 < 1$ . Thus for the left-hand side of Eq. (4.48) to be positive also we must have  $c_*^2 > 1$ . (At a clean fermionic fixed point, the left-hand side must vanish, which can only happen for  $c_*^2 = 1$ .)

#### 4.4.1.1 Fixed points with short-range correlated disorder

We first focus on DFPs with  $\Delta_* \neq 0$  and  $v_* = 0$ , which we term short-range disordered fixed points (SDFPs). From Eq. (4.39) we find that  $h_*^2 = 0$  or  $h_*^2 = \epsilon_\tau/(N+4-n)$ . When the fixed-point value of the Yukawa coupling is zero, we reproduce the results of

Refs. [123, 124, 160] for the purely bosonic  $O(n)$  vector model with random-mass disorder. For  $n = 1$ , there is an accidental degeneracy in the system of equations  $\beta_{\lambda^2} = 0, \beta_{\Delta} = 0$ . The degeneracy is lifted at two-loop order, giving rise to a DFP with  $\lambda_*^2, \Delta_* \sim \mathcal{O}(\sqrt{\epsilon_\tau})$ , for a finite ratio  $\epsilon/\epsilon_\tau$  [123].

Our focus, however, is on fermionic DFPs with nonzero  $h_*^2$ . We find two fermionic SDFPs for  $n = 2, 3$ :

$$\left( c_{*1,2}^2, \frac{N+8-2n \pm \sqrt{D_S}}{8(n-1)(N+4-n)} \epsilon_\tau, \frac{\epsilon_\tau}{N+4-n}, \frac{(n+2)(N \pm \sqrt{D_S}) + 2(4-n)^2}{16(n-1)(N+4-n)} \epsilon_\tau, 0 \right), \quad (4.49)$$

where  $D_S = N^2 - 4(5n-8)N + 4(4-n)^2$ , which we denote by SDFP1 (with  $+\sqrt{D_S}$ ,  $c_*^2 = c_{*1}^2$ ) and SDFP2 (with  $-\sqrt{D_S}$ ,  $c_*^2 = c_{*2}^2$ ). The chiral XY case ( $n = 2$ ) was discussed in Chap. 3: the fixed-point couplings  $\lambda_*^2$ ,  $h_*^2$ , and  $\Delta_*$  are nonnegative, and thus physical, for all  $N \geq 1$ . At  $N = 1$ , SDFP2 merges with the clean GNY fixed point (4.46), while SDFP1 runs off to infinity as it is impossible to satisfy  $\beta_{e^2} = 0$ . (Note that for  $n = 2$ , SDFP1,2 here correspond to DFP1,2 in Chap. 3 and Ref. [2] for  $N < 4$  and to DFP2,1 for  $N > 4$ .) In the chiral Heisenberg case ( $n = 3$ ), the discriminant  $D_S \geq 0$  for  $N \geq N_D \approx 27.856$ , and the SDFPs (4.49) are physical only for  $N > N_D$ .

In the chiral Ising case ( $n = 1$ ), as previously mentioned, the RG equations for  $\lambda^2$  and  $\Delta$  become degenerate for zero Yukawa coupling, and we find only one solution at order  $\mathcal{O}(\epsilon, \epsilon_\tau)$  for  $h_*^2 \neq 0$ :

$$\left( c_*^2, \frac{N\epsilon_\tau}{(N+3)(N+6)}, \frac{\epsilon_\tau}{N+3}, \frac{3(N-6)\epsilon_\tau}{4(N+3)(N+6)}, 0 \right). \quad (4.50)$$

This SDFP is physical for  $N \geq 6$ , and merges with the clean GNY fixed point at  $N = 6$ . There is in principle the possibility of an additional SDFP at two-loop order with  $\lambda_*^2, \Delta_* \sim \mathcal{O}(\sqrt{\epsilon_\tau})$ , as in the bosonic case, and  $h_*^2 \sim \mathcal{O}(\epsilon_\tau)$ . We show in Appendix B.6 that this cannot happen, because it is impossible to satisfy the equation  $\beta_{e^2} = 0$ . We also note that this excludes the possibility of a physical SDFP for the  $N = 1/2$  chiral Ising GNY model, which in the clean limit flows to a conformal field theory with emergent

supersymmetry [148, 212], the  $\mathcal{N} = 1$  Wess-Zumino model. (This theory describes the time-reversal symmetry-breaking transition among the gapless Majorana surface states of a three-dimensional topological superfluid, e.g.,  ${}^3\text{He-B}$  [145].)

For the fermionic SDFPs found in Eqs. (4.49-4.50) above, despite the fact that the equation  $\beta_{c^2} = 0$  is nonlinear in  $c^2$ , one can show analytically that it admits a unique solution  $c_*^2 > 1$ , except for  $N = 1$  in the XY GNY model. The actual fixed-point values of  $c^2$  are obtained by solving the equation numerically, and together with  $h_*^2$  determine via Eq. (4.43) the dynamic critical exponent  $z$  at those fixed points (see Sec. 4.4.3, Fig. 4.6).

#### 4.4.1.2 Fixed points with long-range correlated disorder

We now turn to DFPs with  $v_* \neq 0$ , which we dub long-range disordered fixed points (LDFPs). For vanishing  $h_*^2$ , the purely bosonic random-mass  $O(n)$  vector model for  $n > 1$  was studied in the triple epsilon expansion in Ref. [207], where LDFPs were found. For  $n = 1$ , long-range correlated disorder lifts the previously mentioned degeneracy in the system of fixed-point equations. For nonzero  $h_*^2 = \epsilon_\tau / (N + 4 - n)$ , we find two fermionic LDFPs in all three GNY universality classes,  $n = 1, 2, 3$ :

$$\lambda_{*1,2}^2 = \frac{3(N + 4 - n)\delta - (5N + 4 - n)\epsilon_\tau \pm \sqrt{D_L}}{4(5n + 4)(N + 4 - n)}, \quad (4.51)$$

$$(\Delta_* + v_*)_{1,2} = \frac{-2(n - 1)(N + 4 - n)\delta + [(5n - 2)N - 9 + (n - 1)^2]\epsilon_\tau \pm (2 + n)\sqrt{D_L}}{4(5n + 4)(N + 4 - n)}, \quad (4.52)$$

$$v_{*1,2} = \left(1 + \frac{4(\Delta_* + v_*)_{1,2}}{2\epsilon_\tau - \delta}\right) (\Delta_* + v_*)_{1,2}, \quad (4.53)$$

where  $D_L = [(5N + 4 - n)\epsilon_\tau - 3(N + 4 - n)\delta]^2 - 8(5n + 4)N\epsilon_\tau^2$ . The discriminant  $D_L$  is nonnegative, and thus the fixed-point couplings real, for either:

$$\delta \geq \delta_D \equiv \frac{(5N + 4 - n) + \sqrt{8(5n + 4)N}}{3(N + 4 - n)} \epsilon_\tau, \quad (4.54)$$

or:

$$\delta \leq \delta'_D \equiv \frac{(5N + 4 - n) - \sqrt{8(5n + 4)N}}{3(N + 4 - n)} \epsilon_\tau. \quad (4.55)$$

In addition to being real, the fixed-point couplings (4.51-4.53) must obey the conditions (4.47). By contrast with the SDFPs (4.49-4.50), which are physical above a certain critical value of  $N$  that is independent of  $\delta$ , the LDFPs are physical only in complicated regions of the  $N$ - $\delta$  plane that possess several disconnected components and/or curved boundaries. Since the fixed-point couplings (4.51-4.53) do not depend explicitly on  $c_*^2$ , we first assume a physical solution for  $c_*^2$  exists, and discuss how the remaining conditions delimit those nontrivial regions.

- $\lambda_*^2 \geq 0$ : This condition is satisfied for all  $n = 1, 2, 3$  for both LDFPs provided that  $\delta \geq \delta_D$ . Since  $\delta_D > \delta'_D$  for all  $N > 0$ , LDFPs in the region  $\delta \leq \delta'_D$  of Eq. (4.55) are never physical.
- $\Delta_* + v_* \geq 0$ : For LDFP1, i.e., Eqs. (4.51-4.53) with  $+\sqrt{D_L}$ , the condition is satisfied for different regions of the  $N$ - $\delta$  plane depending on  $n$ :

$$n = 1 : \delta \in \begin{cases} [0, \delta_2] \cup [\delta_1, 4\epsilon_\tau], & N \leq N_2, \\ [0, \delta'_D] \cup [\delta_D, 4\epsilon_\tau], & N > N_2; \end{cases} \quad (4.56)$$

$$n = 2, 3 : \delta \in [0, \delta'_D] \cup \begin{cases} [\delta_1, 4\epsilon_\tau], & N \leq N_2, \\ [\delta_D, 4\epsilon_\tau], & N > N_2. \end{cases} \quad (4.57)$$

For LDFP2, i.e., Eqs. (4.51-4.53) with  $-\sqrt{D_L}$ , we have:

$$n = 1 : \delta \in \cup \begin{cases} \emptyset, & N < N_2, \\ [\delta_2, \delta'_D] \cup [\delta_D, \delta_1], & N \geq N_2; \end{cases} \quad (4.58)$$

$$n = 2, 3 : \delta \in \begin{cases} [\delta_2, \delta'_D], & N \leq N_2, \\ [\delta_2, \delta'_D] \cup [\delta_D, \delta_1], & N \geq N_2. \end{cases} \quad (4.59)$$

Here,

$$\delta_1 \equiv \frac{[(n+14)N+9-(n-1)^2] + (n+2)\sqrt{D_C}}{(n+8)(N+4-n)} \epsilon_\tau, \quad (4.60)$$

$$\delta_2 \equiv \frac{[(n+14)N+9-(n-1)^2] - (n+2)\sqrt{D_C}}{(n+8)(N+4-n)} \epsilon_\tau, \quad (4.61)$$

and  $N_2$  is the value of  $N$ , which depends on  $n$ , at which  $\delta_1 = \delta_D$ . For  $N < N' < N_2$ ,  $\delta'_D < 0$ , in which case  $[0, \delta'_D]$  denotes the empty set. We use the same notational convention whenever the left limit of the interval is greater than the right one.

- $v_* \geq 0$ : For LDFFP1, we have the following constraints depending on the value of  $n$ :

$$n = 1 : \delta \in \begin{cases} [0, \delta_2] \cup [\delta_1, 2\epsilon_\tau), & N \leq N_2, \\ [0, \delta'_D] \cup [\delta_D, 2\epsilon_\tau), & N > N_2; \end{cases} \quad (4.62)$$

$$n = 2 : \delta \in [0, \delta'_D] \cup [\delta_D, 2\epsilon_\tau) \cup \begin{cases} [\delta_1, \delta_4] \cup [\delta_3, 4\epsilon_\tau], 1 \leq N < N_2, \\ [\delta_D, \delta_4] \cup [\delta_3, 4\epsilon_\tau], N_2 \leq N \leq N_3, \\ [\delta_3, 4\epsilon_\tau], N > N_3; \end{cases} \quad (4.63)$$

$$n = 3 : \delta \in [0, \delta'_D] \cup [\delta_D, 2\epsilon_\tau) \cup \begin{cases} [\delta_1, 4\epsilon_\tau], 1 \leq N < N_2, \\ [\delta_D, 4\epsilon_\tau], N_2 \leq N < N_D, \\ [\delta_D, \delta_4] \cup [\delta_3, 4\epsilon_\tau], N_D \leq N \leq N_3, \\ [\delta_3, 4\epsilon_\tau], N > N_3. \end{cases} \quad (4.64)$$

For LDFFP2, we have:

$$n = 1 : \delta \in [\delta_5, \max(2\epsilon_\tau, \delta_1)] \cup \begin{cases} \emptyset, 1 \leq N < N_2, \\ [\delta_2, \delta'_D] \cup [\delta_D, \min(\delta_1, 2\epsilon_\tau)], N \geq N_2; \end{cases} \quad (4.65)$$

$$n = 2, 3 : \delta \in [\delta_2, \delta'_D] \cup [\delta_D, 2\epsilon_\tau) \cup \begin{cases} \emptyset, 1 \leq N < N_2, \\ [\delta_D, \delta_1], N_2 \leq N < N_3, \\ [\delta_4, \delta_1], N \geq N_3. \end{cases} \quad (4.66)$$

We further define

$$\delta_3 \equiv \frac{3[N + 6 + (n - 1)(3N + 6 - 2n)] + (n + 2)\sqrt{D_S}}{4(n - 1)(N + 4 - n)} \epsilon_\tau, \quad (4.67)$$

$$\delta_4 \equiv \frac{3[N + 6 + (n - 1)(3N + 6 - 2n)] - (n + 2)\sqrt{D_S}}{4(n - 1)(N + 4 - n)} \epsilon_\tau, \quad (4.68)$$

$$\delta_5 \equiv \frac{2N^2 + 21N + 18}{(N + 3)(N + 6)} \epsilon_\tau, \quad (4.69)$$

and  $N_3$  is the  $n$ -dependent value of  $N$  at which  $\delta_D = \delta_4$ .

For a given GNY symmetry class  $n$ , the intersection of all those conditions defines regions in the  $N$ - $\delta$  plane in which the various fixed points discussed are physical, and over which fixed-point properties are plotted throughout this chapter.

We now return to the question of whether a physical solution  $c_*^2$  to the nonlinear equation  $\beta_{c^2} = 0$  exists for the LDFPs (4.51-4.53). We solve this equation numerically. For  $n = 1$  and  $n = 3$ , we find a unique solution everywhere in the physical regions of the  $N$ - $\delta$  plane. For  $n = 2$ , we likewise find a unique physical solution in the physical regions, but for LDFP1 computations become increasingly difficult upon approach to the point  $N = 1$ ,  $\delta = 4$ , where  $c_*^2$  grows rapidly. Since exactly at this point LDFP1 coincides with SDFP2, and SDFP2 does not admit a solution to  $\beta_{c^2} = 0$  for  $N = 1$  (see Chap. 3 and Ref. [2]), we conjecture that  $c_*^2$  gradually runs off to infinity as the point  $N = 1$ ,  $\delta = 4$  is approached. Summarizing, we thus find that for all three GNY symmetry classes, a unique solution  $c_*^2 > 1$  exists for the LDFPs (4.51-4.53) everywhere inside the physical regions (4.47) of the  $N$ - $\delta$  plane. As mentioned previously,  $h_*^2$  and  $c_*^2$  together determine the dynamic critical exponent  $z$  at those fixed points (Sec. 4.4.3, Figs. 4.7-4.9).

#### 4.4.2 Linear stability analysis

We now investigate the stability properties of the physical fixed points. All bosonic fixed points (i.e., with  $h_*^2 = 0$ ) are unstable with respect to the  $h^2$  direction. Additionally, for all models, the Gaussian fixed points are unstable with respect to all other directions, and the Wilson-Fisher fixed points are unstable with respect to both short-range and long-range correlated disorder. The stability properties of the bosonic DFPs in the absence of Yukawa coupling have been discussed previously in Refs. [123, 124, 160, 207].

At all fermionic fixed points (i.e., with  $h_*^2 \neq 0$ ), the  $h^2$  direction is irrelevant. Additionally, we find that  $\partial\beta_{c^2}/\partial c^2$  is positive at all such fixed points. Since  $\beta_{c^2}$  is the only beta function in which  $c^2$  appears, this means  $c^2$  is also an irrelevant direction. We can thus exclude  $h^2$  and  $c^2$  from RG flow considerations and investigate stability within the three-

dimensional subspace with fixed  $h_*^2$  and  $c_*^2$  of the full five-dimensional space of couplings. We compute the eigenvalues  $y$  of the stability matrix  $M_{gg'} \equiv -\partial\beta_g/\partial g'$ ,  $g, g' \in \{\lambda^2, \Delta, v\}$ , defined such that  $y > 0$  ( $y < 0$ ) corresponds to a relevant (irrelevant) direction.

#### 4.4.2.1 Stability of the clean fixed point

We first focus on the clean GNY fixed point (4.46), which for the rest of the chapter we refer to as the CFP. The RG eigenvalues at the CFP are:

$$y_1 = -\frac{\sqrt{D_C}}{N+4-n}\epsilon_\tau, \quad y_2 = \frac{(n+2)N + (n+14)(4-n) - (n+2)\sqrt{D_C}}{(n+8)(N+4-n)}\epsilon_\tau, \quad y_3 = \delta - \delta_1, \quad (4.70)$$

and are associated with eigenvectors with nonzero projections along the  $\lambda^2$ ,  $\Delta$ , and  $v$  directions, respectively. The eigenvalue  $y_1$  is negative and thus irrelevant for all  $n$  and  $N$ . For the flow of short-range correlated disorder ( $y_2$ ), we discuss the three GNY symmetry classes in turn.

- $n = 1$ : Disorder is irrelevant for  $N > 6$ . At  $N = 6$ , the CFP merges with the SDFP (4.50), and disorder becomes marginally relevant. For  $N < 6$  (including  $N = 1/2$ ), the SDFP becomes unphysical, and disorder becomes relevant at the CFP.
- $n = 2$ : This case was studied in Chap. 3. Disorder is irrelevant for  $N > 1$ . At  $N = 1$ , SDFP2 [see Eq. (4.49)] merges with the CFP and disorder becomes marginally relevant.
- $n = 3$ : Disorder is irrelevant for all  $N > \frac{2}{15} \approx 0.133$ .

Finally, long-range correlated disorder ( $y_3$ ) is irrelevant for  $\delta$  less than  $\delta_1$ , which is defined in Eq. (4.60). At generic points along the curve  $\delta = \delta_1$  in the  $N$ - $\delta$  plane, one of the LDFPs merges with the CFP, and long-range correlated disorder crosses marginality. At the special point  $N = N_2$  along this curve, the two LDFPs (4.51-4.53) coincide with one another (and with the CFP).

#### 4.4.2.2 Stability of short-range disordered fixed points

We now consider the SDFPs of Sec. 4.4.1.1. We begin with the unique SDFP (4.50) in the chiral Ising class ( $n = 1$ ), which is physical only for  $N \geq 6$ . Long-range correlated disorder is irrelevant at this fixed point provided that  $\delta$  is less than  $\delta_5$ , which is defined in Eq. (4.69). Along the curve  $\delta = \delta_5$  in the  $N$ - $\delta$  plane, the SDFP merges with LDFP2. However, one of the two other eigenvalues is always relevant for  $N > 6$ , thus the SDFP is a multicritical point with at least one relevant direction on the critical hypersurface.

The chiral XY ( $n = 2$ ) and Heisenberg ( $n = 3$ ) classes admit two fermionic SDFPs, Eq. (4.49). Similarly to the chiral Ising case, long-range correlated disorder is irrelevant at SDFP1 (SDFP2) provided that  $\delta < \delta_3$  ( $\delta < \delta_4$ ), with  $\delta_3, \delta_4$  defined in Eqs. (4.67-4.68). The curves  $\delta = \delta_3$  and  $\delta = \delta_4$  correspond to the merger of the corresponding SDFP with one of the LDFPs. When  $\delta_3 = \delta_4$ , the discriminant  $D_S$  vanishes, and the two SDFPs merge with one another. This happens at a critical value of  $N$  which in the XY case is  $N = 4$ , and in the Heisenberg case is  $N = N_D \approx 27.856$ . Besides long-range correlated disorder, the other two directions are irrelevant at SDFP1, thus it is a genuine critical point for  $\delta < \delta_3$ . By contrast, one of those two directions is relevant at SDFP2, thus the latter is a multicritical point.

For the chiral XY and Heisenberg models, and for sufficiently large  $N$ , the two irrelevant eigenvalues at SDFP1 with eigenvectors in the  $\lambda^2$ - $\Delta$  plane form a complex conjugate pair. SDFP1 is then a fixed point of focus type, with spiraling flows near the fixed point. In the XY case, this happens for  $N > \frac{32}{5} = 6.4$ , while for the Heisenberg case, this happens for  $N > 28.087$ . Critical properties in this case are subject to oscillatory corrections to scaling [2, 168].

#### 4.4.2.3 Stability of long-range disordered fixed points

We finally turn to the stability of the LDFPs of Sec. 4.4.1.2. The eigenvalues of the stability matrix depend on  $N$  and  $\delta$  in a complicated way, and we compute them numerically. In Figs. 4.3-4.5, we characterize the stability of the two LDFPs in terms of their number of

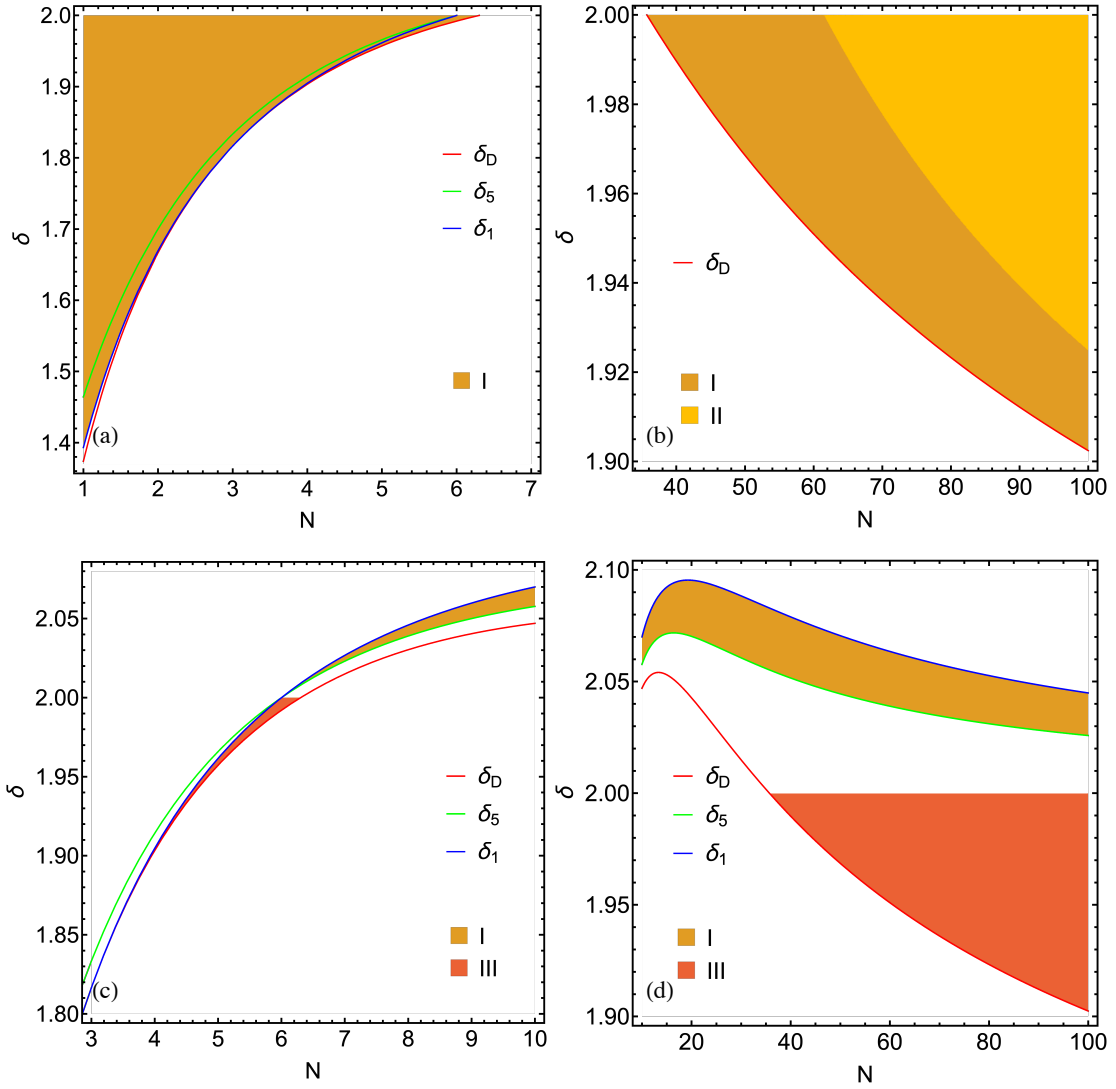


Figure 4.3: Stability in the subspace  $(\lambda^2, \Delta, v)$  of couplings of (a,b) LDFP1 and (c,d) LDFP2 in the chiral Ising GNY model ( $n = 1$ ), as a function of  $N$  and  $\delta$ . I: one relevant eigenvalue; II: one relevant eigenvalue, two complex-conjugate irrelevant eigenvalues; III: two relevant eigenvalues.

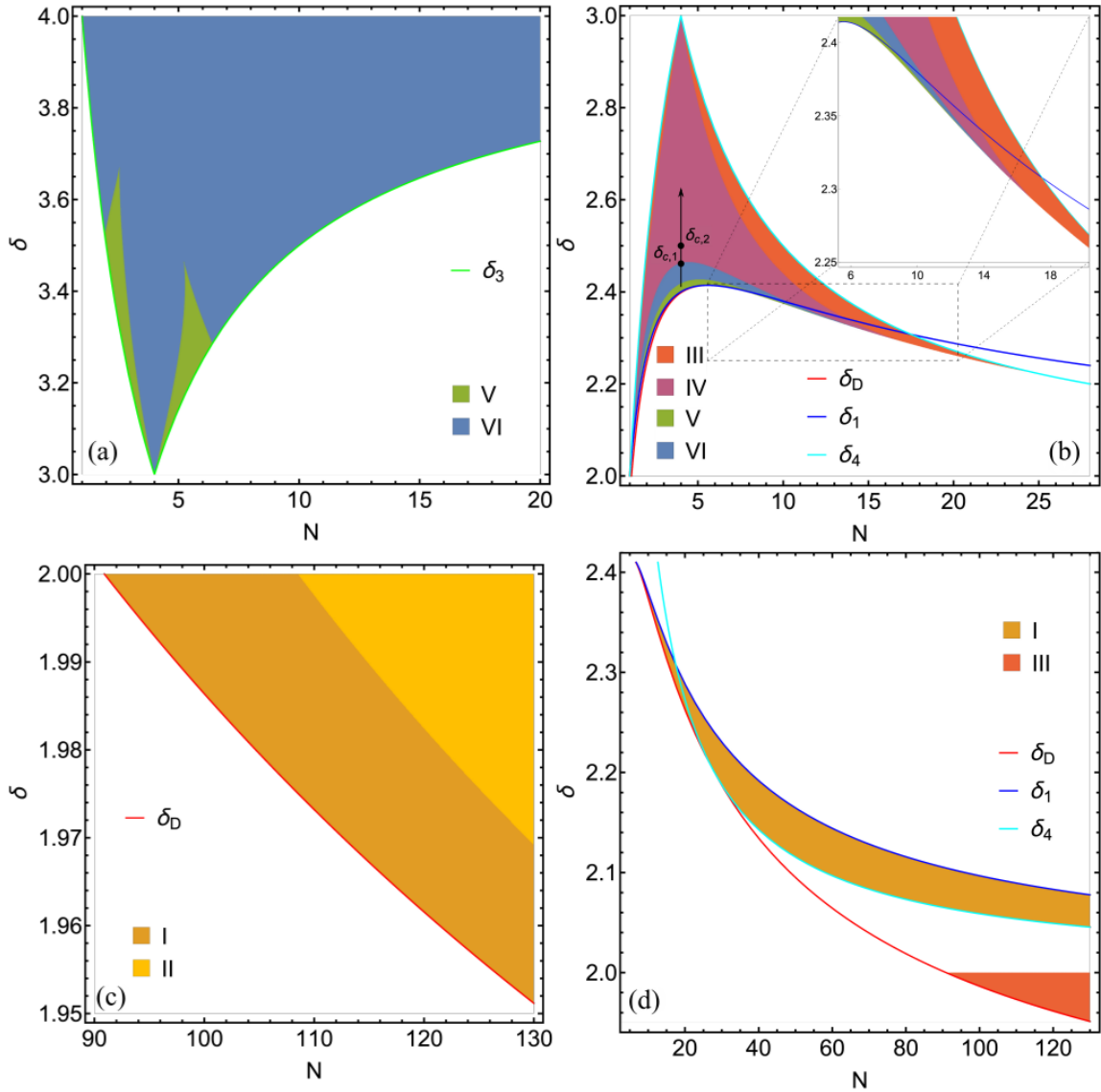


Figure 4.4: Stability in the subspace  $(\lambda^2, \Delta, v)$  of couplings of (a,b) LDFP1 and (c,d) LDFP2 in the chiral XY GNY model ( $n = 2$ ), as a function of  $N$  and  $\delta$ . Regions I-III are defined as in Fig. 4.3. IV: two complex-conjugate relevant eigenvalues; V: no relevant eigenvalues; VI: no relevant eigenvalues, two complex-conjugate irrelevant eigenvalues.

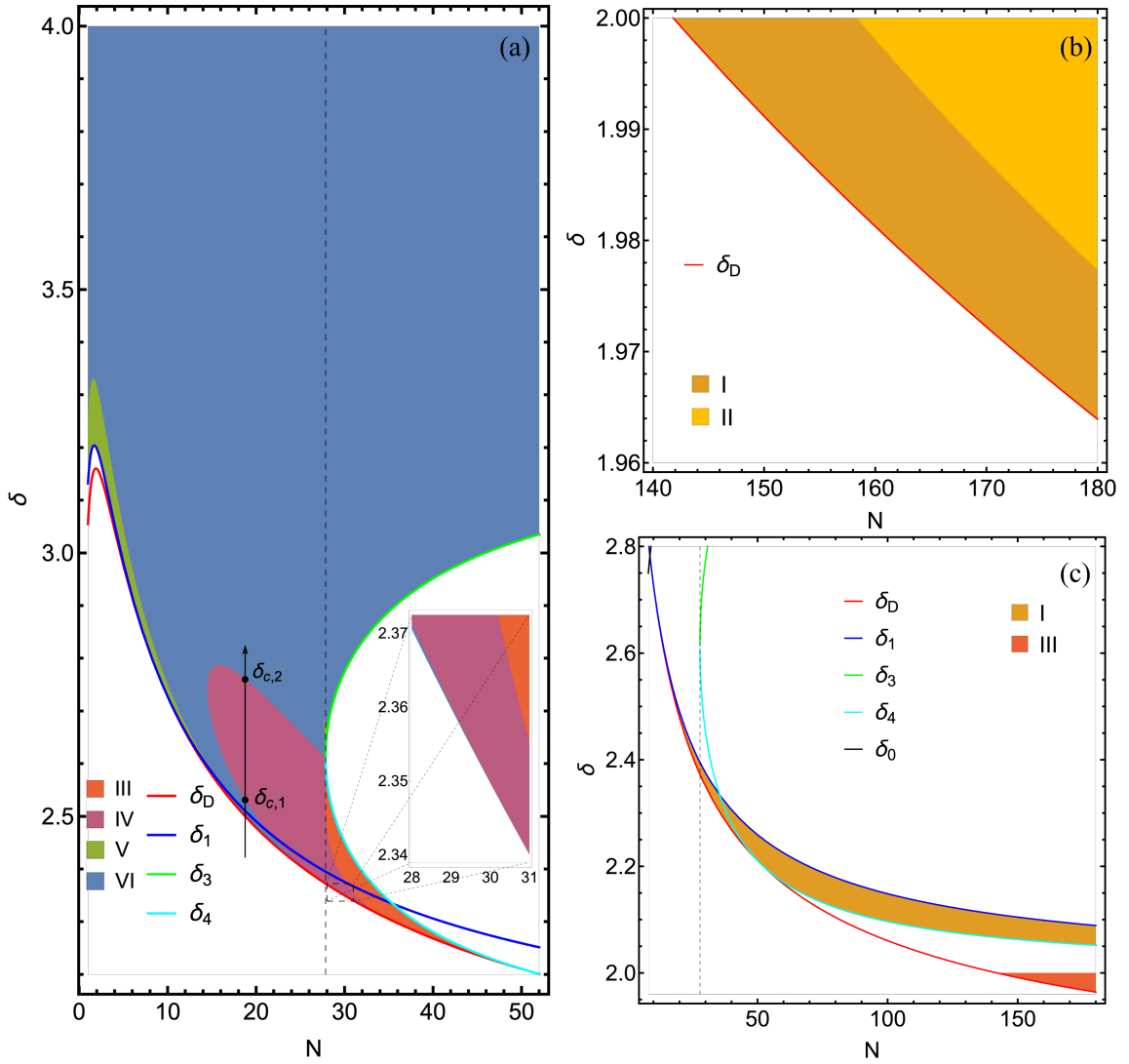


Figure 4.5: Stability in the subspace  $(\lambda^2, \Delta, \nu)$  of couplings of (a,b) LDFP1 and (c) LDFP2 in the chiral Heisenberg GNY model ( $n = 3$ ), as a function of  $N$  and  $\delta$ . Regions are labeled as in Fig. 4.4.

relevant/irrelevant eigenvalues, for each GNY symmetry class. Eigenvalues are real unless otherwise specified; since the stability matrix is real, complex eigenvalues necessarily appear in complex-conjugate pairs, and imply focus-type behavior as discussed above. For all three GNY symmetry classes, the two LDFPs merge along the curve  $\delta = \delta_D$  in the  $N$ - $\delta$  plane, where the discriminant  $D_L$  vanishes. In the Ising case (Fig. 4.3), both LDFPs have at least one relevant eigenvalue on the critical hypersurface and are thus multicritical points (for  $N = 1/2$ , only LDFP1 is physical, for  $\delta_1 \approx 1.143 < \delta < 2$ ). In the XY and Heisenberg cases (Figs. 4.4-4.5), LDFP1 exists in regions (V and VI) in the  $N$ - $\delta$  plane with no relevant eigenvalues, and is thus a *bona fide* critical point in those regions. LDFP2 is always multicritical.

### 4.4.3 Critical exponents

Universal critical exponents at the newly found fermionic DFPs can be computed from Eqs. (4.42-4.45) using the fixed-point couplings found in Sec. 4.4.1.1 and Sec. 4.4.1.2. At the present one-loop order, the fermion  $\eta_\psi$  and boson  $\eta_\phi$  anomalous dimensions depend only on  $h_*^2$ , which is the same at all fermionic fixed points. Thus their values at the DFPs are the same as those for the clean chiral GNY universality classes [140]:  $\eta_\psi = n\epsilon_\tau/[2(N + 4 - n)]$  and  $\eta_\phi = N\epsilon_\tau/(N + 4 - n)$ . At higher loop order the anomalous dimensions are expected to differ at the different fermionic fixed points.

Using Eq. (4.43), the dynamic critical exponent  $z$  at the fermionic DFPs is given by

$$z = 1 + \left(f(c_*^2) - \frac{1}{2}\right) \frac{n\epsilon_\tau}{N + 4 - n}, \quad (4.71)$$

and thus depends on the fixed-point velocity parameter  $c_*^2$ . The latter is a universal function of  $N$  and  $\delta$  for a given DFP but must be computed numerically; we plot the resulting value of  $z$  extrapolated to 2+1 dimensions ( $\epsilon_\tau \rightarrow 1$ ) in Fig. 4.6 for the SDFPs and in Figs. 4.7-4.9 for the LDFPs. Since  $c_*^2 > 1$ , and thus  $f(c_*^2) > \frac{1}{2}$ , at all fermionic DFPs (see Sec. 4.4.1), such DFPs necessarily have  $z > 1$ . This is in agreement with the general expectation

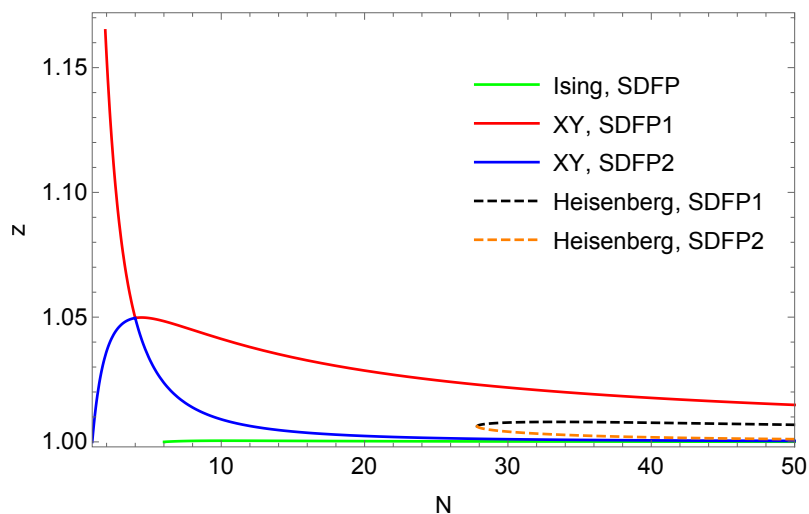


Figure 4.6: Dynamical critical exponent  $z$  at SDFPs for all three chiral GNY symmetry classes, as a function of  $N$ .

that weak disorder increases  $z$  [217]; Refs. [218, 219] also derive the leading-order result  $z - 1 \propto \Delta_* > 0$  at SDFPs obtained by perturbing a conformally invariant QCP with weak short-range correlated disorder. Here we find  $z > 1$  at LDFPs as well.

The inverse correlation length exponent  $\nu^{-1}$ , determined from Eq. (4.42), is the RG eigenvalue associated with the relevant direction  $r$  which tunes across the symmetry-breaking transition. For a *bona fide* critical point,  $\nu$  controls the divergence of the correlation length  $\xi$  at the transition  $r = 0$  via  $\xi \sim r^{-\nu}$ . For multicritical points with additional relevant directions  $g_1, g_2, \dots$  on the critical hypersurface with real, positive eigenvalues  $y_1, y_2, \dots$ , the correlation length behaves near the transition as  $\xi(r, g_1, g_2, \dots) = r^{-\nu} \tilde{\xi}(g_1/r^{\nu y_1}, g_2/r^{\nu y_2}, \dots)$ , where  $\tilde{\xi}(x_1, x_2, \dots)$  is a universal scaling function [220]. Complex-conjugate eigenvalues produce a scaling function with oscillatory behavior. At all LDFPs in all three GNY symmetry classes, we find  $\nu^{-1} = 2 - \frac{1}{2}\delta$ , which alternatively can be written as  $\nu = 2/\alpha$ , with  $\alpha = 4 - \delta$  the exponent controlling long-range disorder correlations in Eq. (4.8). This superuniversal behavior was also found at long-range correlated bosonic DFPs and explained by Weinrib and Halperin [186]. Consider a LDFP with correlation length exponent  $\nu(\alpha)$  in a system with disorder of the type (4.8). If one further perturbs this fixed point with disorder corre-

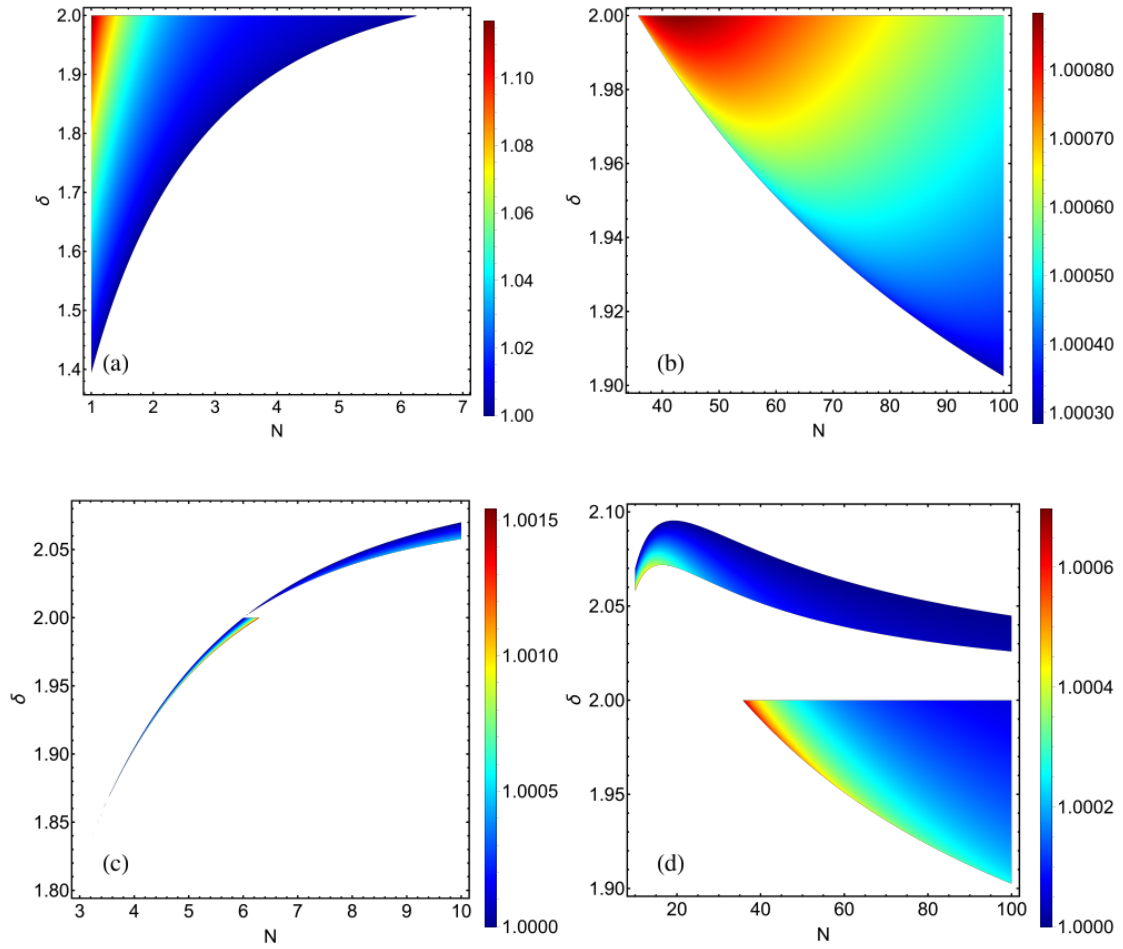


Figure 4.7: Dynamical critical exponent  $z$  in the chiral Ising GNY model ( $n = 1$ ) at (a,b) LDFP1 and (c,d) LDFP2, as a function of  $N$  and  $\delta$ .

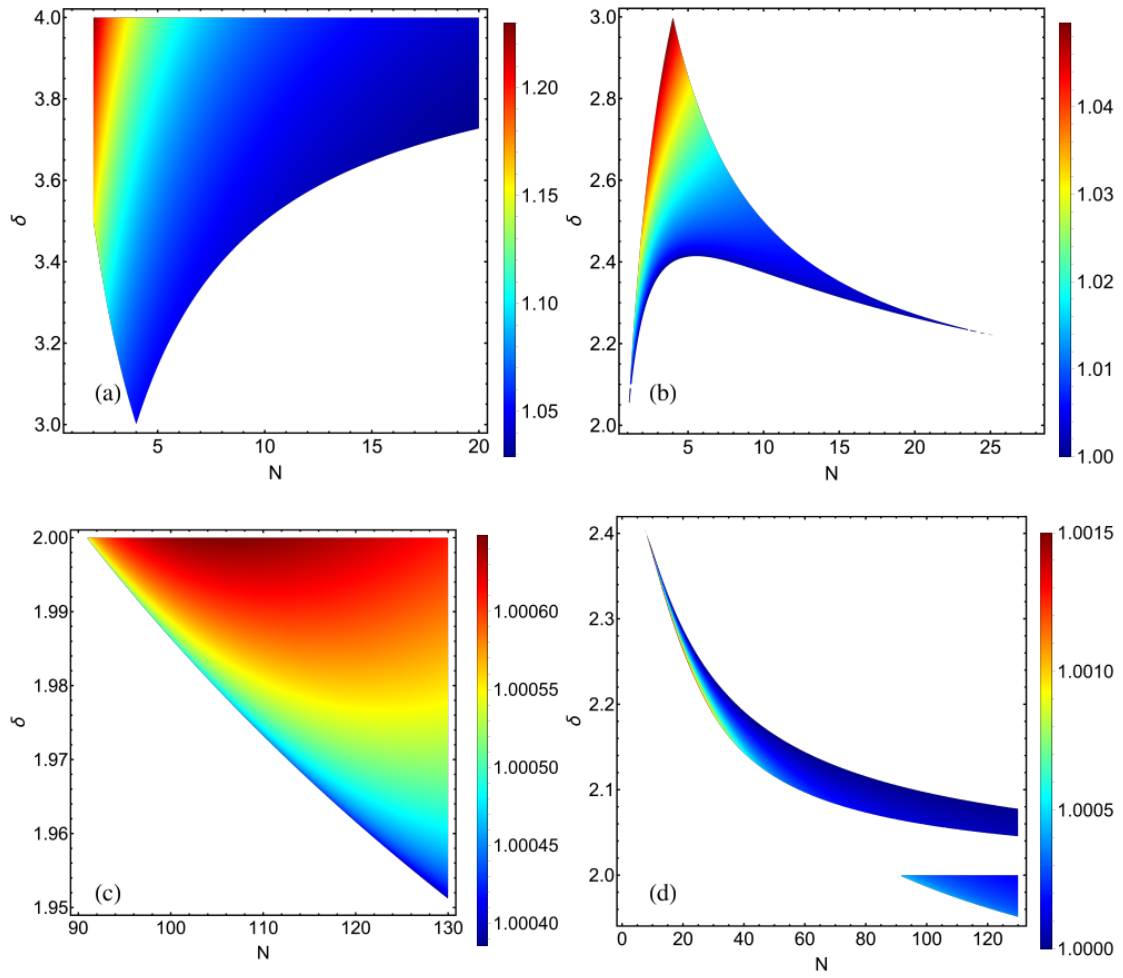


Figure 4.8: Dynamical critical exponent  $z$  in the chiral XY GNY model ( $n = 2$ ) at (a,b) LDFP1 and (c,d) LDFP2, as a function of  $N$  and  $\delta$ .

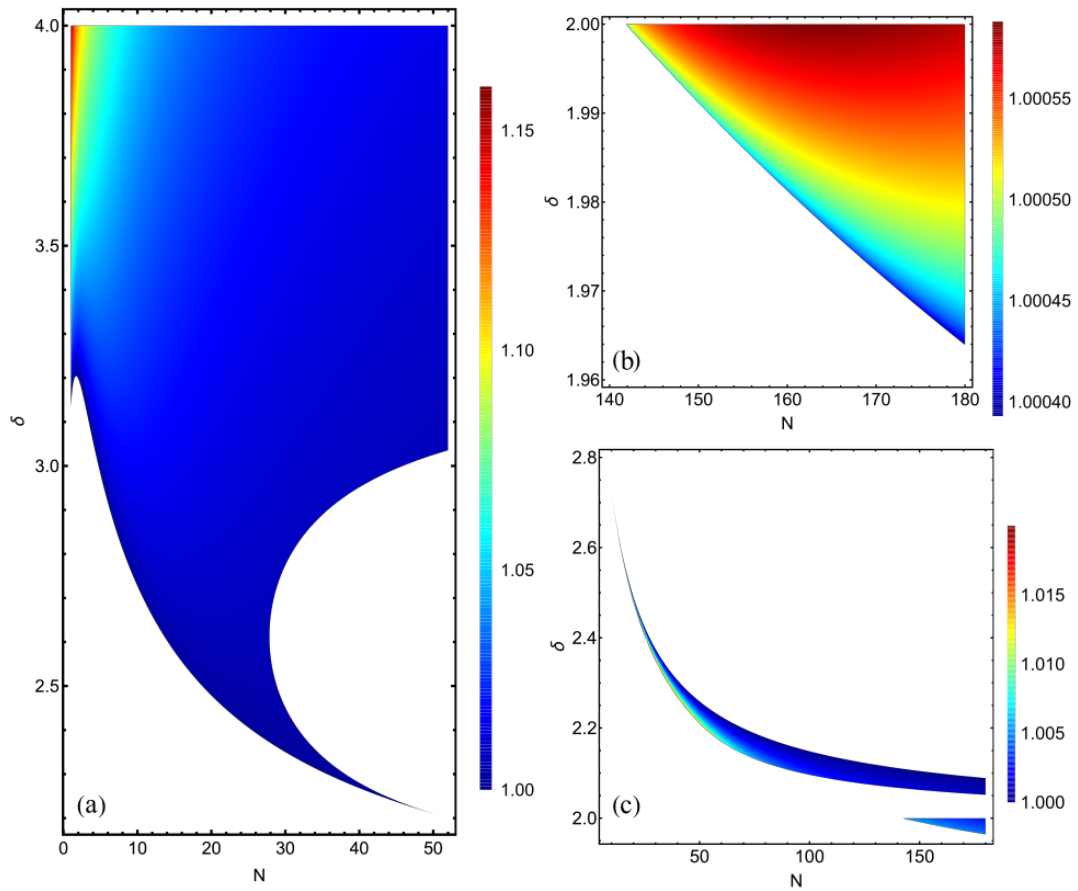


Figure 4.9: Dynamical critical exponent  $z$  in the chiral Heisenberg GNY model ( $n = 3$ ) at (a,b) LDFP1 and (c) LDFP2, as a function of  $N$  and  $\delta$ .

lated according to  $|\mathbf{x} - \mathbf{x}'|^{-\alpha_+}$  such that  $\alpha_+ > \alpha$ , the original asymptotic critical behavior should remain the same, as we expect it is controlled by the longest-range part of the disorder. Conversely, if the perturbation is of the form  $|\mathbf{x} - \mathbf{x}'|^{-\alpha_-}$  with  $\alpha_- < \alpha$ , this falls off more slowly than the original disorder, and the original critical behavior should be unstable. Assuming  $\alpha, \alpha_{\pm} < d$  and applying the modified Harris criterion for long-range correlated disorder, we find  $\nu(\alpha) > 2/\alpha_+$  and  $\nu(\alpha) < 2/\alpha_-$ , for all  $\alpha_- < \alpha < \alpha_+$ . Choosing  $\alpha_{\pm} = \alpha \pm \varepsilon$  and taking the limit  $\varepsilon \rightarrow 0^+$ , we obtain  $\nu(\alpha) = 2/\alpha$ .

The exponent  $\nu$  for the SDFPs can likewise be calculated directly from Eq. (4.42), and we obtain  $\nu^{-1} = 2 - \frac{1}{2}\delta_5$  for the chiral Ising SDFP, with  $\delta_5$  defined in Eq. (4.69). In light of the result above for  $\nu^{-1}$  at LDFPs, this is consistent with the fact that the  $n = 1$  SDFP coalesces with one of the LDFPs at  $\delta = \delta_5$ . Similarly, for both the chiral XY and Heisenberg models we find that SDFP1 has  $\nu^{-1} = 2 - \frac{1}{2}\delta_3$  and SDFP2 has  $\nu^{-1} = 2 - \frac{1}{2}\delta_4$ , with  $\delta_{3,4}$  defined in Eqs. (4.67-4.68). As previously mentioned, the curves  $\delta = \delta_3$  ( $\delta = \delta_4$ ) correspond to the merger of SDFP1 (SDFP2) with a LDFP. We plot  $\nu^{-1}$  at SDFPs for all three GNY models in Fig. 4.10, including  $\nu^{-1}$  at the clean GNY critical point for comparison.

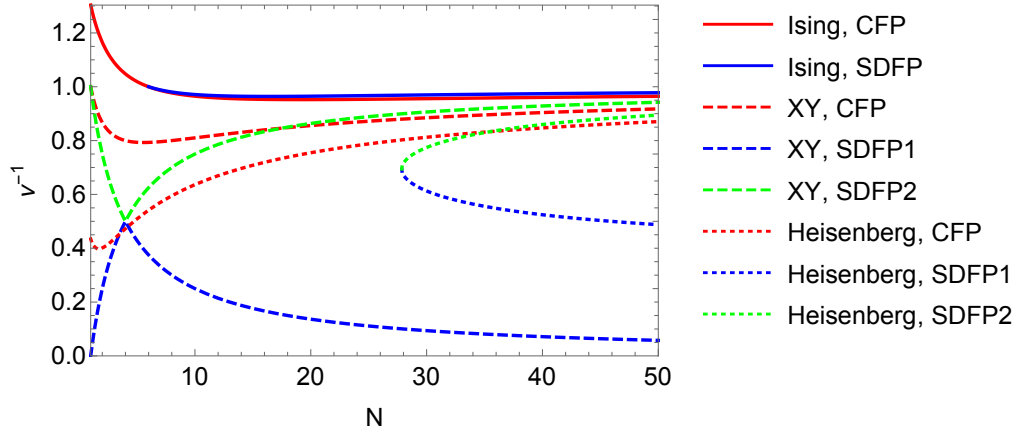


Figure 4.10: Inverse correlation length exponent  $\nu^{-1}$  for the CFP and SDFPs in all three chiral GNY symmetry classes, as a function of  $N$ .

## 4.5 RG flows and bifurcations

Having discussed RG fixed points and their local properties (stability and critical exponents), we now discuss global properties of the RG flow: bifurcations of the flow as the control parameters  $N, \delta$  are varied (Secs. 4.5.1 and 4.5.2), and examples of global phase diagrams for fixed  $N, \delta$  (Sec. 4.5.3). Although the original space of couplings  $(c^2, \lambda^2, h^2, \Delta, v)$  is five-dimensional, as already mentioned the  $c^2$  and  $h^2$  directions are irrelevant at fermionic fixed points, which are the only stable ones. For practical purposes the RG flows thus live in the three-dimensional space  $(\lambda^2, \Delta, v)$ , with  $c^2$  and  $h^2$  assuming their fixed-point values. Since in the chiral Ising case all physical fixed points are multicritical, and for the sake of simplicity, we restrict our attention to the chiral XY and Heisenberg symmetry classes, which exhibit the most interesting phenomena.

### 4.5.1 Transcritical and saddle-node bifurcations

We have already mentioned a number of instances in which two fixed points collide as  $N$  or  $\delta$  are varied. We observe two distinct kinds of bifurcations associated with a collision of two fixed points: the transcritical bifurcation and the saddle-node bifurcation.

The transcritical bifurcation [Fig. 4.11(a)] is a bifurcation at which a stable fixed point and an unstable fixed point pass through each other, exchanging their stability properties, but without annihilating [167]. An example of this bifurcation is the merging of the two chiral XY SDFPs (4.49) as  $N$  is varied through  $N = 4$ . (There is “exchange” of fixed points provided we track individual fixed points on smooth trajectories, as opposed to their arbitrary definition as SDFP1 and SDFP2 in Eq. (4.49).) Unlike the saddle-node bifurcation discussed below, the two fixed points remain real before and after the bifurcation. At the transcritical bifurcation, the beta function (and associated RG flow) is not only marginal, but its derivative with respect to the control parameter, here  $N$ , must vanish as well. Other examples of this bifurcation include the collision of SDFPs with the CFP (at  $N = 1$  for the chiral XY SDFP2), of LDFPs with the CFP (along the curve  $\delta = \delta_1$  in the  $N$ - $\delta$  plane), or

of SDFPs with LDFPs (curves  $\delta = \delta_3$  and  $\delta = \delta_4$ ). At these latter bifurcations, one of the DFPs becomes unphysical, by either  $\Delta_*$ ,  $v_*$ , or  $\Delta_* + v_*$  going through zero and becoming negative. However, since the other fixed point remains physical and thus real, this unphysical fixed point necessarily remains real also (for another RG example of this scenario, see Ref. [141]). Thus the bifurcation is distinct from the saddle-node bifurcation, which we now discuss.

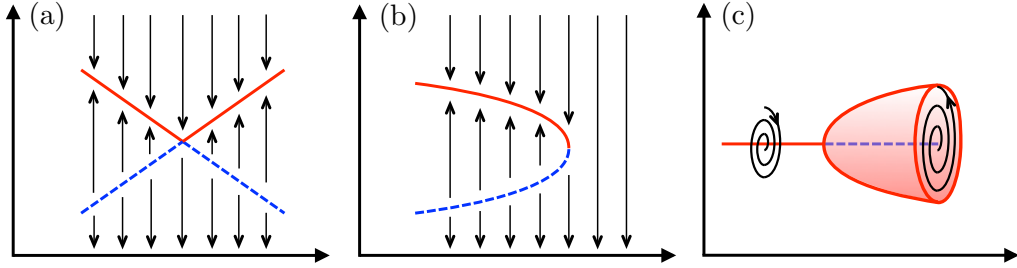


Figure 4.11: Schematic bifurcation diagrams for (a) the transcritical bifurcation, (b) the saddle-node bifurcation, and (c) the supercritical Hopf bifurcation. The horizontal axis represents a direction in the  $N$ - $\delta$  plane, and the vertical axis, the space of running couplings (critical hypersurface). Solid red symbolizes an RG attractor, dashed blue a repeller, and schematic RG trajectories are shown in black.

The saddle-node bifurcation [Fig. 4.11(b)] is a bifurcation at which a stable fixed point and an unstable fixed point merge, leading to marginal behavior as above, but subsequently disappear into the complex plane. This typically happens for a pair of fixed points with critical couplings  $g_{*\pm} \propto A \pm \sqrt{D}$ , such that the discriminant  $D$  continuously goes through zero at the bifurcation and then becomes negative. Both pairs SDFP1,2 and LDFP1,2 are of this type. The two chiral Heisenberg SDFPs, with discriminant  $D = D_S(n = 3)$ , annihilate with decreasing  $N$  at  $N \approx 27.856$ . (For the chiral XY GNY model,  $D = D_S(n = 2)$  touches zero at  $N = 4$  but remains positive elsewhere, which gives the transcritical bifurcation at  $N = 4$ .) Likewise, the two LDFPs in both the XY and Heisenberg cases annihilate on the curve  $\delta = \delta_D$  in the  $N$ - $\delta$  plane, where the discriminant  $D = D_L$  vanishes. Since  $\delta_D$  in Eq. (4.54) is a nonmonotonic function of  $N$ , for fixed  $\delta$  this

fixed-point annihilation can occur for either increasing or decreasing  $N$ .

The saddle-node bifurcation is accompanied by the characteristic phenomenology of walking RG or quasi-critical behavior [166]; we now explain how this manifests itself in the current problem. Focusing on the example above of the annihilation of LDFPs in the chiral XY and Heisenberg GNY models, we first consider a situation where  $\delta$  is slightly above  $\delta_D$ . Small regions in the  $N$ - $\delta$  plane exist such that both LDFPs are physical, with LDFP1 a stable sink-type fixed point (region V) and LDFP2 a multicritical point with one relevant direction (region I). LDFP2 is only physical provided  $\delta < \delta_1$  [see Eq. (4.66)], which implies that the CFP is stable (Sec. 4.4.2.1). For this type of region, numerical studies of the RG flow show that RG trajectories with initial conditions near LDFP2 end up at either LDFP1 or the CFP. We thus consider a curvilinear coordinate system such that one of these coordinates,  $g$ , passes through all three fixed points [Fig. 4.12(a)]. In this section only, we define the infrared (Wilsonian) beta function  $\beta(g) \equiv dg/d\ell$ , where  $\ell$  grows towards the infrared. Denoting by  $g_*$  the common fixed-point coupling of LDFP1 and LDFP2 at the bifurcation  $\delta = \delta_D$ , we assume that for  $\delta$  near  $\delta_D$  and  $g$  near  $g_*$ ,  $\beta(g)$  can be well approximated by a quadratic function,  $\beta(g) \approx A(\delta) + B(\delta)(g - g_*) + C(\delta)(g - g_*)^2$ . Since  $\beta(g_*) = \partial\beta(g_*)/\partial g = 0$  and  $\partial^2\beta(g_*)/\partial g^2 < 0$  at  $\delta = \delta_D$ , we have  $A(\delta_D) = B(\delta_D) = 0$  and  $C(\delta_D) \equiv -\kappa < 0$ . For  $\delta = \delta_D + \varepsilon$  with  $\varepsilon$  small,  $\beta(g)$  should have two real zeros that approach  $g_*$  as  $\varepsilon \rightarrow 0^+$ . Expanding  $A(\delta)$ ,  $B(\delta)$ , and  $C(\delta)$  in powers of  $\varepsilon$ , we find at leading order a pair of zeros of the form  $g_* \pm \sqrt{b\varepsilon/\kappa}$  with  $b \equiv A'(\delta_D)$ , which are real provided that  $b > 0$ , and form a complex-conjugate pair when  $\varepsilon < 0$  ( $\delta < \delta_D$ ). The beta function thus approximately assumes the form  $\beta(g) \approx b(\delta - \delta_D) - \kappa(g - g_*)^2$ , illustrated in Fig. 4.12(b), and considered in Ref. [166].

We now take  $\delta = \delta_D - \varepsilon$  with  $\varepsilon > 0$  small, and consider an RG trajectory with initial coupling  $g_{UV} > g_*$  and “flow velocity”  $\beta(g_{UV})$ , which is generically not small. As  $g$  approaches  $g_*$  from above, the flow velocity decreases considerably (i.e., the running coupling “walks”), since  $\beta(g_*) \approx -b\varepsilon$  is small. This walking behavior persists until  $g_* - g$  becomes on the order of  $\sqrt{b\varepsilon/\kappa}$ , after which the coupling starts “running” again. This determines a

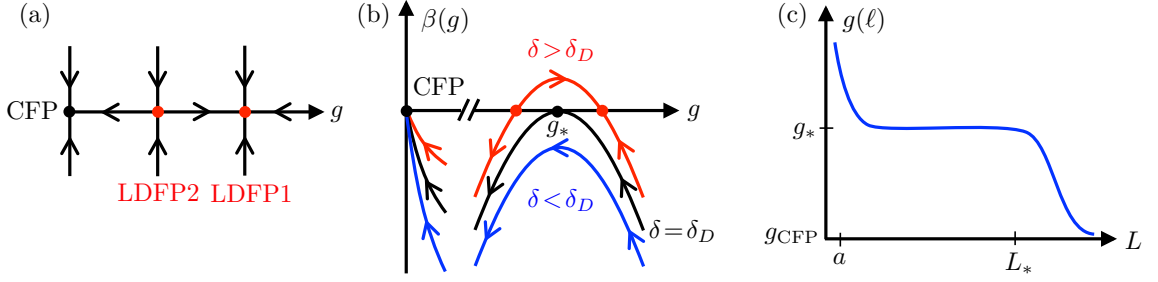


Figure 4.12: Phenomenology of the saddle-node bifurcation at  $\delta = \delta_D$ . (a) Curvilinear coordinate  $g$  along RG trajectories for  $\delta > \delta_D$ ; (b) Wilsonian beta function near the bifurcation; (c) crossover from disordered quasi-critical behavior to clean critical behavior for  $\delta$  slightly below  $\delta_D$ .

characteristic RG time  $\Delta\ell$  insensitive to the initial condition  $g_{\text{UV}}$  of the flow. Approximating  $\beta(g) \approx \beta(g_*) \approx -b\varepsilon$  as constant during the walk, we have  $\beta(g_*) \approx \Delta g / \Delta\ell \sim \sqrt{b\varepsilon/\kappa} / \Delta\ell$ , and thus  $\Delta\ell \sim 1/\sqrt{\kappa b\varepsilon}$ . Alternatively, we may integrate the equation  $dg/d\ell = \beta(g)$  from  $g_{\text{UV}}$  at  $\ell_{\text{UV}}$  to  $g_{\text{IR}} < g_*$  at  $\ell_{\text{IR}}$ . Under the condition  $|g_{\text{UV,IR}} - g_*| \gg \sqrt{b\varepsilon/\kappa}$ , the result of this integration is insensitive to the precise values of  $g_{\text{UV}}$  and  $g_{\text{IR}}$ , and we obtain  $\Delta\ell \equiv \ell_{\text{IR}} - \ell_{\text{UV}} = \pi/\sqrt{\kappa b\varepsilon}$ . In turn, this RG time determines a characteristic infrared length scale  $L_* = L_{\text{IR}} = L_{\text{UV}}e^{\Delta\ell}$ , where we can take  $L_{\text{UV}} \sim a$  to be on the order of a microscopic lattice constant  $a$ . We obtain:

$$L_* \sim a \exp\left(\pi/\sqrt{\kappa b(\delta_D - \delta)}\right), \quad (4.72)$$

as  $\delta$  approaches  $\delta_D$  from below. The exponential inverse-square-root divergence, reminiscent of the divergence of the correlation length at the Kosterlitz-Thouless transition [221], is characteristic of the saddle-node bifurcation [166]. The existence of this exponentially large length scale  $L_* \gg a$  allows for a crossover between two distinct physical regimes [Fig. 4.12(c)]. On intermediate length scales  $a \ll L \ll L_*$ , RG trajectories dwell for an extended period of RG time near  $g = g_*$ , and we have quasi-critical behavior controlled by a complex pair of LDFPs with real part near  $g_*$ . This quasi-critical regime is characterized by approximate power-law scaling and drifting (i.e., scale-dependent) exponents [198]. On

the largest length scales  $a \ll L_* \ll L$ , the transition is controlled by the true infrared fixed point, the CFP, with genuine scale invariance.

### 4.5.2 Supercritical Hopf bifurcation and limit-cycle fermionic quantum criticality

The third type of bifurcation we observe is the supercritical Hopf bifurcation [Fig. 4.11(c)]. This bifurcation occurs as one passes from region VI (blue region) to region IV (purple region) in both the chiral XY [Fig. 4.4(b)] and Heisenberg [Fig. 4.5(a)] models. For instance, one can consider keeping  $N$  fixed and tuning  $\delta$  (black arrow in those figures). In region VI ( $\delta < \delta_{c,1}$ ), LDFP1 is a stable-focus fixed point with two complex-conjugate irrelevant eigenvalues, i.e., complex-conjugate eigenvalues with a negative real part [solid red line on left part of Fig. 4.11(c)]. At the bifurcation ( $\delta = \delta_{c,1}$ ), the real part of those eigenvalues goes through zero and becomes positive for  $\delta > \delta_{c,1}$ . LDFP1 thus loses its stability and becomes an unstable-focus fixed point [dashed blue line on the right part of Fig. 4.11(c)]. At the same time, a stable limit cycle is born [solid red line on the right part of Fig. 4.11(c)], towards which the spiraling RG trajectories coming out of LDFP1 asymptote, and which controls the critical behavior up to a second threshold value  $\delta_{c,2}$  to be discussed shortly. (Trajectories outside the limit cycle also spiral and asymptote to it.)

To our knowledge, this is the first instance in the context of quantum phase transitions where the supercritical Hopf bifurcation [203] appears. After Ref. [222], which studied a holographic model of a critical scalar field perturbed by disorder, our result is the second example of quantum phase transition governed by a stable limit cycle; to our knowledge, it is the first example for fermionic systems. The subcritical Hopf bifurcation [203], where an unstable-focus fixed point becomes stable by giving birth to an unstable limit cycle, has been reported previously in RG studies of classical disordered systems [186, 206]. The general phenomenology of critical behavior controlled by a stable limit cycle was explored in Ref. [205]. For a stable-focus critical point, spiraling trajectories manifest themselves as oscillatory corrections to scaling [2, 168]. By contrast, for a transition governed by a sta-

ble limit cycle, thermodynamic quantities exhibit log-periodic scaling behavior at leading order, i.e., discrete scale invariance. For instance, we show in Appendix B.8 that the order parameter susceptibility  $\chi$  obeys the approximate scaling form:

$$\chi \sim |r|^{-\gamma_{\text{LC}}} \left[ 1 + \gamma_{\text{LC}} \mathcal{F} \left( \nu_{\text{LC}} \ln \left( \frac{r_0}{r} \right) \right) \right], \quad (4.73)$$

where  $\mathcal{F}$  is a periodic function. Here  $\nu_{\text{LC}}$  and  $\gamma_{\text{LC}} = (2 - \eta_\phi)\nu_{\text{LC}}$  are effective correlation-length and susceptibility exponents for the limit cycle,  $r$  is the tuning parameter for the transition, and  $r_0$  is a nonuniversal constant.

As  $\delta$  is further increased past  $\delta_{c,1}$ , the limit cycle eventually disappears at a second critical value  $\delta_{c,2}$ , but in different ways for the chiral XY and Heisenberg GNY models. In the Heisenberg case, the Hopf bifurcation of Fig. 4.11(c) occurs again but in reverse: the limit cycle shrinks to a point, which becomes the stable-focus LDFP1 of region VI. In the XY case, our numerical studies suggest that at least for some values of  $N$ , the limit cycle is destroyed at  $\delta = \delta_{c,2}$  (still within region IV) by colliding with the CFP and SDFP2, which are both saddle points in this regime [see Fig. 4.13(c)]. This is a possible example of heteroclinic bifurcation [223], whose detailed study we reserve for future work.

### 4.5.3 Schematic phase diagrams

From the knowledge of the stability properties of the various fixed points and limit cycles, and numerical investigation of the RG flow connecting those different critical manifolds, schematic phase diagrams can be constructed analogously to those in Chap. 3. For given values of  $N$  and  $\delta$ , we focus on the critical hypersurface ( $r = 0$ ) and ask how the universality class of the transition depends on the bare couplings in the Lagrangian, which determine the initial conditions for the infrared RG flow. We consider a scenario in which the interaction parameters  $h$  and  $\lambda^2$  are fixed, and vary the two types of disorder,  $\Delta$  and  $v$ . Since the number of possibilities is very large, given the complexity of the stability/physicality regions, we focus on the two most interesting regions: those which contain the instances of limit-cycle

quantum criticality discussed in the previous section.

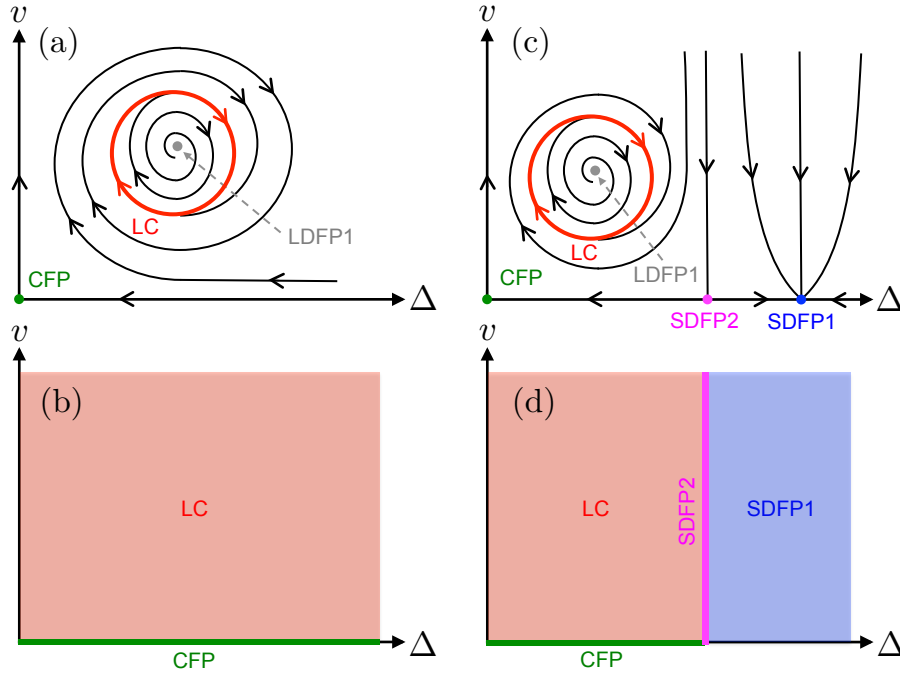


Figure 4.13: Schematic RG flow and critical ( $r = 0$ ) phase diagrams for generic  $N$  and  $\delta_{c,1} < \delta < \delta_{c,2}$  in region IV (see Figs. 4.4-4.5), for (a,b) the chiral Heisenberg GNY model and (c,d) the chiral XY model. In the Heisenberg case, the transition is controlled by a stable limit cycle (LC) for generic bare values of the short-range correlated ( $\Delta$ ) and long-range correlated ( $v$ ) disorder strengths. In the XY case, the transition is controlled by the limit cycle for weak short-range disorder and by a disordered fixed point (SDFP1) for strong short-range disorder.

We first focus on region IV in the chiral Heisenberg GNY model [see Fig. 4.5(a)]. For generic points in this region (e.g., for  $\delta_{c,1} < \delta < \delta_{c,2}$ ), one has  $\delta > \delta_D$  and  $\delta > \delta_1$ . Furthermore, we assume  $N < N_D \approx 27.856$ . From Sec. 4.4.2.1, we conclude that the CFP has two irrelevant directions in the  $\lambda^2$ - $\Delta$  plane, but that long-range correlated disorder  $v$  is relevant, since  $\delta > \delta_1$ . SDFP1,2 are both unphysical, since  $N < N_D$ , and LDFP2 is unphysical as well. As seen in the previous section, LDFP1 is of unstable-focus type, with spiraling flow towards a stable limit cycle. The resulting RG flow is illustrated schematically in Fig. 4.13(a). Consequently, at least for sufficiently small bare values of the disorder, the

transition is controlled by limit-cycle quantum criticality for generic disorder [Fig. 4.13(b)]. If long-range correlated disorder is turned off completely, the transition reverts back to the clean chiral Heisenberg GNY universality class.

We now turn to region IV in the chiral XY GNY model [see Fig. 4.4(b)], assuming  $\delta_{c,1} < \delta < \delta_{c,2}$ . As in the previous case, we generically have  $\delta > \delta_D$ ,  $\delta > \delta_1$ , and also  $\delta < \delta_4$ . As in the Heisenberg case, the CFP has two irrelevant directions in the  $\lambda^2$ - $\Delta$  plane, but  $v$  is relevant. There are now nontrivial SDFPs, whose stability was discussed in Sec. 4.4.2.2. For SDFP1,  $\lambda^2$  and  $\Delta$  are both irrelevant, and  $v$  is irrelevant as well, since  $\delta < \delta_4 < \delta_3$ . For SDFP2,  $v$  is irrelevant since  $\delta < \delta_4$ , but there is one relevant direction with nonzero  $\Delta$  projection. LDFP2 is unphysical, and LDFP1 is an unstable focus with flow towards a stable limit cycle. The resulting RG flow is schematized in Fig. 4.13(c), and the corresponding phase diagram in Fig. 4.13(d). For weak  $\Delta$ , the transition is governed by the limit cycle, but for sufficiently strong  $\Delta$ , the transition is controlled by a disordered fixed point, SDFP1. CFP and SDFP2 appear as multicritical points.

## 4.6 Conclusion

In summary, we have performed a comprehensive study of the three classes of chiral GNY models most relevant for symmetry-breaking quantum phase transitions in (2+1)D gapless Dirac matter—the chiral Ising, XY, and Heisenberg GNY models—in the presence of quenched short-range and long-range correlated random-mass disorder. Using a controlled triple epsilon expansion below the upper critical dimension for these models, we have found several disordered infrared fixed points characterized by finite short-range and/or long-range correlated randomness, and for which we computed critical exponents. The Boyanovsky-Cardy and quantum Weinrib-Halperin fixed points, while present, are destabilized by the Yukawa interaction in favor of new disordered fermionic QCPs, at which the strength of this interaction remains nonzero in the infrared. Besides local stability, using numerical and analytical approaches we analyzed bifurcations of the RG flow. We found instances of the fa-

miliar fixed-point annihilation scenario, which can here be tuned by a genuinely continuous variable—the exponent controlling the algebraic decay of disorder correlations—and with which is associated a parametrically large crossover length scale  $L_*$  that separates a disordered quasi-critical regime ( $L \ll L_*$ ) from a clean regime in the deep infrared ( $L \gg L_*$ ). We also uncovered instances of the transcritical bifurcation, at which fixed points exchange their stability, and the more exotic supercritical Hopf bifurcation. The latter was accompanied by the emergence of a stable limit cycle on the critical hypersurface, thus producing the first instance of fermionic quantum criticality with discrete scale invariance.

Several avenues present themselves for future research. The relative paucity of disordered fixed points found in the chiral Ising class as compared to its continuous-symmetry counterparts, and in fact, the complete absence of *bona fide* critical points in this class, is in agreement with the conjecture by Motrunich *et al.* [127] that all discrete symmetry-breaking transitions in (2+1)D disordered systems should fall in the infinite-randomness universality class. Since infinite-randomness fixed points are not accessible to perturbative RG methods, nonperturbative numerical studies of Ising transitions of interacting Dirac fermions with quenched randomness are desirable, e.g., using quantum Monte Carlo methods [155] or, possibly, incorporating fermions into (2+1)-dimensional adaptations of the strong-disorder RG method [183]. In the presence of gapless Dirac fermions strongly coupled to bosonic order parameter fluctuations, rare-region effects [101,106]—which dominate the low-energy physics at infinite-randomness fixed points—may however lead to a different strong-disorder phenomenology than that found in local bosonic models [224].

Besides the pure GNY universality classes, relevant to symmetry-breaking transitions in systems of itinerant Dirac electrons, our method of analysis may also provide a point of entry to study the effect of quenched disorder on more exotic transitions, such as those involving fractionalized phases. The algebraic or Dirac spin liquid [225–228], a quantum-disordered paramagnet with fractionalized spinon excitations, is described at low energies by (2+1)D quantum electrodynamics (QED<sub>3</sub>) with  $N = 4$  flavors of two-component gapless Dirac fermions. The effect of quenched disorder on QED<sub>3</sub> itself was

studied recently [119–121, 229, 230]; using the methods presented here, one could additionally study the effect of quenched disorder on quantum phase transitions out of the algebraic spin liquid<sup>3</sup>. Transitions towards conventional phases such as VBS states [153, 232, 233] or antiferromagnets [234–236], or transitions towards gapped chiral [237–239] or  $\mathbb{Z}_2$  spin liquids [141], are described by GNY theories in all three (Ising, XY, Heisenberg) symmetry classes, augmented by a coupling to fluctuating  $U(1)$  gauge fields. The effect of random-mass disorder on the critical fixed points of such QED<sub>3</sub>-GNY theories is an interesting topic for future research.

---

<sup>3</sup>As an experimental example of such transitions, Ref. [231] reports the possible observation of a field-induced quantum phase transition between an algebraic spin liquid and a collinear magnetically ordered state in the triangular-lattice frustrated magnet NaYbO<sub>2</sub>.

## Chapter 5

# Conclusion

In this thesis, we theoretically studied the physics of quantum phase transitions in systems of massless Dirac electrons. The latter emerge in certain condensed matter systems and provide a framework for the description of the universal properties of these systems in the low-energy, long-wavelength limit. In particular, massless Dirac fermions form a basis for the description of the low-energy physics in graphene and on the boundaries of topologically nontrivial phases such as 3D topological insulators. The overall finding of this thesis is that the presence of Dirac fermions in the low-energy spectrum can lead to several qualitatively new phenomena in the physics of quantum phase transitions, both in the absence and presence of quenched disorder.

In Chapter 2, to provide a microscopic basis for the phenomenological idea of Pomeranchuk instability in the two-dimensional helical Fermi liquid, applicable to the surface of a 3D topological insulator with a single rotationally invariant Dirac cone, we constructed and analyzed a field-theoretic model of such an instability, which leads to the formation of an unconventional type of nematic order. We found two qualitatively different regimes: the doped one, in which one may neglect one of the helicity bands in the low-energy limit; and the undoped one, in which the Fermi surface shrinks to the Dirac point, and one has to account for both helicity bands. The mean-field solution was found, and the fluctuations about it were considered. We found that, unexpectedly, the nematic transition in

the undoped case is of the first-order kind at low temperature, but becomes continuous above a finite-temperature tricritical point. The nematic transition in the doped case is continuous at zero temperature. Our results predict observable signatures of the nematic phase, such as the partial breakdown of spin-momentum locking and anisotropy in the spin susceptibility. The number and dispersion of collective modes were found to be the same as in spin-degenerate Fermi liquids. However, unlike the spin-degenerate case, we showed that due to spin-orbit coupling, the nematic fluctuations can induce spin fluctuations. While the nematic order in 3D TIs has not been observed to this date, searches for materials featuring strongly correlated Dirac electrons continue not without success. For example, samarium hexaboride ( $\text{SmB}_6$ ) and some other materials are identified as good candidates for being a topological Kondo insulator, in which surface states form in the Kondo gap.

In Chapters 3 and 4, we focused on the interplay of interactions and quenched random-mass disorder at quantum critical points described in the clean limit by the chiral Ising, XY, and Heisenberg GNY models parametrized by the number of low-energy Dirac fermion flavors  $N$ . While disorder couples microscopically to fermions, such a direct coupling is naively irrelevant in the renormalization group sense near the upper critical dimension of the chiral GNY models. However, if disorder does not break the symmetries of the order parameter, at two-loop order, it generates an RG-relevant spatially random boson mass term. To infer the effect of such disorder on universal critical properties, we performed a one-loop perturbative renormalization group study. In the case of uncorrelated disorder, we adopted a double epsilon expansion method introduced initially for purely bosonic systems. For power-law correlated disorder, we introduced a third small “epsilon” parameter – the deviation  $\delta$  of the exponent in the power-law disorder correlation function from the upper critical dimension. For the Ising GNY model, while we found several disordered fixed points, none of them was a *bona fide* quantum critical point. For the XY and Heisenberg GNY models, the phase diagram in the  $N$ - $\delta$  plane is quite rich and complicated in terms of the possible quantum critical points controlling the transition. There are regions where clean, short-range disordered, and long-range disordered fixed points are

quantum critical points. All those disordered quantum critical points are strongly interacting with nonzero Yukawa coupling and characterized by non-Gaussian critical exponents and a noninteger dynamic critical exponent  $z > 1$ . In certain regions in the  $N$ - $\delta$  plane, some of these quantum critical points are of focus type, i.e., renormalization group flows spiral around the fixed point. This spiraling manifests itself in oscillatory corrections to scaling laws. In the XY GNY model, for the case  $N = 1$  corresponding to the surface of a 3D topological insulator, we did not find disordered fixed points, either short-range nor long-range. In turn, disorder becomes marginally relevant at the clean fixed point, leading to runaway flow. One may hope that pursuing the expansion to two-loop order may reveal the fate of the system. Alternatively, one may resort to numerical methods such as quantum Monte Carlo and functional renormalization group methods. As  $N$  and  $\delta$  vary, renormalization group flows undergo different bifurcations. In particular, we revealed instances of the saddle-point bifurcation tuned by the genuinely continuous parameter  $\delta$ . This bifurcation is accompanied by Berezinskii-Kosterlitz-Thouless type scaling, which leads to the existence of the exponentially large crossover length scale  $L_*$  separating the quasi-critical regime, controlled by a disordered fixed point, and the clean critical regime, controlled by the clean fixed point. More exotically, for the XY and Heisenberg GNY models, we found instances of the supercritical Hopf bifurcation, which is accompanied by the birth of a stable limit cycle, controlling the transition and leading to discrete scale invariance. While this finding is interesting, it may be merely an artefact of the triple epsilon expansion used here. The same critique could be applied to the finding of quantum critical points of focus type. To resolve this, the application of nonperturbative methods, such as the numerical methods mentioned above as well as strong-disorder renormalization-group methods, is necessary. The perturbative method we used here might be applicable to quantum phase transitions in other systems featuring emergent massless Dirac fermions, e.g.,  $d$ -wave superconductors or algebraic spin liquids, with quenched random-mass disorder.

# Bibliography

- [1] R. Lundgren, H. Yerzhakov, and J. Maciejko. Nematic order on the surface of a three-dimensional topological insulator. *Phys. Rev. B*, 96(23):235140, December 2017.
- [2] H. Yerzhakov and J. Maciejko. Disordered fermionic quantum critical points. *Phys. Rev. B*, 98(19):195142, November 2018.
- [3] H. Yerzhakov and J. Maciejko. Random-mass disorder in the critical Gross-Neveu-Yukawa models. *arXiv:2008.13663*.
- [4] B. Lenoir, M. Cassart, J.-P. Michenaud, H. Scherrer, and S. Scherrer. Transport properties of Bi-RICH Bi-Sb alloys. *J. Phys. Chem. Solids*, 57(1):89–99, January 1996.
- [5] S.-Q. Shen. *Topological Insulators*. Springer Berlin Heidelberg, 2012.
- [6] H. Zhang, C.-X. Liu, X.-L. Qi, Xi Dai, Z. Fang, and S.-C. Zhang. Topological insulators in  $\text{Bi}_2\text{Se}_3$ ,  $\text{Bi}_2\text{Te}_3$  and  $\text{Sb}_2\text{Te}_3$  with a single Dirac cone on the surface. *Nat. Phys.*, 5(6):438–442, June 2009.
- [7] Y. Xia, D. Qian, D. Hsieh, L. Wray, A. Pal, H. Lin, A. Bansil, D. Grauer, Y. S. Hor, R. J. Cava, and M. Z. Hasan. Observation of a large-gap topological-insulator class with a single Dirac cone on the surface. *Nat. Phys.*, 5(6):398–402, June 2009.

- [8] K. S. Novoselov, A. K. Geim, S. V. Morozov, D. Jiang, M. I. Katsnelson, I. V. Grigorieva, S. V. Dubonos, and A. A. Firsov. Two-dimensional gas of massless Dirac fermions in graphene. *Nature*, 438(7065):197–200, November 2005.
- [9] A. H. Castro Neto, F. Guinea, N. M. R. Peres, K. S. Novoselov, and A. K. Geim. The electronic properties of graphene. *Rev. Mod. Phys.*, 81(1):109–162, January 2009.
- [10] J. von Neumann and E. Wigner. Uber das verhalten von eigenwerten bei adiabatischen prozessen. *Phys. Zeit.*, 30:467–470, November 1929.
- [11] C. L. Kane and E. J. Mele. Quantum spin Hall effect in graphene. *Phys. Rev. Lett.*, 95(22):226801, November 2005.
- [12] O. Vafek and A. Vishwanath. Dirac fermions in solids: From high- $T_c$  cuprates and graphene to topological insulators and Weyl semimetals. *Annu. Rev. Condens. Matter Phys.*, 5(1):83–112, March 2014.
- [13] N. P. Armitage, E. J. Mele, and Ashvin Vishwanath. Weyl and Dirac semimetals in three-dimensional solids. *Rev. Mod. Phys.*, 90(1):015001, January 2018.
- [14] K. V. Klitzing, G. Dorda, and M. Pepper. New method for high-accuracy determination of the fine-structure constant based on quantized Hall resistance. *Phys. Rev. Lett.*, 45(6):494–497, August 1980.
- [15] L. D. Landau. On the theory of phase transitions. I. *Zh. Eksp. Teor. Fiz.*, 7:19, 1937.
- [16] L. D. Landau. On the theory of phase transitions. II. *Zh. Eksp. Teor. Fiz.*, 7:627, 1937.
- [17] W. P. Su, J. R. Schrieffer, and A. J. Heeger. Solitons in polyacetylene. *Phys. Rev. Lett.*, 42(25):1698–1701, June 1979.
- [18] F. D. M. Haldane. Model for a quantum Hall effect without Landau levels: condensed-matter realization of the “parity anomaly”. *Phys. Rev. Lett.*, 61(18):2015–2018, October 1988.

- [19] M. V. Berry. Quantal phase factors accompanying adiabatic changes. *Proc. R. Soc. London. A. Math. Phys. Sci.*, 392(1802):45–57, March 1984.
- [20] C. L. Kane and E. J. Mele.  $Z_2$  topological order and the quantum spin Hall effect. *Phys. Rev. Lett.*, 95(14):146802, September 2005.
- [21] L. Fu and C. L. Kane. Time reversal polarization and a  $Z_2$  adiabatic spin pump. *Phys. Rev. B*, 74(19):195312, November 2006.
- [22] L. Fu, C. L. Kane, and E. J. Mele. Topological insulators in three dimensions. *Phys. Rev. Lett.*, 98(10):106803, March 2007.
- [23] X.-L. Qi, T. L. Hughes, and S.-C. Zhang. Topological field theory of time-reversal invariant insulators. *Phys. Rev. B*, 78(19):195424, November 2008.
- [24] L. Fu and C. L. Kane. Topological insulators with inversion symmetry. *Phys. Rev. B*, 76(4):045302, July 2007.
- [25] D. Hsieh, D. Qian, L. Wray, Y. Xia, Y. S. Hor, R. J. Cava, and M. Z. Hasan. A topological Dirac insulator in a quantum spin Hall phase. *Nature*, 452(7190):970–974, April 2008.
- [26] W.-Y. Shan, H.-Z. Lu, and S.-Q. Shen. Effective continuous model for surface states and thin films of three-dimensional topological insulators. *New J. Phys.*, 12(4):043048, April 2010.
- [27] L. Savary and L. Balents. Quantum spin liquids: a review. *Reports Prog. Phys.*, 80(1):016502, January 2017.
- [28] K. Miyake, S. Schmitt-Rink, and C. M. Varma. Spin-fluctuation-mediated even-parity pairing in heavy-fermion superconductors. *Phys. Rev. B*, 34(9):6554–6556, November 1986.
- [29] D. J. Scalapino, E. Loh, and J. E. Hirsch.  $d$ -wave pairing near a spin-density-wave instability. *Phys. Rev. B*, 34(11):8190–8192, December 1986.

- [30] S. Sachdev. *Quantum Phase Transitions*. Cambridge University Press, 2 edition, 2011.
- [31] K. G. Wilson. The renormalization group and the  $\epsilon$  expansion. *Phys. Rep.*, 12(2):75–199, August 1974.
- [32] K. G. Wilson and M. E. Fisher. Critical exponents in 3.99 dimensions. *Phys. Rev. Lett.*, 28(4):240–243, January 1972.
- [33] J. A. Hertz. Quantum critical phenomena. *Phys. Rev. B*, 14(3):1165–1184, August 1976.
- [34] A. J. Millis. Effect of a nonzero temperature on quantum critical points in itinerant fermion systems. *Phys. Rev. B*, 48(10):7183–7196, September 1993.
- [35] M. A. Metlitski and S. Sachdev. Quantum phase transitions of metals in two spatial dimensions. I. Ising-nematic order. *Phys. Rev. B*, 82(7):075127, August 2010.
- [36] P. Strack, S. Takei, and W. Metzner. Anomalous scaling of fermions and order parameter fluctuations at quantum criticality. *Phys. Rev. B*, 81(12):125103, March 2010.
- [37] J. Zinn-Justin. *Quantum Field Theory and Critical Phenomena*. Oxford University Press, Oxford, 4 edition, 2002.
- [38] E. Fradkin. Electronic Liquid Crystal Phases in Strongly Correlated Systems. In D. Cabra, A. Honecker, and P. Pujol, editors, *Modern Theories of Many-Particle Systems in Condensed Matter Physics*, volume 843 of *Lecture Notes in Physics*, pages 53–116. Springer Berlin Heidelberg, Berlin, Heidelberg, 2012.
- [39] T. C. Lubensky P. M. Chaikin. *Principles of Condensed Matter Physics*. Cambridge University Press, 1995.
- [40] B. I. Halperin and David R. Nelson. Theory of two-dimensional melting. *Phys. Rev. Lett.*, 41(2):121–124, July 1978.

- [41] M. P. Lilly, K. B. Cooper, J. P. Eisenstein, L. N. Pfeiffer, and K. W. West. Evidence for an anisotropic state of two-dimensional electrons in high Landau levels. *Phys. Rev. Lett.*, 82(2):394–397, January 1999.
- [42] R.R. Du, D.C. Tsui, H.L. Stormer, L.N. Pfeiffer, K.W. Baldwin, and K.W. West. Strongly anisotropic transport in higher two-dimensional Landau levels. *Solid State Commun.*, 109(6):389–394, January 1999.
- [43] R. A. Borzi, S. A. Grigera, J. Farrell, R. S. Perry, S. J. S. Lister, S. L. Lee, D. A. Tennant, Y. Maeno, and A. P. Mackenzie. Formation of a nematic fluid at high fields in  $\text{Sr}_3\text{Ru}_2\text{O}_7$ . *Science*, 315(5809):214–217, January 2007.
- [44] Y. Ando, K. Segawa, S. Komiya, and A. N. Lavrov. Electrical resistivity anisotropy from self-organized one dimensionality in high-temperature superconductors. *Phys. Rev. Lett.*, 88(13):137005, March 2002.
- [45] V. Hinkov, D. Haug, B. Fauque, P. Bourges, Y. Sidis, A. Ivanov, C. Bernhard, C. T. Lin, and B. Keimer. Electronic liquid crystal state in the high-temperature superconductor  $\text{YBa}_2\text{Cu}_3\text{O}_{6.45}$ . *Science*, 319(5863):597–600, February 2008.
- [46] C. Xu, M. Müller, and S. Sachdev. Ising and spin orders in the iron-based superconductors. *Phys. Rev. B*, 78(2):020501, July 2008.
- [47] C. Fang, H. Yao, W.-F. Tsai, J. Hu, and S. A. Kivelson. Theory of electron nematic order in  $\text{LaFeAsO}$ . *Phys. Rev. B*, 77(22):224509, June 2008.
- [48] I. I. Mazin and M. D. Johannes. A key role for unusual spin dynamics in ferropnictides. *Nat. Phys.*, 5(2):141–145, February 2009.
- [49] E. Fradkin, S. A. Kivelson, M. J. Lawler, J. P. Eisenstein, and A. P. Mackenzie. Nematic Fermi fluids in condensed matter physics. *Annu. Rev. Condens. Matter Phys.*, 1(1):153–178, August 2010.

- [50] I. Ya. Pomeranchuk. On the stability of a Fermi liquid. *Zh. Eksp. Teor. Fiz.*, 35:524, 1958 [*Sov. Phys. JETP*, 8:361, 1959].
- [51] L. D. Landau. The theory of a Fermi liquid. *Sov. Phys. JETP*, 3(6):920, 1957.
- [52] R. Lundgren and J. Maciejko. Landau theory of helical Fermi liquids. *Phys. Rev. Lett.*, 115(6):066401, August 2015.
- [53] V. Oganesyan, S. A. Kivelson, and E. Fradkin. Quantum theory of a nematic Fermi fluid. *Phys. Rev. B*, 64(19):195109, October 2001.
- [54] E. Berg, M. S. Rudner, and S. A. Kivelson. Electronic liquid crystalline phases in a spin-orbit coupled two-dimensional electron gas. *Phys. Rev. B*, 85(3):035116, January 2012.
- [55] J. Ruhman and E. Berg. Ferromagnetic and nematic non-Fermi liquids in spin-orbit-coupled two-dimensional Fermi gases. *Phys. Rev. B*, 90(23):235119, December 2014.
- [56] M. Z. Hasan and C. L. Kane. *Colloquium* : Topological insulators. *Rev. Mod. Phys.*, 82:3045–3067, Nov 2010.
- [57] X.-L. Qi and S.-C. Zhang. Topological insulators and superconductors. *Rev. Mod. Phys.*, 83:1057–1110, Oct 2011.
- [58] P. G. de Gennes and J. Prost. *The Physics of Liquid Crystals*. International Series of Monographs on Physics. Clarendon Press, 1995.
- [59] Y. Park, S. B. Chung, and J. Maciejko. Surface Majorana fermions and bulk collective modes in superfluid  $^3\text{He-B}$ . *Phys. Rev. B*, 91(5):054507, February 2015.
- [60] L. Fu. Parity-breaking phases of spin-orbit-coupled metals with gyrotropic, ferroelectric, and multipolar orders. *Phys. Rev. Lett.*, 115(2):026401, July 2015.
- [61] M. R. Norman. Dichroism as a probe for parity-breaking phases of spin-orbit coupled metals. *Phys. Rev. B*, 92(7):075113, August 2015.

- [62] C. Wu, K. Sun, E. Fradkin, and S.-C. Zhang. Fermi liquid instabilities in the spin channel. *Phys. Rev. B*, 75:115103, Mar 2007.
- [63] Y. You, G. Y. Cho, and E. Fradkin. Theory of nematic fractional quantum Hall states. *Phys. Rev. X*, 4:041050, Dec 2014.
- [64] I. Khavkine, C.-H. Chung, V. Oganesyan, and H.-Y. Kee. Formation of an electronic nematic phase in interacting fermion systems. *Phys. Rev. B*, 70:155110, Oct 2004.
- [65] H.-Y. Kee, E. H. Kim, and C.-H. Chung. Signatures of an electronic nematic phase at the isotropic-nematic phase transition. *Phys. Rev. B*, 68:245109, Dec 2003.
- [66] M. Garst and A. V. Chubukov. Electron self-energy near a nematic quantum critical point. *Phys. Rev. B*, 81:235105, Jun 2010.
- [67] H. Watanabe and A. Vishwanath. Criterion for stability of Goldstone modes and Fermi liquid behavior in a metal with broken symmetry. *Proc. Natl. Acad. Sci.*, 111:16314–16318, November 2014.
- [68] D. L. Maslov and A. V. Chubukov. Fermi liquid near Pomeranchuk quantum criticality. *Phys. Rev. B*, 81:045110, January 2010.
- [69] M. J. Lawler, D. G. Barci, V. Fernández, E. Fradkin, and L. Oxman. Nonperturbative behavior of the quantum phase transition to a nematic Fermi fluid. *Phys. Rev. B*, 73:085101, Feb 2006.
- [70] P. W. Anderson. Absence of diffusion in certain random lattices. *Phys. Rev.*, 109(5):1492–1505, April 1958.
- [71] R. Nandkishore and D. A. Huse. Many-body localization and thermalization in quantum statistical mechanics. *Annu. Rev. Condens. Matter Phys.*, 6(1):15–38, March 2015.
- [72] K. Binder and A. P. Young. Spin glasses: Experimental facts, theoretical concepts, and open questions. *Rev. Mod. Phys.*, 58(4):801–976, October 1986.

- [73] S.-k. Ma, C. Dasgupta, and C.-k. Hu. Random antiferromagnetic chain. *Phys. Rev. Lett.*, 43(19):1434–1437, November 1979.
- [74] D. S. Fisher. Random antiferromagnetic quantum spin chains. *Phys. Rev. B*, 50(6):3799–3821, August 1994.
- [75] C. Dasgupta and S.-k. Ma. Low-temperature properties of the random Heisenberg antiferromagnetic chain. *Phys. Rev. B*, 22(3):1305–1319, August 1980.
- [76] K. H. Fischer and J. A. Hertz. *Spin glasses*. Cambridge University Press, Cambridge, 1976.
- [77] T. Vojta. Disorder in quantum many-body systems. *Annu. Rev. Condens. Matter Phys.*, 10(1):233–252, March 2019.
- [78] Y. Imry and S.-k. Ma. Random-field instability of the ordered state of continuous symmetry. *Phys. Rev. Lett.*, 35(21):1399–1401, November 1975.
- [79] M. Aizenman and J. Wehr. Rounding of first-order phase transitions in systems with quenched disorder. *Phys. Rev. Lett.*, 62(21):2503–2506, May 1989.
- [80] R. L. Greenblatt, M. Aizenman, and J. L. Lebowitz. Rounding of first order transitions in low-dimensional quantum systems with quenched disorder. *Phys. Rev. Lett.*, 103(19):197201, November 2009.
- [81] M. Aizenman, R. L. Greenblatt, and J. L. Lebowitz. Proof of rounding by quenched disorder of first order transitions in low-dimensional quantum systems. *J. Math. Phys.*, 53(2):023301, February 2012.
- [82] A. B. Harris. Effect of random defects on the critical behaviour of Ising models. *J. Phys. C*, 7(9):1671–1692, May 1974.
- [83] J. T. Chayes, L. Chayes, D. S. Fisher, and T. Spencer. Finite-size scaling and correlation lengths for disordered systems. *Phys. Rev. Lett.*, 57(24):2999–3002, December 1986.

- [84] Z. Huang, D. P. Arovas, and A. V. Balatsky. Impurity scattering in Weyl semimetals and their stability classification. *New J. Phys.*, 15(12):123019, December 2013.
- [85] B. Sbierski, G. Pohl, E. J. Bergholtz, and P. W. Brouwer. Quantum transport of disordered Weyl semimetals at the nodal point. *Phys. Rev. Lett.*, 113(2):026602, July 2014.
- [86] S. V. Syzranov, L. Radzihovsky, and V. Gurarie. Critical transport in weakly disordered semiconductors and semimetals. *Phys. Rev. Lett.*, 114(16):166601, April 2015.
- [87] Y. Ominato and M. Koshino. Quantum transport in three-dimensional Weyl electron system in the presence of charged impurity scattering. *Phys. Rev. B*, 91(3):035202, January 2015.
- [88] Y.X. Zhao and Z.D. Wang. Disordered Weyl semimetals and their topological family. *Phys. Rev. Lett.*, 114(20):206602, May 2015.
- [89] A. Altland and D. Bagrets. Effective field theory of the disordered Weyl semimetal. *Phys. Rev. Lett.*, 114(25):257201, June 2015.
- [90] B. Sbierski, E. J. Bergholtz, and P. W. Brouwer. Quantum critical exponents for a disordered three-dimensional Weyl node. *Phys. Rev. B*, 92(11):115145, September 2015.
- [91] C.-Z. Chen, J. Song, H. Jiang, Q.-F. Sun, Z. Wang, and X. C. Xie. Disorder and metal-insulator transitions in Weyl semimetals. *Phys. Rev. Lett.*, 115(24):246603, December 2015.
- [92] S. Bera, J. D. Sau, and B. Roy. Dirty Weyl semimetals: Stability, phase transition, and quantum criticality. *Phys. Rev. B*, 93(20):201302, May 2016.
- [93] B. Roy, V. Juričić, and S. Das Sarma. Universal optical conductivity of a disordered Weyl semimetal. *Sci. Rep.*, 6:32446, August 2016.

- [94] T. Louvet, D. Carpentier, and A. A. Fedorenko. On the disorder-driven quantum transition in three-dimensional relativistic metals. *Phys. Rev. B*, 94(22):220201, December 2016.
- [95] J. H. Pixley, Y.-Z. Chou, P. Goswami, D. A. Huse, R. Nandkishore, L. Radzihovsky, and S. Das Sarma. Single-particle excitations in disordered Weyl fluids. *Phys. Rev. B*, 95(23):235101, June 2017.
- [96] T. Holder, C.-W. Huang, and P. M. Ostrovsky. Electronic properties of disordered Weyl semimetals at charge neutrality. *Phys. Rev. B*, 96(17):174205, November 2017.
- [97] J. H. Wilson, J. H. Pixley, D. A. Huse, G. Refael, and S. Das Sarma. Do the surface Fermi arcs in Weyl semimetals survive disorder? *Phys. Rev. B*, 97(23):235108, June 2018.
- [98] B. Roy, R.-J. Slager, and V. Juričić. Global phase diagram of a dirty Weyl liquid and emergent superuniversality. *Phys. Rev. X*, 8(3):031076, September 2018.
- [99] S. V. Syzranov and L. Radzihovsky. High-dimensional disorder-driven phenomena in Weyl semimetals, semiconductors, and related systems. *Annu. Rev. Condens. Matter Phys.*, 9(1):35–58, March 2018.
- [100] K. Kobayashi, T. Ohtsuki, K.-I. Imura, and I. F. Herbut. Density of states scaling at the semimetal to metal transition in three dimensional topological insulators. *Phys. Rev. Lett.*, 112(1):016402, January 2014.
- [101] R. Nandkishore, D. A. Huse, and S. L. Sondhi. Rare region effects dominate weakly disordered three-dimensional Dirac points. *Phys. Rev. B*, 89(24):245110, June 2014.
- [102] B. Skinner. Coulomb disorder in three-dimensional Dirac systems. *Phys. Rev. B*, 90(6):060202, August 2014.
- [103] B. Roy and S. Das Sarma. Diffusive quantum criticality in three-dimensional disordered Dirac semimetals. *Phys. Rev. B*, 90(24):241112, December 2014.

- [104] J.H. Pixley, P. Goswami, and S. Das Sarma. Anderson localization and the quantum phase diagram of three dimensional disordered Dirac semimetals. *Phys. Rev. Lett.*, 115(7):076601, August 2015.
- [105] J. H. Pixley, David A. Huse, and S. Das Sarma. Uncovering the hidden quantum critical point in disordered massless Dirac and Weyl semimetals. *Phys. Rev. B*, 94(12):121107, September 2016.
- [106] R. Nandkishore, J. Maciejko, D. A. Huse, and S. L. Sondhi. Superconductivity of disordered Dirac fermions. *Phys. Rev. B*, 87(17):174511, May 2013.
- [107] E. J. König, P. M. Ostrovsky, I. V. Protopopov, I. V. Gornyi, I. S. Burmistrov, and A. D. Mirlin. Interaction and disorder effects in three-dimensional topological insulator thin films. *Phys. Rev. B*, 88(3):035106, July 2013.
- [108] I. Ozfidan, J. Han, and J. Maciejko. Gapless helical superconductivity on the surface of a three-dimensional topological insulator. *Phys. Rev. B*, 94(21):214510, December 2016.
- [109] M. S. Foster and E. A. Yuzbashyan. Interaction-mediated surface-state instability in disordered three-dimensional topological superconductors with Spin SU(2) Symmetry. *Phys. Rev. Lett.*, 109(24):246801, December 2012.
- [110] M. S. Foster, H.-Y. Xie, and Y.-Z. Chou. Topological protection, disorder, and interactions: Survival at the surface of three-dimensional topological superconductors. *Phys. Rev. B*, 89(15):155140, April 2014.
- [111] S. A. A. Ghorashi, S. Davis, and M. S. Foster. Disorder-enhanced topological protection and universal quantum criticality in a spin- $\frac{3}{2}$  topological superconductor. *Phys. Rev. B*, 95(14):144503, April 2017.
- [112] J. Ye. Effects of weak disorders on quantum Hall critical points. *Phys. Rev. B*, 60(11):8290–8303, September 1999.

- [113] T. Stauber, F. Guinea, and M. A. H. Vozmediano. Disorder and interaction effects in two-dimensional graphene sheets. *Phys. Rev. B*, 71(4):041406, January 2005.
- [114] I. F. Herbut, V. Juričić, and O. Vafek. Coulomb interaction, ripples, and the minimal conductivity of graphene. *Phys. Rev. Lett.*, 100(4):046403, January 2008.
- [115] O. Vafek and M. J. Case. Renormalization group approach to two-dimensional Coulomb interacting Dirac fermions with random gauge potential. *Phys. Rev. B*, 77(3):033410, January 2008.
- [116] M. S. Foster and I. L. Aleiner. Graphene via large N: A renormalization group study. *Phys. Rev. B*, 77(19):195413, May 2008.
- [117] J.-R. Wang and G.-Z. Liu. Influence of Coulomb interaction on the anisotropic Dirac cone in graphene. *Phys. Rev. B*, 89(19):195404, May 2014.
- [118] I.-D. Potirniche, J. Maciejko, R. Nandkishore, and S. L. Sondhi. Superconductivity of disordered Dirac fermions in graphene. *Phys. Rev. B*, 90(9):094516, September 2014.
- [119] P. Goswami, H. Goldman, and S. Raghu. Metallic phases from disordered (2+1)-dimensional quantum electrodynamics. *Phys. Rev. B*, 95(23):235145, June 2017.
- [120] A. Thomson and S. Sachdev. Quantum electrodynamics in 2+1 dimensions with quenched disorder: Quantum critical states with interactions and disorder. *Phys. Rev. B*, 95(23):235146, June 2017.
- [121] P.-L. Zhao, A.-M. Wang, and G.-Z. Liu. Effects of random potentials in three-dimensional quantum electrodynamics. *Phys. Rev. B*, 95(23):235144, June 2017.
- [122] S. N. Dorogovtsev. Critical exponents of magnets with lengthy defects. *Phys. Lett. A*, 76(2):169–170, March 1980.
- [123] D. Boyanovsky and J. L. Cardy. Critical behavior of  $m$ -component magnets with correlated impurities. *Phys. Rev. B*, 26(1):154–170, July 1982.

- [124] I. D. Lawrie and V. V. Prudnikov. Static and dynamic properties of systems with extended defects: two-loop approximation. *J. Phys. C*, 17(10):1655, 1984.
- [125] J. Zinn-Justin. Four-fermion interaction near four dimensions. *Nucl. Phys. B*, 367(1):105–122, December 1991.
- [126] B. Rosenstein, H.-L. Yu, and A. Kovner. Critical exponents of new universality classes. *Phys. Lett. B*, 314(3-4):381–386, September 1993.
- [127] O. Motrunich, S.-C. Mau, D. A. Huse, and D. S. Fisher. Infinite-randomness quantum Ising critical fixed points. *Phys. Rev. B*, 61(2):1160–1172, January 2000.
- [128] T. Vojta. Phases and phase transitions in disordered quantum systems. *AIP Conf. Proc.*, 1550(1):188–247, August 2013.
- [129] T. Vojta and J. Schmalian. Quantum Griffiths effects in itinerant Heisenberg magnets. *Phys. Rev. B*, 72(4):045438, July 2005.
- [130] T. Vojta. Rare region effects at classical, quantum and nonequilibrium phase transitions. *J. Phys. A: Math. Gen.*, 39(22):R143–R205, June 2006.
- [131] T. Vojta and J. A. Hoyos. Criticality and quenched disorder: Harris criterion versus rare regions. *Phys. Rev. Lett.*, 112(7):075702, February 2014.
- [132] R.B. Griffiths. Nonanalytic behavior above the critical point in a random Ising ferromagnet. *Phys. Rev. Lett.*, 23(1):17, 1969.
- [133] B. M. McCoy. Incompleteness of the critical exponent description for ferromagnetic systems containing random impurities. *Phys. Rev. Lett.*, 23(7):383–386, August 1969.
- [134] B. M. McCoy. Theory of a two-dimensional Ising model with random impurities. III. *Phys. Rev.*, 188(2):1014, 1969.
- [135] K. G. Wilson. Quantum field - theory models in less than 4 dimensions. *Phys. Rev. D*, 7(10):2911–2926, May 1973.

- [136] D. J. Gross and A. Neveu. Dynamical symmetry breaking in asymptotically free field theories. *Phys. Rev. D*, 10(10):3235–3253, November 1974.
- [137] E. Zhao and A. Paramekanti. BCS-BEC crossover on the two-dimensional honeycomb lattice. *Phys. Rev. Lett.*, 97(23):230404, December 2006.
- [138] N. B. Kopnin and E. B. Sonin. BCS superconductivity of Dirac electrons in graphene layers. *Phys. Rev. Lett.*, 100(24):246808, June 2008.
- [139] B. Roy, V. Juričić, and I. F. Herbut. Quantum superconducting criticality in graphene and topological insulators. *Phys. Rev. B*, 87(4):041401, January 2013.
- [140] N. Zerf, L. N. Mihaila, P. Marquard, I. F. Herbut, and M. M. Scherer. Four-loop critical exponents for the Gross-Neveu-Yukawa models. *Phys. Rev. D*, 96(9):096010, November 2017.
- [141] R. Boyack, C.-H. Lin, N. Zerf, A. Rayyan, and J. Maciejko. Transition between algebraic and  $\mathbb{Z}_2$  quantum spin liquids at large  $N$ . *Phys. Rev. B*, 98(3):035137, July 2018.
- [142] L. Balents, M. P. A. Fisher, and C. Nayak. Nodal liquid theory of the pseudo-gap phase of high- $T_c$  superconductors. *Int. J. Mod. Phys. B*, 12(10):1033–1068, April 1998.
- [143] S. Thomas, talk at the 2005 KITP Conference on Quantum Phase Transitions, Kavli Institute for Theoretical Physics, Santa Barbara, 21 January 2005.
- [144] S.-S. Lee. Emergence of supersymmetry at a critical point of a lattice model. *Phys. Rev. B*, 76(7):075103, 2007.
- [145] T. Grover, D. N. Sheng, and A. Vishwanath. Emergent space-time supersymmetry at the boundary of a topological phase. *Science*, 344(6181):280, April 2014.
- [146] P. Ponte and S.-S. Lee. Emergence of supersymmetry on the surface of three-dimensional topological insulators. *New J. Phys.*, 16(1):013044, January 2014.

- [147] N. Zerf, C.-H. Lin, and J. Maciejko. Superconducting quantum criticality of topological surface states at three loops. *Phys. Rev. B*, 94(20):205106, November 2016.
- [148] L. Fei, S. Giombi, I. R. Klebanov, and G. Tarnopolsky. Yukawa conformal field theories and emergent supersymmetry. *Prog. Theor. Exp. Phys.*, 2016(12):12C105, December 2016.
- [149] Z.-X. Li, A. Vaezi, C. B. Mendl, and H. Yao. Numerical observation of emergent spacetime supersymmetry at quantum criticality. *Sci. Adv.*, 4(11):eaau1463, November 2018.
- [150] C.-Y. Hou, C. Chamon, and C. Mudry. Electron fractionalization in two-dimensional graphenelike structures. *Phys. Rev. Lett.*, 98(18):186809, May 2007.
- [151] Z. Zhou, C. Wu, and Y. Wang. Mott transition in the  $\pi$ -flux  $SU(4)$  Hubbard model on a square lattice. *Phys. Rev. B*, 97(19):195122, May 2018.
- [152] Z.-X. Li, Y.-F. Jiang, S.-K. Jian, and H. Yao. Fermion-induced quantum critical points. *Nat. Commun.*, 8(1):314, August 2017.
- [153] N. Zerf, R. Boyack, P. Marquard, J. A. Gracey, and J. Maciejko. Critical properties of the valence-bond-solid transition in lattice quantum electrodynamics. *Phys. Rev. D*, 101(9):094505, May 2020.
- [154] T. Ando and T. Nakanishi. Impurity scattering in carbon nanotubes - absence of back scattering. *J. Phys. Soc. Jpn*, 67(5):1704–1713, May 1998.
- [155] T. Ma, L. Zhang, C.-C. Chang, H.-H. Hung, and R. T. Scalettar. Localization of interacting Dirac fermions. *Phys. Rev. Lett.*, 120(11):116601, March 2018.
- [156] V. J. Emery. Critical properties of many-component systems. *Phys. Rev. B*, 11(1):239–247, January 1975.
- [157] S. F. Edwards and P. W. Anderson. Theory of spin glasses. *J. Phys. F Met. Phys.*, 5(5):965–974, May 1975.

- [158] T. C. Lubensky. Critical properties of random-spin models from the  $\epsilon$  expansion. *Phys. Rev. B*, 11(9):3573–3580, May 1975.
- [159] B. Roy and S. Das Sarma. Quantum phases of interacting electrons in three-dimensional dirty Dirac semimetals. *Phys. Rev. B*, 94(11):115137, September 2016.
- [160] D. Boyanovsky and J. L. Cardy. Erratum: Critical behavior of  $m$ -component magnets with correlated impurities. *Phys. Rev. B*, 27(11):6971–6971, June 1983.
- [161] T. Vojta, J. Crewse, M. Puschmann, D. Arovas, and Y. Kiselev. Quantum critical behavior of the superfluid-Mott glass transition. *Phys. Rev. B*, 94(13):134501, October 2016.
- [162] J. Crewse, C. Lerch, and T. Vojta. Quantum critical behavior of a three-dimensional superfluid-Mott glass transition. *Phys. Rev. B*, 98(5):054514, August 2018.
- [163] J. Zinn-Justin. *Quantum Field Theory and Critical Phenomena*. Oxford University Press, 4 edition, 2002.
- [164] M. Chanowitz, M. Furman, and I. Hinchliffe. The axial current in dimensional regularization. *Nucl. Phys. B*, 159(1):225–243, November 1979.
- [165] P. B. Weichman and R. Mukhopadhyay. Particle-hole symmetry and the dirty boson problem. *Phys. Rev. B*, 77(21):214516, June 2008.
- [166] D. B. Kaplan, J.-W. Lee, D. T. Son, and M. A. Stephanov. Conformality lost. *Phys. Rev. D*, 80(12):125005, December 2009.
- [167] S. Gukov. RG flows and bifurcations. *Nucl. Phys. B*, 919:583–638, June 2017.
- [168] D. E. Khmel'nitskii. Impurity effect on the phase transition at  $T = 0$  in magnets. Critical oscillations in corrections to the scaling laws. *Phys. Lett. A*, 67(1):59–60, July 1978.

- [169] A. Aharony. Critical properties of random and constrained dipolar magnets. *Phys. Rev. B*, 12(3):1049–1056, August 1975.
- [170] L. Zhao, H. Deng, I. Korzhovska, M. Begliarbekov, Z. Chen, E. Andrade, E. Rosenthal, A. Pasupathy, V. Oganessian, and L. Krusin-Elbaum. Emergent surface superconductivity in the topological insulator  $\text{Sb}_2\text{Te}_3$ . *Nat. Commun.*, 6:8279, September 2015.
- [171] L. Fu. Topological crystalline insulators. *Phys. Rev. Lett.*, 106(10):106802, March 2011.
- [172] T. H. Hsieh, H. Lin, J. Liu, W. Duan, A. Bansil, and L. Fu. Topological crystalline insulators in the SnTe material class. *Nat. Commun.*, 3:982, July 2012.
- [173] Y. Tanaka, Z. Ren, T. Sato, K. Nakayama, S. Souma, T. Takahashi, K. Segawa, and Y. Ando. Experimental realization of a topological crystalline insulator in SnTe. *Nat. Phys.*, 8(11):800–803, November 2012.
- [174] P. Dziawa, B. J. Kowalski, K. Dybko, R. Buczko, A. Szczerbakow, M. Szot, E. Łusakowska, T. Balasubramanian, B. M. Wojek, M. H. Berntsen, O. Tjernberg, and T. Story. Topological crystalline insulator states in  $\text{Pb}_{1-x}\text{Sn}_x\text{Se}$ . *Nat. Mater.*, 11(12):1023–1027, December 2012.
- [175] S.-Y. Xu, C. Liu, N. Alidoust, M. Neupane, D. Qian, I. Belopolski, J. D. Denlinger, Y. J. Wang, H. Lin, L. A. Wray, G. Landolt, B. Slomski, J. H. Dil, A. Marcinkova, E. Morosan, Q. Gibson, R. Sankar, F. C. Chou, R. J. Cava, A. Bansil, and M. Z. Hasan. Observation of a topological crystalline insulator phase and topological phase transition in  $\text{Pb}_{1-x}\text{Sn}_x\text{Te}$ . *Nat. Commun.*, 3:1192, November 2012.
- [176] S. Sasaki, Z. Ren, A. A. Taskin, K. Segawa, L. Fu, and Y. Ando. Odd-parity pairing and topological superconductivity in a strongly spin-orbit coupled semiconductor. *Phys. Rev. Lett.*, 109(21):217004, November 2012.

- [177] T. Sato, Y. Tanaka, K. Nakayama, S. Souma, T. Takahashi, S. Sasaki, Z. Ren, A. A. Taskin, K. Segawa, and Y. Ando. Fermiology of the strongly spin-orbit coupled superconductor  $\text{Sn}_{1-x}\text{In}_x\text{Te}$ : Implications for topological superconductivity. *Phys. Rev. Lett.*, 110(20):206804, May 2013.
- [178] B. J. DeSalvo, M. Yan, P. G. Mickelson, Y. N. Martinez de Escobar, and T. C. Killian. Degenerate Fermi gas of  $^{87}\text{Sr}$ . *Phys. Rev. Lett.*, 105(3):030402, July 2010.
- [179] Z. Zhou, Da Wang, Z. Y. Meng, Yu Wang, and C. Wu. Mott insulating states and quantum phase transitions of correlated  $\text{SU}(2N)$  Dirac fermions. *Phys. Rev. B*, 93(24):245157, June 2016.
- [180] N. Bobev, S. El-Showk, D. Mazáč, and M. F. Paulos. Bootstrapping the three dimensional supersymmetric Ising model. *Phys. Rev. Lett.*, 115(5):051601, July 2015.
- [181] L. Classen, I. F. Herbut, and M. M. Scherer. Fluctuation-induced continuous transition and quantum criticality in Dirac semimetals. *Phys. Rev. B*, 96(11):115132, September 2017.
- [182] R. N. Bhatt and P. A. Lee. Scaling studies of highly disordered spin- $\frac{1}{2}$  antiferromagnetic systems. *Phys. Rev. Lett.*, 48(5):344–347, February 1982.
- [183] S. Iyer, D. Pekker, and G. Refael. Mott glass to superfluid transition for random bosons in two dimensions. *Phys. Rev. B*, 85(9):094202, March 2012.
- [184] R. T. Scalettar, N. Trivedi, and C. Huscroft. Quantum Monte Carlo study of the disordered attractive Hubbard model. *Phys. Rev. B*, 59(6):4364–4375, February 1999.
- [185] R. Boyack, H. Yerzhakov, and J. Maciejko. Quantum phase transitions in Dirac fermion systems. *arXiv:2004.09414*, April 2020.
- [186] A. Weinrib and B. I. Halperin. Critical phenomena in systems with long-range-correlated quenched disorder. *Phys. Rev. B*, 27(1):413–427, January 1983.

- [187] K.-I. Kubota and H. Terao. Dynamical symmetry breaking in QED<sub>3</sub> from the Wilson RG point of view. *Prog. Theor. Phys.*, 105(5):809–825, May 2001.
- [188] K. Kaveh and I. F. Herbut. Chiral symmetry breaking in three-dimensional quantum electrodynamics in the presence of irrelevant interactions: A renormalization group study. *Phys. Rev. B*, 71(18):184519, May 2005.
- [189] H. Gies and J. Jaeckel. Chiral phase structure of QCD with many flavors. *Eur. Phys. J. C*, 46(2):433–438, May 2006.
- [190] J. Braun, C. S. Fischer, and H. Gies. Beyond Miransky scaling. *Phys. Rev. D*, 84(3):034045, August 2011.
- [191] I. F. Herbut. Chiral symmetry breaking in three-dimensional quantum electrodynamics as fixed point annihilation. *Phys. Rev. D*, 94(2):025036, July 2016.
- [192] J. A. Gracey, I. F. Herbut, and D. Roscher. Tensor  $O(N)$  model near six dimensions: Fixed points and conformal windows from four loops. *Phys. Rev. D*, 98(9):096014, November 2018.
- [193] V. Gorbenko, S. Rychkov, and B. Zan. Walking, weak first-order transitions, and complex CFTs. *JHEP*, 10(10):108, October 2018.
- [194] I. F. Herbut and L. Janssen. Topological Mott insulator in three-dimensional systems with quadratic band touching. *Phys. Rev. Lett.*, 113(10):106401, September 2014.
- [195] L. Janssen and I. F. Herbut. Nematic quantum criticality in three-dimensional Fermi system with quadratic band touching. *Phys. Rev. B*, 92(4):045117, July 2015.
- [196] A. Nahum, J. T. Chalker, P. Serna, M. Ortuño, and A. M. Somoza. Deconfined quantum criticality, scaling violations, and classical loop models. *Phys. Rev. X*, 5(4):041048, 2015.
- [197] C. Wang, A. Nahum, M. A. Metlitski, C. Xu, and T. Senthil. Deconfined quantum critical points: Symmetries and dualities. *Phys. Rev. X*, 7(3):031051, September 2017.

- [198] V. Gorbenko, S. Rychkov, and B. Zan. Walking, weak first-order transitions, and complex CFTs II. Two-dimensional Potts model at  $Q > 4$ . *SciPost Phys.*, 5(5):050, November 2018.
- [199] P. Serna and A. Nahum. Emergence and spontaneous breaking of approximate  $O(4)$  symmetry at a weakly first-order deconfined phase transition. *Phys. Rev. B*, 99(19):195110, May 2019.
- [200] B. Ihrig, N. Zerf, P. Marquard, I. F. Herbut, and M. M. Scherer. Abelian Higgs model at four loops, fixed-point collision, and deconfined criticality. *Phys. Rev. B*, 100(13):134507, October 2019.
- [201] R. Ma and C. Wang. Theory of deconfined pseudocriticality. *Phys. Rev. B*, 102(2):020407, July 2020.
- [202] A. Nahum. Note on Wess-Zumino-Witten models and quasiuniversality in 2+1 dimensions. *arXiv:1912.13468*, December 2019.
- [203] J. E. Marsden and M. McCracken. *The Hopf Bifurcation and Its Applications*. Applied Mathematical Sciences. Springer-Verlag, New York, 1976.
- [204] K. G. Wilson. Renormalization group and strong interactions. *Phys. Rev. D*, 3(8):1818–1846, April 1971.
- [205] B. A. Veytsman. Limit cycles in renormalization group flows: thermodynamics controls dances of space patterns. *Phys. Lett. A*, 183(4):315–318, December 1993.
- [206] C. Athorne and I. D. Lawrie. Renormalization group structure of a double replica model of superconductors, spin glasses and cubic ferromagnets. *Nucl. Phys. B*, 257:577–597, January 1985.
- [207] L. De Cesare. Critical properties of systems with anisotropic long-range correlated quenched disorder. *Phys. Rev. B*, 49(17):11742–11748, May 1994.

- [208] B. Roy, V. Jurii, and I. F. Herbut. Emergent Lorentz symmetry near fermionic quantum critical points in two and three dimensions. *JHEP*, 04(4):018, April 2016.
- [209] Y. Nambu and G. Jona-Lasinio. Dynamical model of elementary particles based on an analogy with superconductivity. I. *Phys. Rev.*, 122(1):345–358, April 1961.
- [210] I. F. Herbut. Interactions and phase transitions on graphene’s honeycomb lattice. *Phys. Rev. Lett.*, 97(14):146401, October 2006.
- [211] C. Xu. Time-reversal symmetry breaking at the edge states of a three-dimensional topological band insulator. *Phys. Rev. B*, 81(2):020411, January 2010.
- [212] H. Sonoda. Phase structure of a three-dimensional Yukawa model. *Prog. Theor. Phys.*, 126(1):57–80, 2011.
- [213] P. J. H. Denteneer, R. T. Scalettar, and N. Trivedi. Conducting phase in the two-dimensional disordered hubbard model. *Phys. Rev. Lett.*, 83(22):4610–4613, November 1999.
- [214] W. Witczak-Krempa and J. Maciejko. Optical conductivity of topological surface states with emergent supersymmetry. *Phys. Rev. Lett.*, 116(10):100402, March 2016.
- [215] I. Boettcher and I. F. Herbut. Superconducting quantum criticality in three-dimensional Luttinger semimetals. *Phys. Rev. B*, 93(20):205138, May 2016.
- [216] I. Mandal. Fate of superconductivity in three-dimensional disordered Luttinger semimetals. *Ann. Phys. (N.Y.)*, 392:179–195, May 2018.
- [217] I. F. Herbut. Quantum critical points with the Coulomb interaction and the dynamical exponent: When and why  $z = 1$ . *Phys. Rev. Lett.*, 87(13):137004, September 2001.
- [218] V. Narovlansky and O. Aharony. Renormalization group in field theories with quantum quenched disorder. *Phys. Rev. Lett.*, 121(7):071601, August 2018.

- [219] O. Aharony and V. Narovlansky. Renormalization group flow in field theories with quenched disorder. *Phys. Rev. D*, 98(4):045012, August 2018.
- [220] N. Goldenfeld. *Lectures on Phase Transitions and the Renormalization Group*. Westview Press, Boulder, 1992.
- [221] J. M. Kosterlitz. The critical properties of the two-dimensional  $xy$  model. *J. Phys. C*, 7(6):1046–1060, March 1974.
- [222] S. A. Hartnoll, D. M. Ramirez, and J. E. Santos. Thermal conductivity at a disordered quantum critical point. *JHEP*, 04(4):022, April 2016.
- [223] L. Dingjun, W. Xian, Z. Deming, and H. Maoan. *Bifurcation Theory and Methods of Dynamical Systems*, volume 15 of *Advanced Series in Dynamical Systems*. World Scientific, Singapore, 1997.
- [224] T. Vojta. Disorder-induced rounding of certain quantum phase transitions. *Phys. Rev. Lett.*, 90(10):107202, March 2003.
- [225] I. Affleck and J. B. Marston. Large- $n$  limit of the Heisenberg-Hubbard model: Implications for high- $T_c$  superconductors. *Phys. Rev. B*, 37(7):3774–3777, March 1988.
- [226] D. H. Kim and P. A. Lee. Theory of spin excitations in undoped and underdoped cuprates. *Ann. Phys. (N.Y.)*, 272(1):130–164, February 1999.
- [227] W. Rantner and X.-G. Wen. Electron spectral function and algebraic spin liquid for the normal state of underdoped high  $T_c$  superconductors. *Phys. Rev. Lett.*, 86(17):3871–3874, April 2001.
- [228] M. Hermele, T. Senthil, and M. P. A. Fisher. Algebraic spin liquid as the mother of many competing orders. *Phys. Rev. B*, 72(10):104404, September 2005.
- [229] H. Goldman, M. Mulligan, S. Raghu, G. Torroba, and M. Zimet. Two-dimensional conductors with interactions and disorder from particle-vortex duality. *Phys. Rev. B*, 96(24):245140, December 2017.

- [230] S. Dey. Destabilization of the U(1) Dirac spin liquid phase on the triangular lattice by quenched disorder. *arXiv:2008.12307*, August 2020.
- [231] M. M. Bordelon, E. Kenney, C. Liu, T. Hogan, L. Posthuma, M. Kavand, Y. Lyu, M. Sherwin, N. P. Butch, C. Brown, M. J. Graf, L. Balents, and S. D. Wilson. Field-tunable quantum disordered ground state in the triangular-lattice antiferromagnet NaYbO<sub>2</sub>. *Nat. Phys.*, 15(10):1058–1064, October 2019.
- [232] R. Boyack and J. Maciejko. Critical exponents for the valence-bond-solid transition in lattice quantum electrodynamics. *arXiv:1911.09768*, November 2019.
- [233] L. Janssen, W. Wang, M. M. Scherer, Z. Y. Meng, and X. Y. Xu. Confinement transition in the QED<sub>3</sub>-Gross-Neveu-XY universality class. *Phys. Rev. B*, 101(23):235118, June 2020.
- [234] P. Ghaemi and T. Senthil. Néel order, quantum spin liquids, and quantum criticality in two dimensions. *Phys. Rev. B*, 73(5):054415, February 2006.
- [235] É. Dupuis, M. B. Paranjape, and W. Witczak-Krempa. Transition from a Dirac spin liquid to an antiferromagnet: Monopoles in a QED<sub>3</sub>-Gross-Neveu theory. *Phys. Rev. B*, 100(9):094443, September 2019.
- [236] N. Zerf, R. Boyack, P. Marquard, J. A. Gracey, and J. Maciejko. Critical properties of the Néel–algebraic-spin-liquid transition. *Phys. Rev. B*, 100(23):235130, December 2019.
- [237] L. Janssen and Y.-C. He. Critical behavior of the QED<sub>3</sub>-Gross-Neveu model: Duality and deconfined criticality. *Phys. Rev. B*, 96(20):205113, November 2017.
- [238] B. Ihrig, L. Janssen, L. N. Mihaila, and M. M. Scherer. Deconfined criticality from the QED<sub>3</sub>-Gross-Neveu model at three loops. *Phys. Rev. B*, 98(11):115163, September 2018.

- [239] N. Zerf, P. Marquard, R. Boyack, and J. Maciejko. Critical behavior of the QED<sub>3</sub>-Gross-Neveu-Yukawa model at four loops. *Phys. Rev. B*, 98(16):165125, October 2018.
- [240] G. D. Mahan. *Many-particle physics*. Plenum Press, 1993.
- [241] V. Oganesyan. *Quantum liquid crystals*. PhD thesis, University of California, Los Angeles, January 2001.
- [242] H. Osborn. Weyl consistency conditions and a local renormalisation group equation for general renormalisable field theories. *Nucl. Physics, Sect. B*, 363(2-3):486–526, October 1991.
- [243] A. Kamenev. *Field Theory of Non-Equilibrium Systems*. Cambridge University Press, 2011.
- [244] K. B. Efetov. Supersymmetry method in localization theory. *Sov. Phys. JETP*, 55(3):514, 1982.
- [245] G. Leibbrandt. Introduction to the technique of dimensional regularization. *Rev. Mod. Phys.*, 47(4):849–876, October 1975.
- [246] É. É. Boos and A. I. Davydychev. A method of calculating massive Feynman integrals. *Theor. Math. Phys.*, 89(1):1052–1064, October 1991.
- [247] M. Dudka. Two-loop Feynman integrals for  $\phi^4$  theory with long-range correlated disorder. *J. Math. Phys.*, 56(1):013302, January 2015.
- [248] H. Kleinert and E. Babaev. Two phase transitions in chiral Gross-Neveu model in  $2+\epsilon$  dimensions at low N. *Phys. Lett. B*, 438(34):311–320, October 1998.

# Appendix A

## Calculations for Chapter 2

### A.1 Mean-field phase diagram

The action is

$$S[\psi^\dagger, \psi] = \int_0^\beta d\tau \int d^2r [\psi^\dagger (\partial_\tau - iv_F \hat{z} \cdot (\boldsymbol{\sigma} \times \boldsymbol{\partial}) - \mu) \psi - \frac{f_2}{4} \text{Tr}(\hat{Q}(\mathbf{r})^2)] \quad (\text{A.1})$$

where  $\hat{Q}_{ab}(\mathbf{r}) = -\frac{i}{k_A} \psi^\dagger(\mathbf{r}) (\sigma_a \overleftrightarrow{\partial}_b + \sigma_b \overleftrightarrow{\partial}_a - \delta_{ab} \boldsymbol{\sigma} \cdot \overleftrightarrow{\boldsymbol{\partial}}) \psi(\mathbf{r})$ ,  $\beta = 1/T$  is the inverse temperature, and we consider a dispersive Fermi velocity  $v_F = \bar{v}_F(1 + F(k))$ . We impose a constraint  $1 + F(k) > 0$  for  $k < \Lambda$  to preserve a Dirac-like spectrum in the effective theory.

We introduce an auxiliary bosonic field via the Hubbard-Stratonovich transformation:

$$\int \mathcal{D}\phi e^{-\frac{1}{2} \int d^d x d^d x' \phi(\mathbf{x}) A(\mathbf{x}, \mathbf{x}') \phi(\mathbf{x}') - \int d^d x j(\mathbf{x}) \phi(\mathbf{x})} \propto (\det A)^{\frac{1}{2}} e^{\frac{1}{2} \int d^d x d^d x' j(\mathbf{x}) A^{-1}(\mathbf{x}, \mathbf{x}') j(\mathbf{x}')}. \quad (\text{A.2})$$

For the given case  $j(\mathbf{x}) = (\hat{Q}_{11}(\mathbf{x}), \hat{Q}_{12}(\mathbf{x}), \hat{Q}_{21}(\mathbf{x}), \hat{Q}_{22}(\mathbf{x}))^T$ , and

$$A^{-1} = \begin{pmatrix} 1 & 0 & 0 & 0 \\ 0 & 0 & 1 & 0 \\ 0 & 1 & 0 & 0 \\ 0 & 0 & 0 & 1 \end{pmatrix} \delta(\mathbf{x} - \mathbf{x}') \frac{f_2}{2}. \quad (\text{A.3})$$

Then

$$A = \begin{pmatrix} 1 & 0 & 0 & 0 \\ 0 & 0 & 1 & 0 \\ 0 & 1 & 0 & 0 \\ 0 & 0 & 0 & 1 \end{pmatrix} \delta(\mathbf{x} - \mathbf{x}') \frac{2}{f_2}. \quad (\text{A.4})$$

Thus, using  $Q_{ab}(\mathbf{r})$  for the components of the auxiliary field, the effective action becomes:

$$S[\psi^\dagger, \psi, Q_{ab}(\mathbf{r})] = \int_0^\beta d\tau \int d^2r [\psi^\dagger (\partial_\tau - iv_F \hat{z} \cdot (\boldsymbol{\sigma} \times \boldsymbol{\partial}) - \mu) \psi + \frac{1}{f_2} \sum_{ab} Q_{ab}(\mathbf{r}) Q_{ba}(\mathbf{r}) - i \sum_{ab} \frac{Q_{ab}(\mathbf{r})}{k_A} (\psi^\dagger(\mathbf{r}) (\sigma_a \overleftrightarrow{\partial}_b + \sigma_b \overleftrightarrow{\partial}_a - \delta_{ab} \boldsymbol{\sigma} \cdot \overleftrightarrow{\boldsymbol{\partial}}) \psi(\mathbf{r}))]. \quad (\text{A.5})$$

Partially going into  $(\mathbf{k}, i\nu_n)$ -space, assuming a constant order parameter  $Q_{ab}(\mathbf{q}, i\nu_n) = (2\pi)^2 \delta_{\nu_n, 0} \delta(\mathbf{q}) \bar{Q}_{ab}$ , and integrating out the fermion fields, we obtain for the partition function

$$Z = \int \mathcal{D}Q_{ab} e^{-\left(\frac{1}{f_2} \int_0^\beta d\tau \int d^2r \text{Tr}(Q^2) - \frac{1}{\beta} \sum_{i\nu_n} \int \frac{d^2k}{(2\pi)^2} \ln \det(-i\nu_n + v_F \hat{z} \cdot (\boldsymbol{\sigma} \times \mathbf{k}) - \mu + \frac{Q_{ab}}{k_A} (\sigma_a k_b + \sigma_b k_a - \delta_{ab} \boldsymbol{\sigma} \cdot \mathbf{k}))\right)}. \quad (\text{A.6})$$

By rotational invariance, we may set

$$\bar{Q} = \begin{pmatrix} 0 & \bar{Q} \\ \bar{Q} & 0 \end{pmatrix}. \quad (\text{A.7})$$

Then, calculating the determinant, we obtain

$$Z = \int \mathcal{D}\bar{Q}_{ab} e^{-\left(\frac{2}{f_2} \int_0^\beta d\tau \int d^2r \bar{Q}^2 - \frac{1}{\beta V} \sum_{i\nu_n} \sum_{\mathbf{k}} \ln((\nu_n - i\mu)^2 + \epsilon_{\mathbf{k}}^2(\bar{Q}))\right)}, \quad (\text{A.8})$$

where

$$\epsilon_{\mathbf{k}}(\bar{Q}) = v_F k \sqrt{(1 + F(k))^2 - 2\Delta(1 + F(k)) \cos(2\theta) + \Delta^2} \quad (\text{A.9})$$

and  $\Delta = \frac{2\bar{Q}}{v_F k_A}$ . To sum over Matsubara frequencies in the expression

$$I = \frac{1}{\beta} \sum_{i\nu_n} \ln((\nu_n - i\mu)^2 + \epsilon_{\mathbf{k}}^2(\bar{Q})), \quad (\text{A.10})$$

we use the residue theorem:

$$S = \sum_n h(\nu_n) = \frac{\xi}{2\pi i} \oint dz g(z) h(-iz) = \xi \sum_n \text{Res}(g(z) h(-iz)) \Big|_{z=i\nu_n} \quad (\text{A.11})$$

where  $g(z) = \frac{\beta}{e^{\beta z} - \xi}$ , and  $\xi = \pm 1$  for bosons and fermions, respectively. One may perform this calculation by directly applying the above formula to the sum  $I$  with  $h(\nu_n) = \frac{1}{\beta} \ln((\nu_n - i\mu)^2 + \epsilon^2(\bar{Q}))$ . But it is technically easier to first take a partial derivative with respect to  $\epsilon_{\mathbf{k}}$ ,

$$\frac{\partial I}{\partial \epsilon_{\mathbf{k}}(\bar{Q})} = \frac{1}{\beta} \sum_{i\nu_n} \frac{2\epsilon_{\mathbf{k}}(\bar{Q})}{(\nu_n - i\mu)^2 + \epsilon_{\mathbf{k}}(\bar{Q})^2} = \frac{1}{\beta} \sum_{i\nu_n} \left( \frac{1}{i\nu_n + \epsilon_{\mathbf{k}}(\bar{Q}) + \mu} - \frac{1}{i\nu_n - (\epsilon_{\mathbf{k}}(\bar{Q}) - \mu)} \right), \quad (\text{A.12})$$

then perform the Matsubara sum using the well known sums (see, e.g., Ref. [240]),

$$\frac{\partial I}{\partial \epsilon_{\mathbf{k}}(\bar{Q})} = - \left( n_F(\epsilon_{\mathbf{k}}(\bar{Q}) - \mu) - n_F(-\epsilon_{\mathbf{k}}(\bar{Q}) - \mu) \right) = \left( -n_F(\epsilon_{\mathbf{k}}(\bar{Q}) - \mu) - n_F(\epsilon_{\mathbf{k}}(\bar{Q}) + \mu) + 1 \right), \quad (\text{A.13})$$

and integrate the obtained result:

$$I = \left( -\epsilon_{\mathbf{k}}(\bar{Q}) + \frac{1}{\beta} \ln(1 + e^{\beta(\epsilon_{\mathbf{k}}(\bar{Q}) - \mu)}) + \frac{1}{\beta} \ln(1 + e^{\beta(\epsilon_{\mathbf{k}}(\bar{Q}) + \mu)}) \right), \quad (\text{A.14})$$

which up to an irrelevant constant shift in the free energy gives the value we are interested in. Upon adjusting this constant,  $I$  may also be rewritten in a more symmetric form:

$$I = \frac{1}{\beta} \sum_{i\nu_n} \ln((\nu_n - i\mu)^2 + \epsilon_{\mathbf{k}}^2(\bar{Q})) = \frac{1}{\beta} \ln(1 + e^{-\beta(\epsilon_{\mathbf{k}}(\bar{Q}) - \mu)}) + \frac{1}{\beta} \ln(1 + e^{\beta(\epsilon_{\mathbf{k}}(\bar{Q}) + \mu)}). \quad (\text{A.15})$$

We need to consider the undoped,  $\mu = 0$ , and doped,  $\mu \neq 0$ , cases separately.

### A.1.1 Undoped limit, zero temperature

In the  $T \rightarrow 0$  limit, for the free energy density, which at  $T = 0$  is the ground state energy per unit volume  $\mathcal{E}$ , we have

$$\mathcal{E} = \frac{2\bar{Q}^2}{f_2} - \int \frac{d^2k}{(2\pi)^2} \epsilon_{\mathbf{k}}(\bar{Q}), \quad (\text{A.16})$$

where we switched from the discrete sum to an integral over  $\mathbf{k}$  by working in the thermodynamic limit  $V \rightarrow \infty$ . In the nodal (undoped) limit, we integrate to a cutoff  $\Lambda$  in momentum space:  $\int \frac{d^2k}{(2\pi)^2} = \int_0^\Lambda \frac{dkk}{2\pi} \int_0^{2\pi} \frac{d\theta}{2\pi}$ . Introducing dimensionless variables  $k = \Lambda y$ ,  $\lambda = \frac{2f_2}{3\pi^2 v_F}$ , the expression for the ground state energy is

$$\begin{aligned} \mathcal{E} &= \frac{v_F \Lambda^3}{3\pi^2} \left( \frac{\Delta^2}{\lambda} - 3 \int_0^1 dy y^2 \int d\theta \sqrt{(1 + F(\Lambda y))^2 - 2(1 + F(\Lambda y))\Delta \cos 2\theta + \Delta^2} \right) \\ &= \frac{v_F \Lambda^3}{3\pi^2} \left( \frac{\Delta^2}{\lambda} - 3 \int_0^1 dy y^2 (1 + F(\Lambda y) - \Delta) \sqrt{1 + 4 \frac{(1 + F(\Lambda y))\Delta}{(1 + F(\Lambda y) - \Delta)^2} \sin^2 \theta} \right) \\ &= \frac{v_F \Lambda^3}{3\pi^2} \left( \frac{\Delta^2}{\lambda} - 3 \int_0^1 dy y^2 (1 + F(\Lambda y) - \Delta) E \left( -4 \frac{(1 + F(\Lambda y))\Delta}{(1 + F(\Lambda y) - \Delta)^2} \right) \right), \quad (\text{A.17}) \end{aligned}$$

where  $E(m) = \int_0^{\frac{\pi}{2}} d\theta \sqrt{1 - m^2 \sin^2 \theta}$  is the complete elliptic integral of the second kind. For the constant Fermi velocity, the integral over  $\mathbf{k}$  may be performed analytically, and the ground state energy is as given in Eq. (2.15):

$$\mathcal{E}(\Delta) = \frac{v_F \Lambda^3}{3\pi^2} \left[ \frac{\Delta^2}{\lambda} - |\Delta - 1| E \left( -\frac{4\Delta}{(\Delta - 1)^2} \right) \right]. \quad (\text{A.18})$$

The ground state energy as a function of  $\Delta$  for  $F(k) = 1 + \alpha k^2$ ,  $\alpha = -0.61$ , is plotted in Fig. 2.2. As discussed in the main text, the zero temperature transition is first-order<sup>1</sup>. In the next subsection we investigate the transition still in the nodal limit,  $\mu = 0$ , but at finite temperature.

---

<sup>1</sup>There is nothing special about the particular value of  $\alpha$  above; we only want to show by example that corrections to strict linearity in the dispersion affect the magnitude of the first-order jump in the order parameter.

### A.1.2 Undoped limit, finite temperature

In dimensionless units ( $\lambda = \frac{2f_2\Lambda}{3\pi^2v_F}$ ;  $\beta v_F\Lambda \rightarrow \beta$ ;  $\frac{k}{\Lambda} \rightarrow k$ ) the free energy density becomes:

$$F(\Delta) = \frac{v_F\Lambda^3}{3\pi^2} \left( \frac{\Delta^2}{\lambda} - \frac{3\pi^2}{\beta} \int_0^1 \frac{dk}{(2\pi)^2} \int_0^{2\pi} d\theta k \left\{ \ln\left(1 + e^{-\beta\epsilon_k(\bar{Q})}\right) + \ln\left(1 + e^{\beta\epsilon_k(\bar{Q})}\right) \right\} \right). \quad (\text{A.19})$$

Omitting lengthy algebra, after integration over  $k$  it acquires the following form:

$$F(\Delta) = \frac{v_F\Lambda^3}{3\pi^2} \left( \frac{\Delta^2}{\lambda} - \frac{3\pi^2}{\beta} \int_0^{2\pi} \frac{d\theta}{(2\pi)^2} \left\{ \frac{1}{2} \ln\left(1 + e^{-\beta f(\theta)}\right) + \frac{1}{2} \ln\left(1 + e^{\beta f(\theta)}\right) - \frac{\beta f(\theta)}{6} - \frac{2}{(\beta f(\theta))^2} \text{Li}_3(-1) + \text{Li}_1(-e^{-\beta f(\theta)}) + \frac{2}{\beta f(\theta)} \text{Li}_2(-e^{-\beta f(\theta)}) + \frac{2}{(\beta f(\theta))^2} \text{Li}_3(-e^{-\beta f(\theta)}) \right\} \right), \quad (\text{A.20})$$

where

$$f(\theta) = \sqrt{1 - 2\Delta \cos(2\theta) + \Delta^2}, \text{ and } \text{Li}_n(z) = \sum_{k=1}^{\infty} \frac{z^k}{k^n} \text{ is the polylogarithm.} \quad (\text{A.21})$$

The integral over  $\theta$  is not amenable to analytical evaluation, but numerical investigation reveals that the first-order phase transition changes to a continuous one above a finite temperature  $T_{\text{TCP}}$  (see Fig. 2.3a), corresponding to a tricritical point, as discussed in the main text. To complete the investigation, we expand the free energy around  $\Delta = 0$ .

We first expand the integrand up to sixth order in  $\Delta$ . Denoting

$$f_{\pm}(\Delta) = \ln\left(1 + e^{\pm\beta k f(\theta)}\right), \quad (\text{A.22})$$

the derivatives at  $\Delta = 0$  are (here  $\xi = \pm$ ):

$$\begin{aligned}
\left. \frac{\partial f_\xi}{\partial \Delta} \right|_{\Delta=0} &= -\xi \frac{\beta k}{1 + e^{-\xi \beta k}} \cos(2\theta) = a_{1\xi}, \\
\left. \frac{\partial^2 f_\xi}{\partial \Delta^2} \right|_{\Delta=0} &= \frac{(\beta k)^2}{4 \cosh^2(\frac{\beta k}{2})} \cos^2(2\theta) + \xi \frac{\beta k}{1 + e^{-\xi \beta k}} \sin^2(2\theta) = a_{2\xi}, \\
\left. \frac{\partial^3 f_\xi}{\partial \Delta^3} \right|_{\Delta=0} &= \frac{(\beta k)^3 \sinh(\frac{\beta k}{2})}{4 \cosh^3(\frac{\beta k}{2})} \cos^3(2\theta) - \frac{3(\beta k)^2}{4 \cosh^2(\frac{\beta k}{2})} (\cos(2\theta) - \cos^3(2\theta)) + \\
&\quad \xi \frac{3\beta k}{1 + e^{-\xi \beta k}} (\cos(2\theta) - \cos^3(2\theta)) = a_{3\xi}, \tag{A.23}
\end{aligned}$$

$$\begin{aligned}
\left. \frac{\partial^4 f_\xi}{\partial \Delta^4} \right|_{\Delta=0} &= \frac{(\beta k)^4}{8} \left( 4 \tanh^2\left(\frac{\beta k}{2}\right) - 3 \tanh^4\left(\frac{\beta k}{2}\right) - 1 \right) \cos^4(2\theta) - \\
&\quad \frac{3}{2} (\beta k)^3 \frac{\sinh(\frac{\beta k}{2})}{\cosh^3(\frac{\beta k}{2})} \cos^2(2\theta) \sin^2(2\theta) + \frac{3(\beta k)^2}{4 \cosh^2(\frac{\beta k}{2})} (\sin^4(2\theta) - 4 \cos^2(2\theta) \sin^2(2\theta)) - \\
&\quad 3\xi \frac{\beta k}{1 + e^{-\xi \beta k}} \sin^2(2\theta) (1 - 5 \cos^2(2\theta)) = a_{4\xi}. \tag{A.24}
\end{aligned}$$

We do not show formulas for the fifth and sixth derivatives but note that analogically to the second and third derivatives,  $\left. \frac{\partial^5 f_\xi}{\partial \Delta^5} \right|_{\Delta=0}$  contains only odd powers of  $\cos(2\theta)$ , and  $\left. \frac{\partial^6 f_\xi}{\partial \Delta^6} \right|_{\Delta=0}$  contains only even powers. Then, after integration over  $\theta$ , odd powers of  $\Delta$  in the expansion of the free energy vanish, and we obtain

$$F(\Delta, T) - F(0, T) = \frac{v_F \Lambda^3}{3\pi^2} (a_2 \Delta^2 + a_4 \Delta^4 + a_6 \Delta^6), \tag{A.25}$$

where

$$\begin{aligned}
a_2 &= \left( \frac{1}{\lambda} - \frac{3\pi^2}{8\beta} \int_0^1 \frac{dk}{2\pi} k \left\{ \frac{(\beta k)^2}{\cosh^2(\frac{\beta k}{2})} + 2\beta k \tanh \frac{\beta k}{2} \right\} \right), \\
a_4 &= -\frac{3\pi^2}{64\beta} \int_0^1 \frac{dk}{2\pi} k \left\{ (\beta k)^4 \left( -\frac{1}{\cosh^2(\frac{\beta k}{2})} + 3\frac{\tanh^2(\frac{\beta k}{2})}{\cosh^2(\frac{\beta k}{2})} \right) - (\beta k)^3 \frac{\tanh(\frac{\beta k}{2})}{\cosh^2(\frac{\beta k}{2})} - \right. \\
&\quad \left. \frac{(\beta k)^2}{2\cosh^2(\frac{\beta k}{2})} + \beta k \tanh\left(\frac{\beta k}{2}\right) \right\}, \\
a_6 &= \frac{\pi}{6144} \int_0^1 dk k^2 \left( \beta k \operatorname{sech}^2\left(\frac{\beta k}{2}\right) \left( -2\beta^4 k^4 + 6\beta^2 k^2 + 3\beta k \left( -5\beta^3 k^3 \operatorname{sech}^4\left(\frac{\beta k}{2}\right) + \right. \right. \right. \\
&\quad \left. \left. \left. 2(\beta^2 k^2 + 2) \tanh\left(\frac{\beta k}{2}\right) + \beta k \left( 5\beta^2 k^2 - 6\beta k \tanh\left(\frac{\beta k}{2}\right) - 3 \right) \operatorname{sech}^2\left(\frac{\beta k}{2}\right) \right) \right) + \right. \\
&\quad \left. 18 \right) - 36 \tanh\left(\frac{\beta k}{2}\right) \Big). \tag{A.26}
\end{aligned}$$

In these expressions, it is possible to calculate the integrals analytically, and the result will contain polylogarithms of  $(-\exp(\frac{\beta k}{2}))$ . However, the final expression is rather long and complicates further investigation. Therefore, a better strategy is to evaluate the coefficients in the expansion numerically as a function of temperature. The temperature dependence of the fourth- and sixth-order coefficients is depicted in Fig. (A.1).

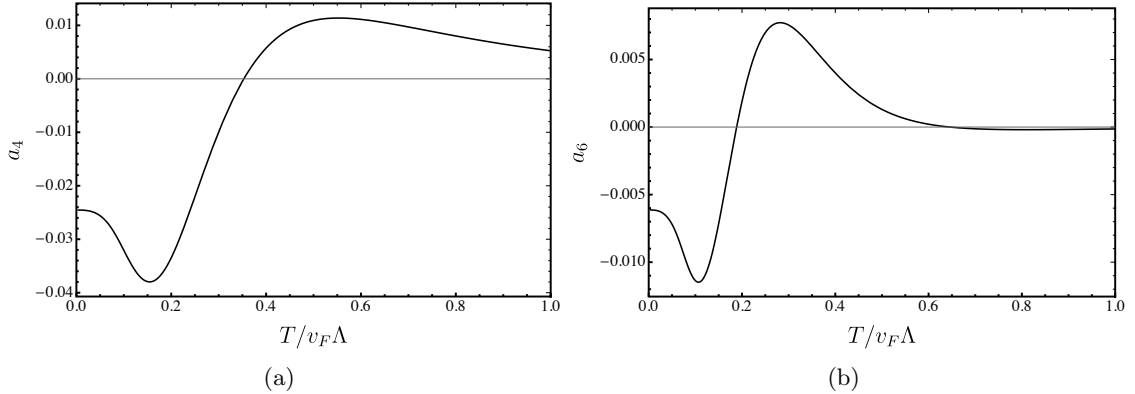


Figure A.1: Temperature dependence of  $a_4$  (a) and  $a_6$  (b) in Eq. (A.25).

The tricritical temperature  $T_{\text{TCP}}$ , above which the order of the transition changes from first to second and is determined from  $a_4(T) = 0$ , is approximately 0.353. Note that  $a_6 > 0$  in the vicinity of  $T = T_{\text{TCP}}$ , which stabilizes the free energy. The phase diagram in

the  $\lambda$ - $T$  plane is given in Fig. 2.3b.

### A.1.3 Doped limit, zero temperature

We now calculate the free energy density for the doped case at zero temperature. We consider only a constant Fermi velocity. In the  $T \rightarrow 0$  limit, neglecting a constant term (see Eq. (A.14)), we may write

$$\mathcal{F}(\bar{Q}) = \frac{2\bar{Q}^2}{f_2} - \frac{1}{\beta} \sum_{\mathbf{k}} \ln\left(1 + e^{\beta(\epsilon_{\mathbf{k}}(\bar{Q}) - \mu)}\right). \quad (\text{A.27})$$

We denote  $G_{\mathbf{k}} = \frac{1}{\beta} \ln\left(1 + e^{\beta(\epsilon_{\mathbf{k}}(\bar{Q}) - \mu)}\right)$ . For the doped case,  $\epsilon_{\mathbf{k}}(\bar{Q}) = v_F k \sqrt{1 - 2\Delta \cos(2\theta_{\mathbf{k}}) + \Delta^2}$ , where  $\Delta = \frac{2\bar{Q}}{v_F k} = \frac{2\bar{Q}}{\epsilon_{\mathbf{k}}(0)}$ . In the following, whenever we write  $\epsilon_{\mathbf{k}}$  we mean  $\epsilon_{\mathbf{k}}(0)$ ; we also use  $\theta$  for  $\theta_{\mathbf{k}}$ . The first order term in the expansion of  $\sum_{\mathbf{k}} G_{\mathbf{k}}$  is

$$\begin{aligned} \sum_{\mathbf{k}} \frac{\partial G_{\mathbf{k}}(\Delta)}{\partial \Delta} \Big|_{\Delta=0} \Delta &= (1 - n_F(\epsilon_{\mathbf{k}}(\Delta))) \frac{\partial \epsilon_{\mathbf{k}}(\Delta)}{\partial \Delta} \Big|_{\Delta=0} = (1 - n_F(\epsilon_{\mathbf{k}}))(-v_F k \cos 2\theta) \\ &= \sum_{\mathbf{k}} (1 - n_F(\epsilon_{\mathbf{k}}))(-\epsilon_{\mathbf{k}} \cos 2\theta) \Delta = 0, \end{aligned} \quad (\text{A.28})$$

$$\begin{aligned} \frac{1}{2} \sum_{\mathbf{k}} \frac{\partial^2 G_{\mathbf{k}}}{\partial \Delta^2} \Big|_{\Delta=0} \Delta^2 &= \frac{1}{2} \sum_{\mathbf{k}} \left( \frac{\partial^2 \epsilon_{\mathbf{k}}(\Delta)}{\partial \Delta^2} (1 - n_F(\epsilon_{\mathbf{k}}(\Delta))) - \left( \frac{\partial \epsilon_{\mathbf{k}}(\Delta)}{\partial \Delta} \right) \frac{\partial n_F(\epsilon_{\mathbf{k}})}{\partial \epsilon_{\mathbf{k}}} \right) \Delta^2 \\ &= \frac{1}{2} \sum_{\mathbf{k}} \left( \epsilon_{\mathbf{k}} (1 - \cos^2 \theta) (1 - n_F(\epsilon_{\mathbf{k}})) - \cos^2 \theta \frac{\partial n_F}{\partial \epsilon_{\mathbf{k}}} \epsilon_{\mathbf{k}}^2 \right) \Delta^2 \\ &= \frac{Q^2}{2} \sum_{\mathbf{k}} \left( \epsilon_{\mathbf{k}} (1 - \cos^2 \theta) (1 - n_F(\epsilon_{\mathbf{k}})) - \cos^2 \theta \frac{\partial n_F}{\partial \epsilon_{\mathbf{k}}} \epsilon_{\mathbf{k}}^2 \right) \frac{1}{\epsilon_{\mathbf{k}}^2} \\ &= \frac{Q^2}{2} \int_{k_{F-\Lambda}}^{k_{F+\Lambda}} \frac{dk}{2\pi} \left( \epsilon_{\mathbf{k}} (1 - n_F(\epsilon_{\mathbf{k}})) - \frac{\partial n_F}{\partial \epsilon_{\mathbf{k}}} \epsilon_{\mathbf{k}}^2 \right) \frac{1}{\epsilon_{\mathbf{k}}^2} \\ &= \frac{Q^2}{4} \int d\epsilon \mathcal{N}(\epsilon) \left( \epsilon (1 - n_F(\epsilon)) - \frac{\partial n_F}{\partial \epsilon} \epsilon^2 \right) \frac{1}{\epsilon^2} \\ &= \frac{Q^2}{4} \int d\epsilon \mathcal{N}(\epsilon) \delta(\epsilon - \mu) = \frac{\mathcal{N}(\mu)}{4} \bar{Q}^2. \end{aligned} \quad (\text{A.29})$$

Here we introduced the density of states  $\mathcal{N}(\epsilon)$  and neglected the first term in the last expression in the penultimate line as it produces a term linear in  $\Lambda$ , vanishing in the limit  $\Lambda/k_F \ll 1$ .

$$\begin{aligned} \left. \frac{\partial^3 G_{\mathbf{k}}}{\partial \Delta^3} \right|_{\Delta=0} &= \left( \frac{\partial^3 \epsilon_{\mathbf{k}}(\Delta)}{\partial \Delta^3} (1 - n_F(\epsilon_{\mathbf{k}})) - 3 \frac{\partial \epsilon_{\mathbf{k}}(\Delta)}{\partial \Delta} \frac{\partial^2 \epsilon_{\mathbf{k}}(\Delta)}{\partial \Delta^2} \frac{\partial n_F}{\partial \epsilon_{\mathbf{k}}} - \left( \frac{\partial \epsilon_{\mathbf{k}}(\Delta)}{\partial \Delta} \right)^3 \frac{\partial^2 n_F}{\partial \epsilon_{\mathbf{k}}^2} \right) \Big|_{\Delta=0} \\ &= \left( 3(1 - n_F(\epsilon_{\mathbf{k}}))(\cos 2\theta - \cos^3 2\theta)\epsilon_{\mathbf{k}} + 3\epsilon_{\mathbf{k}} \cos 2\theta(1 - \cos^2 2\theta) \frac{\partial n_F}{\partial \epsilon_{\mathbf{k}}} + \epsilon_{\mathbf{k}}^3 \cos^3 2\theta \frac{\partial^2 n_F}{\partial \epsilon_{\mathbf{k}}^2} \right). \end{aligned} \quad (\text{A.30})$$

Therefore, integrating over  $\theta$ , we conclude that  $\frac{1}{3!} \sum_{\mathbf{k}} \frac{\partial^3 G_{\mathbf{k}}}{\partial \Delta^3} \Big|_{\Delta=0} \Delta^3 = 0$ . For the fourth order term we obtain

$$\begin{aligned} \frac{1}{4!} \sum_{\mathbf{k}} \frac{\partial^4 G_{\mathbf{k}}}{\partial \Delta^4} \Big|_{\Delta=0} \Delta^4 &= \frac{1}{4!} \sum_{\mathbf{k}} \left( \frac{\partial^4 \epsilon_{\mathbf{k}}(\Delta)}{\partial \Delta^4} (1 - n_F(\epsilon_{\mathbf{k}})) \right. \\ &\quad \left. - \left( 4 \frac{\partial \epsilon_{\mathbf{k}}(\Delta)}{\partial \Delta} \frac{\partial^3 \epsilon_{\mathbf{k}}(\Delta)}{\partial \Delta^3} + 3 \left( \frac{\partial^2 \epsilon_{\mathbf{k}}(\Delta)}{\partial \Delta^2} \right)^2 \right) \frac{\partial n_F}{\partial \epsilon_{\mathbf{k}}} \right. \\ &\quad \left. - 6 \left( \frac{\partial \epsilon_{\mathbf{k}}(\Delta)}{\partial \Delta} \right)^2 \frac{\partial^2 \epsilon_{\mathbf{k}}(\Delta)}{\partial \Delta^2} \frac{\partial^2 n_F}{\partial \epsilon_{\mathbf{k}}^2} - \left( \frac{\partial \epsilon_{\mathbf{k}}(\Delta)}{\partial \Delta} \right)^4 \frac{\partial^3 n_F}{\partial \epsilon_{\mathbf{k}}^3} \right) \Big|_{\Delta=0} \Delta^4 \\ &= \frac{\bar{Q}^4}{4! \cdot 8} \int d\epsilon \mathcal{N}(\epsilon) \left( 3\epsilon^{-3}(1 - n_F(\epsilon)) + 3\epsilon^{-2} \frac{\partial n_F}{\partial \epsilon} - 6\epsilon^{-1} \frac{\partial^2 n_F}{\partial \epsilon^2} + 3 \frac{\partial^3 n_F}{\partial \epsilon^3} \right) \end{aligned} \quad (\text{A.31})$$

$$\begin{aligned} &\stackrel{\Lambda \rightarrow 0}{=} \frac{\bar{Q}^4}{4! \cdot 8} \left( -3 \frac{\mathcal{N}(\mu)}{\mu^2} + 6 \frac{d}{d\epsilon} \left( \frac{\mathcal{N}(\epsilon)}{\epsilon} \right) \Big|_{\epsilon=\mu} + 3 \frac{d^2}{d\epsilon^2} (\mathcal{N}(\epsilon)) \Big|_{\epsilon=\mu} \right) \\ &= -\frac{\bar{Q}^4}{64} \frac{\mathcal{N}(\mu)}{\mu^2}. \end{aligned} \quad (\text{A.32})$$

Altogether, the free energy at zero temperature is

$$\mathcal{F}(\bar{Q}) - \mathcal{F}(0) = \left( \frac{2}{f_2} - \frac{\mathcal{N}(\mu)}{4} \right) \bar{Q}^2 + \frac{\mathcal{N}(\mu)}{64\mu^2} \bar{Q}^4 + O(\bar{Q}^6). \quad (\text{A.33})$$

This expansion corresponds to a continuous phase transition.

## A.2 Spin susceptibility in the nematic phase

In this section, we derive formulas given in Eq. (2.27) and Eq. (2.41): the in-plane spin susceptibility anisotropy in the nematic phase in the nodal and doped limits. In the presence of an in-plane magnetic field, the mean-field quasiparticle Hamiltonian takes the form

$$H = \sum_{\mathbf{k}} \psi_{\mathbf{k}}^{\dagger} \left( v_F \hat{\mathbf{z}} \cdot (\boldsymbol{\sigma} \times \mathbf{k}) - \mu + 2 \frac{\bar{Q}}{k_A} (\sigma_x k_y + \sigma_y k_x) - \frac{1}{2} g \mu_B \mathbf{B} \cdot \boldsymbol{\sigma} \right) \psi_{\mathbf{k}}. \quad (\text{A.34})$$

For  $\mathbf{B} = B \hat{x}$  and  $\mathbf{B} = B \hat{y}$ , the energy spectrum is given, respectively, by

$$\begin{aligned} E_{x\pm}(\mathbf{k}, \bar{Q}, B) &= \pm E_x = \pm \sqrt{\epsilon_{\mathbf{k}}(\bar{Q})^2 + \frac{g^2 \mu_B B^2}{4} - g \mu_B B \left( 2\bar{Q} \frac{k}{k_A} + v_F k \right) \sin \theta_{\mathbf{k}}}, \\ E_{y\pm}(\mathbf{k}, \bar{Q}, B) &= \pm E_y = \pm \sqrt{\epsilon_{\mathbf{k}}(\bar{Q})^2 + \frac{g^2 \mu_B B^2}{4} - g \mu_B B \left( 2\bar{Q} \frac{k}{k_A} - v_F k \right) \cos \theta_{\mathbf{k}}}, \end{aligned} \quad (\text{A.35})$$

and the corresponding normalized eigenstates are

$$\begin{aligned} |\psi_{x\chi}(\mathbf{k}, \bar{Q}, B)\rangle &= \frac{1}{\sqrt{2}} \begin{pmatrix} \chi \frac{iv_F k e^{-i\theta_{\mathbf{k}}} - i2\bar{Q} \frac{k}{k_A} e^{i\theta_{\mathbf{k}}} - \frac{g\mu_B B}{2}}{E_x(\mathbf{k}, \bar{Q}, B)} \\ 1 \end{pmatrix}, \\ |\psi_{y\chi}(\mathbf{k}, \bar{Q}, B)\rangle &= \frac{1}{\sqrt{2}} \begin{pmatrix} \chi \frac{iv_F k e^{-i\theta_{\mathbf{k}}} - i2\bar{Q} \frac{k}{k_A} e^{i\theta_{\mathbf{k}}} + i\frac{g\mu_B B}{2}}{E_x(\mathbf{k}, \bar{Q}, B)} \\ 1 \end{pmatrix}, \end{aligned} \quad (\text{A.36})$$

where  $\chi = \pm 1$ . Using these eigenstates, we find

$$\begin{aligned} \langle \psi_{x\chi}(\mathbf{k}, \bar{Q}, B) | \sigma_x | \psi_{x\chi}(\mathbf{k}, \bar{Q}, B) \rangle &= \frac{\chi}{E_x(\mathbf{k}, \bar{Q}, B)} \left( -\frac{g\mu_B B}{2} + (v_F k + 2\bar{Q} \frac{k}{k_A}) \sin \theta_{\mathbf{k}} \right), \\ \langle \psi_{y\chi}(\mathbf{k}, \bar{Q}, B) | \sigma_y | \psi_{y\chi}(\mathbf{k}, \bar{Q}, B) \rangle &= \frac{\chi}{E_y(\mathbf{k}, \bar{Q}, B)} \left( -\frac{g\mu_B B}{2} + (-v_F k + 2\bar{Q} \frac{k}{k_A}) \cos \theta_{\mathbf{k}} \right). \end{aligned} \quad (\text{A.37})$$

In the limit  $B \rightarrow 0$ , for  $k = k_F$ , these equations reproduce Eq. (2.38) in the main text. We consider the undoped limit first.

### A.2.1 Undoped Limit

We will consider small  $\bar{Q}$  and  $B$  so that we will be able to expand  $\chi_{xx}$  and  $\chi_{yy}$  in these parameters. In the undoped limit, the nematic transition is a first-order transition at zero temperature and becomes continuous at  $T = T_{\text{TCP}}$ . Thus, we work at finite temperature where  $\bar{Q}$  can be small near the transition. The expectation value of the  $\sigma_x$  operator, proportional to the  $x$ -component of spin, in an in-plane magnetic field parallel to the  $x$ -axis is

$$\langle \sigma_x(B, \bar{Q}) \rangle = \sum_{\chi} \int \frac{d^2k}{(2\pi)^2} \langle \psi_{x\chi}(\mathbf{k}, \bar{Q}, B) | \sigma_x | \psi_{x\chi}(\mathbf{k}, \bar{Q}, B) \rangle n_F(E_{x\chi}(\mathbf{k}, \bar{Q}, B)), \quad (\text{A.38})$$

where the sum is over both helicity branches. The expression for  $\langle \sigma_y \rangle$  in an in-plane magnetic field parallel to the  $y$ -axis is analogical:

$$\langle \sigma_y(B, \bar{Q}) \rangle = \sum_{\chi} \int \frac{d^2k}{(2\pi)^2} \langle \psi_{y\chi}(\mathbf{k}, \bar{Q}, B) | \sigma_y | \psi_{y\chi}(\mathbf{k}, \bar{Q}, B) \rangle n_F(E_{y\chi}(\mathbf{k}, \bar{Q}, B)); \quad (\text{A.39})$$

and the anisotropy in the in-plane spin susceptibility is given by

$$\chi_{xx}(\bar{Q}) - \chi_{yy}(\bar{Q}) = \frac{g\mu_B}{2} \frac{\partial}{\partial B} \left( \langle \sigma_x(B, \bar{Q}) \rangle - \langle \sigma_y(B, \bar{Q}) \rangle \right). \quad (\text{A.40})$$

Using that  $n_F(-x) = 1 - n_F(x)$  and  $\langle \psi_{\alpha-} | \sigma_{\alpha} | \psi_{\alpha-} \rangle = -\langle \psi_{\alpha+} | \sigma_{\alpha} | \psi_{\alpha+} \rangle$ , where  $\alpha = x, y$ , we may write

$$\langle \sigma_x \rangle - \langle \sigma_y \rangle = - \int_0^{2\pi} \frac{d\theta_{\mathbf{k}}}{2\pi} \int_0^{\Lambda} \frac{dk k}{2\pi} \left( \langle \psi_{x+} | \sigma_x | \psi_{x+} \rangle \tanh\left(\frac{E_{x+}}{2T}\right) - \langle \psi_{y+} | \sigma_y | \psi_{y+} \rangle \tanh\left(\frac{E_{y+}}{2T}\right) \right). \quad (\text{A.41})$$

Substituting Eq. (A.37) into the last equation, expanding to second order in  $\bar{Q}$  and  $B$ , and

integrating over the angle  $\theta_{\mathbf{k}}$ , we find

$$\langle \sigma_x \rangle - \langle \sigma_y \rangle = -\frac{g\mu_B B \bar{Q}}{8\pi\Lambda T^2 v_F^2} \int_0^\Lambda dk \operatorname{sech}^2\left(\frac{kv_F}{2T}\right) \left( T^2 \sinh\left(\frac{kv_F}{T}\right) + k^2 v_F^2 \tanh\left(\frac{kv_F}{2T}\right) - kv_F T \right). \quad (\text{A.42})$$

Introducing a dimensionless variable  $y = \frac{kv_F}{T}$  and switching to  $\Delta = \frac{2\bar{Q}}{v_F\Lambda}$ , we obtain

$$\chi_{xx}(\bar{Q}) - \chi_{yy}(\bar{Q}) = -\frac{g^2 \mu_B^2 \Lambda \Delta}{32\pi v_F^2} F(x), \quad (\text{A.43})$$

which is Eq. (2.27) in the main text, where

$$F(x) = x \int_0^{\frac{1}{x}} dy \operatorname{sech}^2\left(\frac{y}{2}\right) \left( \sinh y + y \left( y \tanh\left(\frac{y}{2}\right) - 1 \right) \right). \quad (\text{A.44})$$

## A.2.2 Doped Limit

In the doped limit, the transition is continuous already at  $T = 0$ . Assuming  $\mu > 0$ , it is sufficient to retain only the positive helicity branch in calculations. Thus, at zero temperature,

$$\begin{aligned} \langle \sigma_x(B, \bar{Q}) \rangle &= \int \frac{d^2k}{(2\pi)^2} \langle \psi_{x+}(\mathbf{k}, \bar{Q}, B) | \sigma_x | \psi_{x+}(\mathbf{k}, \bar{Q}, B) \rangle, \\ \langle \sigma_y(B, \bar{Q}) \rangle &= \int \frac{d^2k}{(2\pi)^2} \langle \psi_{y+}(\mathbf{k}, \bar{Q}, B) | \sigma_y | \psi_{y+}(\mathbf{k}, \bar{Q}, B) \rangle. \end{aligned} \quad (\text{A.45})$$

The theory we work with assumes interaction within a small shell of thickness  $\Lambda$  around the FS. Thus we approximate  $\int \frac{d^2k}{(2\pi)^2} f(k, \theta_{\mathbf{k}}) \approx \frac{k_F \Lambda}{\pi} \int_0^{2\pi} \frac{d\theta_{\mathbf{k}}}{2\pi} f(k_F, \theta_{\mathbf{k}})$ . Then, expanding integrands to second order in  $B$  and  $\Delta_F = \frac{2Q}{v_F k_F}$ , and integrating over  $\theta_{\mathbf{k}}$ , we find

$$\begin{aligned} \langle \sigma_x(B, \bar{Q}) \rangle &\approx \frac{k_F \Lambda}{2\pi} \frac{g\mu_B B}{2v_F k_F} \left( -1 + \frac{1}{2} \Delta_F \right), \\ \langle \sigma_y(B, \bar{Q}) \rangle &\approx \frac{k_F \Lambda}{2\pi} \frac{g\mu_B B}{2v_F k_F} \left( -1 - \frac{1}{2} \Delta_F \right). \end{aligned} \quad (\text{A.46})$$

And thus

$$\chi_{xx}(\bar{Q}) - \chi_{yy}(\bar{Q}) = \frac{k_F \Lambda g^2 \mu_B^2 B}{8\pi v_F k_F} \Delta_F = \frac{\Lambda \mathcal{N}(\mu) g^2 \mu_B^2 B}{4 k_F} \Delta_F, \quad (\text{A.47})$$

reproducing Eq. (2.41) in the main text.

### A.3 Inverse propagator for the nematic field

In this section, we calculate the effects of fluctuations about mean field theory. For convenience, we reproduce here the Hamiltonian

$$\hat{H} = \int \frac{d^2k}{(2\pi)^2} \psi_{\mathbf{k}}^\dagger (v_F \hat{\mathbf{z}} \cdot (\boldsymbol{\sigma} \times \mathbf{k}) - \mu) \psi_{\mathbf{k}} - \frac{f_2}{4} \int d^2r \text{tr} \left( \hat{Q}(\mathbf{r})^2 \right), \quad (\text{A.48})$$

where

$$\hat{Q}_{ab}(\mathbf{r}) = -\frac{i}{k_A} \psi^\dagger(\mathbf{r}) (\sigma_a \overleftrightarrow{\partial}_b + \sigma_b \overleftrightarrow{\partial}_a - \delta_{ab} \boldsymbol{\sigma} \cdot \overleftrightarrow{\boldsymbol{\partial}}) \psi(\mathbf{r}), \quad (\text{A.49})$$

and

$$\psi^\dagger(\mathbf{r}) \overleftrightarrow{\partial}_b \psi(\mathbf{r}) = \frac{1}{2} \left( \psi^\dagger(\mathbf{r}) \partial_b \psi(\mathbf{r}) + \partial_b \psi^\dagger(\mathbf{r}) \psi(\mathbf{r}) \right). \quad (\text{A.50})$$

The order parameter may be rewritten in the form

$$\hat{Q} = \psi^\dagger \Delta_1 \psi \tau_z + \psi^\dagger \Delta_2 \psi \tau_x, \quad (\text{A.51})$$

where for the doped limit

$$\Delta_1 = -i(\sigma_x \overleftrightarrow{\hat{\partial}}_x - \sigma_y \overleftrightarrow{\hat{\partial}}_y), \quad \Delta_2 = -i(\sigma_x \overleftrightarrow{\hat{\partial}}_y + \sigma_y \overleftrightarrow{\hat{\partial}}_x), \quad (\text{A.52})$$

with  $\hat{\partial}_\alpha = \frac{\partial}{|\boldsymbol{\partial}|}$ ,  $\alpha = x, y$ .

Introducing an auxiliary field  $\mathbf{n}$  via the Hubbard-Stratonovich transformation, the

action takes the form

$$S[\psi^\dagger, \psi, \mathbf{n}] = \int_0^{1/T} d\tau \int d^2r \left[ \psi^\dagger (\hat{\mathcal{G}}_0^{-1} - \mathbf{n} \cdot \boldsymbol{\Delta}) \psi + \frac{1}{2f_2} \mathbf{n}^2 \right]. \quad (\text{A.53})$$

Passing to the momentum-frequency domain for the fermionic terms, we may write it as

$$\begin{aligned} S[\psi^\dagger, \psi, \mathbf{n}] &= \int_0^\beta d\tau \int d^2r \frac{\mathbf{n}^2}{2f_2} + \frac{1}{\beta V} \sum_{\vec{k}_1} \psi_{\vec{k}_1}^\dagger (-i\omega_{1n} + v_F \hat{z} \cdot (\boldsymbol{\sigma} \times \mathbf{k}_1) - \mu) \psi_{\vec{k}_1} \\ &\quad - \frac{1}{\beta^2 V^2} \sum_{\vec{k}_1, \vec{k}_2} \psi_{\vec{k}_1}^\dagger \left\{ n_1 (\vec{k}_1 - \vec{k}_2) \left( \sigma_x \frac{\hat{k}_{1x} + \hat{k}_{2x}}{2} - \sigma_y \frac{\hat{k}_{1y} + \hat{k}_{2y}}{2} \right) \right. \\ &\quad \left. + n_2 (\vec{k}_1 - \vec{k}_2) \left( \sigma_x \frac{\hat{k}_{1y} + \hat{k}_{2y}}{2} + \sigma_y \frac{\hat{k}_{1x} + \hat{k}_{2x}}{2} \right) \right\} \psi_{\vec{k}_2}, \end{aligned} \quad (\text{A.54})$$

where  $\vec{k}_i = (i\omega_{in}, \mathbf{k}_i)$ ,  $i = 1, 2$ , is a 3-vector with Matsubara frequency and momentum components, and  $\hat{\mathbf{k}}_i$  is a unit vector in the direction of  $\mathbf{k}_i$ . Integrating out the fermionic fields, we obtain

$$S_{\text{eff}}[\mathbf{n}] = \int_0^\beta d\tau \int d^2r \left[ \frac{\mathbf{n}^2}{2f_2} - \text{Tr} \ln \left( \mathcal{G}_0^{-1} - \mathbf{n} \cdot \boldsymbol{\Delta} \right) \right]. \quad (\text{A.55})$$

In the isotropic phase close to the QCP (so that  $\mathbf{n}$  is small), expanding the trace to second order in  $\mathbf{n}$ , we obtain

$$S_{\text{eff}}[\mathbf{n}] = \int_0^\beta d\tau \int d^2r \frac{\mathbf{n}^2}{2f_2} + \frac{1}{2} \text{Tr} \left( \mathcal{G}_0 \mathbf{n} \cdot \boldsymbol{\Delta} \mathcal{G}_0 \mathbf{n} \cdot \boldsymbol{\Delta} \right) + O((\mathbf{n}^2)^2). \quad (\text{A.56})$$

Denoting  $\Delta_{\mathbf{k}_1, \mathbf{k}_2}^1 = \sigma_x \frac{\hat{k}_{1x} + \hat{k}_{2x}}{2} - \sigma_y \frac{\hat{k}_{1y} + \hat{k}_{2y}}{2}$  and  $\Delta_{\mathbf{k}_1, \mathbf{k}_2}^2 = \sigma_x \frac{\hat{k}_{1y} + \hat{k}_{2y}}{2} + \sigma_y \frac{\hat{k}_{1x} + \hat{k}_{2x}}{2}$ , we may write

$$\begin{aligned} \frac{1}{2} \text{Tr} \left( \mathcal{G}_0 \mathbf{n} \cdot \boldsymbol{\Delta} \mathcal{G}_0 \mathbf{n} \cdot \boldsymbol{\Delta} \right) &= \frac{1}{\beta^2 V^2} \sum_{ij} \sum_{\vec{q}} n_{i, \vec{q}} \left( \frac{1}{2} \text{tr} \sum_{\vec{k}} G_{\vec{k}+\vec{q}} \Delta_{\mathbf{k}, \mathbf{k}+\vec{q}}^i G_{\vec{k}} \Delta_{\mathbf{k}+\vec{q}, \mathbf{k}}^j \right) n_{j, -\vec{q}} \\ &= \frac{1}{\beta^2 V^2} \sum_{ij} \sum_{\vec{q}} n_{i, \vec{q}} \chi_{ij}^{-1}(\mathbf{q}, i\Omega_m) n_{j, -\vec{q}}, \end{aligned} \quad (\text{A.57})$$

where  $\vec{q} = (i\Omega_m, \mathbf{q})$  and

$$\chi_{ij}^{-1}(\mathbf{q}, i\Omega_m) = \frac{1}{2} \frac{1}{\beta V} \text{tr} \sum_{\vec{k}} G_{\vec{k}+\vec{q}}^{-} \Delta_{\mathbf{k}, \mathbf{k}+\mathbf{q}}^i G_{\vec{k}}^{-} \Delta_{\mathbf{k}+\mathbf{q}, \mathbf{k}}^j. \quad (\text{A.58})$$

It is convenient to introduce

$$\beta_1 = \hat{k}_x + \widehat{(\mathbf{k} + \mathbf{q})}_x; \quad \beta_2 = \hat{k}_y + \widehat{(\mathbf{k} + \mathbf{q})}_y, \quad (\text{A.59})$$

which appear in the nematic form factors  $\Delta_{\mathbf{k}, \mathbf{k}+\mathbf{q}}^1$  and  $\Delta_{\mathbf{k}, \mathbf{k}+\mathbf{q}}^2$ . After some algebra we find

$$\chi_{ij}^{-1}(\mathbf{q}, i\Omega_m) = \frac{1}{4} \frac{1}{\beta V} \sum_{\mathbf{k}, i\omega_n} \frac{(i\omega_n + i\Omega_m + \mu)(i\omega_n + \mu) \alpha_{\mathbf{k}, \mathbf{q}}^{ij} + \gamma_{\mathbf{k}, \mathbf{q}}^{ij}}{\left( (i\omega_n + i\Omega_m + \mu)^2 - v_F^2 |\mathbf{k} + \mathbf{q}|^2 \right) \left( (i\omega_n + \mu)^2 - v_F^2 |\mathbf{k}|^2 \right)}, \quad (\text{A.60})$$

where

$$\begin{aligned} \alpha_{\mathbf{k}, \mathbf{q}}^{ij} &= (\beta_1^2 + \beta_2^2) \delta_{ij} = \left( 2 + 2 \cos(\theta_{\mathbf{k}} - \theta_{\mathbf{k}-\mathbf{q}}) \right) \delta_{ij}, \\ \gamma_{\mathbf{k}, \mathbf{q}}^{11} &= -\gamma_{\mathbf{k}, \mathbf{q}}^{22} = v_F^2 k |\mathbf{k} + \mathbf{q}| \left( -\cos(\theta_{\mathbf{k}} + \theta_{\mathbf{k}+\mathbf{q}}) (\beta_1^2 - \beta_2^2) + 2 \sin(\theta_{\mathbf{k}} + \theta_{\mathbf{k}+\mathbf{q}}) \beta_1 \beta_2 \right) \\ &= -v_F^2 k |\mathbf{k} + \mathbf{q}| \left( \cos(3\theta_{\mathbf{k}} + \theta_{\mathbf{k}+\mathbf{q}}) + \cos(3\theta_{\mathbf{k}+\mathbf{q}} + \theta_{\mathbf{k}}) + 2 \cos(2\theta_{\mathbf{k}+\mathbf{q}} + 2\theta_{\mathbf{k}}) \right), \\ \gamma_{\mathbf{k}, \mathbf{q}}^{12} &= \gamma_{\mathbf{k}, \mathbf{q}}^{21} = v_F^2 k |\mathbf{k} + \mathbf{q}| \left( -\sin(\theta_{\mathbf{k}} + \theta_{\mathbf{k}+\mathbf{q}}) (\beta_1^2 - \beta_2^2) - 2 \cos(\theta_{\mathbf{k}} + \theta_{\mathbf{k}+\mathbf{q}}) \beta_1 \beta_2 \right) \\ &= -v_F^2 k |\mathbf{k} + \mathbf{q}| \left( \sin(3\theta_{\mathbf{k}} + \theta_{\mathbf{k}+\mathbf{q}}) + \sin(3\theta_{\mathbf{k}+\mathbf{q}} + \theta_{\mathbf{k}}) + 2 \sin(2\theta_{\mathbf{k}+\mathbf{q}} + 2\theta_{\mathbf{k}}) \right). \end{aligned} \quad (\text{A.61})$$

Using partial fractions, we may represent the expression above as a sum over intra-band ( $\chi = \chi'$ ) and interband ( $\chi \neq \chi'$ ) contributions to the pair bubble:

$$\chi_{ij}^{-1}(\mathbf{q}, i\Omega_m) = \frac{1}{16} \frac{1}{\beta V} \sum_{\mathbf{k}, i\omega_n} \sum_{\chi, \chi' = \pm 1} \frac{\alpha_{\mathbf{k}, \mathbf{q}}^{ij} + \chi \chi' \frac{\gamma_{\mathbf{k}, \mathbf{q}}^{ij}}{v_F^2 k |\mathbf{k} + \mathbf{q}|}}{(i\omega_n + i\Omega_m + \mu - \chi v_F |\mathbf{k} + \mathbf{q}|)(i\omega_n + \mu - \chi' v_F k)}, \quad (\text{A.62})$$

where we may keep only the term with  $\chi = \chi' = 1$  (positive helicity branch) as all other terms are negligible in the low-frequency, long-wavelength limit. Thus

$$\chi_{ij}^{-1}(\mathbf{q}, i\Omega_m) \approx \frac{1}{16} \frac{1}{\beta V} \sum_{\mathbf{k}, i\omega_n} \frac{\alpha_{\mathbf{k}, \mathbf{q}}^{ij} + \frac{\gamma_{\mathbf{k}, \mathbf{q}}^{ij}}{v_F^2 k |\mathbf{k} + \mathbf{q}|}}{(i\omega_n + i\Omega_m + \mu - v_F |\mathbf{k} + \mathbf{q}|)(i\omega_n + \mu - v_F k)}. \quad (\text{A.63})$$

After carrying out a standard Matsubara frequency summation (see, e.g., Ref. [240]), we obtain

$$\chi_{ij}^{-1}(\mathbf{q}, i\Omega_m) \approx \frac{1}{16} \frac{1}{V} \sum_{\mathbf{k}} \frac{n_F(v_F k) - n_F(v_F |\mathbf{k} + \mathbf{q}|)}{i\Omega_m + v_F k - v_F |\mathbf{k} + \mathbf{q}|} \left( \alpha_{\mathbf{k}, \mathbf{q}}^{ij} + \frac{\gamma_{\mathbf{k}, \mathbf{q}}^{ij}}{v_F^2 k |\mathbf{k} + \mathbf{q}|} \right). \quad (\text{A.64})$$

To proceed further, we use another approximation, representing the inverse propagator as a sum of static and dynamical parts:

$$\chi_{ij}^{-1}(\mathbf{q}, i\Omega_m) \approx \chi_{ij}^{-1}(0, i\Omega_m) + \chi_{ij}^{-1}(\mathbf{q}, 0). \quad (\text{A.65})$$

Let us first consider the static limit.

### A.3.1 Static limit

In the static limit,  $i\Omega_m \rightarrow 0$ ; and at  $T \rightarrow 0$ , we have

$$n_F(v_F k) = \frac{1}{e^{\beta(v_F k - \mu)} + 1} \rightarrow \theta(-(v_F k - \mu)). \quad (\text{A.66})$$

Let us denote  $\xi_{\mathbf{k}} = v_F k$ . Taylor expanding around  $\xi_{\mathbf{k}}$ , for the first factor in the summand of Eq. (A.64) we obtain

$$\begin{aligned} \frac{n_F(\xi_{\mathbf{k}}) - n_F(\xi_{\mathbf{k} + \mathbf{q}})}{\xi_{\mathbf{k}} - \xi_{\mathbf{k} + \mathbf{q}}} &= \frac{\frac{\partial n_F}{\partial \xi_{\mathbf{k}}} \Big|_{\xi_{\mathbf{k}}} (\xi_{\mathbf{k}} - \xi_{\mathbf{k} + \mathbf{q}}) + \frac{1}{2} \frac{\partial^2 n_F}{\partial \xi_{\mathbf{k}}^2} \Big|_{\xi_{\mathbf{k}}} (\xi_{\mathbf{k}} - \xi_{\mathbf{k} + \mathbf{q}})^2 + \frac{1}{6} \frac{\partial^3 n_F}{\partial \xi_{\mathbf{k}}^3} \Big|_{\xi_{\mathbf{k}}} (\xi_{\mathbf{k}} - \xi_{\mathbf{k} + \mathbf{q}})^3 + \dots}{\xi_{\mathbf{k}} - \xi_{\mathbf{k} + \mathbf{q}}} \\ &= \frac{\partial n_F(\xi_{\mathbf{k}})}{\partial \xi_{\mathbf{k}}} + \frac{1}{2} \cos(\theta_{\mathbf{k}} - \theta_{\mathbf{q}}) v_F q \frac{\partial^2 n_F(\xi_{\mathbf{k}})}{\partial \xi_{\mathbf{k}}^2} + \left( \frac{\sin^2(\theta_{\mathbf{k}} - \theta_{\mathbf{q}})}{4 \xi_{\mathbf{k}}} \frac{\partial^2 n_F(\xi_{\mathbf{k}})}{\partial \xi_{\mathbf{k}}^2} \right. \\ &\quad \left. + \frac{\cos^2(\theta_{\mathbf{k}} - \theta_{\mathbf{q}})}{6} \frac{\partial^3 n_F(\xi_{\mathbf{k}})}{\partial \xi_{\mathbf{k}}^3} \right) (v_F q)^2 + O(q^3). \end{aligned} \quad (\text{A.67})$$

Then

$$\begin{aligned}
\chi_{ij}^{-1}(\mathbf{q}, 0) = & \frac{1}{16} \int_{k_F-\Lambda}^{k_F+\Lambda} \frac{kdk}{(2\pi)^2} \int_0^{2\pi} d\theta_{\mathbf{k}} \left( -\delta(\xi_{\mathbf{k}}) - \frac{1}{2} \cos(\theta_{\mathbf{k}} - \theta_{\mathbf{q}}) v_F q \delta(\xi_{\mathbf{k}}) \frac{d}{d\xi_{\mathbf{k}}} - \right. \\
& \left. \left( \frac{\sin^2(\theta_{\mathbf{k}} - \theta_{\mathbf{q}})}{4\xi_{\mathbf{k}}} \delta(\xi_{\mathbf{k}}) \frac{d}{d\xi_{\mathbf{k}}} + \frac{\cos^2(\theta_{\mathbf{k}} - \theta_{\mathbf{q}})}{6} \delta(\xi_{\mathbf{k}}) \frac{d^2}{d\xi_{\mathbf{k}}^2} \right) (v_F q)^2 \right) \left( \left( 2 + 2 \cos(\theta_{\mathbf{k}} - \theta_{\mathbf{k}-\mathbf{q}}) \right) \delta_{ij} - \right. \\
& \left. \left( \sin\left(3\theta_{\mathbf{k}} + \theta_{\mathbf{k}+\mathbf{q}} + \left[\frac{\pi}{2} + \pi\delta_{i,2}\right]\delta_{i,j}\right) + \sin\left(3\theta_{\mathbf{k}+\mathbf{q}} + \theta_{\mathbf{k}} + \left[\frac{\pi}{2} + \pi\delta_{i,2}\right]\delta_{i,j}\right) + \right. \right. \\
& \left. \left. 2 \sin\left(2\theta_{\mathbf{k}+\mathbf{q}} + 2\theta_{\mathbf{k}} + \left[\frac{\pi}{2} + \pi\delta_{i,2}\right]\delta_{i,j}\right) \right) \right). \tag{A.68}
\end{aligned}$$

The  $\gamma_{\mathbf{k},\mathbf{q}}^{ij}$  terms in Eq. (A.64), i.e., the last two lines of Eq. (A.68), contribute only at  $q^4$  and higher orders. To first order in  $q$ ,  $\theta_{\mathbf{k}-\mathbf{q}} \approx \theta_{\mathbf{k}} - \frac{q}{k_F} \sin(\theta_{\mathbf{q}} - \theta_{\mathbf{k}})$ . Thus,  $\alpha_{\mathbf{k},\mathbf{q}}^{ij}$  is approximately

$$\left( 2 + 2 \cos(\theta_{\mathbf{k}} - \theta_{\mathbf{k}-\mathbf{q}}) \right) \delta_{ij} \approx \left( 4 - \left( \frac{q}{k} \right)^2 \right) \delta_{ij}. \tag{A.69}$$

Thus, to second order in  $q$ , the static part of the inverse propagator equals

$$\begin{aligned}
\chi_{ij}^{-1}(\mathbf{q}, 0) = & \frac{1}{16} \int_{k_F-\Lambda}^{k_F+\Lambda} \frac{kdk}{2\pi} \int_0^{2\pi} d\theta_{\mathbf{k}} \left( -\delta(\xi_{\mathbf{k}}) - \frac{1}{2} \cos(\theta_{\mathbf{k}} - \theta_{\mathbf{q}}) v_F q \delta(\xi_{\mathbf{k}}) \frac{d}{d\xi_{\mathbf{k}}} \right) \left( 4 - \left( \frac{q}{k} \right)^2 \right) \delta_{ij} \\
= & -\frac{1}{4} \mathcal{N}(\mu) \left( 1 - \frac{1}{8} \left( \frac{q}{k_F} \right)^2 \right) \delta_{ij}, \tag{A.70}
\end{aligned}$$

where  $\mathcal{N}(\mu) = \frac{\mu}{2\pi v_F^2} = \frac{k_F}{2\pi v_F}$  is the density of states at the Fermi energy.

### A.3.2 Dynamical Limit

In the dynamical limit, we evaluate Eq. (A.64) in the limit  $q \rightarrow 0$ . We rewrite

$$\frac{n_F(\xi_{\mathbf{k}}) - n_F(\xi_{\mathbf{k}+\mathbf{q}})}{i\Omega_m + \xi_{\mathbf{k}} - \xi_{\mathbf{k}+\mathbf{q}}} \xrightarrow{q \rightarrow 0} \frac{dn_F}{d\xi_{\mathbf{k}}} \frac{1}{1 - i \frac{\Omega_m}{\xi_{\mathbf{k}} - \xi_{\mathbf{k}+\mathbf{q}}}} \approx \delta(\xi_{\mathbf{k}} - \mu) \frac{\cos(\theta_{\mathbf{k}} - \theta_{\mathbf{q}})}{is - \cos(\theta_{\mathbf{k}} - \theta_{\mathbf{q}})}, \tag{A.71}$$

where  $s = \frac{\Omega_m}{v_F q}$ .

Then, using  $\frac{1}{V} \sum_{\mathbf{k}} = \int \frac{kd\mathbf{k}}{(2\pi)^2} \int d\theta_{\mathbf{k}} = \frac{1}{2\pi} \int \mathcal{N}(\xi) d\xi \int d\theta_{\mathbf{k}}$ , we find

$$\chi_{ij,dyn}^{-1} = \frac{1}{16} \int d\xi \mathcal{N}(\xi) \int_0^{2\pi} \frac{d\theta_{\mathbf{k}}}{2\pi} \delta(\xi - \mu) \frac{\cos(\theta_{\mathbf{k}} - \theta_{\mathbf{q}})}{is - \cos(\theta_{\mathbf{k}} - \theta_{\mathbf{q}})} \left( \alpha_{\mathbf{k},\mathbf{q}=0}^{ij} + \frac{\gamma_{\mathbf{k},\mathbf{q}=0}^{ij}}{v_F^2 k^2} \right). \quad (\text{A.72})$$

Using  $\frac{\cos(\theta_{\mathbf{k}} - \theta_{\mathbf{q}})}{is - \cos(\theta_{\mathbf{k}} - \theta_{\mathbf{q}})} = \frac{is}{is - \cos(\theta_{\mathbf{k}} - \theta_{\mathbf{q}})} - 1$ , we rewrite the previous expression in the matrix form as follows

$$\begin{aligned} \chi_{dyn}^{-1} &= \frac{\mathcal{N}(\mu)}{4} \int_0^{2\pi} \frac{d\theta_{\mathbf{k}}}{2\pi} \frac{is}{is - \cos(\theta_{\mathbf{k}} - \theta_{\mathbf{q}})} \begin{pmatrix} 1 - \cos(4\theta_{\mathbf{k}}) & -\sin 4\theta_{\mathbf{k}} \\ -\sin 4\theta_{\mathbf{k}} & 1 + \cos 4\theta_{\mathbf{k}} \end{pmatrix} \\ &= \frac{\mathcal{N}(\mu)}{4} \int_0^{2\pi} \frac{d\theta_{\mathbf{k}}}{2\pi} \begin{pmatrix} 1 - \cos(4\theta_{\mathbf{k}}) & -\sin 4\theta_{\mathbf{k}} \\ -\sin 4\theta_{\mathbf{k}} & 1 + \cos 4\theta_{\mathbf{k}} \end{pmatrix}. \end{aligned} \quad (\text{A.73})$$

The last term is just  $-\delta_{ij} \frac{\mathcal{N}(\mu)}{4}$ .

The angular integrals in Eq. (A.73) may be evaluated using the residue theorem. We will also encounter a similar integral in the expression for the fermion self-energy; thus, we devote some space to the derivation of these integrals. First of all, we notice

$$\begin{aligned} \int_0^{2\pi} \frac{d\theta}{2\pi} \frac{is}{is - \cos(\theta_{\mathbf{k}} - \theta_{\mathbf{q}})} &= \int_0^{2\pi} \frac{d\theta}{2\pi} \frac{is}{is - \cos(\theta_{\mathbf{k}})}, \\ is \int_0^{2\pi} \frac{d\theta_{\mathbf{k}}}{2\pi} \frac{\cos(4\theta_{\mathbf{k}})}{is - \cos(\theta_{\mathbf{k}} - \theta_{\mathbf{q}})} &= is \int_{\theta_{\mathbf{q}}}^{2\pi + \theta_{\mathbf{q}}} \frac{d\theta_{\mathbf{k}}}{2\pi} \frac{(\cos(4\theta_{\mathbf{k}}) \cos(4\theta_{\mathbf{q}}) - \sin(4\theta_{\mathbf{k}}) \sin(4\theta_{\mathbf{q}}))}{is - \cos \theta_{\mathbf{k}}} \\ &= is \int_0^{2\pi} \frac{d\theta_{\mathbf{k}}}{2\pi} \frac{\cos(4\theta_{\mathbf{k}}) \cos(4\theta_{\mathbf{q}})}{is - \cos \theta_{\mathbf{k}}} = is \cos(4\theta_{\mathbf{q}}) \int_0^{2\pi} \frac{d\theta_{\mathbf{k}}}{2\pi} \frac{2 \cos^2(2\theta_{\mathbf{k}}) - 1}{is - \cos \theta_{\mathbf{k}}}, \\ is \int_0^{2\pi} \frac{d\theta_{\mathbf{k}}}{2\pi} \frac{\sin(4\theta_{\mathbf{k}})}{is - \cos(\theta_{\mathbf{k}} - \theta_{\mathbf{q}})} &= is \int_0^{2\pi} \frac{d\theta_{\mathbf{k}}}{2\pi} \frac{\cos(4\theta_{\mathbf{k}}) \sin(4\theta_{\mathbf{q}})}{is - \cos \theta_{\mathbf{k}}}. \end{aligned} \quad (\text{A.74})$$

We start with the integral  $I_1 = \int_0^{2\pi} \frac{d\theta}{2\pi} \frac{\cos^2(2\theta)}{is + \cos \theta}$ . Introducing a new variable  $z = e^{i\theta}$ , we convert the integral over  $\theta$  into a contour integral over the unit circle:

$$I_1 = \int_0^{2\pi} \frac{d\theta}{2\pi} \frac{\cos^2(2\theta)}{is + \cos \theta} = \oint \frac{dz}{iz} \frac{z^8 + 2z^4 + 1}{4z^4(is + \frac{z+z^{-1}}{2})} = \int \frac{dz}{2i} \frac{z^8 + 2z^4 + 1}{z^4(z^2 + 2is z + 1)} \quad (\text{A.75})$$

The poles of the integrand are at  $z_0 = 0$  (4-fold) and  $z_{1,2} = -is \pm \sqrt{(is)^2 - 1}$ .

Because  $z_1 z_2 = 1$ , only one of these poles is inside the unit circle.

The corresponding residues are:

$$\text{Res}(f(z), z_0) = \frac{1}{3!} \frac{1}{2i} \lim_{z \rightarrow z_0} \frac{d^3}{(dz)^3} \left( \frac{z^8 + 2z^4 + 1}{z^2 + 2isz + 1} \right) = -2s(-1 + 2(is)^2), \quad (\text{A.76})$$

$$\text{Res}(f(z), z_1) = \frac{1}{2i} \frac{z_1^8 + 2z_1^4 + 1}{z_1^4(z_1 - z_2)} = \frac{1}{2i} \frac{(z_1^2 + z_2^2)^2}{(z_1 - z_2)} = -i \frac{(2(is)^2 - 1)^2}{\sqrt{(is)^2 - 1}}, \quad (\text{A.77})$$

$$\text{Res}(f(z), z_2) = -\text{Res}(f(z), z_1). \quad (\text{A.78})$$

When  $s > 0$ ,  $z_1$  lies inside the unit circle, whereas for  $s < 0$ ,  $z_2$  is inside. Combining everything together, we find

$$I_1 = \int_0^{2\pi} \frac{d\theta}{2\pi} \frac{\cos^2(2\theta)}{is + \cos\theta} = 2\pi \left( -is(2(is)^2 - 1) + \frac{(2(is)^2 - 1)^2}{\sqrt{(is)^2 - 1}} \text{sgn}(s) \right) \quad (\text{A.79})$$

Analogously, we obtain

$$I_2 = \int_0^{2\pi} \frac{d\theta}{2\pi} \frac{1}{is + \cos\theta} = \frac{\text{sgn}(s)}{\sqrt{(is)^2 - 1}}. \quad (\text{A.80})$$

After a simple change of variables to reduce the integrals of Eq. (A.74) to  $I_1$  or  $I_2$ , we finally obtain:

$$\begin{aligned} \int_0^{2\pi} \frac{d\theta}{2\pi} \frac{is}{is - \cos(\theta_{\mathbf{k}} - \theta_{\mathbf{q}})} &= \frac{|s|}{\sqrt{1 + s^2}} \approx |s|, \\ is \int_0^{2\pi} \frac{d\theta_{\mathbf{k}}}{2\pi} \frac{\cos(4\theta_{\mathbf{k}})}{is - \cos(\theta_{\mathbf{k}} - \theta_{\mathbf{q}})} &= \left( \frac{-4s^2 \sqrt{1 + s^2} (1 + 2s^2) + (1 + 8(s^2 + s^4)) |s|}{\sqrt{1 + s^2}} \right) \cos(4\theta_{\mathbf{q}}) \\ &\approx \cos(4\theta_{\mathbf{q}}) (|s| - 4s^2), \\ is \int_0^{2\pi} \frac{d\theta_{\mathbf{k}}}{2\pi} \frac{\sin(4\theta_{\mathbf{k}})}{is - \cos(\theta_{\mathbf{k}} - \theta_{\mathbf{q}})} &= \left( \frac{-4s^2 \sqrt{1 + s^2} (1 + 2s^2) + (1 + 8(s^2 + s^4)) |s|}{\sqrt{1 + s^2}} \right) \sin(4\theta_{\mathbf{q}}) \\ &\approx \sin(4\theta_{\mathbf{q}}) (|s| - 4s^2), \end{aligned} \quad (\text{A.81})$$

where the approximation is done for small  $s^2$ . Then, to lowest order in  $s$ , the dynamical

---

<sup>2</sup>Note that since  $z > 1$ , the approximation  $s \ll 1$  remains consistent even in the small- $q$  limit.

part of the inverse propagator is:

$$\chi_{dyn}^{-1} = -\delta_{ij} \frac{\mathcal{N}(\mu)}{4} + \frac{g(\mu)}{4} \begin{pmatrix} |s| - \cos(4\theta_{\mathbf{q}})(|s| - 4s^2) & -\sin(4\theta_{\mathbf{q}})(|s| - 4s^2) \\ -\sin(4\theta_{\mathbf{q}})(|s| - 4s^2) & |s| + \cos(4\theta_{\mathbf{q}})(|s| - 4s^2) \end{pmatrix}. \quad (\text{A.82})$$

### A.3.3 Inverse propagator in the nematic phase

In the nematic phase,  $\mathbf{n} = \bar{\mathbf{n}} + \delta\mathbf{n}$ . Close to the QCP, so that  $\mathbf{n}$  is still small, we may use the same expansion about  $\mathbf{n} = 0$  as in the isotropic phase, but we have to include terms of fourth order in  $\mathbf{n}$ . Using rotational invariance of the action, we may write, up to fourth order in  $\mathbf{n}$ ,

$$\begin{aligned} S_{\text{eff}}[\mathbf{n}] &= \frac{1}{2} \frac{1}{\beta V} \sum_{\vec{q}} (\mathbf{n}_{\vec{q}}^T \chi_{\text{is}}^{-1}(\mathbf{q}, i\Omega_n) \mathbf{n}_{-\vec{q}}) + \lambda \int d^2r d\tau (\mathbf{n}(\mathbf{r}, \tau)^2)^2 \\ &= \frac{1}{2} \frac{1}{\beta V} \sum_{\vec{q}} (\delta \mathbf{n}_{\vec{q}}^T \chi^{-1}(\mathbf{q}, i\Omega_n) \delta \mathbf{n}_{-\vec{q}}), \end{aligned} \quad (\text{A.83})$$

where  $\chi_{\text{is},ij}^{-1}(\mathbf{q}, i\Omega_n) = \delta_{ij}(r + \kappa q^2) + M_{ij}(\mathbf{q}, i\Omega_n)$  is the inverse propagator in the isotropic phase. In the rest of this subsection, to simplify notation, we omit the  $\frac{1}{\beta V}$  factor. Without loss of generality, we may set  $\mathbf{n}(\mathbf{r}, \tau) = (n_0 + \delta n_1(\mathbf{r}, \tau), \delta n_2(\mathbf{r}, \tau))^T$ , which in momentum space is  $\mathbf{n}_{\vec{q}} = (n_0 \delta_{\vec{q},0} + \delta n_{1,\vec{q}}, \delta n_{2,\vec{q}})^T$ . Substituting this into Eq. (A.83), we obtain

$$\begin{aligned} S_{\text{eff}}[\mathbf{n}] &= \frac{1}{2} (n_0 + \delta n_{1,\vec{0}}, \delta n_{2,\vec{0}}) \chi_{\text{is}}^{-1}(\mathbf{0}, 0) (n_0 + \delta n_{1,\vec{0}}, \delta n_{2,\vec{0}})^T + \frac{1}{2} \sum_{\vec{q}} (\delta \mathbf{n}_{\vec{q}}^T \chi_{\text{is}}^{-1}(\mathbf{q}, i\Omega_n) \delta \mathbf{n}_{-\vec{q}}) \\ &\quad + \lambda \int d^2r d\tau (n_0^4 + 4n_0^3 \delta n_1 + 6n_0^2 \delta n_1^2 + 2n_0^2 \delta n_2^2 + \mathcal{O}((\delta \mathbf{n})^2)), \end{aligned} \quad (\text{A.84})$$

where the prime above the sum sign means that we omit the term corresponding to  $\vec{q} = \vec{0}$ . In the nematic phase,  $r < 0$ ,  $\chi_{\text{is}}^{-1}(\mathbf{0}, 0)_{ij} = r\delta_{ij}$ . Then, to second order in  $\delta\mathbf{n}$ ,

$$S_{\text{eff}}[\mathbf{n}] = \frac{r}{2}n_0^2 + (rn_0 + 4\lambda n_0^3)\delta n_{1,\vec{0}} + \sum_{\vec{q}} \left( \frac{r}{2} + 6\lambda n_0^2 \right) \delta n_{1,\vec{q}} \delta n_{1,-\vec{q}} \\ + \sum_{\vec{q}} \left( \frac{r}{2} + 2\lambda n_0^2 \right) \delta n_{2,\vec{q}} \delta n_{2,-\vec{q}} + \frac{1}{2} \sum_{\vec{q}} (\delta \mathbf{n}_{i,\vec{q}}^T (\delta_{ij} \kappa q^2 + M_{ij}(\mathbf{q}, i\Omega_n))) \delta \mathbf{n}_{j,-\vec{q}}. \quad (\text{A.85})$$

Because  $\bar{\mathbf{n}} = (n_0, 0)^T$  minimizes the action, the linear in  $\delta\mathbf{n}$  term must vanish. Thus,  $\lambda n_0^2 = -\frac{r}{4}$ , and we find that  $\chi^{-1}(\mathbf{q}, i\Omega_n) = \delta\chi^{-1} + \chi_{\text{is}}^{-1}(\mathbf{q}, i\Omega_n)$ , where

$$\delta\chi^{-1} = \begin{pmatrix} -3r & 0 \\ 0 & -r \end{pmatrix}. \quad (\text{A.86})$$

Thus, we obtain the expression Eq. (2.61) of the main text.

## A.4 Electron self-energy

To compute the fermionic self-energy, we consider the Yukawa-like coupling of fermionic quasiparticles to fluctuations of the nematic order parameter:

$$S = \frac{1}{2\beta V} \sum_{\mathbf{q}, iq_n} \mathbf{n}(\mathbf{q}, iq_n)^T \chi^{-1}(\mathbf{q}, iq_n) \mathbf{n}(-\mathbf{q}, -iq_n) + \frac{1}{\beta V} \sum_{\mathbf{k}, ik_n} \psi^\dagger(\mathbf{k}, ik_n) \mathcal{G}_0^{-1}(\mathbf{k}, ik_n) \psi(\mathbf{k}, ik_n) \\ - \frac{1}{\beta^2 V^2} \sum_{\substack{\mathbf{k}, ik_n \\ \mathbf{q}, iq_n}} \mathbf{n}(\mathbf{q}, iq_n)^T \psi^\dagger(\mathbf{k} - \mathbf{q}, ik_n - iq_n) \Delta(\mathbf{k}) \psi(\mathbf{k}, ik_n). \quad (\text{A.87})$$

Then, at one loop order, the self-energy is given by

$$\Sigma(\mathbf{k}, ik_n) = \frac{T}{V} \sum_{\mathbf{q}, i\omega_m} \sum_{i,j} \Delta_{\mathbf{k}, \mathbf{k}-\mathbf{q}}^i \mathcal{G}_0(\mathbf{k} - \mathbf{q}, ik_n - i\omega_m) \Delta_{\mathbf{k}-\mathbf{q}, \mathbf{k}}^j \chi_{ij}(\mathbf{q}, i\omega_m), \quad (\text{A.88})$$

where the nematic field propagator in the nematic phase is

$$\chi(\mathbf{q}, i\omega_n) = \frac{1}{\chi_{\perp}^{-1}(\mathbf{q}, i\omega_n)\chi_{\parallel}^{-1}(\mathbf{q}, i\omega_n)} \begin{pmatrix} \kappa q^2 + M_{22}(\mathbf{q}, i\omega_n) & -M_{12}(\mathbf{q}, i\omega_n) \\ -M_{12}(\mathbf{q}, i\omega_n) & 2|r| + \kappa q^2 + M_{11}(\mathbf{q}, i\omega_n) \end{pmatrix}. \quad (\text{A.89})$$

Here the dynamical matrix  $M$  is

$$M(\mathbf{q}, i\omega_n) = a(s) [\sigma_0 - b(s) (\sigma_z \cos 4\theta_{\mathbf{q}} + \sigma_x \sin 4\theta_{\mathbf{q}})], \quad (\text{A.90})$$

where

$$a(s) = \frac{\mathcal{N}(\mu)}{2} \frac{|s|}{\sqrt{s^2 + 1}}; \quad b(s) = (\sqrt{s^2 + 1} - |s|)^4. \quad (\text{A.91})$$

At  $r = 0$ , Eq. (A.89) reduces to the nematic propagator at the QCP.

After some algebra, we find the following expression for the self-energy

$$\Sigma(\mathbf{k}, ik_n) = \frac{1}{4V} \sum_{\mathbf{q}, i\Omega_m} \frac{1}{(ik_n - i\Omega_m + \mu)^2 - v_F^2 |\mathbf{k} - \mathbf{q}|^2} \frac{1}{\chi_{\perp}^{-1}(\mathbf{q}, i\Omega_m)\chi_{\parallel}^{-1}(\mathbf{q}, i\Omega_m)} \begin{pmatrix} A_{11} & A_{12} \\ A_{12}^* & A_{22} \end{pmatrix}. \quad (\text{A.92})$$

where

$$A_{11} = (\beta_1^2 + \beta_2^2)(ik_n - i\Omega_m + \mu)[2r + 2\kappa q^2 + 2a(s)], \quad (\text{A.93})$$

$$A_{12} = iv_F |\mathbf{k} - \mathbf{q}| [(\beta_1^2 - \beta_2^2) + 2i\beta_1\beta_2] e^{i\theta_{\mathbf{k}-\mathbf{q}}} [2r - 2a(s)b(s)e^{-i4\theta_{\mathbf{q}}}], \quad (\text{A.94})$$

$$A_{22} = (\beta_1^2 + \beta_2^2)(ik_n - i\Omega_m + \mu)[2r + 2\kappa q^2 + 2a(s)], \quad (\text{A.95})$$

and

$$\begin{aligned}\chi_{\perp}^{-1} &= \frac{1}{2} \left[ 2\kappa q^2 + 2r + 2a(s) - \sqrt{[2r + 2a(s)b(s)]^2 - 16ra(s)b(s) \cos^2 2\theta_{\mathbf{q}}} \right], \\ \chi_{\parallel}^{-1} &= \frac{1}{2} \left[ 2\kappa q^2 + 2r + 2a(s) + \sqrt{[2r + 2a(s)b(s)]^2 - 16ra(s)b(s) \cos^2 2\theta_{\mathbf{q}}} \right].\end{aligned}\quad (\text{A.96})$$

Note that

$$\begin{aligned}\chi_{\perp}^{-1} + \chi_{\parallel}^{-1} &= 2 [\kappa q^2 + r + a(s)], \\ \chi_{\parallel}^{-1} - \chi_{\perp}^{-1} &= 2\sqrt{[r + a(s)b(s)]^2 - 4ra(s)b(s) \cos^2 2\theta_{\mathbf{q}}},\end{aligned}\quad (\text{A.97})$$

which allows us to rewrite

$$\begin{aligned}\frac{1}{\chi_{\perp}^{-1} \chi_{\parallel}^{-1}} &= \frac{1}{2 [\kappa q^2 + r + a(s)]} \left( \frac{1}{\chi_{\perp}^{-1}} + \frac{1}{\chi_{\parallel}^{-1}} \right), \\ \frac{1}{\chi_{\perp}^{-1} \chi_{\parallel}^{-1}} &= \frac{1}{\chi_{\parallel}^{-1} - \chi_{\perp}^{-1}} \left( \frac{1}{\chi_{\perp}^{-1}} - \frac{1}{\chi_{\parallel}^{-1}} \right).\end{aligned}\quad (\text{A.98})$$

Also

$$\begin{aligned}\frac{ik_n - i\Omega_m + \mu}{(ik_n - i\Omega_m + \mu)^2 - v_F^2 |\mathbf{k} - \mathbf{q}|^2} &= \frac{1}{2} \frac{1}{ik_n - i\Omega_m + \mu - v_F |\mathbf{k} - \mathbf{q}|} + \frac{1}{2} \frac{1}{ik_n - i\Omega_m + \mu + v_F |\mathbf{k} - \mathbf{q}|}, \\ \frac{v_F |\mathbf{k} - \mathbf{q}|}{(ik_n - i\Omega_m + \mu)^2 - v_F^2 |\mathbf{k} - \mathbf{q}|^2} &= \frac{1}{2} \frac{1}{ik_n - i\Omega_m + \mu - v_F |\mathbf{k} - \mathbf{q}|} - \frac{1}{2} \frac{1}{ik_n - i\Omega_m + \mu + v_F |\mathbf{k} - \mathbf{q}|}.\end{aligned}\quad (\text{A.99})$$

Using the first expressions in Eqs. (A.98) and (A.99), for the diagonal components we have:

$$\begin{aligned}\Sigma_{11} = \Sigma_{22} &= \frac{1}{8V} \sum_{\mathbf{q}, i\Omega_m} \left( \frac{1}{ik_n - i\Omega_m + \mu - v_F |\mathbf{k} - \mathbf{q}|} + \frac{1}{ik_n - i\Omega_m + \mu + v_F |\mathbf{k} - \mathbf{q}|} \right) \\ &\quad \times \left( \frac{1}{\chi_{\perp}^{-1}} + \frac{1}{\chi_{\parallel}^{-1}} \right) (\beta_1^2 + \beta_2^2).\end{aligned}\quad (\text{A.100})$$

Analogically, but using the second expression in Eqs. (A.98) and (A.99), for the off-diagonal components, we obtain

$$\begin{aligned}
\Sigma_{12} &= \frac{1}{8V} \sum_{\mathbf{q}, i\Omega_m} \left( \frac{1}{ik_n - i\Omega_m + \mu - v_F |\mathbf{k} - \mathbf{q}|} - \frac{1}{ik_n - i\Omega_m + \mu + v_F |\mathbf{k} - \mathbf{q}|} \right) \\
&\quad \times \left( \frac{1}{\chi_{\perp}^{-1}} - \frac{1}{\chi_{\parallel}^{-1}} \right) \frac{i(\beta_1 + i\beta_2)^2 e^{i\theta_{\mathbf{k}-\mathbf{q}}} [2r - 2a(s)b(s)e^{-i4\theta_{\mathbf{q}}}]}{\chi_{\parallel}^{-1} - \chi_{\perp}^{-1}}, \\
\Sigma_{21} &= \frac{1}{8V} \sum_{\mathbf{q}, i\Omega_m} \left( \frac{1}{ik_n - i\Omega_m + \mu - v_F |\mathbf{k} - \mathbf{q}|} - \frac{1}{ik_n - i\Omega_m + \mu + v_F |\mathbf{k} - \mathbf{q}|} \right) \\
&\quad \times \left( \frac{1}{\chi_{\perp}^{-1}} - \frac{1}{\chi_{\parallel}^{-1}} \right) \left[ \frac{i(\beta_1 + i\beta_2)^2 e^{i\theta_{\mathbf{k}-\mathbf{q}}} [2r - 2a(s)b(s)e^{-i4\theta_{\mathbf{q}}}]}{\chi_{\parallel}^{-1} - \chi_{\perp}^{-1}} \right]^*. \tag{A.101}
\end{aligned}$$

In the following, we will neglect the interband scattering contribution, i.e. terms containing the  $\frac{1}{ik_n - i\Omega_m + \mu + v_F |\mathbf{k} - \mathbf{q}|}$  factor. Also, close to the FS, we may approximate

$$\frac{1}{ik_n - i\Omega_m + \mu - v_F |\mathbf{k} - \mathbf{q}|} \approx \frac{1}{ik_n - i\Omega_m + v_F q \cos(\theta_{\mathbf{q}} - \theta_{\mathbf{k}})}. \tag{A.102}$$

#### A.4.1 Quantum Critical Point

At the QCP,  $r = 0$ , the longitudinal mode with dynamic critical exponent  $z = 3$  is dominant, and we neglect the contribution from the transverse  $z = 2$  mode. Thus, we are interested in calculating

$$\begin{aligned}
\Sigma_{11} = \Sigma_{22} &\approx \frac{1}{8V} \sum_{\mathbf{q}, i\Omega_m} \frac{1}{ik_n - i\Omega_m + v_F q \cos(\theta_{\mathbf{q}} - \theta_{\mathbf{k}})} \frac{\beta_1^2 + \beta_2^2}{\chi_{\parallel}^{-1}}, \\
\Sigma_{12} &\approx \frac{1}{8V} \sum_{\mathbf{q}, i\Omega_m} \frac{1}{ik_n - i\Omega_m + v_F q \cos(\theta_{\mathbf{q}} - \theta_{\mathbf{k}})} \frac{1}{\chi_{\parallel}^{-1}} \frac{i(\beta_1 + i\beta_2)^2 e^{i\theta_{\mathbf{k}-\mathbf{q}}} 2a(s)b(s)e^{-i4\theta_{\mathbf{q}}}}{\chi_{\parallel}^{-1} - \chi_{\perp}^{-1}}, \\
\Sigma_{21} &\approx \frac{1}{8V} \sum_{\mathbf{q}, i\Omega_m} \frac{1}{ik_n - i\Omega_m + v_F q \cos(\theta_{\mathbf{q}} - \theta_{\mathbf{k}})} \frac{1}{\chi_{\parallel}^{-1}} \left[ \frac{i(\beta_1 + i\beta_2)^2 e^{i\theta_{\mathbf{k}-\mathbf{q}}} 2a(s)b(s)e^{-i4\theta_{\mathbf{q}}}}{\chi_{\parallel}^{-1} - \chi_{\perp}^{-1}} \right]^* \\
&= -\Sigma_{12}^*. \tag{A.103}
\end{aligned}$$

At the QCP,  $\chi_{\parallel}^{-1} = \kappa q^2 + a(s) + a(s)b(s)$ , which to first order in  $s$  is  $\chi_{\parallel}^{-1} \approx \kappa q^2 + \mathcal{N}(\mu)|s|$ . Recall that<sup>3</sup>

$$\beta_1 = \hat{k}_x + \widehat{(k-q)}_x; \beta_2 = \hat{k}_y + \widehat{(k-q)}_y. \quad (\text{A.104})$$

So

$$\begin{aligned} \beta_1^2 + \beta_2^2 &= 2 + 2 \cos(\theta_{\mathbf{k}} - \theta_{\mathbf{k}-\mathbf{q}}) \approx 4 - \left(\frac{q}{k}\right)^2 \approx 4, \\ (\beta_1 + i\beta_2)^2 &= e^{2i\theta_{\mathbf{k}-\mathbf{q}}} \left(1 + e^{i(\theta_{\mathbf{k}} - \theta_{\mathbf{k}-\mathbf{q}})}\right)^2 \approx 4e^{2i\theta_{\mathbf{k}}}. \end{aligned} \quad (\text{A.105})$$

Combining everything together, we need to calculate

$$\begin{aligned} \Sigma_{11} = \Sigma_{22} &\approx \frac{1}{2} \frac{T}{V} \sum_{\mathbf{q}, i\Omega_m} \frac{1}{ik_n - i\Omega_m + v_F q \cos(\theta_{\mathbf{q}} - \theta_{\mathbf{k}})} \frac{1}{\kappa q^2 + \mathcal{N}(\mu)|s|}, \\ \Sigma_{12} &\approx \frac{1}{2} \frac{T}{V} \sum_{\mathbf{q}, i\Omega_m} \frac{1}{ik_n - i\Omega_m + v_F q \cos(\theta_{\mathbf{q}} - \theta_{\mathbf{k}})} \frac{ie^{3i\theta_{\mathbf{k}}} e^{-i4\theta_{\mathbf{q}}}}{\kappa q^2 + \mathcal{N}(\mu)|s|} = -\Sigma_{12}^*. \end{aligned} \quad (\text{A.106})$$

At zero temperature and in the thermodynamic limit, discrete sums over frequency and momentum turn into integrals:  $\frac{T}{V} \sum_{\mathbf{q}, i\Omega_m} \rightarrow \int \frac{d\Omega}{2\pi} \int \frac{d^2\mathbf{q}}{(2\pi)^2} = \int \frac{d\Omega}{2\pi} \int \frac{dq q}{(2\pi)^2} \int_0^{2\pi} d\theta_{\mathbf{q}}$ . Using Eq. (A.80), we find that in the regime  $|\frac{k_n - \Omega}{v_F q}| \ll 1$ :

$$\int_0^{2\pi} d\varphi \frac{1}{ik_n - i\Omega_m + v_F q \cos(\varphi - \varphi_0)} \approx -\frac{2\pi i}{v_F q} \text{sgn}(k_n - \Omega_m). \quad (\text{A.107})$$

Since  $\chi_{\parallel}$  is even with respect to  $\Omega$ , the expression for the self-energy may be simplified. Let us denote  $f(\Omega) = \int_0^{\infty} dq \chi_{\parallel}(q, i\Omega)$ . If  $k_n > 0$ :

$$\begin{aligned} \int_{-\infty}^{\infty} d\Omega \text{sgn}(k_n - \Omega) f(\Omega) &= \int_{-\infty}^{k_n} d\Omega f(\Omega) - \int_{k_n}^{\infty} d\Omega f(\Omega) \\ &= \int_{-\infty}^{-k_n} d\Omega f(\Omega) + \int_{-k_n}^{k_n} d\Omega f(\Omega) - \int_{k_n}^{\infty} d\Omega f(\Omega) = 2 \int_0^{k_n} d\Omega f(\Omega). \end{aligned} \quad (\text{A.108})$$

---

<sup>3</sup>Note that we changed the sign of  $\mathbf{q}$  in comparison to Eq. (A.59), which does not affect any physical conclusions.

If  $k_n < 0$ :

$$\begin{aligned} \int_{-\infty}^{\infty} d\Omega \operatorname{sgn}(k_n - \Omega_n) f(\Omega) &= \int_{-\infty}^{-|k_n|} d\Omega f(\Omega) - \int_{-|k_n|}^{\infty} d\Omega f(\Omega) \\ &= \int_{-\infty}^{-|k_n|} d\Omega f(\Omega) - \int_{-|k_n|}^{|k_n|} d\Omega f(\Omega) - \int_{|k_n|}^{\infty} d\Omega f(\Omega) = -2 \int_0^{|k_n|} d\Omega f(\Omega). \end{aligned} \quad (\text{A.109})$$

So, for the **diagonal component**, we may write

$$\begin{aligned} \Sigma_{11} &= -\frac{i}{v_F} \operatorname{sgn}(k_n) \int \frac{dq}{2\pi} \int_0^{|k_n|} \frac{d\Omega}{2\pi} \chi_{\parallel} = -\frac{i}{v_F} \operatorname{sgn}(k_n) \int \frac{dq}{2\pi} \int_0^{|k_n|} \frac{d\Omega}{2\pi} \frac{1}{\kappa q^2 + \mathcal{N}(\mu)|s|} \\ &= -\frac{i}{v_F \kappa} \operatorname{sgn}(k_n) \int \frac{dq}{2\pi} \int_0^{|k_n|} \frac{d\Omega}{2\pi} \frac{q}{q^3 + \frac{\mathcal{N}(\mu)}{v_F \kappa} \Omega}. \end{aligned} \quad (\text{A.110})$$

To evaluate the integral over  $q$ , we decompose it into the sum of simple fractions. However, we will evaluate an integral with a more general integrand:  $\int \frac{dq}{2\pi} \frac{q}{q^3 + r q + \Omega}$ , which could be used for evaluating contributions from the gapped mode in the nematic phase (which will not be done in this thesis). Using Cardano's formula, solutions for the cubic equation  $q^3 + r q + \Omega = 0$  are:

$$q_1 = \alpha + \beta, \quad q_{2,3} = -\frac{\alpha + \beta}{2} \pm i \frac{\alpha - \beta}{2} \sqrt{3}, \quad (\text{A.111})$$

where  $\alpha = \sqrt[3]{-\frac{\Omega}{2} + \sqrt{\left(\frac{r}{3}\right)^3 + \left(\frac{\Omega}{2}\right)^2}}$ . For  $\frac{|\omega|^2}{r^3} \gg 1$ , which is satisfied for  $r \rightarrow 0$ , the solution of the cubic equation simplifies to

$$q_1 \approx -\Omega^{\frac{1}{3}}, \quad q_{2,3} \approx \Omega^{\frac{1}{3}} \left( \frac{1}{2} \pm i \frac{\sqrt{3}}{2} \right) = \Omega^{\frac{1}{3}} e^{\pm i\pi/3}. \quad (\text{A.112})$$

In our theory, we have a cutoff  $\Lambda$  around the FS. But the integrand decays fast enough, and we approximate the result by extending the range of integration over  $q$  to

infinity. Then the integral over  $q$  becomes

$$\begin{aligned}
\int_0^\infty dq \frac{q}{q^3 + rq + \Omega} &\approx \int_0^\infty dq \frac{q}{(q + \Omega^{\frac{1}{3}})((q - \frac{\Omega^{\frac{1}{3}}}{2})^2 + \frac{3}{4}\Omega^{\frac{2}{3}})} \\
&= \int_0^\infty dq \left( -\frac{1}{3\Omega^{\frac{1}{3}}} \frac{1}{q + \Omega^{\frac{1}{3}}} + \frac{1}{2} \frac{1}{(q - \frac{\Omega^{\frac{1}{3}}}{2})^2 + \frac{3}{4}\Omega^{\frac{2}{3}}} + \frac{1}{3\Omega^{\frac{1}{3}}} \frac{q - \frac{\Omega^{\frac{1}{3}}}{2}}{(q - \frac{\Omega^{\frac{1}{3}}}{2})^2 + \frac{3}{4}\Omega^{\frac{2}{3}}} \right) \\
&= -\frac{1}{3\Omega^{\frac{1}{3}}} \ln(q + \Omega^{\frac{1}{3}}) \Big|_0^\infty + \frac{1}{\sqrt{3}\Omega^{\frac{1}{3}}} \arctan \frac{2(q - \frac{\Omega^{\frac{1}{3}}}{2})}{\sqrt{3}\Omega^{\frac{1}{3}}} \Big|_0^\infty \\
&+ \frac{1}{3\Omega^{\frac{1}{3}}} \ln \sqrt{(q - \frac{\Omega^{\frac{1}{3}}}{2})^2 + \frac{3}{4}\Omega^{\frac{2}{3}}} \Big|_0^\infty = \frac{1}{3\Omega^{\frac{1}{3}}} \ln \left( \frac{\sqrt{(q - \frac{\Omega^{\frac{1}{3}}}{2})^2 + \frac{3}{4}\Omega^{\frac{2}{3}}}}{q + \Omega^{\frac{1}{3}}} \right) \Big|_0^\infty \\
&- \frac{1}{3\Omega^{\frac{1}{3}}} \ln \left( \frac{\sqrt{\frac{\Omega^{\frac{2}{3}}}{4} + \frac{3}{4}\Omega^{\frac{2}{3}}}}{\Omega^{\frac{1}{3}}} \right) + \frac{1}{\sqrt{3}\Omega^{\frac{1}{3}}} \left( \frac{\pi}{2} + \frac{\pi}{6} \right) = \frac{2\pi}{3\sqrt{3}} \Omega^{-\frac{1}{3}}. \quad (\text{A.113})
\end{aligned}$$

Using this result, and integrating over  $\Omega$ , for the diagonal components of the self-energy, we find

$$\Sigma_{11}(\mathbf{k}, ik_n) \approx -\frac{i}{4\sqrt{3}\pi} \text{sgn}(k_n) \omega_0^{\frac{1}{3}} |k_n|^{\frac{2}{3}} = \Sigma_0(\mathbf{k}, ik_n), \quad (\text{A.114})$$

where  $\omega_0 = (v_F^2 \kappa^2 \mathcal{N}(\mu))^{-1}$ .

To calculate the **off-diagonal components**, we use another approximation: the fermion Green's function is peaked at  $\theta_{\mathbf{q}} = \theta_{\mathbf{k}} \pm \frac{\pi}{2}$ , and, therefore, we may substitute other factors in the expression for the self-energy with their values at  $\theta_{\mathbf{q}} = \theta_{\mathbf{k}} \pm \frac{\pi}{2}$  [68, 69]. Thus,

$$\begin{aligned}
\Sigma_{12}(\mathbf{k}, ik_n) &\approx \frac{1}{2} \frac{T}{V} \sum_{\mathbf{q}, i\Omega_m} \frac{1}{ik_n - i\Omega_m + v_F q \cos(\theta_{\mathbf{q}} - \theta_{\mathbf{k}})} \frac{ie^{-i\theta_{\mathbf{k}}}}{\kappa q^2 + \mathcal{N}(\mu)|s|} \\
&\approx -\frac{i}{4\sqrt{3}\pi} \text{sgn}(k_n) \omega_0^{\frac{1}{3}} |k_n|^{\frac{2}{3}} ie^{-i\theta_{\mathbf{k}}}. \quad (\text{A.115})
\end{aligned}$$

Combining everything together, we find:

$$\Sigma(\mathbf{k}, ik_n) = \begin{pmatrix} 1 & i \cos \theta_{\mathbf{k}} + \sin \theta_{\mathbf{k}} \\ -i \cos \theta_{\mathbf{k}} + \sin \theta_{\mathbf{k}} & 1 \end{pmatrix} \Sigma_0(\mathbf{k}, ik_n) = \left( \mathbb{I}_2 + \left( \boldsymbol{\sigma} \times \hat{\mathbf{k}} \right)_z \right) \Sigma_0(\mathbf{k}, ik_n). \quad (\text{A.116})$$

#### A.4.2 Nematic phase

In the nematic phase, the longitudinal mode becomes gapped, and the transverse (Goldstone) mode is dominant. Thus, for the self-energy we have

$$\Sigma(\mathbf{k}, ik_n) = \frac{1}{2} \frac{T}{V} \sum_{\mathbf{q}, i\Omega_m} \frac{1}{ik_n - i\Omega_m + v_F q \cos(\theta_{\mathbf{q}} - \theta_{\mathbf{k}})} \frac{1}{\chi_{\perp}^{-1}} \times \begin{pmatrix} \frac{\beta_1^2 + \beta_2^2}{4} & \frac{i(\beta_1 + i\beta_2)^2 e^{i\theta_{\mathbf{k}} - \mathbf{q}} [r - a(s)b(s)e^{-i4\theta_{\mathbf{q}}}]}{2(\chi_{\parallel}^{-1} - \chi_{\perp}^{-1})} \\ \frac{-i(\beta_1 - i\beta_2)^2 e^{-i\theta_{\mathbf{k}} - \mathbf{q}} [r - a(s)b(s)e^{i4\theta_{\mathbf{q}}}]}{2(\chi_{\parallel}^{-1} - \chi_{\perp}^{-1})} & \frac{\beta_1^2 + \beta_2^2}{4} \end{pmatrix}. \quad (\text{A.117})$$

To second order in  $|s|$ ,

$$\chi_{\perp}^{-1}(\mathbf{q}, i\Omega_m) = \kappa q^2 + \mathcal{N}(\mu)|s| \cos^2 2\theta_{\mathbf{q}} - \mathcal{N}(\mu) \left( \cos 4\theta_{\mathbf{q}} + \frac{\mathcal{N}(\mu)}{16|r|} \sin^2 4\theta_{\mathbf{q}} \right) 2s^2 + O(s^3),$$

$$\chi_{\parallel}^{-1} - \chi_{\perp}^{-1} \approx 2r - \mathcal{N}(\mu)|s| \cos 4\theta_{\mathbf{q}}. \quad (\text{A.118})$$

Thus,

$$\begin{aligned}
\Sigma_{11} &\approx \frac{1}{8} \frac{T}{V} \sum_{\mathbf{q}, i\Omega_m} \frac{1}{ik_n - i\Omega_m + v_F q \cos(\theta_{\mathbf{q}} - \theta_{\mathbf{k}})} \\
&\quad \times \frac{2 + 2 \cos(\theta_{\mathbf{k}} - \theta_{\mathbf{k}-\mathbf{q}})}{\kappa q^2 + \mathcal{N}(\mu)|s| \cos^2 2\theta_{\mathbf{q}} - \mathcal{N}(\mu) \left( \cos 4\theta_{\mathbf{q}} + \frac{\mathcal{N}(\mu)}{16|r|} \sin^2 4\theta_{\mathbf{q}} \right) 2s^2}, \\
\Sigma_{12} &\approx \frac{1}{8} \frac{T}{V} \sum_{\mathbf{q}, i\Omega_m} \frac{1}{ik_n - i\Omega_m + v_F q \cos(\theta_{\mathbf{q}} - \theta_{\mathbf{k}})} \\
&\quad \times \frac{1}{\kappa q^2 + \mathcal{N}(\mu)|s| \cos^2 2\theta_{\mathbf{q}} - \mathcal{N}(\mu) \left( \cos 4\theta_{\mathbf{q}} + \frac{\mathcal{N}(\mu)}{16|r|} \sin^2 4\theta_{\mathbf{q}} \right) 2s^2} \\
&\quad \times \frac{ie^{2i\theta_{\mathbf{k}-\mathbf{q}}} (1 + e^{i(\theta_{\mathbf{k}} - \theta_{\mathbf{k}-\mathbf{q}})})^2 e^{i\theta_{\mathbf{k}-\mathbf{q}}} (2r - \mathcal{N}(\mu)|s|e^{-i4\theta_{\mathbf{q}}})}{2r - \mathcal{N}(\mu)|s| \cos 4\theta_{\mathbf{q}}} = -\Sigma_{12}^*. \tag{A.119}
\end{aligned}$$

Again, we substitute  $\theta_{\mathbf{q}} = \frac{\pi}{2} \pm \theta_{\mathbf{k}}$  everywhere except in the fermion Green's function. Then, for a generic angle we may do calculations keeping terms up to first order in  $s$  in  $\chi_{\perp}$ , and zeroth order term in  $s$  in the third factor of the off-diagonal components of the self-energy in Eq. (A.119). However, for  $\theta_{\mathbf{k}} = \frac{\pi}{4} + \frac{\pi}{2}m$ ,  $m \in \mathbb{Z}$ , the first order term in  $s$  in the inverse propagator of the Goldstone mode vanishes, and we have to keep second order terms.

We first consider a generic angle. In this case, the calculation of the self-energy proceeds in the same way as for the QCP, and we obtain

$$\begin{aligned}
\Sigma_{11}(\mathbf{k}, ik_n) &\approx (\cos 2\theta_{\mathbf{k}})^{-\frac{2}{3}} \Sigma_0(\mathbf{k}, ik_n), \\
\Sigma_{12}(\mathbf{k}, ik_n) &\approx (\cos 2\theta_{\mathbf{k}})^{-\frac{2}{3}} \Sigma_0(\mathbf{k}, ik_n) ie^{i3\theta_{\mathbf{k}}}. \tag{A.120}
\end{aligned}$$

In matrix form, the self-energy in the nematic phase is:

$$\Sigma(\mathbf{k}, ik_n) = (\mathbb{I}_2 - \sigma_y \cos 3\theta_{\mathbf{k}} - \sigma_x \sin 3\theta_{\mathbf{k}}) |\cos 2\theta_{\mathbf{k}}|^{-2/3} \Sigma_0(\mathbf{k}, ik_n). \tag{A.121}$$

Now let us consider points on the FS along the principal axes of nematic order, i.e.,  $\theta_{\mathbf{k}} = \pm \frac{\pi}{4}, \pm \frac{3\pi}{4}$ . We first project the self-energy onto the FS. Instead of the original field operator  $\psi_{\mathbf{k}\sigma}$ , which annihilates a fermion of definite spin  $\sigma$ , one may introduce operators

$\psi_{\mathbf{k}\pm}$ , which annihilate fermions of fixed helicity:

$$\psi_{\mathbf{k}\pm} = \frac{1}{\sqrt{2}} \left( i e^{-i\theta_{\mathbf{k}}} \psi_{\mathbf{k}\uparrow} \pm \psi_{\mathbf{k}\downarrow} \right). \quad (\text{A.122})$$

Inverting this, we find that

$$\psi_{\mathbf{k}\uparrow} = \frac{i e^{-i\theta_{\mathbf{k}}}}{\sqrt{2}} (\psi_{\mathbf{k}+} + \psi_{\mathbf{k}-}), \quad \psi_{\mathbf{k}\downarrow} = \frac{1}{\sqrt{2}} (\psi_{\mathbf{k}+} - \psi_{\mathbf{k}-}). \quad (\text{A.123})$$

Assuming that the FS is above the Dirac point, projecting onto the FS, we may get rid of states of negative helicity, i.e., abandon the operator  $\psi_{\mathbf{k}-}$  in the above expressions. Thus, effectively we may substitute  $\psi_{\mathbf{k}\uparrow} \rightarrow \frac{i e^{-i\theta_{\mathbf{k}}}}{\sqrt{2}} \psi_{\mathbf{k}+}$ ,  $\psi_{\mathbf{k}\downarrow} \rightarrow \frac{1}{\sqrt{2}} \psi_{\mathbf{k}+}$ . Below we omit the momentum label  $\mathbf{k}$  in the helicity operators.

Considering only the matrix in brackets in Eq. (A.117) for convenience, in the  $s \rightarrow 0$  limit, we obtain

$$\begin{aligned} \psi_{\mathbf{k}}^{\dagger} \left[ \begin{array}{cc} \frac{1+\cos(\theta_{\mathbf{k}}-\theta_{\mathbf{k}-\mathbf{q}})}{2} & \frac{i e^{3i\theta_{\mathbf{k}}-\mathbf{q}} (1+e^{i(\theta_{\mathbf{k}}-\theta_{\mathbf{k}-\mathbf{q}})})^2}{4} \\ \frac{-i e^{-3i\theta_{\mathbf{k}}-\mathbf{q}} (1+e^{-i(\theta_{\mathbf{k}}-\theta_{\mathbf{k}-\mathbf{q}})})^2}{4} & \frac{1+\cos(\theta_{\mathbf{k}}-\theta_{\mathbf{k}-\mathbf{q}})}{2} \end{array} \right] \psi_{\mathbf{k}} \\ = \frac{\psi_{+}^{\dagger} \psi_{+}}{2} (1 + \cos(\theta_{\mathbf{k}} - \theta_{\mathbf{k}-\mathbf{q}})) 2 \cos^2(\theta_{\mathbf{k}} + \theta_{\mathbf{k}-\mathbf{q}}). \end{aligned} \quad (\text{A.124})$$

Shifting the angle,  $\theta_{\mathbf{k}} \rightarrow \theta_{\mathbf{k}} + \frac{\pi}{4}$ , we obtain

$$\psi_{+}^{\dagger} \psi_{+} (1 + \cos(\theta_{\mathbf{k}} - \theta_{\mathbf{k}-\mathbf{q}})) \cos^2(\theta_{\mathbf{k}} + \theta_{\mathbf{k}-\mathbf{q}}) = \psi_{+}^{\dagger} \psi_{+} (1 + \cos(\theta_{\mathbf{k}} - \theta_{\mathbf{k}-\mathbf{q}})) \sin^2(\theta_{\mathbf{k}} + \theta_{\mathbf{k}-\mathbf{q}}). \quad (\text{A.125})$$

Thus, to first order in  $\frac{q}{k}$ , the projection of the self-energy onto the helical band becomes

$$\Sigma_{proj}(\mathbf{k}, ik_n) = \frac{1}{2V} \sum_{\mathbf{q}, i\Omega_m} \frac{1}{ik_n - i\Omega_m + v_{Fq} \cos(\theta_{\mathbf{q}} - \theta_{\mathbf{k}})} \frac{1}{\chi_{\perp}^{-1}} \sin^2 \left( 2\theta_{\mathbf{k}} - \frac{q}{k_F} \sin(\theta_{\mathbf{q}} - \theta_{\mathbf{k}}) \right), \quad (\text{A.126})$$

which is the same as the expression for the self-energy to first order in  $\frac{q}{k_F}$  in Ref. [241]. Following the subsequent analysis in this reference, we conclude that at these points of high symmetry the self-energy is proportional to  $k_n^{3/2}$ .

## A.5 Spin-nematic susceptibility

In this section, we calculate the retarded correlation function Eq. (2.65),

$$\Pi_{ij}^R(\mathbf{r}, t) = -i\theta(t) \left\langle \left[ (\psi^\dagger \sigma_i \psi)_{(\mathbf{r}, t)}, (\psi^\dagger \Delta_j \psi)_{(\mathbf{0}, 0)} \right] \right\rangle, \quad (\text{A.127})$$

corresponding to a spin-nematic susceptibility, in the isotropic phase.

Switching to the momentum-Matsubara frequency domain, the corresponding time-ordered correlator is

$$\Pi_{ij}(\mathbf{q}, iq_n) = \frac{T}{V} \sum_{\mathbf{p}, ip_n} \text{tr} \sigma_i \mathcal{G}_0(\mathbf{p} + \mathbf{q}, ip_n + iq_n) \Delta_j(\mathbf{p}, \mathbf{p} + \mathbf{q}) \mathcal{G}_0(\mathbf{p}, ip_n). \quad (\text{A.128})$$

Our strategy is to compute first the imaginary part, and the real part might then be determined via a Kramers-Kronig relation. Using the spectral representation for fermionic Green's functions and standard Matsubara summation formulae, then analytically continuing  $iq_n \rightarrow \omega + i\eta$ , we find

$$\Pi_{ij}^R(\mathbf{q}, \omega) = \text{tr} \int \frac{d^2p}{(2\pi)^2} \int d\epsilon \int d\epsilon' \frac{A(\mathbf{p} + \mathbf{q}, \epsilon) \Delta_j A(\mathbf{p}, \epsilon')}{\omega + i\eta + \epsilon' - \epsilon} (n_F(\epsilon') - n_F(\epsilon)) \sigma_i, \quad (\text{A.129})$$

where  $\eta$  is a positive infinitesimal. Using the identity  $\frac{1}{\omega + i\eta} = \mathcal{P} \frac{1}{\omega} - i\pi \delta(\omega)$ , for the imaginary part, we obtain

$$\begin{aligned} \text{Im} \Pi_{ij}^R(\mathbf{q}, \omega) &= -\pi \text{tr} \int \frac{d^2p}{(2\pi)^2} \int d\epsilon \int d\epsilon' \delta(\omega + \epsilon' - \epsilon) A(\mathbf{p} + \mathbf{q}, \epsilon) \Delta_j A(\mathbf{p}, \epsilon') (n_F(\epsilon') - n_F(\epsilon)) \sigma_i \\ &= -\pi \text{tr} \int \frac{d^2p}{(2\pi)^2} \int d\epsilon' A(\mathbf{p} + \mathbf{q}, \epsilon) \Delta_j A(\mathbf{p}, \epsilon') (n_F(\epsilon') - n_F(\epsilon' + \omega)) \sigma_i. \end{aligned} \quad (\text{A.130})$$

For definiteness, let us consider  $\omega > 0$ . Then  $\int d\epsilon(n_F(\epsilon') - n_F(\epsilon' + \omega)) \rightarrow \int_{-\omega}^0 d\epsilon$ . Also, the fermion spectral function is  $A(\mathbf{p}, \epsilon) = -\pi \left( \sigma_0 + \frac{v_F \hat{z} (\boldsymbol{\sigma} \times \mathbf{p})}{\mu + \epsilon} \right) \delta(\epsilon - v_F p + \mu)$ , where  $\sigma_0$  denotes the  $2 \times 2$  identity matrix. Then

$$\begin{aligned} \text{Im } \Pi_{ij}^R(\mathbf{q}, \omega) &= -\pi^3 \text{tr} \int \frac{d^2 p}{(2\pi)^2} \int_{-\omega}^0 d\epsilon X_{ij}(\mathbf{p} + \mathbf{q}, \epsilon + \omega; \mathbf{p}, \epsilon) \delta(\epsilon + \omega - v_F |\mathbf{p} + \mathbf{q}| + \mu) \delta(\epsilon - v_F p + \mu) \\ &= -\pi^3 \text{tr} \int' \frac{d^2 p}{(2\pi)^2} X_{ij}(\mathbf{p} + \mathbf{q}, v_F p - \mu + \omega; \mathbf{p}, v_F p - \mu) \delta(\omega + v_F p - v_F |\mathbf{p} + \mathbf{q}|), \end{aligned} \quad (\text{A.131})$$

where

$$\begin{aligned} X_{ij}(\mathbf{p} + \mathbf{q}, \epsilon + q_n; \mathbf{p}, \epsilon) &= \text{tr} \left( \sigma_0 + \frac{\hat{z} \cdot (\boldsymbol{\sigma}) \times (\mathbf{p} + \mathbf{q})}{|\mathbf{p} + \mathbf{q}|} \right) [\sigma_x \beta_{\alpha_j} + (-1)^j \sigma_y \beta_{\alpha_{j+1}}] \\ &\quad \times \left( \sigma_0 + \frac{\hat{z} \cdot (\boldsymbol{\sigma}) \times \mathbf{p}}{p} \right) [\sigma_x \delta_{1,i} + \sigma_y \delta_{2,i}]. \end{aligned} \quad (\text{A.132})$$

Here  $\alpha_1 = \alpha_3 = 2$ , and  $\alpha_2 = 1$ . In the last equation in the  $(-1)^i$  factor,  $i$  is an integer, taking values 1 or 2. In Eq. (A.131), we integrated over  $\epsilon$  using  $\delta(\epsilon - v_F p + \mu)$ . Because the limits in the integral over  $\epsilon$  are  $-\omega$  and 0, in  $\int' \frac{d^2 p}{(2\pi)^2}$ , the modulus of  $\mathbf{p}$  lies in the range  $[\frac{\mu - \omega}{v_F}, \frac{\mu}{v_F}] \cap [p_F - \Lambda, p_F + \Lambda]$ . Because we work in the limit  $\frac{\omega}{v_F q} \ll 1$  (therefore  $\frac{\omega}{v_F \Lambda} \ll 1$ ),  $\int' \frac{d^2 p}{(2\pi)^2} = \int_{\frac{\mu - \omega}{v_F}}^{\frac{\mu}{v_F}} \frac{dk k}{2\pi} \frac{d\theta_p}{2\pi}$ . After some algebra, we find

$$X_{ij} = \alpha_{ij} + \gamma_{ij}, \quad (\text{A.133})$$

where the matrices  $\alpha_{ij}$  and  $\gamma_{ij}$  are

$$\begin{aligned} \alpha &= \begin{pmatrix} \beta_1 & -\beta_2 \\ \beta_2 & \beta_1 \end{pmatrix} = \begin{pmatrix} \cos \theta_{\mathbf{p}} + \cos \theta_{\mathbf{p}+\mathbf{q}} & -\sin \theta_{\mathbf{p}} - \sin \theta_{\mathbf{p}+\mathbf{q}} \\ \sin \theta_{\mathbf{p}} + \sin \theta_{\mathbf{p}+\mathbf{q}} & \cos \theta_{\mathbf{p}} + \cos \theta_{\mathbf{p}+\mathbf{q}} \end{pmatrix} \\ \gamma &= \begin{pmatrix} -(\cos(2\theta_{\mathbf{p}} + \theta_{\mathbf{p}+\mathbf{q}}) + (\cos(\theta_{\mathbf{p}} + 2\theta_{\mathbf{p}+\mathbf{q}}))) & -(\sin(2\theta_{\mathbf{p}} + \theta_{\mathbf{p}+\mathbf{q}}) + (\sin(\theta_{\mathbf{p}} + 2\theta_{\mathbf{p}+\mathbf{q}}))) \\ -(\sin(2\theta_{\mathbf{p}} + \theta_{\mathbf{p}+\mathbf{q}}) + (\sin(\theta_{\mathbf{p}} + 2\theta_{\mathbf{p}+\mathbf{q}}))) & \cos(2\theta_{\mathbf{p}} + \theta_{\mathbf{p}+\mathbf{q}}) + (\cos(\theta_{\mathbf{p}} + 2\theta_{\mathbf{p}+\mathbf{q}})) \end{pmatrix}. \end{aligned} \quad (\text{A.134})$$

Integration over the angle  $\theta_{\mathbf{p}}$  in Eq. (A.131) picks a specific angle determined (up to  $\left(\frac{q}{p}\right)^2$ ) by  $\omega = v_F q \cos(\theta_{\mathbf{p}} - \theta_{\mathbf{q}})$ . The solution of this equation is  $\theta_{\mathbf{p};1,2} = \theta_{\mathbf{q}} \pm \arccos(s)$ , where  $s = \frac{\omega}{v_F q}$ . Then, the delta function is

$$\begin{aligned} \delta(\omega + v_F p - v_F |\mathbf{p} + \mathbf{q}|) &\approx \delta(\omega - v_F q \cos(\theta_{\mathbf{p}} - \theta_{\mathbf{q}})) = \frac{\delta(\theta_{\mathbf{p}} - \theta_{\mathbf{p};1})}{|v_F q \sin(\theta_{\mathbf{p}} - \theta_{\mathbf{q}})|} + \frac{\delta(\theta_{\mathbf{p}} - \theta_{\mathbf{p};2})}{|v_F q \sin(\theta_{\mathbf{p}} - \theta_{\mathbf{q}})|} \\ &= \frac{\delta(\theta_{\mathbf{p}} - \theta_{\mathbf{p};1})}{v_F q \sqrt{1 - s^2}} + \frac{\delta(\theta_{\mathbf{p}} - \theta_{\mathbf{p};2})}{v_F q \sqrt{1 - s^2}}. \end{aligned} \quad (\text{A.135})$$

Then, approximating  $\theta_{\mathbf{p}+\mathbf{q}} \approx \theta_{\mathbf{p}} - \frac{q}{k_F} \sin(\theta_{\mathbf{p}} - \theta_{\mathbf{q}})$  and performing integration over  $\mathbf{p}$ , we find

$$\text{Im } \Pi^R(\mathbf{q}, \omega) = -\frac{\pi}{4} \frac{\mu^2 - (\mu - \omega)^2}{v_F^2} \frac{1}{v_F q \sqrt{1 - s^2}} \left( \begin{pmatrix} a_1 & a_2 \\ -a_2 & a_1 \end{pmatrix} - \begin{pmatrix} b_1 & b_2 \\ b_2 & -b_1 \end{pmatrix} \right), \quad (\text{A.136})$$

where

$$\begin{aligned} a_1 &= \cos \theta_{\mathbf{q}} \cos \phi + \cos \theta_{\mathbf{q}} \cos \left( \phi - \frac{q}{k_F} \sin \phi \right), \\ a_2 &= \sin \theta_{\mathbf{q}} \cos \phi + \sin \theta_{\mathbf{q}} \cos \left( \phi - \frac{q}{k_F} \sin \phi \right), \\ b_1 &= \cos 3\theta_{\mathbf{q}} \cos \left( 3\phi - \frac{q}{k_F} \sin \phi \right) + \cos 3\theta_{\mathbf{q}} \cos \left( 3\phi - 2\frac{q}{k_F} \sin \phi \right), \\ b_2 &= \sin 3\theta_{\mathbf{q}} \cos \left( 3\phi - \frac{q}{k_F} \sin \phi \right) + \sin 3\theta_{\mathbf{q}} \cos \left( 3\phi - 2\frac{q}{k_F} \sin \phi \right), \end{aligned} \quad (\text{A.137})$$

and we denoted  $\arccos(s)$  by  $\phi$ . Also,

$$\begin{aligned}
\frac{\mu^2 - (\mu - \omega)^2}{2\pi v_F^2 v_F q \sqrt{1 - s^2}} &\approx \frac{2\mu\omega}{2\pi v_F^2 v_F q} = 2\mathcal{N}(\mu)s, \quad \cos \phi = s, \\
\cos\left(\phi - a\frac{q}{k_F}\sin\phi\right) &= \cos\phi \cos\left(a\frac{q}{k_F}\sin\phi\right) + \sin\phi \sin\left(a\frac{q}{k_F}\sin\phi\right) \\
&\approx s\left(1 - \frac{1}{2}\left(a\frac{q}{k_F}\sqrt{1 - s^2}\right)^2\right) + \sqrt{1 - s^2}a\frac{q}{k_F}\sqrt{1 - s^2}, \\
\cos\left(3\phi - a\frac{q}{k_F}\sin\phi\right) &= \cos 3\phi \cos\left(a\frac{q}{k_F}\sin\phi\right) + \sin 3\phi \sin\left(a\frac{q}{k_F}\sin\phi\right) \\
&\approx (4s^3 - 3s)\left(1 - \frac{1}{2}\left(a\frac{q}{k_F}\sqrt{1 - s^2}\right)^2\right) + \sqrt{1 - (4s^3 - 3s)^2}a\frac{q}{k_F}\sqrt{1 - s^2},
\end{aligned} \tag{A.138}$$

where  $a$  is a number (we are interested in  $a = 1, 3$ ). Thus, to leading order in  $s$ , we find:

$$\text{Im } \Pi^R(\mathbf{q}, \omega) \sim s\frac{q}{k_F} \begin{pmatrix} \cos\theta_{\mathbf{q}} & \sin\theta_{\mathbf{q}} \\ -\sin\theta_{\mathbf{q}} & \cos\theta_{\mathbf{q}} \end{pmatrix} - 3s\frac{q}{k_F} \begin{pmatrix} \cos 3\theta_{\mathbf{q}} & \sin 3\theta_{\mathbf{q}} \\ \sin 3\theta_{\mathbf{q}} & -\cos 3\theta_{\mathbf{q}} \end{pmatrix}. \tag{A.139}$$

The structure in momentum space of Eq. (A.139) may be verified by symmetry. Under rotations, the spin operator transforms like a vector, and the nematic operator, correspond to angular momentum  $l = 2$ , rotates twice as fast as a vector (intuitively, a headless vector returns to itself after rotation by  $\pi$ ). Therefore, we expect:

$$\Pi_{i'j'}^R(R(\theta)\mathbf{q}, \omega) = R(\theta)_{i'i}R(2\theta)_{j'j}\Pi_{ij}^R(\mathbf{q}, \omega) \implies \Pi^R(R(\theta)\mathbf{q}, \omega) = R(\theta)\Pi^R(\mathbf{q}, \omega)R^T(2\theta), \tag{A.140}$$

where  $R(\theta)$  is an  $SO(2)$  rotation matrix through angle  $\theta$  counterclockwise.

One may check that both matrices in Eq. (A.139) satisfy Eq. (A.140). This is especially clear for the first matrix as it also corresponds directly to  $R(\theta)$ , and  $R(\theta)^2 = R(2\theta)$ .

# Appendix B

## Calculations for Chapters 3 and 4

In this Appendix, we show details for the RG calculations done in Chaps. 3 and 4.

### B.1 Replica trick: general idea

Let us suppose that our goal is to calculate the disorder averaged observable  $\overline{\langle O \rangle}$  in a quantum many-body system described by the imaginary-time action  $S$  (the overline is used to denote disorder averaging):

$$\overline{\langle O \rangle} = \frac{\overline{\int D\phi e^{-S[\phi]} O_\phi}}{Z_d}, \quad (\text{B.1})$$

where  $\phi$  denotes an arbitrary collection of quantum fields, bosonic and/or fermionic. The problem in averaging is due to the disorder dependent partition function  $Z_d$  in the denominator. Different theoretical approaches have been developed to circumvent this problem. The most straightforward, but perhaps also most laborious, is local RG in real space [242]. An approach developed by Keldysh [243] assumes integration over a closed contour in real time. This implies that  $Z_d = 1$ , but at the expense of working with matrix-valued real-time propagators. An approach by Efetov based on supersymmetry likewise forces  $Z_d = 1$ , but only applies to noninteracting systems [244]. Here we use the replica trick [30, 156, 157], which applies to arbitrary interacting systems and is formulated directly in imaginary time.

One introduces  $m$  replicas (copies) of the same system and at the end of the calculation takes the  $m \rightarrow 0$  limit:

$$\lim_{m \rightarrow 0} \overline{\int D\phi_1 D\phi_2 \dots D\phi_m e^{-S[\phi_1] - S[\phi_2] - \dots - S[\phi_m]} O_{\phi_1}} = \lim_{m \rightarrow 0} \overline{\int D\phi_1 e^{-S[\phi_1]} O_{\phi_1} Z_d^{m-1}} = \overline{\langle O \rangle}. \quad (\text{B.2})$$

The connection to the partition function of the disordered system is given by

$$\overline{\log Z_d} = \lim_{m \rightarrow 0} \frac{\overline{Z_d^m} - 1}{m} = \lim_{m \rightarrow 0} \frac{1}{m} \log \overline{Z_d^m}. \quad (\text{B.3})$$

As will be shown soon, averaging over quenched disorder via the replica trick in a quantum system introduces a term nonlocal in time in the action of the replicated theory. This may raise a question about the validity of application of RG techniques for studying such systems. In Refs. [218, 219] it has been shown via nonperturbative arguments that the replicated theory in the  $m \rightarrow 0$  limit is equivalent to the local original disordered theory, provided we are only interested in disorder-averaged observables.

### B.1.1 Replica trick: application

We consider the action

$$S = \int d^2 \mathbf{x} d\tau (\mathcal{L}_\phi + \mathcal{L}_\psi + \mathcal{L}_{\psi\phi}), \quad (\text{B.4})$$

where each term for the chiral Ising, XY, and Heisenberg GNY models is defined in the main text.

To describe the random-mass quenched disorder  $r(\mathbf{x}) = r_0 + \delta r(\mathbf{x})$  it is sufficient to specify the first two cumulants as other cumulants generate irrelevant terms near four dimensions:

$$\begin{aligned} \overline{\delta r(\mathbf{x})} &= 0, \\ \overline{\delta r(\mathbf{x}) \delta r(\mathbf{y})} &= g(|\mathbf{x} - \mathbf{y}|) = \frac{v}{|\mathbf{x} - \mathbf{y}|^a} + \Delta \delta(\mathbf{x} - \mathbf{y}). \end{aligned} \quad (\text{B.5})$$

The replicated action is

$$S = \sum_{a=1}^n \int d^d \mathbf{x} d\tau (\mathcal{L}_{\phi_a} + \mathcal{L}_{\psi_a} + \mathcal{L}_{\psi_a \phi_a}). \quad (\text{B.6})$$

Averaging over disorder, we use the cumulant expansion:

$$\overline{e^{f(x)}} = e^{\overline{f(x)} + \frac{1}{2}(\overline{f(x)^2} - \overline{f(x)}^2) + \dots}, \quad (\text{B.7})$$

where  $f(x)$  is a random variable. Specifically,

$$\left\langle e^{\sum_a \int d^d \mathbf{x} d\tau \delta r(\mathbf{x}) \phi^2(\mathbf{x})} \right\rangle_{\text{disorder}} = e^{\frac{1}{2} \int d^d \mathbf{x} d\tau d^d \mathbf{x}' d\tau' \sum_{a,b} \phi_a^2(\mathbf{x}, \tau) \overline{\delta r(\mathbf{x}) \delta r(\mathbf{x}') \phi_b^2(\mathbf{x}', \tau')}}. \quad (\text{B.8})$$

Thus, averaging over disorder in the replicated theory introduces a term that is nonlocal in time (and nonlocal in space for long-range correlated disorder):

$$S = \int d^d \mathbf{x} d\tau (\mathcal{L}_{\phi} + \mathcal{L}_{\psi} + \mathcal{L}_{\psi\phi}) - \frac{1}{2} \int d^d \mathbf{x} d\tau d^d \mathbf{x}' d\tau' \sum_{a,b} \phi_a^2(\mathbf{x}, \tau) \overline{\delta r(\mathbf{x}) \delta r(\mathbf{x}') \phi_b^2(\mathbf{x}', \tau)}. \quad (\text{B.9})$$

## B.2 Field-theoretic RG

We use the field-theoretic RG method, which is built around three functionals [163]:

- the generating functional of correlation functions:

$$Z[J, \bar{\eta}, \eta] = \int \mathcal{D}\phi \mathcal{D}\bar{\psi} \mathcal{D}\psi e^{-S[\phi, \bar{\psi}, \psi] + \int d^d x (J\phi + \bar{\eta}\psi + \bar{\psi}\eta)}. \quad (\text{B.10})$$

- the generating functional of connected correlation functions:

$$W[J, \bar{\eta}, \eta] = \ln Z[J, \bar{\eta}, \eta], \quad (\text{B.11})$$

- and the generating functional of proper vertices, also known as the one-particle irre-

ducible (1PI) effective action:

$$\Gamma [\phi', \bar{\psi}', \psi'] = -W [\phi', \bar{\psi}', \psi'] + \int d^d x (J\phi' + \bar{\eta}\psi' + \bar{\psi}'\eta), \quad (\text{B.12})$$

which is the Legendre transform of  $W$ .

To calculate  $\Gamma$  to one-loop order, we expand the generating functional  $Z$  about the classical (saddle point) solution to quadratic order in the fields:

$$\begin{aligned} Z[J, \bar{\eta}, \eta] &= \int \mathcal{D}\delta\phi \mathcal{D}\delta\bar{\psi} \mathcal{D}\delta\psi e^{(-S[\phi_{\text{cl}}+\delta\phi, \bar{\psi}_{\text{cl}}+\delta\bar{\psi}, \psi_{\text{cl}}+\delta\psi] + \int d^d x (J\phi + \bar{\eta}\psi + \bar{\psi}\eta))} \\ &= \int \mathcal{D}\delta\phi \mathcal{D}\delta\bar{\psi} \mathcal{D}\delta\psi e^{-S_{\text{cl}} + \int d^d x (J\phi_{\text{cl}} + \bar{\eta}\psi_{\text{cl}} + \bar{\psi}_{\text{cl}}\eta) - \delta^2 S + \dots}, \end{aligned} \quad (\text{B.13})$$

where the classical solutions are determined from

$$\frac{\delta S}{\delta\phi_{\text{cl}}} = J, \quad \frac{\delta S}{\delta\bar{\psi}_{\text{cl}}} = \eta, \quad \frac{\delta S}{\delta\psi_{\text{cl}}} = -\bar{\eta}. \quad (\text{B.14})$$

For the Ising model, we find

$$\begin{aligned} \delta^2 S &= \sum_a \int d^d \mathbf{x} d\tau (i\delta\bar{\psi}_a (\not{\partial}_\tau + \not{\nabla}) \delta\psi_a + \delta\phi_a (-\partial_b^2 + r) \delta\phi_a + 6\lambda^2 \phi_a^2 \delta\phi_a^2 \\ &\quad + ih\phi_a \delta\bar{\psi}_a \delta\psi_a + ih\bar{\psi}_a \delta\phi_a \delta\psi_a + ih\delta\phi_a \bar{\psi}_a \delta\psi_a) \\ &\quad - \frac{1}{2} \int d^d \mathbf{x} d\tau d^d \mathbf{x}' d\tau' \sum_{a,b} \delta\phi_a(\mathbf{x}, \tau) M_{ab}(\mathbf{x}\tau; \mathbf{x}'\tau') \delta\phi_b(\mathbf{x}', \tau'), \end{aligned} \quad (\text{B.15})$$

where

$$M_{ab} = 2\delta(\mathbf{x} - \mathbf{x}')\delta(\tau - \tau')\delta_{ab} \sum_c \int d^d \mathbf{x}'' d\tau'' g(\mathbf{x} - \mathbf{x}'')\phi_c^2(\mathbf{x}'', \tau'') + 4g(\mathbf{x} - \mathbf{x}')\phi_a(\mathbf{x}, \tau)\phi_b(\mathbf{x}', \tau'). \quad (\text{B.16})$$

For the XY model, we first recast the theory in terms of Nambu spinors  $\Psi = (\psi, C\bar{\psi}^T)$ , where  $C = i\sigma_2$  is a charge-conjugation matrix:

$$S = \sum_a \int d^d x d^{\epsilon\tau} \tau \left( \frac{1}{2} \Psi_a^T \mathcal{C} (\mathcal{G}_0^{-1} + X_a) \Psi_a + |\partial_\mu \phi_a|^2 + r |\phi_a|^2 + \lambda^2 |\phi_a|^4 \right), \quad (\text{B.17})$$

where

$$\mathcal{C} = \begin{pmatrix} C & 0 \\ 0 & C \end{pmatrix}, \quad \mathcal{G}_0^{-1} = \begin{pmatrix} 0 & G_0^{-1} \\ G_0^{-1} & 0 \end{pmatrix}, \quad X_a = \begin{pmatrix} 2h\phi_a^* & 0 \\ 0 & -2h\phi_a \end{pmatrix}, \quad (\text{B.18})$$

and  $G_0^{-1}$  is the inverse propagator of the original (not replicated) system. Then

$$\begin{aligned} \delta^2 S &= \sum_a \int d^d x d^{\epsilon\tau} \tau \left( \delta\phi_a^* (-\partial^2 + r) \delta\phi_a + \lambda^2 (\phi_a^2 \delta\phi_a^{*2} + 4|\phi_a|^2 \delta\phi_a^* \delta\phi_a + \phi_a^{*2} \delta\phi_a^2) \right. \\ &\quad \left. + \frac{1}{2} \delta\Psi_a^T \mathcal{C} (\mathcal{G}_0^{-1} + X_a) \delta\Psi_a + \Psi_a^T \mathcal{C} \delta X_a \delta\Psi_a \right) \\ &\quad - \frac{1}{2} \int d^d \mathbf{x} d\tau d^d \mathbf{x}' d\tau' \sum_{a,b} \delta\phi_a(\mathbf{x}, \tau) M_{ab}(\mathbf{x}\tau; \mathbf{x}'\tau') \delta\phi_b(\mathbf{x}', \tau'), \end{aligned} \quad (\text{B.19})$$

where  $M_{ab}$  is a  $2 \times 2$  matrix with components

$$\begin{aligned} M_{ab}^{11} &= 2g(\mathbf{x} - \mathbf{x}') \phi_a(\mathbf{x}, \tau) \phi_b(\mathbf{x}', \tau'), \\ M_{ab}^{12} &= 2 \int d^d \mathbf{x}'' d\tau'' g(\mathbf{x} - \mathbf{x}'') \sum_c \phi^2(\mathbf{x}'', \tau'') \delta(\mathbf{x} - \mathbf{x}') \delta(\tau - \tau') \delta_{ab} \delta_{ij} + 2g(\mathbf{x} - \mathbf{x}') \phi_a(\mathbf{x}, \tau) \phi_b^*(\mathbf{x}', \tau'), \\ M_{ab}^{21} &= (M_{ab}^{12})^*, \quad M_{ab}^{22} = (M_{ab}^{11})^*. \end{aligned} \quad (\text{B.20})$$

For the Heisenberg model,

$$\begin{aligned} \delta^2 S &= \sum_a \int d^d \mathbf{x} d\tau \left( i\delta\bar{\psi}_a (\not{\partial}_\tau + \not{\nabla}) \delta\psi_a + \delta\phi_a (-\partial_b^2 + r) \delta\phi_a + \lambda^2 \sum_{ij} \delta\phi_a^i (4\phi_a^i \phi_a^j + 2\phi_a^2 \delta_{ij}) \delta\phi_a^j \right. \\ &\quad \left. + ih\delta\bar{\psi}_a \phi_a \cdot \boldsymbol{\sigma} \delta\psi_a + ih\delta\phi_a \cdot \delta\bar{\psi}_a \boldsymbol{\sigma} \psi_a + ih\delta\phi_a \cdot \bar{\psi}_a \boldsymbol{\sigma} \delta\psi_a \right) \\ &\quad - \frac{1}{2} \int d^d \mathbf{x} d\tau d^d \mathbf{x}' d\tau' \sum_{a,b} \delta\phi_a(\mathbf{x}, \tau) M_{ab}(\mathbf{x}\tau; \mathbf{x}'\tau') \delta\phi_b(\mathbf{x}', \tau'), \end{aligned} \quad (\text{B.21})$$

where the Pauli matrices only act in spin space, and  $M_{ab}$  is a  $3 \times 3$  matrix with components

$$M_{ab}^{ij} = 2\delta(\mathbf{x} - \mathbf{x}')\delta(\tau - \tau')\delta_{ab} \sum_c \int d^d \mathbf{x}'' d\tau'' g(\mathbf{x} - \mathbf{x}'')\phi^2(\mathbf{x}'', \tau'') + 4\phi_a^i(\mathbf{x}, \tau)\phi_b^j(\mathbf{x}', \tau'). \quad (\text{B.22})$$

One may see that for the Ising model the matrix  $M_{ab}$  has the same form as the matrix  $M_{ab}$  in the Heisenberg case. For the XY model, in the vector representation of the bosonic field, the corresponding matrix  $M_{ab}$  would also have the same form as in the Heisenberg case. Thus, for all three models, we expect the same contribution to beta functions from the diagrams that include only disorder vertices.

Integrating out the fermionic fields, we obtain:

- for the Ising model:

$$\int \prod_{a=1}^m \mathcal{D}\delta\psi_a \mathcal{D}\delta\bar{\psi}_a e^{-\sum_a \int d^d \mathbf{x} d\tau (i\delta\bar{\psi}_a (\not{\partial}_\tau + \not{\nabla}) \delta\psi_a + ih\phi_a \delta\bar{\psi}_a \delta\psi_a + ih\bar{\psi}_a \delta\phi_a \delta\psi_a + ih\delta\phi_a \bar{\psi}_a \delta\psi_a)} = \prod_{a=1}^m \det(G_0^{-1} + ih\phi_a) e^{-\sum_a \int d^d \mathbf{x} d\tau h\bar{\psi}_a \delta\phi_a (G_0^{-1} + ih\phi_a)^{-1} h\psi_a \delta\phi_a}, \quad (\text{B.23})$$

- for the XY model:

$$\int \prod_{a=1}^m \mathcal{D}\delta\Psi_a \exp\left(-\sum_a \int d^d \mathbf{x} d\tau \left(\frac{1}{2}\delta\Psi_a^T \mathcal{C} (\mathcal{G}_0^{-1} + X_a) \delta\Psi_a + \Psi_a^T \mathcal{C} \delta X \delta\Psi_a\right)\right) = \prod_{a=1}^m (\det \mathcal{C} (\mathcal{G}_0^{-1} + X_a))^{\frac{1}{2}} e^{-\sum_a \int d^d \mathbf{x} d\tau \left(\frac{1}{2}\Psi_a^T \mathcal{C} \delta X_a (\mathcal{G}_0^{-1} + X_a)^{-1} \mathcal{C}^{-1} \delta X_a^T \mathcal{C}^T \Psi_a\right)}, \quad (\text{B.24})$$

- for the Heisenberg model:

$$\begin{aligned}
& \int \prod_{a=1}^m \mathcal{D}\delta\psi_a \mathcal{D}\delta\bar{\psi}_a e^{-\sum_a \int d^d \mathbf{x} d\tau (i\delta\bar{\psi}_a (\not{\partial}_\tau + \nabla) \delta\psi_a + ih\delta\bar{\psi}_a \phi_a \cdot \sigma \delta\psi_a + ih\delta\phi_a \cdot \delta\bar{\psi}_a \sigma \psi_a + ih\delta\phi_a \cdot \bar{\psi}_a \sigma \delta\psi_a)} = \\
& \prod_{a=1}^m \det (G_0^{-1} + h\phi_a \cdot \sigma) e^{-\sum_a \int d^d \mathbf{x} d\tau h\bar{\psi}_a \delta\phi_a \cdot \sigma (G_0^{-1} + h\phi_a \cdot \sigma)^{-1} h\delta\phi_a \cdot \sigma \psi_a}.
\end{aligned} \tag{B.25}$$

Finally, reexponentiating determinants using  $\det M = \exp(\text{Tr} \ln M)$  and integrating out bosonic fields, we obtain for the effective action at one-loop order:

$$\Gamma = \text{Tr} \ln \left( G^{-1} + X \right) + \frac{1}{2} \text{Tr} \ln \left( D^{-1} + \Xi - \frac{M}{2} \right), \tag{B.26}$$

where  $G^{-1}$  and  $D^{-1}$  are the inverse of the propagators of the replicated system defined in Eqs. (3.34), (3.35) and (4.25). We will also use propagators for an individual replica  $G_a$  and  $D_a$  such that  $G = \bigoplus_{a=1}^m G_a$  and  $D = \bigoplus_{a=1}^m D_a$ , where  $\bigoplus$  denotes the matrix direct sum, and we also denote the operator which in momentum space has the form  $\frac{1}{c^2 p_0^2 + \mathbf{p}^2 + \mu^2 r}$  by  $D^0$ . The form of the matrices  $X$  and  $\Xi$  depends on the model:

- for the Ising model we have

$$X = \bigoplus_{a=1}^m X_a = \bigoplus_{a=1}^m h\phi_a, \quad \Xi = \bigoplus_{a=1}^m \Xi_a = \bigoplus_{a=1}^m \left( 6\lambda^2 \phi_a^2 + h^2 \bar{\psi}_a \left( G_{0,a}^{-1} + X_a \right)^{-1} \psi_a \right). \tag{B.27}$$

- for the XY model we have

$$X = \bigoplus_{a=1}^m X_a, \quad \Xi = \bigoplus_{a=1}^m \Xi_a = \bigoplus_{a=1}^m \left( 2\lambda^2 \begin{pmatrix} \phi_a^2 & 2|\phi_a|^2 \\ 2|\phi_a|^2 & \phi_a^{*2} \end{pmatrix} - 4h^2 Y_a^T \mathcal{C} \left( \mathcal{G}_{0,a}^{-1} + X_a \right)^{-1} Y_a \right), \tag{B.28}$$

where

$$Y_a = \begin{pmatrix} \psi_a & 0 \\ 0 & -C\psi_a^T \end{pmatrix}, \quad (\text{B.29})$$

and we also explicitly write down the expression for  $D^{-1}$  in complex boson notation

$$D^{-1} = \bigoplus_{a=1}^m D_a^{-1} = \bigoplus_{a=1}^m \begin{pmatrix} 0 & -\partial^2 + r \\ -\partial^2 + r & 0 \end{pmatrix}. \quad (\text{B.30})$$

- for the Heisenberg model

$$X = \bigoplus_{a=1}^m X_a = \bigoplus_{a=1}^m ih\phi_a \cdot \boldsymbol{\sigma}, \quad \Xi = \bigoplus_{a=1}^m \Xi_a, \quad (\text{B.31})$$

where  $\Xi_a$  is a  $3 \times 3$  matrix with components

$$\Xi_a^{ij} = \lambda^2(4\phi_a^i\phi_a^j + 2\phi^2\delta_{ij}) + h^2\bar{\psi}_a\sigma_i \left(G_{0,a}^{-1} + X_a\right)^{-1} \sigma_j\psi_a. \quad (\text{B.32})$$

Expanding logarithms to quadratic order in the couplings  $h^2$ ,  $\lambda^2$ ,  $\Delta$ , and  $v$ , which are all of the same order in the epsilon expansion, we find for the divergent part of the effective action:

$$\begin{aligned} \Gamma_{\text{div}} = & -\text{Tr} \left\{ GX - \frac{1}{2}(GX)^2 + \frac{1}{3}(GX)^3 - \frac{1}{4}(GX)^4 \right\} \\ & + \frac{1}{2}\text{Tr} \left\{ D\Xi - \Pi\frac{M}{2} - \frac{1}{2}(D\Xi)^2 + D\Xi D\frac{M}{2} - \frac{1}{2}\left(D\frac{M}{2}\right)^2 \right\}. \end{aligned} \quad (\text{B.33})$$

UV divergences in the one-loop effective action appear as simple poles in linear combinations of the small epsilon parameters. The renormalization constants are then obtained by demanding the cancellation of these divergences by appropriate infinite counterterms.

### B.2.1 Calculating traces

In this section we calculate traces. First, it is easy to notice that traces of odd powers of  $GX$  vanish. For the trace of the second power of  $GX$  we have:

$$\begin{aligned} \text{Tr}(GXGX) &= \text{tr} \sum_{\text{all indices}} G_{\mathbf{x}\tau, \mathbf{x}'\tau'} X_{\mathbf{x}'\tau', \mathbf{x}''\tau''} G_{\mathbf{x}''\tau'', \mathbf{x}'''\tau'''} X_{\mathbf{x}'''\tau''', \mathbf{x}\tau} \\ &= \text{tr} \sum_{\text{all indices}} G_{\mathbf{x}\tau, \mathbf{x}'\tau'} X(\mathbf{x}'\tau') G_{\mathbf{x}'\tau', \mathbf{x}\tau} X(\mathbf{x}\tau), \end{aligned} \quad (\text{B.34})$$

where going from the first to the second line we used the fact that  $X_{\mathbf{x}\tau, \mathbf{x}'\tau'} = X(\mathbf{x}\tau)\delta(\mathbf{x} - \mathbf{x}')\delta(\tau - \tau')$ . Here by sum over continuous variables (spatial and time coordinates) we mean integrals, and use this notation for convenience. By a lowercase tr we mean a trace over the remaining discrete indices (field components, flavor, and replica indices). Analogously,

$$\begin{aligned} \text{Tr}(GXGX)^2 &= \text{tr} \sum_{\text{all indices}} G_{\mathbf{x}\tau, \mathbf{x}'\tau'} X(\mathbf{x}'\tau') G_{\mathbf{x}'\tau', \mathbf{x}''\tau''} X(\mathbf{x}''\tau'') \\ &\quad \times G_{\mathbf{x}''\tau'', \mathbf{x}'''\tau'''} X(\mathbf{x}'''\tau''') G_{\mathbf{x}'''\tau''', \mathbf{x}\tau} X(\mathbf{x}\tau). \end{aligned} \quad (\text{B.35})$$

To pick out the divergent part in  $\text{Tr}(D\Xi)$ , it is sufficient to expand the second term in  $\Xi_a$  to first order in  $G_a X_a$ . As a concrete example, we use the Ising model:

$$\Xi_a = 6\lambda^2 \phi_a^2 + h^2 \bar{\psi}_a \left( G_{0,a}^{-1} + X_a \right)^{-1} \psi_a \rightarrow 6\lambda^2 \phi_a^2 + h^2 \bar{\psi}_a G_a \psi_a + h^2 \bar{\psi}_a G_a^2 X_a \psi_a. \quad (\text{B.36})$$

Analogously, for other models, the first and second terms in  $\Xi_a$  include only  $\phi$  and  $\psi$  fields, respectively. The third term contains both  $\phi$  and  $\psi$  fields. To keep calculations general, we write

$$\Xi = \Xi_\phi + L_\psi \left( G_a^{-1} + X_a \right)^{-1} R_\psi \rightarrow \Xi_\phi + L_\psi G_a R_\psi - L_\psi G_a^2 X_a R_\psi, \quad (\text{B.37})$$

where  $L_\psi$  and  $R_\psi$  for each model are identified by comparison with Eqs. (B.27), (B.28) and (B.32).

Thus, we have

$$\begin{aligned} \text{Tr}(D\Xi) &= \sum_{\text{all indices}} D_{\mathbf{x}\tau, \mathbf{x}\tau} \Xi(\mathbf{x}\tau) + \sum_{\text{all indices}} D_{\mathbf{x}\tau, \mathbf{x}'\tau'} L_\psi(\mathbf{x}'\tau') G_{\mathbf{x}'\tau', \mathbf{x}\tau} R_\psi(\mathbf{x}\tau) \\ &\quad - \sum_{\text{all indices}} D_{\mathbf{x}\tau, \mathbf{x}'\tau'} L_\psi(\mathbf{x}'\tau') G_{\mathbf{x}'\tau', \mathbf{x}''\tau''} G_{\mathbf{x}''\tau'', \mathbf{x}\tau} X_a(\mathbf{x}\tau) R_\psi(\mathbf{x}\tau). \end{aligned} \quad (\text{B.38})$$

To evaluate the divergent part in  $\text{Tr}(D\Xi)^2$ , it is sufficient to retain the first term in  $\Xi$ :

$$\text{Tr}(D\Xi)^2 \rightarrow \text{Tr}(D\Xi_\phi)^2 = \sum_{\text{all indices}} D_{\mathbf{x}\tau, \mathbf{x}'\tau'} \Xi_\phi(\mathbf{x}'\tau') D_{\mathbf{x}'\tau', \mathbf{x}\tau} \Xi_\phi(\mathbf{x}\tau). \quad (\text{B.39})$$

At one-loop order, traces that include disorder vertices induce corrections only to purely bosonic vertices. As was mentioned before, the structure of the matrix  $M$  is the same for all three models, and we write these traces using the vector representation of the  $O(n)$  bosonic field. We have

$$\begin{aligned} \text{Tr}\left(D\frac{M}{2}\right) &= \sum_{\text{all indices}} D_{\mathbf{x}\tau, \mathbf{x}'\tau'}^0 \delta_{ij} \delta_{ab} \frac{M_{ba}^{ji}}{2} = \sum_{\text{all indices}} D_{\mathbf{x}\tau, \mathbf{x}'\tau'}^0 \frac{M_{aa}^{ii}}{2} \\ &= \sum_a \int d^D x d^D x' \frac{d^D p}{(2\pi)^D} \frac{1}{c^2 p_0^2 + \mathbf{p}^2 + \mu^2 r} \sum_c \int d^d \mathbf{x}'' d\tau'' g(\mathbf{x} - \mathbf{x}'') \phi^2(\mathbf{x}'', \tau'') \\ &\quad + 2 \sum_{a,i} \int d^D x d^D x' \frac{d^D p}{(2\pi)^D} \frac{e^{-ip \cdot (\mathbf{x} - \mathbf{x}')}}{c^2 p_0^2 + \mathbf{p}^2 + \mu^2 r} g(\mathbf{x}' - \mathbf{x}) \phi_a^i(\mathbf{x}, \tau) \phi_a^i(\mathbf{x}', \tau'), \end{aligned} \quad (\text{B.40})$$

where  $D$  in the superscripts of the integration measures (not to be confused with the propagator  $D$ ) is the dimensionality of space-time.

To assess the divergent part in  $\text{Tr}(D\Xi D\frac{M}{2})$ , we again may retain only the first term

in  $\Xi$ :

$$\begin{aligned}
\text{Tr} \left( D \Xi D \frac{M}{2} \right) &\rightarrow \text{Tr} \left( D \Xi_\phi D \frac{M}{2} \right) = \sum_{\text{all indices}} D_{aa;\mathbf{x}\tau,\mathbf{x}'\tau'}^{ii} \Xi_{\phi a}^{ij}(\mathbf{x}', \tau') D_{aa;\mathbf{x}'\tau',\mathbf{x}''\tau''}^{jj} \frac{M_{aa}^{ji}}{2} \\
&= \lambda^2 \sum_{\text{all indices}} D_{aa;\mathbf{x}\tau,\mathbf{x}'\tau'}^{ii} (4\phi_a^i \phi_a^j + 2\phi^2 \delta_{ij}) \Big|_{(\mathbf{x}', \tau')} D_{aa;\mathbf{x}'\tau',\mathbf{x}''\tau''}^{jj} (\delta(\mathbf{x}'' - \mathbf{x}) \delta(\tau'' - \tau) \\
&\quad \sum_c \int d^d \mathbf{x}''' d\tau''' g(\mathbf{x}'' - \mathbf{x}''') \phi^2(\mathbf{x}''', \tau''') + 2\phi_a^j(\mathbf{x}'', \tau'') \phi_a^i(\mathbf{x}, \tau)).
\end{aligned} \tag{B.41}$$

Expanding, we obtain

$$\begin{aligned}
\text{Tr} \left( D \Xi D \frac{M}{2} \right) &= \lambda^2 \sum_{a;\mathbf{x}\tau,\mathbf{x}'\tau',\mathbf{x}''\tau''} \left\{ 8 \sum_{ij} D_{aa;\mathbf{x}\tau,\mathbf{x}'\tau'}^{ii} \phi_a^i \phi_a^j \Big|_{(\mathbf{x}', \tau')} \right. \\
&\quad \times D_{aa;\mathbf{x}'\tau',\mathbf{x}''\tau''}^{jj} \phi_a^j(\mathbf{x}'', \tau'') \phi_a^i(\mathbf{x}, \tau) g(\mathbf{x}'' - \mathbf{x}) \\
&\quad + 4 \sum_i D_{aa;\mathbf{x}\tau,\mathbf{x}'\tau'}^{ii} \phi_a^2(\mathbf{x}', \tau') D_{aa;\mathbf{x}'\tau',\mathbf{x}''\tau''}^{ii} \phi_a^i(\mathbf{x}'', \tau'') \phi_a^i(\mathbf{x}, \tau) g(\mathbf{x}'' - \mathbf{x}) \\
&\quad + 4 D_{aa;\mathbf{x}\tau,\mathbf{x}'\tau'}^{ii} \phi_a^2(\mathbf{x}', \tau') D_{aa;\mathbf{x}'\tau',\mathbf{x}\tau}^{ii} \int d^d \mathbf{x}'' d\tau'' g(\mathbf{x}'' - \mathbf{x}) \sum_c \phi_c^i(\mathbf{x}'', \tau'')^2 \\
&\quad \left. + 2 \sum_i D_{aa;\mathbf{x}\tau,\mathbf{x}'\tau'}^{ii} \phi_a^2(\mathbf{x}', \tau') D_{aa;\mathbf{x}'\tau',\mathbf{x}\tau}^{ii} \int d^d \mathbf{x}'' d\tau'' g(\mathbf{x}'' - \mathbf{x}) \sum_c \phi_c^i(\mathbf{x}'', \tau'')^2 \right\}.
\end{aligned} \tag{B.42}$$

Grouping similar terms, we finally have

$$\begin{aligned}
\text{Tr} \left( D \Xi D \frac{M}{2} \right) &= \lambda^2 \sum_{a;\mathbf{x}\tau,\mathbf{x}'\tau',\mathbf{x}''\tau''} \left\{ 8 \sum_{ij} D_{aa;\mathbf{x}\tau,\mathbf{x}'\tau'}^{ii} \phi_a^i \phi_a^j \Big|_{(\mathbf{x}', \tau')} \right. \\
&\quad \times D_{aa;\mathbf{x}'\tau',\mathbf{x}''\tau''}^{jj} \phi_a^j(\mathbf{x}'', \tau'') \phi_a^i(\mathbf{x}, \tau) g(\mathbf{x}'' - \mathbf{x}) \\
&\quad + 4 \sum_i D_{aa;\mathbf{x}\tau,\mathbf{x}'\tau'}^{ii} \phi_a^2(\mathbf{x}', \tau') D_{aa;\mathbf{x}'\tau',\mathbf{x}''\tau''}^{ii} \phi_a^i(\mathbf{x}'', \tau'') \phi_a^i(\mathbf{x}, \tau) g(\mathbf{x}'' - \mathbf{x}) \\
&\quad \left. + 2(n+2) D_{aa;\mathbf{x}\tau,\mathbf{x}'\tau'}^{ii} \phi_a^2(\mathbf{x}', \tau') D_{aa;\mathbf{x}'\tau',\mathbf{x}\tau}^{ii} \int d^d \mathbf{x}'' d\tau'' g(\mathbf{x}'' - \mathbf{x}) \sum_c \phi_c^i(\mathbf{x}'', \tau'')^2 \right\}.
\end{aligned} \tag{B.43}$$

Finally, for  $\text{Tr} \left( \Pi \frac{M}{2} \right)^2$ , we obtain

$$\begin{aligned}
\text{Tr} \left( \Pi \frac{M}{2} \right)^2 &= \sum_{a; \mathbf{x}\tau, \mathbf{x}'\tau', \mathbf{x}''\tau''} \left\{ \sum_i D_{aa; \mathbf{x}\tau, \mathbf{x}\tau}^{ii} \int d^d \mathbf{x}' d\tau' g(\mathbf{x}' - \mathbf{x}) \sum_c \phi_c^i(\mathbf{x}', \tau')^2 \right. \\
&\times D_{aa; \mathbf{x}\tau, \mathbf{x}\tau}^{ii} \int d^d \mathbf{x}'' d\tau'' g(\mathbf{x}'' - \mathbf{x}) \sum_c \phi_c^i(\mathbf{x}'', \tau'')^2 \\
&+ 2 \sum_i D_{aa; \mathbf{x}\tau, \mathbf{x}'\tau'}^{ii} \int d^d \mathbf{x}''' d\tau''' g(\mathbf{x}''' - \mathbf{x}') \sum_c \phi_c^i(\mathbf{x}''', \tau''')^2 D_{aa; \mathbf{x}'\tau', \mathbf{x}''\tau''}^{ii} g(\mathbf{x}'' - \mathbf{x}) \phi_a^i(\mathbf{x}'', \tau'') \phi_a^i(\mathbf{x}, \tau) \\
&+ 2 D_{aa; \mathbf{x}\tau, \mathbf{x}'\tau'}^{ii} g(\mathbf{x}' - \mathbf{x}'') \phi_a^i(\mathbf{x}', \tau') \phi_a^i(\mathbf{x}'', \tau'') D_{aa; \mathbf{x}''\tau'', \mathbf{x}\tau}^{ii} \int d^d \mathbf{x}''' d\tau''' g(\mathbf{x}''' - \mathbf{x}) \sum_c \phi_c^i(\mathbf{x}''', \tau''')^2 \\
&\left. + 4 D_{aa; \mathbf{x}\tau, \mathbf{x}'\tau'}^{ii} g(\mathbf{x}' - \mathbf{x}'') \phi_a^i(\mathbf{x}', \tau') \phi_a^j(\mathbf{x}'', \tau'') D_{aa; \mathbf{x}''\tau'', \mathbf{x}'''\tau'''}^{ii} g(\mathbf{x}''' - \mathbf{x}) \phi_b^j(\mathbf{x}''', \tau''') \phi_a^i(\mathbf{x}, \tau) \right\}. \tag{B.44}
\end{aligned}$$

### B.3 Calculating Feynman diagrams

In this section we evaluate expressions obtained in the previous section. We focus on the XY GNY model with short-range correlated disorder first, which is the focus of Chapter 3. Contributions from long-range correlated disorder are considered in the next section.

#### B.3.1 Boson two-point function

The diagrams are given in Fig. 3.3(a,b,c). The diagram in Fig. 3.3(a) is produced by the first term in the expression for  $\text{Tr}(D\xi)$  (Eq. (B.38)), for which we obtain

$$\delta\Gamma_{\text{div}}^{(a)} = 4\lambda^2 \int \frac{d^{\epsilon_\tau} p_0}{(2\pi)^{\epsilon_\tau}} \int \frac{d^d \mathbf{p}}{(2\pi)^d} \frac{1}{c^2 p_0^2 + \mathbf{p}^2 + r\mu^2} \sum_a \int d^d \mathbf{x} \int d^{\epsilon_\tau} \tau |\phi_a|^2. \tag{B.45}$$

Here and in the rest of this Appendix momentum integrals are evaluated in the limit  $\epsilon, \epsilon_\tau \rightarrow 0$ , discarding all finite terms. We obtain

$$\int \frac{d^{\epsilon_\tau} p_0}{(2\pi)^{\epsilon_\tau}} \int \frac{d^d \mathbf{p}}{(2\pi)^d} \frac{1}{c^2 p_0^2 + \mathbf{p}^2 + r\mu^2} = -\frac{r\mu^2}{8\pi^2(\epsilon - \epsilon_\tau)}, \tag{B.46}$$

thus

$$\delta Z_r^{(a)} = \frac{\lambda^2}{2\pi^2(\epsilon - \epsilon_\tau)}. \quad (\text{B.47})$$

The diagram in Fig. 3.3(c) is produced by the second term in the expression for  $\text{Tr}(D\frac{M}{2})$  (Eq. (B.40)) (the first term vanishes in the replica limit  $m \rightarrow 0$ ), for which we have

$$\delta\Gamma_{\text{div}}^{(c)} = -\Delta \sum_a \int \frac{d^D k}{(2\pi)^D} |\phi_a(k)|^2 \int \frac{d^d \mathbf{p}}{(2\pi)^d} \frac{1}{c^2 k_0^2 + \mathbf{p}^2 + r\mu^2}, \quad (\text{B.48})$$

where  $d^D k = d^{\epsilon_\tau} k_0 d^d \mathbf{k}$ . Using

$$\int \frac{d^d \mathbf{p}}{(2\pi)^d} \frac{1}{c^2 k_0^2 + \mathbf{p}^2 + r\mu^2} = -\frac{c^2 k_0^2 + r\mu^2}{8\pi^2 \epsilon}, \quad (\text{B.49})$$

we find

$$\delta Z_3^{(c)} = -\frac{\Delta}{8\pi^2 \epsilon}, \quad \delta Z_r^{(c)} = -\frac{\Delta}{8\pi^2 \epsilon}. \quad (\text{B.50})$$

The diagram in Fig. 3.3(b) is produced by  $\text{Tr}((GX)^2)$  (Eq. (B.34)), for which we have

$$\delta\Gamma_{\text{div}}^{(b)} = -2Nh^2 \sum_a \int \frac{d^D k}{(2\pi)^D} \phi_a^*(k) \int \frac{d^D p}{(2\pi)^D} \text{tr} \frac{\not{p}(\not{p} + \not{k})}{p^2(p+k)^2} \phi_a(k), \quad (\text{B.51})$$

where  $\text{tr}$  denotes a trace over spinor indices. Using Feynman parameters to express

$$\frac{1}{p^2(p+k)^2} = \int_0^1 \frac{dx}{[xp^2 + (1-x)(p+k)^2]^2}, \quad (\text{B.52})$$

and shifting the integration variable  $p \rightarrow p - (1-x)k$ , we obtain

$$\int \frac{d^D p}{(2\pi)^D} \text{tr} \frac{\not{p}(\not{p} + \not{k})}{p^2(p+k)^2} = -\frac{k^2}{8\pi^2(\epsilon - \epsilon_\tau)}, \quad (\text{B.53})$$

using the fact that the gamma matrices are two-dimensional, as well as the 't Hooft-Veltman prescription [245],

$$\int \frac{d^D p}{(2\pi)^D} \frac{1}{p^2} = 0. \quad (\text{B.54})$$

We thus obtain

$$\delta Z_3^{(\text{b})} = -\frac{Nh^2 c^{-2}}{4\pi^2(\epsilon - \epsilon_\tau)}, \quad \delta Z_4^{(\text{b})} = -\frac{Nh^2}{4\pi^2(\epsilon - \epsilon_\tau)}. \quad (\text{B.55})$$

### B.3.2 Fermion two-point function

A unique diagram, Fig. 3.3(d), contributes to the renormalization of the fermion two-point function. It is produced by the second term in the expression for  $\text{Tr}(D\Xi)$  (Eq. (B.38)), and the corresponding divergent part of the effective action is

$$\delta\Gamma_{\text{div}}^{(\text{d})} = 4h^2 \sum_a \int \frac{d^D k}{(2\pi)^D} \bar{\psi}_a(k) \int \frac{d^D p}{(2\pi)^D} \frac{\not{p} + \not{k}}{(c^2 p_0^2 + \mathbf{p}^2)(p+k)^2} \psi_a(k). \quad (\text{B.56})$$

Using Feynman parameters as in Eq. (B.52), and shifting  $\mathbf{p} \rightarrow \mathbf{p} - (1-x)\mathbf{k}$  to perform the integral over  $\mathbf{p}$  first, we have

$$I_1 \equiv \int \frac{d^D p}{(2\pi)^D} \frac{\not{p} + \not{k}}{(c^2 p_0^2 + \mathbf{p}^2)(p+k)^2} = \frac{\Gamma(\epsilon/2)}{(4\pi)^{d/2}} \int_0^1 dx \int \frac{d^{\epsilon_\tau} p_0}{(2\pi)^{\epsilon_\tau}} \frac{\gamma_0(p_0 + k_0) + x\gamma \cdot \mathbf{k}}{(M^2)^{\epsilon/2}}, \quad (\text{B.57})$$

where

$$M^2 = (1 + (c^2 - 1)x) \left[ \ell_0^2 + \frac{x(1-x)\mathbf{k}^2}{1 + (c^2 - 1)x} + \frac{x(1-x)c^2 k_0^2}{(1 + (c^2 - 1)x)^2} \right], \quad (\text{B.58})$$

with

$$\ell_0 = p_0 + \frac{(1-x)k_0}{1 + (c^2 - 1)x}. \quad (\text{B.59})$$

Shifting the integral over  $p_0$  to one over  $\ell_0$ , we have, in the limit  $\epsilon, \epsilon_\tau \rightarrow 0$ ,

$$\begin{aligned} I_1 &= \frac{1}{8\pi^2(\epsilon - \epsilon_\tau)} \int_0^1 dx \left( \frac{xc^2}{1 + (c^2 - 1)x} \gamma_0 k_0 + x \boldsymbol{\gamma} \cdot \mathbf{k} \right) \\ &= \frac{1}{8\pi^2(\epsilon - \epsilon_\tau)} \left( \frac{c^2(c^2 - 1 - \ln c^2)}{(c^2 - 1)^2} \gamma_0 k_0 + \frac{1}{2} \boldsymbol{\gamma} \cdot \mathbf{k} \right). \end{aligned} \quad (\text{B.60})$$

We thus obtain

$$\delta Z_1^{(\text{d})} = -\frac{h^2 f(c^2)}{2\pi^2(\epsilon - \epsilon_\tau)}, \quad \delta Z_2^{(\text{d})} = -\frac{h^2}{4\pi^2(\epsilon - \epsilon_\tau)}, \quad (\text{B.61})$$

with  $f(c^2)$  defined in Eq. (3.44).

### B.3.3 Boson self-interaction

The relevant diagrams are given in Fig. 3.3(e,f,g), where (e) and (g) are meant to include diagrams in all three ( $s, t, u$ ) scattering channels.

The diagram in Fig. 3.3(e) is produced by  $\text{Tr}(D\Xi)^2$  (Eq. (B.38)), for which we have

$$\begin{aligned} \delta\Gamma_{\text{div}}^{(\text{e})} &= -2\lambda^4 \sum_a \int \frac{d^D k}{(2\pi)^D} (4|\phi_a|_{-k}^2 |\phi_a|_k^2 + (\phi_a^{*2})_{-k} (\phi_a^2)_k) \\ &\quad \times \int \frac{d^D p}{(2\pi)^D} \frac{1}{(c^2 p_0^2 + \mathbf{p}^2)(c^2(p_0 + k_0)^2 + (\mathbf{p} + \mathbf{k})^2)}. \end{aligned} \quad (\text{B.62})$$

As before, we use Feynman parameters to perform the integral over  $\mathbf{p}$  first, shifting  $\mathbf{p} \rightarrow \mathbf{p} - (1-x)\mathbf{k}$ ,

$$\begin{aligned} I_2 &\equiv \int \frac{d^D p}{(2\pi)^D} \frac{1}{(c^2 p_0^2 + \mathbf{p}^2)(c^2(p_0 + k_0)^2 + (\mathbf{p} + \mathbf{k})^2)} \\ &= \frac{\Gamma(\epsilon/2)}{(4\pi)^{d/2}} \int_0^1 dx \int \frac{d^{\epsilon_\tau} \ell_0}{(2\pi)^{\epsilon_\tau}} \frac{1}{(c^2 \ell_0^2 + Q^2)^{\epsilon/2}}, \end{aligned} \quad (\text{B.63})$$

with  $Q^2 = x(1-x)(c^2 k_0^2 + \mathbf{k}^2)$ , and we have shifted the integral over  $p_0$  to one over  $\ell_0 = p_0 + (1-x)k_0$ . Performing the integrals over  $\ell_0$  and  $x$ , we obtain  $I_2 = 1/[8\pi^2(\epsilon - \epsilon_\tau)]$ ,

and thus

$$\delta Z_5^{(e)} = \frac{5\lambda^2}{4\pi^2(\epsilon - \epsilon_\tau)}. \quad (\text{B.64})$$

The diagram in Fig. 3.3(f) is produced by  $\text{Tr}((GX)^4)$  (Eq. (B.35)), for which we have

$$\begin{aligned} \delta\Gamma_{\text{div}}^{(f)} &= 4Nh^4 \left( \prod_{i=1}^4 \int \frac{d^D k_i}{(2\pi)^D} \right) (2\pi)^D \delta \left( \sum_{i=1}^4 k_i \right) \phi_a^*(-k_1) \phi(k_2) \phi_a^*(-k_3) \phi_a(k_4) \int \frac{d^D p}{(2\pi)^D} \\ &\quad \times \text{tr} \frac{\not{p}(\not{p} - \not{k}_1)(\not{p} - \not{k}_1 - \not{k}_2)(\not{p} + \not{k}_4)}{p^2(p - k_1)^2(p - k_1 - k_2)^2(p + k_4)^2}. \end{aligned} \quad (\text{B.65})$$

Using four Feynman parameters,

$$\frac{1}{A_1 A_2 A_3 A_4} = 3! \int_0^1 dx \int_0^1 dy \int_0^1 dz \int_0^1 dw \frac{\delta(x + y + z + w - 1)}{(xA_1 + yA_2 + zA_3 + wA_4)^4}, \quad (\text{B.66})$$

as well as

$$\text{tr} \gamma_\mu \gamma_\lambda \gamma_\nu \gamma_\rho = 2(\delta_{\mu\lambda} \delta_{\nu\rho} + \delta_{\lambda\nu} \delta_{\mu\rho} - \delta_{\mu\nu} \delta_{\lambda\rho}), \quad (\text{B.67})$$

to perform the spinor trace, we find that after shifting  $p$  appropriately the denominator can be expressed as  $(p^2 + P^2)^4$  where  $P^2$  is independent of  $p$ , and the numerator contains powers of  $p$  ranging from one to four. For  $D = 4 - (\epsilon - \epsilon_\tau)$ , only the term with  $(p^2)^2$  will give a pole in  $\epsilon - \epsilon_\tau$ . Using

$$\int_0^1 dx \int_0^1 dy \int_0^1 dz \int_0^1 dw \delta(x + y + z + w - 1) = \frac{1}{3!}, \quad (\text{B.68})$$

we find

$$\delta\Gamma_{\text{div}}^{(f)} = \frac{Nh^4}{\pi^2(\epsilon - \epsilon_\tau)} \sum_a \int d^D x |\phi_a|^4, \quad (\text{B.69})$$

and thus

$$\delta Z_5^{(f)} = -\frac{Nh^4\lambda^{-2}}{\pi^2(\epsilon - \epsilon_\tau)}. \quad (\text{B.70})$$

The diagrams with one disorder vertex and one boson self-interaction vertex contribute to the renormalization of both  $\lambda^2$  [Fig. 3.3(g)] and  $\Delta$  [Fig. 3.3(h)]. Here we focus only on those diagrams that contribute to the renormalization of  $\lambda^2$ , which are produced by the first two terms in  $\text{Tr} (D\Xi D\frac{M}{2})$  (Eq. (B.43)). We have

$$\begin{aligned} \delta\Gamma_{\text{div}}^{(g)} &= 2\lambda^2\Delta \sum_a \int \frac{d^D k}{(2\pi)^D} \int \frac{d^D q}{(2\pi)^D} \left( |\phi_a|_{-k}^2 \phi_a^\alpha(k+q)\phi_a^\alpha(-q) + 2(\phi_a^\alpha\phi_a^\beta)_{-k} \phi_a^\alpha(k+q)\phi_a^\beta(-q) \right) \\ &\quad \times \int \frac{d^d \mathbf{p}}{(2\pi)^d} \frac{1}{(c^2q_0^2 + \mathbf{p}^2)(c^2(q_0 + k_0)^2 + (\mathbf{p} + \mathbf{k})^2)}, \end{aligned} \quad (\text{B.71})$$

denoting  $\phi_a^1 = \text{Re } \phi_a$ ,  $\phi_a^2 = \text{Im } \phi_a$ , and with sums over repeated indices  $\alpha, \beta = 1, 2$  understood. Denoting  $m_1^2 = c^2q_0^2$  and  $m_2^2 = c^2(q_0 + k_0)^2$ , the loop integral is

$$\int \frac{d^d \mathbf{p}}{(2\pi)^d} \frac{1}{(\mathbf{p}^2 + m_1^2)((\mathbf{p} + \mathbf{k})^2 + m_2^2)} = \frac{1}{8\pi^2\epsilon}, \quad (\text{B.72})$$

using Feynman parameters and shifting  $\mathbf{p} \rightarrow \mathbf{p} - (1-x)\mathbf{k}$ . We thus obtain

$$\delta\Gamma_{\text{div}}^{(g)} = \frac{3\lambda^2\Delta}{4\pi^2\epsilon} \sum_a \int d^D x |\phi_a|^4, \quad (\text{B.73})$$

and

$$\delta Z_5^{(g)} = -\frac{3\Delta}{4\pi^2\epsilon}. \quad (\text{B.74})$$

### B.3.4 Disorder strength

The two diagrams are Fig. 3.3(h) and (i). The diagram in Fig. 3.3(h) is produced by the third term in  $\text{Tr}(D\Xi D\frac{M}{2})$  (Eq. (B.43)), for which we have

$$\delta\Gamma_{\text{div}}^{(h)} = 4\lambda^2\Delta \sum_{ab} \int \frac{d^d\mathbf{k}}{(2\pi)^d} \int d^{\epsilon_\tau}\tau \int d^{\epsilon_\tau}\tau' |\phi_a|_{-\mathbf{k},\tau}^2 |\phi_b|_{\mathbf{k},\tau'}^2 \int \frac{d^D\mathbf{p}}{(2\pi)^D} \frac{1}{(c^2p_0^2 + \mathbf{p}^2)(c^2p_0^2 + (\mathbf{p} + \mathbf{k})^2)}. \quad (\text{B.75})$$

The loop integral is the same as  $I_2$  in Eq. (B.63), but with  $k_0 = 0$ , which does not change the result  $I_2 = 1/[8\pi^2(\epsilon - \epsilon_\tau)]$  in the limit  $\epsilon, \epsilon_\tau \rightarrow 0$ . We thus have

$$\delta\Gamma_{\text{div}}^{(h)} = \frac{\lambda^2\Delta}{2\pi^2(\epsilon - \epsilon_\tau)} \sum_{ab} \int d^d\mathbf{x} d^{\epsilon_\tau}\tau d^{\epsilon_\tau}\tau' |\phi_a|_{\mathbf{x},\tau}^2 |\phi_b|_{\mathbf{x},\tau'}^2, \quad (\text{B.76})$$

hence

$$\delta Z_7^{(h)} = \frac{\lambda^2}{\pi^2(\epsilon - \epsilon_\tau)}. \quad (\text{B.77})$$

The first term in  $\text{Tr}(D\Xi D\frac{M}{2})$  (Eq. (B.43)) vanishes in the replica limit  $m \rightarrow 0$ , and the rest of the terms produce nonvanishing contributions to the diagram in Fig. 3.3(i). The second and third terms in Eq. (B.43) give:

$$\begin{aligned} \delta\Gamma_{\text{div}}^{(i,1)} &= -\Delta^2 \sum_{ab} \int \frac{d^d\mathbf{k}}{(2\pi)^d} \int d^{\epsilon_\tau}\tau \int \frac{d^D\mathbf{q}}{(2\pi)^D} |\phi_a|_{-\mathbf{k},\tau}^2 \phi_b^\alpha(\mathbf{k} + \mathbf{q}, q_0) \phi_b^\alpha(-q) \\ &\quad \times \int \frac{d^d\mathbf{p}}{(2\pi)^d} \frac{1}{(c^2q_0^2 + \mathbf{p}^2)(c^2q_0^2 + (\mathbf{p} + \mathbf{k})^2)}, \end{aligned} \quad (\text{B.78})$$

and the last term in Eq. (B.43) contribute

$$\begin{aligned} \delta\Gamma_{\text{div}}^{(i,2)} &= -\Delta^2 \sum_{ab} \left( \prod_{i=1}^4 \int \frac{d^d\mathbf{k}_i}{(2\pi)^d} \right) (2\pi)^d \delta \left( \sum_{i=1}^4 \mathbf{k}_i \right) \int \frac{d^{\epsilon_\tau}p_0}{(2\pi)^{\epsilon_\tau}} \int \frac{d^{\epsilon_\tau}q_0}{(2\pi)^{\epsilon_\tau}} \\ &\quad \times \phi_a^\alpha(\mathbf{k}_1, p_0) \phi_a^\alpha(\mathbf{k}_4, -p_0) \phi_b^\beta(\mathbf{k}_3, q_0) \phi_b^\beta(\mathbf{k}_2, -q_0) \int \frac{d^d\mathbf{p}}{(2\pi)^d} \frac{1}{(c^2p_0^2 + \mathbf{p}^2)(c^2q_0^2 + (\mathbf{p} + \mathbf{k}_3 + \mathbf{k}_4)^2)}. \end{aligned} \quad (\text{B.79})$$

Both integrals over the loop momentum  $\mathbf{p}$  are of the form (B.72), and thus evaluate to  $1/(8\pi^2\epsilon)$ . Performing the remaining integrals, we obtain

$$\delta\Gamma_{\text{div}}^{(i,1)} + \delta\Gamma_{\text{div}}^{(i,2)} = -\frac{\Delta^2}{4\pi^2\epsilon} \sum_{ab} \int d^d\mathbf{x} d^{\epsilon_\tau}\tau d^{\epsilon_\tau}\tau' |\phi_a|^2(\mathbf{x},\tau) |\phi_b|^2(\mathbf{x},\tau'), \quad (\text{B.80})$$

thus

$$\delta Z_7^{(i)} = -\frac{\Delta}{2\pi^2\epsilon}. \quad (\text{B.81})$$

Adding up the various contributions and rescaling the couplings  $\lambda^2$ ,  $h^2$ , and  $\Delta$  by  $(4\pi)^2$ , we obtain the renormalization constants in Eqs. (3.36)-(3.43).

## B.4 Yukawa coupling

In this section we calculate the counter-term for the Yukawa coupling. The contribution to  $\delta Z_6$  comes from the last term in the expression for  $\text{Tr}(\Pi\Xi)$  (Eq. (B.38)). In the XY model, at one-loop order, there is no diagram consistent with the Feynman rules in Fig. 3.2 that can renormalize the Yukawa vertex; thus  $\delta Z_6 = 0$  at this order. We perform calculations for the Ising and Heisenberg models separately. Let us first consider the Ising model, for which we have

$$\begin{aligned} \delta\Gamma_{\text{div}}^{(f)} &= -i\frac{h^3}{2} \int \frac{d^D k_1}{(2\pi)^D} \int \frac{d^D k_2}{(2\pi)^D} \phi_a(k_2) \bar{\psi}_a(k_1) \psi_a(k_1 - k_2) \\ &\quad \times \int \frac{d^D p}{(2\pi)^D} \frac{1}{c^2 p_0^2 + \mathbf{p}^2} \frac{(\not{p} + \not{k}_1)(\not{p} + \not{k}_1 - \not{k}_2)}{(p + k_1)^2 (p + k_1 - k_2)^2} \\ &= -i\frac{h^3}{(4\pi)^2} \frac{1}{\epsilon - \epsilon_\tau} \int \frac{d^D k_1}{(2\pi)^D} \int \frac{d^D k_2}{(2\pi)^D} \phi_a(k_2) \bar{\psi}_a(k_1) \psi_a(k_1 - k_2). \end{aligned} \quad (\text{B.82})$$

Here the superscript (f) in  $\delta\Gamma_{\text{div}}^{(f)}$  refers to Fig. 4.2(f). The calculation of the integral over  $p$  is performed similarly to the one done in Sec. (B.3.2). To simplify the calculation, we may set the external momentum  $k_2$  to zero in the fermion propagator, since we are only interested in corrections to the local Yukawa vertex, and the integral reduces to the one in Eq. (B.57)

with  $(\not{p} + \not{k}) \rightarrow 1$  in the nominator. Rescaling  $h^2$  by  $(4\pi)^2$ , for the Ising model we obtain

$$\delta Z_6^{(f)} = \frac{h^2}{\epsilon - \epsilon_\tau}. \quad (\text{B.83})$$

For the Heisenberg model, we have

$$\begin{aligned} \delta \Gamma_{\text{div}}^{(f)} &= -i \frac{h^3}{2} \int \frac{d^D k_1}{(2\pi)^D} \int \frac{d^D k_2}{(2\pi)^D} \int \frac{d^D p}{(2\pi)^D} \sum_i \bar{\psi}_a(k_1) \frac{1}{c^2 p_0^2 + \mathbf{p}^2} \sigma_i \\ &\quad \times \frac{(\not{p} + \not{k}_1)(\not{p} + \not{k}_1 - \not{k}_2)}{(p + k_1)^2 (p + k_1 - k_2)^2} (\phi_a(k_2) \cdot \boldsymbol{\sigma}) \sigma_i \psi_a(k_1 - k_2) \\ &\rightarrow -i \frac{h^3}{2} \int \frac{d^D k_1}{(2\pi)^D} \int \frac{d^D k_2}{(2\pi)^D} \bar{\psi}_a(k_1) (\phi_a(k_2) \cdot \boldsymbol{\sigma}) \psi_a(k_1 - k_2) \int \frac{d^D p}{(2\pi)^D} \frac{1}{c^2 p_0^2 + \mathbf{p}^2} \frac{1}{(p + k_1)^2} \\ &= i \frac{h^3}{(4\pi)^2} \frac{1}{\epsilon - \epsilon_\tau} \int \frac{d^D k_1}{(2\pi)^D} \int \frac{d^D k_2}{(2\pi)^D} \bar{\psi}_a(k_1) (\phi_a(k_2) \cdot \boldsymbol{\sigma}) \psi_a(k_1 - k_2), \end{aligned} \quad (\text{B.84})$$

where going from the second to the third line we simplified calculations by setting  $k_2 = 0$  in the fermion propagator as before, which does not change  $\delta Z_6$ . Thus, in the Heisenberg model, rescaling  $h^2$  by  $(4\pi)^2$ , we obtain

$$\delta Z_6^{(f)} = -\frac{h^2}{\epsilon - \epsilon_\tau}. \quad (\text{B.85})$$

Combining these results altogether, we may compactly write a generic expression for all three models considered:

$$\delta Z_6^{(f)} = (2 - n) \frac{h^2}{\epsilon - \epsilon_\tau}. \quad (\text{B.86})$$

## B.5 Long-range correlated disorder contributions

In this section we detail the computation of diagrams involving long-range correlated disorder. All diagrams listed below refer to Fig. 4.2. Throughout the calculations we use the vector representation of bosonic fields for all models.

### B.5.1 Boson two-point function

The diagram (d) in Fig. 4.2 contributes to  $\delta Z_3$  and  $\delta Z_r$  and is produced by the long-range part of the second term in the expression for  $\text{Tr}(D^{\frac{M}{2}})$  (Eq. (B.40)). Its contribution to the divergent part of the effective action is:

$$\delta\Gamma_{\text{div}}^{(d)} = -v \sum_a \int \frac{d^D k}{(2\pi)^D} \phi_a(-k) \cdot \phi_a(k) \int \frac{d^d \mathbf{p}}{(2\pi)^d} \frac{|\mathbf{p}|^{\epsilon-\delta}}{c^2 k_0^2 + (\mathbf{k} + \mathbf{p})^2 + r\mu^2}. \quad (\text{B.87})$$

Since we anticipate a renormalization of both the time-derivative term [218, 219] and the scalar mass term, the latter being necessary to compute the correlation length exponent, we must keep the “mass squared”  $c^2 k_0^2 + r$  in the denominator. Such massive Feynman integrals can be evaluated using the Mellin-Barnes representation of hypergeometric functions [246, 247]. We have:

$$I \equiv \int \frac{d^d \mathbf{p}}{(2\pi)^d} \frac{|\mathbf{p}|^{\epsilon-\delta}}{c^2 k_0^2 + (\mathbf{k} + \mathbf{p})^2 + r\mu^2} = (c^2 k_0^2 + r\mu^2)^{1-\delta/2} S_{4-\epsilon} \frac{\Gamma(-1 + \frac{\delta}{2}) \Gamma(2 - \frac{\delta}{2})}{2\Gamma(1)} \times {}_2F_1\left(\frac{\delta - \epsilon}{2}, -1 + \frac{\delta}{2}; 2 - \frac{\epsilon}{2}; -\frac{\mathbf{k}^2}{c^2 k_0^2 + r\mu^2}\right), \quad (\text{B.88})$$

where  ${}_2F_1(a, b; c; z)$  is the Gauss hypergeometric function, and  $S_d = 2/[(4\pi)^{d/2} \Gamma(d/2)]$ . Taking the limit  $\delta, \epsilon \rightarrow 0$ , the hypergeometric function evaluates to a constant:  ${}_2F_1(0, -1; 2; z) = 1$ . The only divergent factor in this limit is  $\Gamma(-1 + \frac{\delta}{2}) \rightarrow -2/\delta$ , and we obtain:

$$I = -\frac{2(c^2 k_0^2 + r\mu^2)}{(4\pi)^2 \delta}. \quad (\text{B.89})$$

After rescaling the couplings by  $(4\pi)^2$ , we thus obtain:

$$\delta Z_3^{(d)} = \delta Z_r^{(d)} = -\frac{2v}{\delta}. \quad (\text{B.90})$$

### B.5.2 Boson self-interaction

The diagram (j) contributes to the boson self-interaction vertex and is produced by the long-range part in the first two terms in  $\text{Tr} (D \Xi D \frac{M}{2})$  (Eq. (B.43)):

$$\begin{aligned} \delta\Gamma_{\text{div}}^{(j)} &= 6\lambda^2 v \sum_a \int \frac{d^D k}{(2\pi)^D} \int \frac{d^D k'}{(2\pi)^D} \int \frac{d^D k''}{(2\pi)^D} \phi_a^i(-k) \phi_a^j(-k') \phi_a^i(k'') \phi_a^j(k + k' - k'') \\ &\times \int \frac{d^d \mathbf{p}}{(2\pi)^d} \frac{|\mathbf{p}|^{\epsilon-\delta}}{[c^2(k_0 + k'_0 - k''_0)^2 + (\mathbf{k} + \mathbf{k}' - \mathbf{k}'' + \mathbf{p})^2 + r\mu^2][c^2(k''_0)^2 + (\mathbf{k}'' - \mathbf{p})^2 + r\mu^2]}. \end{aligned} \quad (\text{B.91})$$

Since we are looking for the correction to a local four-point vertex, we can set the external momenta  $k, k', k''$  to zero in the integral over the loop momentum  $\mathbf{p}$ . Using standard Euclidean integrals,

$$\int \frac{d^d \ell}{(2\pi)^d} \frac{\ell^m}{(\ell^2 + \Delta^2)^n} = \frac{1}{(4\pi)^{d/2}} \frac{\Gamma(\frac{d+m}{2}) \Gamma(n - \frac{d+m}{2})}{\Gamma(d/2) \Gamma(n)} \left(\frac{1}{\Delta^2}\right)^{n-(d+m)/2}, \quad (\text{B.92})$$

we then have, in the limit  $\epsilon, \delta \rightarrow 0$ ,

$$\int \frac{d^d \mathbf{p}}{(2\pi)^d} \frac{|\mathbf{p}|^{\epsilon-\delta}}{(\mathbf{p}^2 + r\mu^2)^2} = \frac{2}{(4\pi)^2 \delta}. \quad (\text{B.93})$$

Rescaling  $v$  by  $(4\pi)^2$ , we obtain:

$$\delta Z_5^{(j)} = -\frac{12v}{\delta}. \quad (\text{B.94})$$

### B.5.3 Short-range correlated disorder strength

The diagrams (l) and (m), which involve long-range correlated disorder, both contribute to the renormalization of the short-range disorder strength. Diagrams of the type (l) give two

distinct contributions, of the form:

$$\delta\Gamma_{\text{div}}^{(l;1,2)} = -\Delta v \sum_{ab} \int \frac{d^D k}{(2\pi)^D} \int \frac{d^D k'}{(2\pi)^D} \int \frac{d^d \mathbf{k}''}{(2\pi)^d} \phi_a^i(-k) \phi_b^j(-k') \phi_a^i(\mathbf{k}'', k_0) \phi_b^j(\mathbf{k} + \mathbf{k}' - \mathbf{k}'', k'_0) \\ \times \mathcal{I}_{1,2}(k, k', \mathbf{k}''), \quad (\text{B.95})$$

where

$$\mathcal{I}_1(k, k', \mathbf{k}'') = 2 \int \frac{d^d \mathbf{p}}{(2\pi)^d} \frac{|\mathbf{p}|^{\epsilon-\delta}}{[c^2 k_0^2 + (\mathbf{k} + \mathbf{p})^2 + r\mu^2] [c^2 (k'_0)^2 + (\mathbf{k}' - \mathbf{p})^2 + r\mu^2]}, \quad (\text{B.96})$$

$$\mathcal{I}_2(k, k', \mathbf{k}'') = \int \frac{d^d \mathbf{p}}{(2\pi)^d} \frac{|\mathbf{p}|^{\epsilon-\delta}}{[c^2 (k'_0)^2 + (\mathbf{k} + \mathbf{k}' - \mathbf{k}'' - \mathbf{p})^2 + r\mu^2] [c^2 (k'_0)^2 + (\mathbf{k}' - \mathbf{p})^2 + r\mu^2]}. \quad (\text{B.97})$$

The first contribution ( $\mathcal{I}_1$ ) comes from the fourth term in the expression for  $\text{Tr}(D\frac{M}{2})^2$  (Eq. (B.44)), and the second contribution ( $\mathcal{I}_2$ ) is produced by the second and the third terms in the same expression. As in the previous section, we can set  $k = k' = 0$ ,  $\mathbf{k}'' = 0$  in those loop integrals, which then simply reduce to Eq. (B.93). With  $v$  rescaled by  $(4\pi)^2$  as before, we then obtain:

$$\delta Z_7^{(l)} = -\frac{12v}{\delta}. \quad (\text{B.98})$$

The diagram (m) is produced by the fourth term in the expression for  $\text{Tr}(D\frac{M}{2})^2$  (Eq. (B.44)) and illustrates that long-range correlated disorder perturbatively generates short-range correlated disorder. We obtain:

$$\delta\Gamma_{\text{div}}^{(m)} = -v^2 \sum_{ab} \int \frac{d^D k}{(2\pi)^D} \int \frac{d^D k'}{(2\pi)^D} \int \frac{d^d \mathbf{k}''}{(2\pi)^d} \phi_a^i(-k) \phi_b^j(-k') \phi_a^i(\mathbf{k}'', k_0) \phi_b^j(\mathbf{k} + \mathbf{k}' - \mathbf{k}'', k'_0) \\ \times \int \frac{d^d \mathbf{p}}{(2\pi)^d} \frac{|\mathbf{p}|^{\epsilon-\delta} |\mathbf{k} - \mathbf{k}'' + \mathbf{p}|^{\epsilon-\delta}}{[c^2 k_0^2 + (\mathbf{k} + \mathbf{p})^2 + r\mu^2] [c^2 (k'_0)^2 + (\mathbf{k}' - \mathbf{p})^2 + r\mu^2]}, \quad (\text{B.99})$$

an expression analogous to Eqs. (B.95-B.96), but with an additional factor  $|\mathbf{k} - \mathbf{k}'' + \mathbf{p}|^{\epsilon-\delta}$

in the loop integral. Again, the loop integral can be evaluated in the limit of vanishing external momenta. Using Eq. (B.92), we obtain:

$$\int \frac{d^d \mathbf{p}}{(2\pi)^d} \frac{|\mathbf{p}|^{2(\epsilon-\delta)}}{(\mathbf{p}^2 + r\mu^2)^2} = \frac{2}{(4\pi)^2(2\delta - \epsilon)}, \quad (\text{B.100})$$

in the limit  $\epsilon, \delta \rightarrow 0$ , and the corresponding renormalization constant is:

$$\delta Z_7^{(m)} = -\frac{4v^2 \Delta^{-1}}{2\delta - \epsilon}. \quad (\text{B.101})$$

#### B.5.4 Long-range correlated disorder strength

The diagrams in Fig. 4.2(j,l,m) contribute to the long-range disorder coupling renormalization. The diagram (j) is produced by the third term in the expression for the  $\text{Tr}(D\Xi D\frac{M}{2})$  (Eq. (B.43)) and gives:

$$\begin{aligned} \delta\Gamma_{\text{div}}^{(j)} &= (n+2)\lambda^2 v \sum_{ab} \int \frac{d^D k}{(2\pi)^D} \int \frac{d^D k'}{(2\pi)^D} \int \frac{d^d \mathbf{k}''}{(2\pi)^d} \phi_a^i(-k) \phi_b^j(-k') \phi_a^i(\mathbf{k}'', k_0) \phi_b^j(\mathbf{k} + \mathbf{k}' - \mathbf{k}'', k'_0) \\ &\quad \times |\mathbf{k} - \mathbf{k}''|^{\epsilon-\delta} \int \frac{d^D p}{(2\pi)^D} \frac{1}{(c^2 p_0^2 + \mathbf{p}^2 + r\mu^2) [c^2 p_0^2 + (\mathbf{k} - \mathbf{k}'' - \mathbf{p})^2 + r\mu^2]}. \end{aligned} \quad (\text{B.102})$$

The interaction term induced by long-range correlated disorder in Eq. (4.9) can be Fourier transformed to momentum space:

$$\begin{aligned} \int d^d \mathbf{x} d^d \mathbf{x}' d^{\epsilon\tau} \tau d^{\epsilon\tau} \tau' \frac{\phi_a^2(\mathbf{x}, \tau) \phi_b^2(\mathbf{x}, \tau')}{|\mathbf{x} - \mathbf{x}'|^\alpha} &= \int \frac{d^D k}{(2\pi)^D} \int \frac{d^D k'}{(2\pi)^D} \int \frac{d^d \mathbf{k}''}{(2\pi)^d} \phi_a^i(-k) \phi_b^j(-k') \phi_a^i(\mathbf{k}'', k_0) \\ &\quad \times \phi_b^j(\mathbf{k} + \mathbf{k}' - \mathbf{k}'', k'_0) |\mathbf{k} - \mathbf{k}''|^{\epsilon-\delta}, \end{aligned} \quad (\text{B.103})$$

using  $d = 4 - \epsilon$  and  $\alpha = 4 - \delta$ . Here, we include a constant prefactor arising during the Fourier transformation of the disorder correlation function into a redefinition of  $v$ . Comparing with Eq. (B.102), we see that we can evaluate the loop integral in the limit of zero external

momenta:

$$\int \frac{d^D p}{(2\pi)^D} \frac{1}{(c^2 p_0^2 + \mathbf{p}^2 + r\mu^2)^2} = \frac{\Gamma(\epsilon/2)}{(4\pi)^{d/2}} \int \frac{d^{\epsilon_\tau} p_0}{(2\pi)^{\epsilon_\tau}} \frac{1}{(c^2 p_0^2 + r\mu^2)^{\epsilon/2}} = \frac{2}{(4\pi)^2(\epsilon - \epsilon_\tau)}, \quad (\text{B.104})$$

in the limit  $\epsilon, \epsilon_\tau \rightarrow 0$ . We correspondingly have:

$$\delta Z_8^{(j)} = \frac{4(n+2)\lambda^2}{\epsilon - \epsilon_\tau}. \quad (\text{B.105})$$

The diagram (l) is produced by the second and third terms in the expression for  $\text{Tr} \left( D \frac{M}{2} \right)^2$  (Eq. (B.44)) and gives:

$$\begin{aligned} \delta \Gamma_{\text{div}}^{(l)} = & -\Delta v \sum_{ab} \int \frac{d^D k}{(2\pi)^D} \int \frac{d^D k'}{(2\pi)^D} \int \frac{d^d \mathbf{k}''}{(2\pi)^d} \phi_a^i(-k) \phi_b^j(-k') \phi_a^i(\mathbf{k}'', k_0) \phi_b^j(\mathbf{k} + \mathbf{k}' - \mathbf{k}'', k'_0) \\ & \times |\mathbf{k} - \mathbf{k}''|^{\epsilon-\delta} \int \frac{d^d \mathbf{p}}{(2\pi)^d} \frac{1}{[c^2(k'_0)^2 + \mathbf{p}^2 + r\mu^2] [c^2(k'_0)^2 + (\mathbf{k} - \mathbf{k}'' - \mathbf{p})^2 + r\mu^2]}. \end{aligned} \quad (\text{B.106})$$

Once again, the loop integral can be performed setting to zero the external momenta:

$$\int \frac{d^d \mathbf{p}}{(2\pi)^d} \frac{1}{(\mathbf{p}^2 + r\mu^2)^2} = \frac{2}{(4\pi)^2 \epsilon}, \quad (\text{B.107})$$

in the limit  $\epsilon \rightarrow 0$ , and we obtain:

$$\delta Z_8^{(l)} = -\frac{4\Delta}{\epsilon}. \quad (\text{B.108})$$

Finally, the diagram (m), which is also produced by the fourth term in the expression for  $\text{Tr} \left( D \frac{M}{2} \right)^2$  (Eq. (B.44)), gives a contribution similar to the diagram (l), but with an extra

$\mathbf{p}$ -dependent factor in the loop integrand:

$$\begin{aligned} \delta\Gamma_{\text{div}}^{(\text{m})} = & -v^2 \sum_{ab} \int \frac{d^D k}{(2\pi)^D} \int \frac{d^D k'}{(2\pi)^D} \int \frac{d^d \mathbf{k}''}{(2\pi)^d} \phi_a^i(-k) \phi_b^j(-k') \phi_a^i(\mathbf{k}'', k_0) \phi_b^j(\mathbf{k} + \mathbf{k}' - \mathbf{k}'', k_0) \\ & \times |\mathbf{k} - \mathbf{k}''|^{\epsilon-\delta} \int \frac{d^d \mathbf{p}}{(2\pi)^d} \frac{|\mathbf{k} + \mathbf{k}' - \mathbf{k}'' - \mathbf{p}|^{\epsilon-\delta}}{[c^2(k_0')^2 + \mathbf{p}^2 + r\mu^2] [c^2(k_0')^2 + (\mathbf{k} - \mathbf{k}'' - \mathbf{p})^2 + r\mu^2]}. \end{aligned} \quad (\text{B.109})$$

In the limit of vanishing external momenta, the loop integral reduces to Eq. (B.93), and we have:

$$\delta Z_8^{(\text{m})} = -\frac{4v}{\delta}. \quad (\text{B.110})$$

## B.6 Absence of fermionic short-range disordered fixed point at $\mathcal{O}(\sqrt{\epsilon_\tau})$ in the chiral Ising GNY model

In the random-mass chiral Ising GNY model ( $n = 1$ ), we found a single SDFP at one-loop order [Eq. (4.50)], by contrast with the chiral XY and Heisenberg models where we found two SDFPs [Eq. (4.49)]. This is a consequence of the accidental degeneracy of the system of equations  $\beta_{\lambda^2}/\lambda^2 = 0$ ,  $\beta_{\Delta}/\Delta = 0$  in the bosonic limit  $h^2 = 0$ . In the bosonic theory, this accidental degeneracy is lifted at two-loop order, which leads to a SDFP with  $\lambda_*^2, \Delta_* \sim \mathcal{O}(\sqrt{\epsilon_\tau})$  for a fixed ratio  $\epsilon/\epsilon_\tau$  [123, 124, 160]. Setting  $\epsilon/\epsilon_\tau = 2$ , we investigate the possibility of an additional fermionic SDFP with  $\lambda_*^2, \Delta_* \sim \mathcal{O}(\sqrt{\epsilon_\tau})$  in the random-mass chiral Ising GNY model.

At higher loop orders, for a reason that will become clearer towards the end of this Appendix, it is technically more convenient [123, 124] to work with rescaled couplings  $\tilde{\lambda}^2$  and  $\tilde{h}^2$ , defined via  $\lambda^2 = c^{\epsilon_\tau} \tilde{\lambda}^2$  and  $h^2 = c^{\epsilon_\tau} \tilde{h}^2$ . Using Eqs. (4.17-4.19), the beta functions

for those rescaled couplings are:

$$\beta_{\tilde{\lambda}^2} = (-\epsilon_\tau + 2\gamma_4 - \gamma_5 + \frac{\epsilon_\tau}{2}(\gamma_3 - \gamma_4)) \tilde{\lambda}^2, \quad (\text{B.111})$$

$$\beta_{\tilde{h}^2} = (-\epsilon_\tau + 2(\gamma_2 - \gamma_6) + \gamma_4 + \frac{\epsilon_\tau}{2}(\gamma_3 - \gamma_4)) \tilde{h}^2. \quad (\text{B.112})$$

At one-loop order, those beta functions reduce to those previously found [Eqs. (4.38-4.39)] with  $\lambda \rightarrow \tilde{\lambda}$  and  $h \rightarrow \tilde{h}$ . Indeed, there is no change in the divergent part of the one-loop effective action in the limit  $\epsilon_\tau \rightarrow 0$ , and thus in the  $\overline{\text{MS}}$  renormalization constants, and the terms  $\frac{\epsilon_\tau}{2}(\gamma_3 - \gamma_4)$  in Eqs. (B.111-B.112) are dropped at this order. At two-loop order, ignoring these latter terms for now, the beta functions for  $\tilde{\lambda}^2$ ,  $\Delta$ , and  $\tilde{h}^2$  read:

$$\beta_{\tilde{\lambda}^2} = -\epsilon_\tau \tilde{\lambda}^2 + 6(3\tilde{\lambda}^2 - 2\Delta)\tilde{\lambda}^2 + 2N\tilde{h}^2\tilde{\lambda}^2 - N\tilde{h}^4 + (\text{cubic in } \tilde{h}^2, \tilde{\lambda}^2, \Delta), \quad (\text{B.113})$$

$$\beta_\Delta = -2\epsilon_\tau \Delta + 4(3\tilde{\lambda}^2 - 2\Delta)\Delta + 2N\tilde{h}^2\Delta + (\text{quadratic in } \tilde{h}^2, \tilde{\lambda}^2, \Delta) \times \Delta, \quad (\text{B.114})$$

$$\beta_{\tilde{h}^2} = -\epsilon_\tau \tilde{h}^2 + (N + 3)\tilde{h}^4 + (\text{quadratic in } \tilde{h}^2, \tilde{\lambda}^2, \Delta) \times \tilde{h}^2. \quad (\text{B.115})$$

where the form of the two-loop term in Eq. (B.114) follows from the fact that a disorder vertex cannot be generated perturbatively from a clean theory. Similarly, Eq. (B.115) follows from the fact that a Yukawa vertex cannot be generated from a theory of decoupled bosons and fermions.

We expand the fixed-point couplings  $\tilde{\lambda}_*^2$ ,  $\Delta_*$ , and  $\tilde{h}_*^2$  in increasing powers of  $\epsilon_\tau$ :

$$\tilde{\lambda}_*^2 = \lambda_1^2 + \lambda_2^2 + \dots, \quad \Delta_* = \Delta_1 + \Delta_2 + \dots, \quad \tilde{h}_*^2 = h_1^2 + h_2^2 + \dots, \quad (\text{B.116})$$

where the leading power for each coupling remains to be determined. The SDFP (4.50) previously found was obtained assuming that  $3\lambda_1^2 - 2\Delta_1 \neq 0$ , which gives  $\lambda_1^2, \Delta_1, h_1^2 \propto \epsilon_\tau$ . Here we consider the possibility that  $3\lambda_1^2 - 2\Delta_1 = 0$ , with  $\lambda_1^2, \Delta_1 \propto \sqrt{\epsilon_\tau}$  [123, 124, 160]. First, in Eq. (B.115), the two-loop term is at most  $\propto \epsilon_\tau \tilde{h}^2$ , thus the equation  $\beta_{\tilde{h}^2} = 0$  may in general be solved to  $\mathcal{O}(\epsilon_\tau^2)$  to yield a nontrivial solution  $h_1^2 \propto \epsilon_\tau \neq 0$ . In fact,  $\beta_{\tilde{h}^2}$  also contains the term  $\frac{\epsilon_\tau}{2}(\gamma_3 - \gamma_4)\tilde{h}^2$  [see Eq. (B.112)], but at leading order this term is  $\mathcal{O}(\epsilon_\tau^{5/2})$

and does not affect  $h_1^2$ .

At leading order, the equations  $\beta_{\tilde{\chi}^2} = 0$  and  $\beta_{\Delta} = 0$  become:

$$0 = -\epsilon_{\tau}\lambda_1^2 + 6(3\lambda_2^2 - 2\Delta_2)\lambda_1^2 + 2Nh_1^2\lambda_1^2 - Nh_1^4 + (\text{cubic in } h_1^2, \lambda_1^2, \Delta_1), \quad (\text{B.117})$$

$$0 = -2\epsilon_{\tau}\Delta_1 + 4(3\lambda_2^2 - 2\Delta_2)\Delta_1 + 2Nh_1^2\Delta_1 + (\text{quadratic in } h_1^2, \lambda_1^2, \Delta_1) \times \Delta_1. \quad (\text{B.118})$$

These equations may in general be solved to  $\mathcal{O}(\epsilon_{\tau}^{3/2})$  to yield nontrivial solutions  $\lambda_1^2, \Delta_1 \propto \sqrt{\epsilon_{\tau}}$ , with  $\lambda_2^2, \Delta_2 \propto \epsilon_{\tau}$ . As with  $\beta_{\tilde{h}^2}$ , Eq. (B.117) in fact contains the additional term  $\frac{\epsilon_{\tau}}{2}(\gamma_3 - \gamma_4)\tilde{\lambda}^2$  on the right-hand side [see Eq. (B.111)], but at leading order this term is  $\mathcal{O}(\epsilon_{\tau}^2)$  and does not affect  $\lambda_1^2, \Delta_1$ .

Thus far we have seen that a common zero of  $\beta_{\tilde{\chi}^2}, \beta_{\tilde{h}^2}, \beta_{\Delta}$  with  $\tilde{\lambda}_*^2, \Delta_* \sim \mathcal{O}(\sqrt{\epsilon_{\tau}})$  and  $\tilde{h}_*^2 \sim \mathcal{O}(\epsilon_{\tau})$  is in principle possible at two-loop order. We now turn to the remaining equation,  $\beta_{c^2} = 0$ . At two-loop order, the beta function for  $c^2$  reads:

$$\beta_{c^2} = -2\Delta c^2 + \tilde{h}^2 [N(c^2 - 1) + c^2(2f(c^2) - 1)] + \beta_{c^2}^{(2L)}, \quad (\text{B.119})$$

where the two-loop part,

$$\beta_{c^2}^{(2L)} = \left(2\gamma_1^{(2L)} - 2\gamma_2^{(2L)} - \gamma_3^{(2L)} + \gamma_4^{(2L)}\right) c^2, \quad (\text{B.120})$$

depends on  $\gamma_i^{(2L)}$ ,  $i = 1, \dots, 4$ , the two-loop contributions to the anomalous dimensions  $\gamma_i = d \ln Z_i / d \ln \mu$ . These contributions are quadratic in the couplings  $\tilde{h}^2, \tilde{\lambda}^2, \Delta$ , but may have a nontrivial dependence on  $c^2$ . We separate  $\beta_{c^2}^{(2L)}$  into a purely bosonic part and a part depending on the Yukawa coupling:

$$\beta_{c^2}^{(2L)} = (\text{quadratic in } \tilde{\lambda}^2, \Delta) \times f_1(c^2)c^2 + (\text{linear in } \tilde{h}^2, \tilde{\lambda}^2, \Delta) \times \tilde{h}^2 f_2(c^2)c^2, \quad (\text{B.121})$$

where  $f_1$  and  $f_2$  are potentially nontrivial functions of  $c^2$ . We look for solutions  $c_*^2$  to the equation  $\beta_{c^2} = 0$ , evaluated at  $\tilde{\lambda}_*^2, \Delta_* \sim \mathcal{O}(\sqrt{\epsilon_{\tau}})$  and  $\tilde{h}_*^2 \sim \mathcal{O}(\epsilon_{\tau})$ . Since  $c^2$  is not a

perturbative coupling, we assume  $c_*^2 \sim \mathcal{O}(1)$ , as in the DFPs studied in the rest of the thesis. The first term in (B.119) is then  $\mathcal{O}(\sqrt{\epsilon_\tau})$  while the remaining terms are  $\mathcal{O}(\epsilon_\tau)$ , so there is no consistent  $c_*^2 \neq 0$  solution.

We can at last look for a fixed point with  $c_*^2 = 0$ , such that  $\beta_{c^2} = -N\tilde{h}_*^2 + \beta_{c^2}^{(2L)}$ . If we can show that  $f_1(c^2) = \text{const.}$ , this solution is again inconsistent at leading order in  $\epsilon_\tau$  since, even if  $f_2(c^2)c^2$  remains finite in the limit  $c_*^2 \rightarrow 0$ , the  $\tilde{h}^2$ -dependent term in Eq. (B.121) is then  $\mathcal{O}(\epsilon_\tau^{3/2})$ . We now proceed to show that  $f_1(c^2)$  is in fact independent of  $c^2$ . To do so, we can restrict ourselves to the purely bosonic theory with  $\tilde{h}^2 = 0$ . In this case one has  $\gamma_1 = \gamma_2 = 0$  at all loop orders, since the fermions decouple and remain free fields, and we need only consider the contributions of  $\gamma_3^{(2L)}$  and  $\gamma_4^{(2L)}$  to  $\beta_{c^2}^{(2L)}$ , i.e., two-loop corrections to the boson two-point function in the bosonic theory. These are essentially the standard double tadpole and sunset diagrams of two-loop  $\phi^4$  theory, but with  $V_\lambda$  self-interaction vertices and  $V_\Delta$  disorder vertices such that  $V_\lambda + V_\Delta = 2$ . Schematically, these corrections are of the form:

$$\delta D(k_0, \mathbf{k}) \propto \left(c^{\epsilon_\tau} \tilde{\lambda}^2\right)^{V_\lambda} \Delta^{V_\Delta} \int d^{\epsilon_\tau} p_0 d^{\epsilon_\tau} p'_0 d^d \mathbf{p} d^d \mathbf{p}' \left[\delta^{(\epsilon_\tau)}(k_0, p_0, p'_0)\right]^{V_\Delta} I(ck_0, \mathbf{k}; cp_0, cp'_0, \mathbf{p}, \mathbf{p}'), \quad (\text{B.122})$$

where  $k = (k_0, \mathbf{k})$  is the external momentum,  $p = (p_0, \mathbf{p})$  and  $p' = (p'_0, \mathbf{p}')$  are the two independent loop momenta, and  $[\delta^{(\epsilon_\tau)}(k_0, p_0, p'_0)]^{V_\Delta}$  symbolizes the fact that each disorder vertex is accompanied by an  $\epsilon_\tau$ -dimensional delta function involving linear combinations of the frequencies  $k_0, p_0, p'_0$  in the diagram (see Fig. 4.1). Performing the change of integration variables  $p_0 \rightarrow \tilde{p}_0 = cp_0$ ,  $p'_0 \rightarrow \tilde{p}'_0 = cp'_0$ , and using the property  $\delta^{(\epsilon_\tau)}(q_0/c) = c^{\epsilon_\tau} \delta^{(\epsilon_\tau)}(q_0)$ , Eq. (B.122) becomes:

$$\begin{aligned} \delta D(k_0, \mathbf{k}) &\propto c^{(V_\lambda + V_\Delta - 2)\epsilon_\tau} \left(\tilde{\lambda}^2\right)^{V_\lambda} \Delta^{V_\Delta} \\ &\quad \times \int d^{\epsilon_\tau} \tilde{p}_0 d^{\epsilon_\tau} \tilde{p}'_0 d^d \mathbf{p} d^d \mathbf{p}' \left[\delta^{(\epsilon_\tau)}(ck_0, \tilde{p}_0, \tilde{p}'_0)\right]^{V_\Delta} I(ck_0, \mathbf{k}; \tilde{p}_0, \tilde{p}'_0, \mathbf{p}, \mathbf{p}'), \end{aligned} \quad (\text{B.123})$$

which, since  $V_\lambda + V_\Delta = 2$ , depends on  $c$  only through  $c^2 k_0^2$ . Since the latter appears in the unperturbed propagator (4.25),  $\gamma_3^{(2L)}$  and  $\gamma_4^{(2L)}$ , and thus  $f_1(c^2)$  in Eq. (B.121), are necessarily independent of  $c^2$ . Similar reasoning shows that counter-term insertions in one-loop diagrams do not generate a dependence on  $c^2$  either. According to the argument above, a fixed point with  $c_*^2 = 0$  is thus impossible.

## B.7 Oscillatory corrections to scaling

We derive the existence of oscillatory corrections to scaling [168] at the DFPs due to the presence of a pair of complex-conjugate eigenvalues of the stability matrix. Passing over to a Wilsonian description, and ignoring corrections to the dynamic critical exponent, the two-point function of the order parameter  $\chi(\mathbf{q}) = \langle \phi(\mathbf{q})\phi^*(\mathbf{q}) \rangle$  (for the XY model in the complex boson representation) obeys the scaling relation  $\chi(\mathbf{q}, r(0)) = e^{(2-\eta_\phi)\ell} \chi(e^\ell \mathbf{q}, r(\ell))$ , where  $\ell$  is an infrared scale parameter,  $r(0)$  is the bare relevant tuning parameter for the transition, and  $r(\ell)$  is the renormalized tuning parameter, which obeys the differential equation

$$\frac{dr(\ell)}{d\ell} = [2 - \gamma_4(\mathbf{g}(\ell)) + \gamma_r(\mathbf{g}(\ell))]r(\ell) = [2 - \gamma_{m^2}(\mathbf{g}(\ell))]r(\ell). \quad (\text{B.124})$$

Similarly,  $\mathbf{g}(\ell) = (c^2, h^2, \lambda^2, \Delta, v)$  is a vector of renormalized couplings, which obeys the differential equation

$$\frac{d\mathbf{g}(\ell)}{d\ell} = \boldsymbol{\beta}(\mathbf{g}(\ell)), \quad (\text{B.125})$$

where  $\boldsymbol{\beta} = (\beta_{c^2}, \beta_{h^2}, \beta_{\lambda^2}, \beta_\Delta, \beta_v)$  is a vector of beta functions given by Eq. (4.37)-(4.41), but with a minus sign since  $d\ell = -d \ln \mu$ . Defining  $\ell_r$  such that  $r(\ell_r) = r_0$  for some arbitrary constant  $r_0$ , we find that the uniform thermodynamic susceptibility behaves as  $\chi(\mathbf{q} = 0, r) \sim e^{(2-\eta_\phi)\ell_r}$  where we now denote  $r(0)$  by  $r$  for simplicity, and  $\ell_r$  depends on  $r$

in a manner to be determined. Integrating Eq. (B.124) from  $\ell = 0$  to  $\ell = \ell_r$ , we find

$$\ln\left(\frac{r_0}{r}\right) = \int_0^{\ell_r} d\ell [2 - \gamma_{m^2}(\mathbf{g}(\ell))]. \quad (\text{B.126})$$

Linearizing Eq. (B.125) near the fixed point  $\mathbf{g}_*$ , we have

$$\frac{d}{d\ell}(\mathbf{g}(\ell) - \mathbf{g}_*) = M(\mathbf{g}(\ell) - \mathbf{g}_*), \quad (\text{B.127})$$

which is solved by diagonalizing  $M = PDP^{-1}$  where  $D$  is a diagonal matrix. Now,  $\gamma_{m^2}$  in Eq. (B.126) can be read off from Eq. (4.42), and is linear in the couplings:

$$\gamma_{m^2}(\mathbf{g}(\ell)) = \mathbf{a} \cdot \mathbf{g}(\ell) = \mathbf{a} \cdot \mathbf{g}_* + \sum_i u_i(0) \mathbf{a} \cdot \mathbf{v}_i e^{-\omega_i \ell}, \quad (\text{B.128})$$

where the eigenvalues of  $M$  are denoted as  $-\omega_i$ ,  $\mathbf{v}_i$  are the respective eigenvectors, and  $\mathbf{u}(0)$  is a vector of initial conditions,

$$\mathbf{u}(0) = P^{-1}(\mathbf{g}(0) - \mathbf{g}_*). \quad (\text{B.129})$$

Substituting into Eq. (B.126), we obtain

$$\ln\left(\frac{r_0}{r}\right) = \nu^{-1} \ell_r + \sum_i \frac{u_i(0)}{\omega_i} \mathbf{a} \cdot \mathbf{v}_i \left(e^{-\omega_i \ell_r} - 1\right), \quad (\text{B.130})$$

where  $\nu^{-1} = 2 - \gamma_{m^2}(\mathbf{g}_*)$ . Assuming that the deviation (B.129) from the fixed point is small, we can solve for  $\ell_r$  to  $\mathcal{O}(\mathbf{u}(0))$ ,

$$\ell_r = \nu \ln\left(\frac{r_0}{r}\right) - \sum_i \frac{\nu u_i(0)}{\omega_i} \mathbf{a} \cdot \mathbf{v}_i \left[\left(\frac{r}{r_0}\right)^{\nu \omega_i} - 1\right] + \mathcal{O}(\mathbf{u}(0)^2). \quad (\text{B.131})$$

The susceptibility thus becomes

$$\chi \sim |r|^{-\gamma} \left[ 1 - \sum_i \frac{\gamma u_i(0)}{\omega_i} \mathbf{a} \cdot \mathbf{v}_i \left(\frac{r}{r_0}\right)^{\nu \omega_i} + \mathcal{O}(\mathbf{u}(0)^2) \right], \quad (\text{B.132})$$

where  $\gamma = (2 - \eta_\phi)\nu$  is the usual susceptibility exponent.

Real (positive) eigenvalues  $\omega \in \mathbb{R}$  produce the usual corrections to scaling  $\chi \sim |r|^{-\gamma}(1 + C|r|^{\nu\omega} + \dots)$  [220]. Since the stability matrix  $M$  in Eq. (B.127) is real, complex eigenvalues  $\omega = \omega' + i\omega''$ , if any, must come in complex-conjugate pairs  $\omega, \omega^*$ . The associated eigenvectors  $\mathbf{v}, \mathbf{v}^*$  are also complex conjugates since  $M\mathbf{v} = -\omega\mathbf{v}$  and  $M$  is real. Finally, since the components  $u_i$  obey the differential equation  $du_i/d\ell = -\omega_i u_i$ , the component of  $\mathbf{u}(0)$  associated with  $\omega^*$  must also be the complex conjugate of the component associated with  $\omega$ . As a result the corrections to scaling due to a single pair of complex-conjugate eigenvalues  $\omega' \pm i\omega''$  are of the form

$$\begin{aligned} \chi &\sim |r|^{-\gamma} \left[ 1 + \left( \frac{1}{2} C e^{i\phi} \left( \frac{r}{r_0} \right)^{\nu(\omega' + i\omega'')} + \text{c.c.} \right) + \dots \right] \\ &\sim |r|^{-\gamma} \left[ 1 + C \left| \frac{r}{r_0} \right|^{\nu\omega'} \cos \left( \nu\omega'' \ln \left| \frac{r}{r_0} \right| + \phi \right) + \dots \right], \end{aligned} \quad (\text{B.133})$$

where  $C$  and  $\phi$  are nonuniversal constants, but the exponents  $\omega'$  and  $\omega''$  are universal.

## B.8 Log-periodic scaling laws from limit-cycle criticality

In this section we derive the effects of limit-cycle criticality on scaling laws. As in the previous section, we focus on the uniform static susceptibility  $\chi$ , but the derivation can be extended to other thermodynamic observables.

Again, the uniform thermodynamic susceptibility is  $\chi(\mathbf{q} = 0, r) \sim e^{(2 - \eta_\phi)\ell_r}$ , and the goal is to determine  $\ell_r$  as a function of  $r$ . Note that at one-loop order,  $\eta_\phi$  depends only on  $h_*^2$ , and is thus constant everywhere on the limit cycle. From Eq. (B.124), we find

$$\ln \left( \frac{r_0}{r} \right) = \int_0^{\ell_r} d\ell [2 - \gamma_{m^2}(\mathbf{g}(\ell))]. \quad (\text{B.134})$$

For initial values of couplings  $\mathbf{g}(0)$  such that they are on the limit cycle, the integration of Eq. (B.125) gives periodic functions  $\mathbf{g}(l)$  with period  $\ell_{\text{LC}}$ , which can then be expanded as

a Fourier series:

$$\mathbf{g}(\ell) = \sum_{n=-\infty}^{\infty} \mathbf{g}_n e^{2\pi i n \ell / \ell_{\text{LC}}}, \quad (\text{B.135})$$

with  $\mathbf{g}_n = \mathbf{g}_{-n}^*$  since  $\mathbf{g}(\ell)$  is real. At one-loop order,  $\gamma_{m^2}$  is linear in the couplings,  $\gamma_{m^2}(\mathbf{g}(\ell)) = \mathbf{a} \cdot \mathbf{g}(\ell)$ . Performing the integration over  $\ell$  in Eq. (B.134), we obtain:

$$\ln\left(\frac{r_0}{r}\right) = \nu_{\text{LC}}^{-1} \ell_r - \mathcal{F}(\ell_r), \quad (\text{B.136})$$

where

$$\nu_{\text{LC}}^{-1} = 2 - \mathbf{a} \cdot \langle \mathbf{g} \rangle_{\text{LC}}, \quad (\text{B.137})$$

is an effective inverse correlation-length exponent associated with the critical limit cycle, and the function  $\mathcal{F}$  defined as

$$\mathcal{F}(\ell_r) = \mathbf{a} \cdot \int_0^{\ell_r} d\ell [\mathbf{g}(\ell) - \langle \mathbf{g} \rangle_{\text{LC}}] = \sum_{n \neq 0} \mathbf{a} \cdot \mathbf{g}_n \frac{e^{2\pi i n \ell / \ell_{\text{LC}}} - 1}{2\pi i n / \ell_{\text{LC}}}, \quad (\text{B.138})$$

is periodic in  $\ell_r$  with the period  $\ell_{\text{LC}}$  of the limit cycle. In Eqs. (B.137-B.138),  $\langle \mathbf{g} \rangle_{\text{LC}}$  is the “center” of the limit cycle, i.e., the average of  $\mathbf{g}(\ell)$  over one period,

$$\langle \mathbf{g} \rangle_{\text{LC}} = \frac{1}{\ell_{\text{LC}}} \int_0^{\ell_{\text{LC}}} d\ell \mathbf{g}(\ell), \quad (\text{B.139})$$

and coincides with the zeroth Fourier component  $\mathbf{g}_0$ . For limit cycles with inversion symmetry with respect to the enclosed unstable-focus fixed point  $\mathbf{g}_*$  (see Sec. 4.5.2),  $\nu_{\text{LC}}$  would coincide with the correlation-length exponent at this fixed point.

If the limit cycle is small, e.g., near the Hopf bifurcation, we see from Eq. (B.138) that  $\mathcal{F}$  is also small, in which case Eq. (B.136) can be solved perturbatively in the radius

of the limit cycle. To first order in this radius, we thus obtain:

$$\ell_r \approx \nu_{\text{LC}} \ln \left( \frac{r_0}{r} \right) + \nu_{\text{LC}} \mathcal{F} \left( \nu_{\text{LC}} \ln \left( \frac{r_0}{r} \right) \right). \quad (\text{B.140})$$

Substituting into  $\chi \equiv \chi(\mathbf{q} = 0, r) \sim e^{(2-\eta_\phi)\ell_r}$ , and consistently working to first order in  $\mathcal{F}$ , we obtain:

$$\chi \sim |r|^{-\gamma_{\text{LC}}} \left[ 1 + \gamma_{\text{LC}} \mathcal{F} \left( \nu_{\text{LC}} \ln \left( \frac{r_0}{r} \right) \right) \right], \quad (\text{B.141})$$

which is Eq. (4.73) in the main text, where we have defined  $\gamma_{\text{LC}} = (2 - \eta_\phi)\nu_{\text{LC}}$ .

## B.9 Relation between two-component and four-component formulations of the chiral XY GNY model

In this section we prove the equivalence between the two-component formulation of the chiral XY GNY model, used in this thesis and in Ref. [147], and its four-component formulation, used in Ref. [139, 140]. We are only concerned with the fermion part of the Lagrangian, and will set  $c_f = 1$  for simplicity, without loss of generality. Consider an even number  $N = 2N_f$  of flavors of two-component Dirac fermions  $\psi_\alpha$ ,  $\alpha = 1, \dots, N$ . Combining those into  $N_f$  four-component Dirac spinors,

$$\Psi_\alpha = \begin{pmatrix} \psi_\alpha \\ i\psi_{\alpha+N_f} \end{pmatrix}, \quad \alpha = 1, \dots, N_f, \quad (\text{B.142})$$

the fermion Lagrangian can be written as

$$\mathcal{L}_f = \sum_{\alpha=1}^{N_f} \bar{\Psi}_\alpha \not{\partial} \Psi_\alpha + h \left( \phi^* \sum_{\alpha=1}^{N_f} \Psi_\alpha^T i\Gamma_2 \Psi_\alpha + \text{H.c.} \right), \quad (\text{B.143})$$

where  $\bar{\Psi}_\alpha = \Psi_\alpha^\dagger \Gamma_0$ ,  $\not{\partial} = \Gamma_\mu \partial_\mu$ , and we define the  $4 \times 4$  gamma matrices

$$\Gamma_\mu = \begin{pmatrix} \gamma_\mu & 0 \\ 0 & -\gamma_\mu \end{pmatrix}, \quad \mu = 0, 1, 2. \quad (\text{B.144})$$

One can easily check that the Lagrangian of Sec. 3.2 is reproduced by a suitable choice of  $2 \times 2$  gamma matrices, such as  $\gamma_0 = \sigma_3$ ,  $\gamma_1 = \sigma_1$ , and  $\gamma_2 = \sigma_2$ . One can further define the two Hermitian matrices

$$\Gamma_3 = \begin{pmatrix} 0 & -i \\ i & 0 \end{pmatrix}, \quad \Gamma_5 = \Gamma_0 \Gamma_1 \Gamma_2 \Gamma_3 = \begin{pmatrix} 0 & 1 \\ 1 & 0 \end{pmatrix}, \quad (\text{B.145})$$

which square to the identity and anticommute with the gamma matrices (B.144). Defining the charge conjugation matrix  $C = i\Gamma_2$ , we now perform a change of variables to a new set of  $N_f$  four-component spinors  $\chi_\alpha$  [248],

$$\Psi_\alpha = P_- \chi_\alpha + P_+ C \bar{\chi}_\alpha^T, \quad (\text{B.146})$$

where  $P_\pm = \frac{1}{2}(1 \pm \Gamma_5)$  are projectors obeying  $P_\pm^2 = P_\pm$  and  $P_+ P_- = P_- P_+ = 0$ . Using the properties  $C \Gamma_\mu C^{-1} = -\Gamma_\mu^T$  and  $P_\pm \Gamma_\mu = \Gamma_\mu P_\mp$ ,  $\mu = 0, 1, 2$ , the conjugate spinor is given by

$$\bar{\Psi}_\alpha = \bar{\chi}_\alpha P_+ + \chi_\alpha^T C P_- . \quad (\text{B.147})$$

Inserting Eq. (B.146)-(B.147) into the Lagrangian (B.143), and using the properties  $C P_\pm C^{-1} = P_\mp$ ,  $P_\pm^T = P_\pm$ , and  $C^T = C^{-1} = C^\dagger = -C$ , we find

$$\mathcal{L}_f = \sum_{\alpha=1}^{N_f} \bar{\chi}_\alpha \not{\partial} \chi_\alpha + 2h \sum_{\alpha=1}^{N_f} \bar{\chi}_\alpha (\phi_1 + i\phi_2 \Gamma_5) \chi_\alpha, \quad (\text{B.148})$$

where  $\phi = \phi_1 + i\phi_2$ , which is the form of the chiral XY GNY model given in Ref. [139, 140].

In graphene  $N_f = 2$ , thus in the notation of Chap. 3, for us  $N = 2N_f = 4$ .